AN ABSTRACT OF THE THESIS OF

Leslie Groom for the degree of Doctor of Philosophy in Forest Products presented on June 16, 1988.

Title: Experimental Verification and Nonlinear Modeling of Truss-plate Joints by Runge-Kutta Numerical Technique.

Signature redacted for privacy.

Abstract approved : _____
Anton Polensek

The growing use of light-frame wood trusses in the residential and commercial construction has generated the need for general analysis procedures for predicting deformations and ultimate load of truss-plate joints, which are the basis for accurate evaluation of structural performance and design of complete truss assemblies. This dissertation was aimed at developing such a model.

The developed model incorporates mechanisms of load transfer from one wood member through the truss plate and into another wood member and predicts the load-deflection trace and ultimate load. It treats plate teeth as beams on elastic foundation and applies Runge-Kutta numerical analysis to solve the governing differential equations. The nonlinear response of the foundation is accounted for by a linear step-by-step procedure. Additional theoretical investigation consisted of using an existing program to perform finite element analysis of plate joints to determine the interaction of plate teeth arranged in

columns or in rows. This analysis showed some interaction among teeth in columns and none among teeth in rows.

To develop data for model verification, tests were performed on joints made of Douglas-fir lumber and 20-gauge truss plates with die-punched teeth for various grain and plate orientations. Foundation moduli of test joints were obtained by embedment testing under compression loads.

Comparisons between theoretical and experimental load-deflection traces show acceptable agreement. Ultimate load was accurately predicted for specimens which failed as a result of tooth withdrawal, but not for either plate failure or wood failure perpendicular-to-grain, neither of which was included in the model. Possible future model improvements should consist of incorporating these two failure modes and a mechanism associated with moment transfer through plate joints.

EXPERIMENTAL VERIFICATION AND NONLINEAR MODELING OF TRUSS-PLATE JOINTS BY RUNGE-KUTTA NUMERICAL TECHNIQUE

by

LESLIE GROOM

A THESIS

submitted to

Oregon State University

in partial fulfillment of

the requirements for the

degree of

Doctor of Philosophy

Completed June 16, 1988

Commencement June 1989

APPROVED:

Signature redacted for privacy.

Professor of Forest Products in charge of major

Signature redacted for privacy.

Head of Department of Forest Products

Signature redacted for privacy.

Dean of Graduate School

Date thesis is presented 16 June 1988

Typed by Leslie Groom for Leslie Groom

ACKNOWLEDGEMENTS

I would like to express my sincere gratitude and appreciation to the following: Anton 'Tony' Polensek for his guidance, encouragement, and knowledge; Phil Humphrey and Ronald Guenther for their many helpful suggestions; Helmuth 'Dad' Resch for his encouragement and contagious enthusiasm; Boyd A. Schimel for his computer and basketball lessons; Ken Bastendorff for his assistance with specimen testing; and all the guys in the shop who transformed the work plan into a reality.

I would also like to express my thanks to: my parents, who began this whole process 31 years ago, for their neverending encouragement, love, and (of course) financial support; Cath Kendrick for her friendship and invaluable advice; Kevin Groom who has helped to make my last 5 years in Corvallis the best in my life; and to the team of Stan Lebow and Miller, G. D. who gave me many laughs and preserved my sanity.

Lastly, this thesis is dedicated to Mary Ann Reddoch for her unfailing love and without whom I would have never experienced waysays and brochettes.

TABLE OF CONTENTS

I. INTRODUCTION 1

1.1. Justification 2
1.2. Objectives 4

II. LITERATURE REVIEW 5

2.1. Theoretical modeling 5
2.2. Empirical modeling 16

III. THEORETICAL PROCEDURE 19

3.1. Modeling principles 19
3.2. Beam on elastic foundation concept 21
3.2.1. Nonlinear Differential Equation governing tooth-wood interaction 21
3.2.2. Runge-Kutta technique 27
3.2.2.1. Basic concepts 28
3.2.2.2. Application of Runge-Kutta technique to higher order differential equations 31
3.2.2.3. Procedure for evaluating displacements and forces for complete tooth 40
3.2.2.4. Options for varying tooth cross-section and nonlinear foundation modulus 42
3.2.3. Equations for nonlinear foundation modulus 43
3.3. Computer program for Runge-Kutta solution 44
3.4. Evaluation of interaction among teeth ... 47

IV. EXPERIMENTAL PROCEDURE 51

4.1. Joint specimens 51
4.1.1. Material selection 51
4.1.2. Specimen construction 52
4.1.3. Testing procedure 58
4.2. Evaluation of material properties 58
4.2.1. Material selection 60
4.2.2. Testing procedure 60
4.2.2.1. Specific gravity and moisture content 60
4.2.2.2. Tooth embedment 60
4.2.2.3. Tooth withdrawal 63

V. RESULTS AND DISCUSSION 66

5.1. Specific model for specimens tested 66
5.1.1. Multiple tooth effect 66

5.1.1.1. Material data base 66
5.1.1.2. Stress distribution under single tooth 68
5.1.1.3. Stress distribution among multiple teeth in rows and columns .. 70
5.1.2. Analogy of beam-on-elastic-foundation 77
5.1.2.1. Evaluation of material properties 77
5.1.2.2. Foundation modulus of wood .. 79
5.2. Evaluation of the accuracy of theoretical model 91
5.2.1. Joints with four teeth in a row or column 91
5.2.2. Complete truss-plate joints 98
5.3. Proposed modifications for the theoretical model 111
5.3.1. Inclusion of additional failure mechanisms 111
5.3.2. Option for combined loading 111
5.4. Sensitivity analysis: Effects of material properties 115
5.4.1. Effect of foundation modulus on theoretical model 115
5.4.2. Effect of friction coefficient 122
5.4.3. Interaction between effects of changes in foundation moduli and friction coefficient 124

VI. CONCLUSIONS AND RECOMMENDATIONS 133

6.1. Conclusions 133
6.2. Recommendations 136

BIBLIOGRAPHY 137

APPENDICES

A. Truss-plate model TRUSSCON 143

B. Truss manufacturer survey 165

C. Plate-wood stiffness comparison 167

D. Load-embedment traces 173

E. Specific gravity and moisture content 199

F. Tooth withdrawal data 201

LIST OF FIGURES

Figure		Page
2.1.	Deflection pattern under uniform load for: (a) Winkler foundation, and (b) elastic foundation.....	7
2.2.	Typical load-displacement trace that Foschi found in testing embedment specimens.....	13
3.1.	Flow chart of modeling procedures.....	20
3.2.	(a) Cross-section and (b) free-body diagram of elastic beam of finite length, L, on an elastic foundation.....	22
3.3.	(a) Cross-section and (b) free-body diagram of beam on an elastic foundation with lateral shear, moment, and axial loading considered...	24
3.4.	(a) Cross-section and (b) free-body diagram of a beam on an elastic foundation with lateral shear, and axial load in conjunction with friction.....	26
3.5.	Graphic representation of Runge-Kutta technique for initial-value, first-order differential equation.....	29
3.6.	Graphic representation of solution for second order differential equation with boundary conditions using Runge-Kutta technique.....	32
3.7.	Flow chart of the program TRUSSCON used in this study to determine joint response using beam-on-elastic-foundation theory and solved using Runge-Kutta techniques.....	45
3.8.	Finite element models used in this study to determine stress contours under each truss-plate tooth.....	49
4.1.	Truss plate dimensions used in this investigation.....	53
4.2.	Joint types tested in this study to determine the effect of multiple teeth on truss-plate behavior. Joints shown contain (a) Type 1: single tooth, (b) Type 2: 4 teeth in a row, and (c) Type 3: 4 teeth in a column.....	54

4.3. Joint types tested with complete sets of teeth to determine effect of grain and plate orientation on ultimate joint load..... 55

4.4. Apparatus used to assemble truss-plate joint specimens..... 57

4.5. Typical joint type 1 specimen during testing.. 59

4.6. Apparatus used in this study to determine foundation modulus using tooth embedment..... 62

4.7. Apparatus used to (a) assemble tooth withdrawal specimens, and (b) conduct withdrawal test..... 64

5.1. Moduli of elasticity for the finite element analysis for: (a) wood; longitudinal, (b) wood, radial and tangential, and (c) steel.... 67

5.2. Stress distributions for (a) tooth face bearing on end grain and (b) tooth edge bearing on end grain determined by nonlinear finite element analysis (Stresses shown are in kips/in2)..... 69

5.3. Percent of load distributed per 1/8-section of tooth length for the load applied at tooth head for: (a) face and (b) edge orientated tooth..... 71

5.4. Stress distribution obtained in the finite-element analysis of a system with four teeth bearing on faces and arranged in a column at: (a) 67 lbs, (b) 83 lbs (typical failure load), and (c) 100 lbs per tooth..... 73

5.5. Stress distribution obtained in the finite-element analysis of a system with four teeth bearing on edges and arranged in a column at (a) 75 lbs, (b) 100 lbs (typical failure load), and (c) 125 lbs per tooth..... 74

5.6. Stress distribution obtained in the finite-element analysis of four teeth in a row embedded in wood and transferring the load through their edges at a load of 125 lbs/ tooth..... 76

5.7. Load-embedment traces obtained in test of tooth face bearing on end grain for: (a) board no. 1, joint types 1, 2, and 3, and (b) board no. 1, joint types 4, 5, 6, and 7... 81

5.8. Average load-embedment traces obtained in test of tooth face bearing on end grain for: (a) board no. 1, joint types 1, 2, and 3, and (b) board no. 1, joint types 4, 5, 6, and 7..... 82

5.9. Average load-embedment traces for boards 1 through 5 adjusted for specimen alignment and standardized to 1-in. basis in tests of tooth bearing on end grain for joint types 1, 2, and 3..... 83

5.10. Average load-embedment traces for boards 1 through 5 adjusted for specimen alignment and standardized to 1-in. basis in tests of tooth bearing on end grain for joint types 4, 5, 6, and 7..... 84

5.11. Average load-embedment traces for boards 1 through 5 adjusted for specimen alignment and standardized to 1-in. basis in tests of tooth bearing on side grain for joint types 4, 5, 6, and 7..... 85

5.12. Average load-embedment traces for boards 1 through 5 adjusted for specimen alignment and standardized to 1-in. basis in tests of tooth edge bearing on end grain for joint types 4, 5, 6, and 7..... 86

5.13. Average load-embedment traces for boards 1 through 5 adjusted for specimen alignment and standardized to 1-in. basis in tests of tooth edge bearing on side grain for joint types 4, 5, 6, and 7..... 87

5.14. Load-embedment trace and corresponding linear moduli and deflection limits for a tooth face bearing on end grain specimen..... 89

5.15. Load-embedment trace and least-squares nonlinear regression curve for a tooth bearing with face on side grain specimen..... 90

5.16. Experimental and theoretical traces for joints with one tooth (Joint type 1) with tooth face bearing on end grain..... 93

5.17. Experimental and theoreticaal traces for joints with 4 teeth in a row (Joint type 2) and tooth face bearing on end grain..... 94

5.18. Experimental and theoreticaal traces for joints with 4 teeth in a column (Joint type 2) and tooth face bearing on end grain..... 95

5.19. Experimental and theoretical traces for specimens 1 through 5 with tooth face bearing on end grain (Joint type 4)..... 99

5.20. Experimental and theoretical traces for specimens 1 through 5 with tooth edge bearing on end grain (Joint type 5)..... 100

5.21. Experimental and theoretical traces for specimens 1 through 5 with tooth face bearing on side grain (Joint type 6).....101

5.22. Experimental and theoretical traces for specimens 1 through 5 with tooth edge bearing on side grain (Joint type 7).....102

5.23. Typical failure of joint type 4 with teeth face bearing on end grain.....104

5.24. Typical failure of joint type 5 with teeth edge bearing on end grain.....106

5.25. Typical failure of joint types 6 and 7 illustrating wood failure.....107

5.26. Typical elbow joint showing location of truss plate, teeth, and load application. Centers of rotation determined from shear and couple loading and resultant loads on selected teeth also shown..... 113

5.27. Effect of foundation modulus on the theoretical displacement at 75 lb. load per tooth for a truss-plate joint with teeth face bearing on end grain..... 117

5.28. Effect of foundation modulus on the deflected tooth shape for a tooth embedded in wood with face bearing on the end grain at a constant load of 75 lb. Displacement values are given along tooth length from tooth head (tooth-plate juncture) to the tooth end..... 118

5.29. Effect of foundation modulus on the deflected tooth shape for a tooth embedded in wood with face bearing on the end grain and displacements are given along tooth length from tooth head to the tooth end..... 119

5.30. Effect of foundation modulus on the joint failure for tooth face bearing on end grain... 120

5.31. Effect of foundation modulus on joint displacement at failure for tooth face bearing on end grain..... 121

5.32. Effect of friction coefficient on the deflected tooth shape for a tooth embedded in wood with face bearing on the end grain at a constant load of 75 lb. Displacement values are given along tooth length from tooth head to the tooth end..... 123

5.33. Effect of friction coefficient on joint failure load with tooth face bearing on end grain..... 125

5.34. Effect of friction coefficient on joint displacement at failure with tooth face bearing on end grain..... 126

5.35. Effect of friction coefficient on the deflected tooth shape at failure load. The tooth is embedded in wood with face bearing on the eng grain. Displacement values are given along tooth length from tooth head to the tooth end..... 127

5.36. Interaction between foundation modulus and friction coefficient in terms of failure load of joints with tooth face bearing on end grain..... 131

5.37. Interaction between foundation modulus and friction coefficient in terms of displacement at failure load of joints with tooth face bearing on end grain..... 132

LIST OF TABLES

Table		Page
3.1	First-order differential equations equivalent to higher-order equations (3.21) and (3.22).....	38
3.2	Initial conditions for the first-order differential equations representing the behavior of a tooth embedded in wood.....	39
5.1	Input parameters used in the theoretical analysis of experimental plate joints of this study.....	78
5.2	Summary of parameters defining foundation modulus.....	92
5.3	Comparison between the theoretical and experimental ultimate loads characterized by tooth withdrawal for tooth face bearing on end grain.....	97
5.4	Theoretical and experimental failure loads (lbs/tooth) and mode of failure for joint types 4, 5, 6, and 7.....	109
5.5	Effects of single- and multiple-parameter changes of foundation modulus and friction coefficient for failure load and deflection at failure for tooth faces bearing on end grain.....	129

MODELING OF TRUSS-PLATE JOINTS USING NONLINEAR STIFFNESS AND RUNGE-KUTTA NUMERICAL ANALYSIS

I. INTRODUCTION

Light-frame wood trusses are extensively used for supporting roofs and floors in the construction of residential, commercial, and farm buildings. Hundreds of millions of trusses have been built in the United States during the past 25 years (29). Roof trusses with pitched top chords have spans that vary from about 20 feet in residential to about 70 feet in commercial construction. The use of floor trusses with parallel chords has recently shown a strong upward trend and constitutes about 20% of the present wood floor market (22). In all-wood trusses, light-gauge steel plates with die-punched teeth or holes for nailing are the most common fasteners for constructing truss joints. Although there are many patented plates and assembly processes and new plate types continue to be introduced, all the plates exhibit similar structural behavior. A general analysis procedure that predicts deformation and ultimate load of existing and newly introduced plate joints would offer an efficient way to evaluate the structural performance of and design complete truss assemblies and their joints.

1.1. Justification

In trusses, joints are structurally as important as wood elements. A major reason for failure is stress concentrations at joints. Even small deformations in joints can often cause disproportionally large truss deflections. Therefore, strength and stiffness of truss joints are extremely important parameters in truss design.

Stress transfer and resulting deformations within truss-plate joints are very complex structurally. Such joints should be visualized as structural systems to better model this complexity. Once a model accurately represents all the mechanisms in the system, loading that simulates actual loads can be applied to the model. Solving the interaction equations between the loading and mathematical representation of the model results in parameters, such as critical stresses and deformations, which can be used as design guidelines.

Roof trusses were among one of the eight research areas that were evaluated at a recent workshop on structural wood research (22, 29). Representatives from universities, federal laboratories, wood industry, and engineering consultants decided that the behavior of truss-plate joints subjected to combinations of loads was a topic of high research priority. To improve the understanding of this behavior, the mechanism of stress transfer from one wood member through the plate into another wood member has

to be identified. To be able to apply this knowledge in the design of trusses and joints, this mechanism should be modeled theoretically by a computer-based procedure that should be efficient and economical. This dissertation involves theoretical and experimental studies that lead to such a mechanism and procedure.

Allowable design loads for truss-plate joints are not available in codes and specifications because of the proprietary nature of the plates (29). Therefore, procedures for evaluating design properties of the plates vary in details (2, 11, 39), but the same general considerations apply to all; joint strength usually governs the design and the joints are supposed to transfer full tensile load with provisions made for bending or compression loads (29). The allowable loads are purely empirical, based on testing of tension specimens with plates acting in double shear. Testing procedures vary, because no universally accepted testing standard exists.

This study was aimed at developing a theoretical model to improve existing design methods for trusses. This model provides a procedure for evaluating plate connections constructed of traditional structural materials and a means for developing technical data that should assist with acceptance of domestic truss systems by overseas building codes. Applications of the model should also provide data for the limit-state design of trusses, which is expected to

improve structural reliability and economy in truss manufacturing.

1.2. Objectives

The overall objective was to develop a theoretical procedure that predicts stress transfer through and associated deformations in truss-plate joints. The specific objectives were:

1) To theoretically model mechanisms of load transfer and develop a close-form solution for the strength and stiffness analysis of truss-plate joints;

2) To experimentally assess the accuracy of the theoretical models by physical testing of typical joints; and

3) To define the effect of material properties on joint behavior by performing a sensitivity analysis.

II. LITERATURE REVIEW

The overall strength and stiffness of truss systems are directly proportional to the strength and stiffness properties of the truss-plate joints. Thus the modeling of joints has been the main focus in the past decade among researchers attempting to define truss behavior and improve its design. The models were theoretical and empirical.

2.1. Theoretical Modeling

The light-gauge steel plates with die-punched teeth are currently the most common truss-plate, but they have only been used in construction for the past few decades. The precursor to the die-punched plates were plates with evenly spaced holes for nailing. For this reason, most of the models developed for truss-plates have concepts which utilize or originate from nail theory.

The earliest models designed to show the interaction between nail and wood involved solutions for a beam on an elastic foundation. Winkler (47), in 1867, first introduced the concept and mathematical solutions of a bending beam on an elastic foundation. The principle, originally prompted by a need to analyze railroad tracks and ties, was based on the assumption that reaction forces of the elastic foundation are proportional to the deflection of the beam.

Winkler's concept and its modification by H. Zimmerman (50) assume that the foundation deflects only directly under the beam when the load is applied, so that the adjacent foundation material is unaffected (Figure 2.1). This assumption introduces some error since, in actuality, deflections of elastic foundations diminish continuously with increasing distance from the beam. However, this error is minimal when the foundation exhibits a nonlinear response (10).

It should be noted that there is a limitation to the Winkler solution: The contact area between the beam and the foundation must remain continuous (10). This results in a downward pressure when the beam deflects upward. Without this assumption, the response of the beam would become nonlinear as the contact zone would be dependent on the beam deflection. Fortunately for fasteners embedded in wood, this restriction of a continuous contact area causes no problem since the tooth is pushed under pressure into the wood, which creates equal pressure on the upper and lower part of the tooth.

Hetenyi (18), in 1946, expanded the solutions of Winkler and Zimmerman to include beams of finite length and varying stiffness. He also presented solutions for deflection, slope, moment, and shear for variables such as beam length, boundary conditions, and loading.

Kuenzi (24) was the first to use beam-on-elastic-

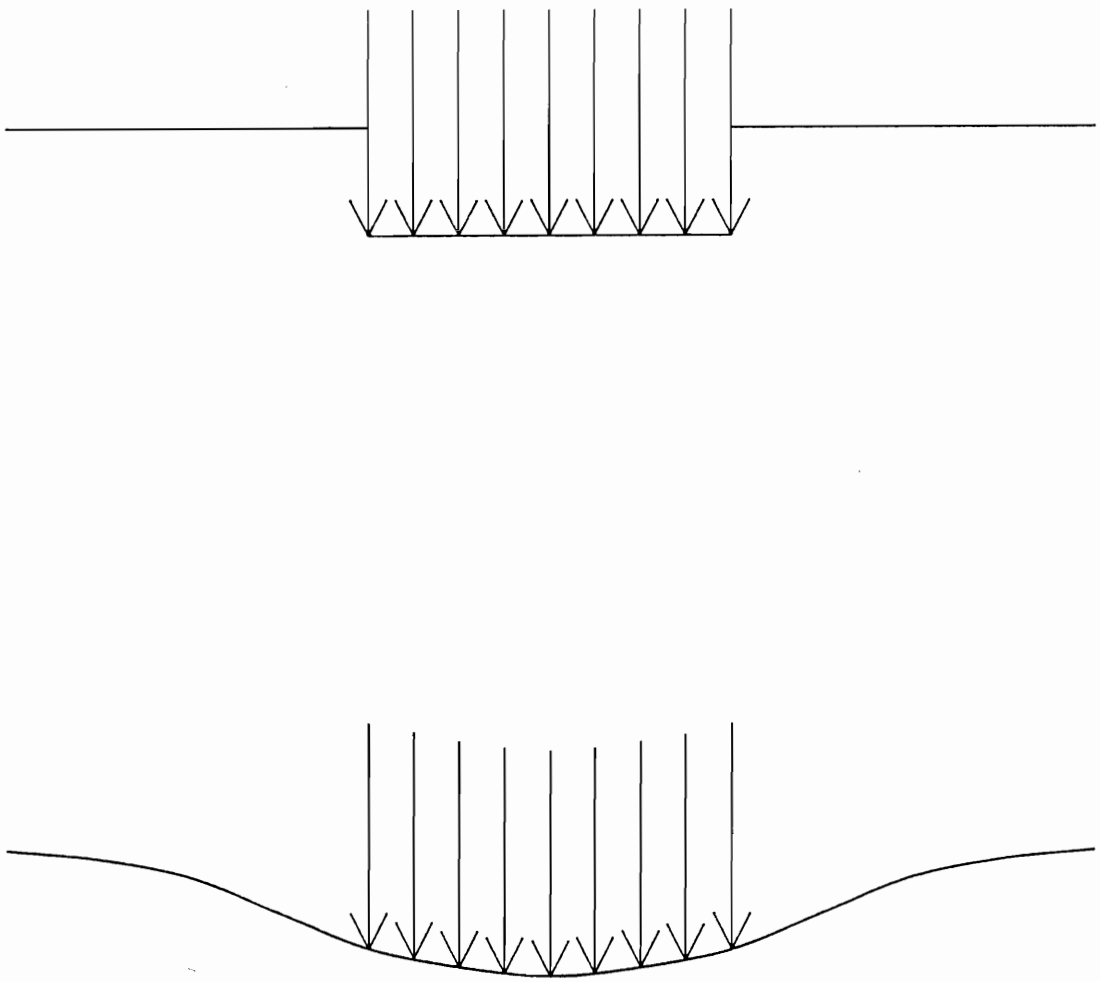

Figure 2.1. Deflection pattern under uniform load for: (a) Winkler foundation, and (b) elastic foundation.

foundation theory to model laterally loaded nail or bolt joints. He applied solutions of Hetenyi in treating a nail or bolt as a beam which rested on wood visualized as an elastic foundation. His development starts with the following governing differential equation for the deflection of the nail/bolt bearing on wood:

$$EI \frac{d^4y}{dx^4} = - ky \qquad (2.1)$$

where: E = nail/bolt modulus of elasticity;
I = nail/bolt moment of inertia;
y = deflection at point x; and
k = foundation modulus of wood.

The solution of eq. (2.1) results in expressions containing the following character:

$$= \sqrt[4]{\frac{k}{4EI}} \qquad (2.2)$$

Kuenzi developed expressions for deflections, slopes, moments, and shears at any point along the length of the nail or bolt which depend upon . The total joint slip was the sum of the nail or bolt deflection in each connected member at their contact area.

This model is limited to the elastic behavior of a wood foundation. Although wood does behavior linearly when compressed by small loads, it behaves nonlinearly in joints due to the crushing of the wood during nail penetration. Under large loads both nail and bolt joint behave nonlinearly. Therefore, Kuenzi's methods had to be

modified to represent the actual joint behavior more accurately.

In 1962, Noren (32) developed a nonlinear equation to define the load-slip relationship for nailed joints. He expanded upon Kuenzi's methods to define a slip modulus which relates foundation modulus, nail diameter, and (eq. (2.2)).

In the first of 5 publications, Wilkinson (43) presented a theoretical analysis based on Kuenzi's work and derived the following expression which relates single shear load and joint slip:

$$P = 0.1667\ E^{1/4} k_o^{3/4} d^{7/4} y \qquad (2.3)$$

where: P = lateral load;
E = nail modulus of elasticity;
k_o = elastic bearing constant;
d = nail diameter; and
y = joint slip.

Wilkinson defined the elastic bearing constant as the foundation modulus divided by the nail width. He determined the elastic bearing constant by cyclic loading of joints to an initial slip of 0.015 in., a point at which two successive cycles of load-slip traces coincided. Wilkinson assumed a linear relationship between elastic bearing constant and specific gravity, and used it to determine regression relations for foundation moduli for varying specific gravity; relations are valid only at slip levels below 0.011-in.

Wilkinson (45) expanded upon his previous research to include joints constructed of wooden members with dissimilar properties by adding a term to eq. (2.3). He determined elastic bearing constants by relating them to specific gravity of wooden members and to three nail types. As in the case of similar members, Wilkinson limited the validity range of his expressions to regions below 0.011-in. slip.

Wilkinson continued his work on dissimilar members with three papers which dealt with determination of the elastic bearing constant. He (44) demonstrated the effect of deformed shanks, prebored lead holes, and grain orientation on the elastic bearing constant. The second study of this series (47) showed the effect of moisture content on the elastic bearing constant as it pertained to assembled joints. In the final study of this series, he (46) developed material properties that enable the use of eq. (2.3) for joints with various sheathing materials such as plywood, hardboard, insulation board, particleboard, and gypsum board.

Foschi (12), in 1974, used a finite element approach to successfully model the load-slip characteristics of "Glulam Rivets". Glulam Rivets, also called Griplam nails, were commonly used in the 1970's with predrilled steel plates. This combination was an early precursor to truss-plates with die-punched teeth commonly used today.

Foschi's model included yielding of the nail in bending and a nonlinear bearing behavior of the wood under the nail. He developed the following exponential form:

$$p = (p_o + p_1 w)(1 - e^{\frac{-kw}{p_o}}) \qquad (2.4)$$

where: p = load;
w = nail penetration;
k = initial tangent modulus;
p_o = constant; and
p_1 = constant.

The initial tangent modulus and constants p_o and p_1 were determined by nonlinear least squares fitting of experimental data. By combining eq. (2.4) with the finite element analysis, Foschi could predict both linear and nonlinear joint deformations.

In a subsequent paper, Foschi (16) expanded his earlier theory by including pressure that wood exerts on a driven nail, which he accomplished by loading and unloading the nail-embedment specimens before determination of k, p_o, and p_1. This resulted in an altered load-deformation trace and modified constants for eq. (2.4). The resulting procedure yielded a good estimate of both initial stiffness of the connection and ultimate load, but substantially deviate from experimental data at intermediate slips.

Foschi and Longworth (17) postulated and verified an analysis technique which for the first time applied procedures for nail joints to predict metal-plate-fastener

strength. For Griplam nails and predrilled steel side plates, they used a semi-analytical finite element approach (49) to determine the maximum stresses in the wood member for parallel to grain loading. Failure mode was governed by either shear stresses around the nail or by nail yielding. This approach was verified by testing fasteners with nail penetration lengths of 3.0-in. while varying nail spacing, number of nails, and nail end distance. Results showed that close nail spacing produces wood failure, usually by shear around the nail group, while a larger spacing produces nail yielding.

Foschi (13, 14) continued his work on truss-plates with die-punched teeth by applying the computer program SADT, that had been developed at the Western Forest Products Laboratory in Vancouver, B.C. The program treats connections as continuous systems and calculates slip values by the method of virtual work as follows:

$$[K]\{x\} = R_0 + R_1(\{x\}) \qquad (2.5)$$

where: $[K]$ = stiffness matrix in linear region;
$\{x\}$ = global vector of unknown displacements;
R_0 = load vector; and
R_1 = nonlinear vector, function of $\{x\}$

which is solved by iteration. In references (13) and (14), the constants p_0 and p_1 were substituted by m_0 and m_1. These constants and k were determined empirically rather than from statistical correlation equations (Figure 2.2). The modulus was modified for grain and plate angle using

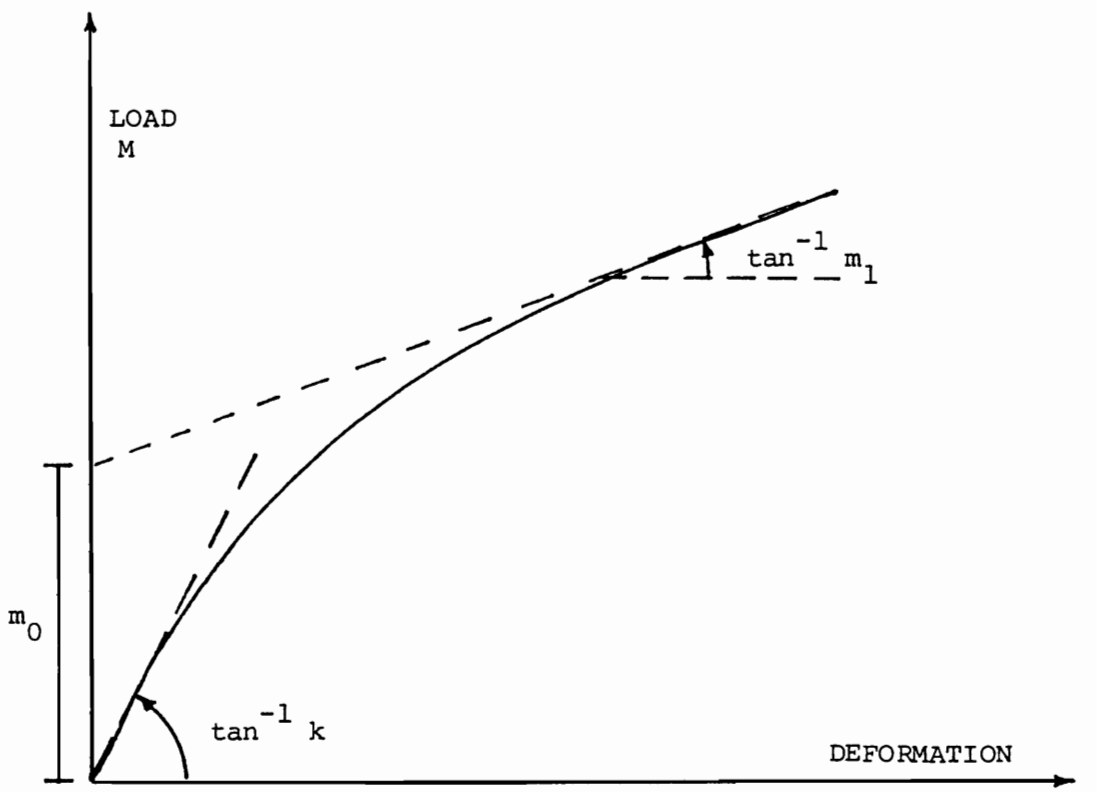

Figure 2.2. Typical load-displacement trace that Foschi found in testing embedment specimens.

the Hankinson's formula. Other parameters in the model included gaps between connected members, the buckling capacity of the plate, and plate yielding in tension or shear. The model was experimentally verified using elbow joints with specified gaps among the connected components. The verification was carried out at low load levels, but poor agreement was observed following the gap closure when wood failure occurred that was not accounted for in the model.

McCarthy and Wolfe (28) used Foschi's model to assess truss-plate performance in trusses made with southern pine lumber. Using four standard and two nonstandard joint configurations, they found that modulus of elasticity has no effect on the parameters of eq. (2.4). McCarthy and Wolfe also reported that the strain in the truss-plate itself was less than 0.001 in. at or near the maximum load, thus concluding that the elastic strain in the plate did not have a measurable influence on joint deformation curves.

Foschi (15) modified his earlier version of SADT to analyze entire truss systems. The modified program, called SAT, incorporates the main features of SADT to predict the deformation and ultimate load of the truss system.

Maraghechi and Itani (27) modeled truss-plate connectors in light-frame wood buildings. They considered the truss-plate joint as a two-dimensional element with

axial linear springs, shear, and rotational degrees of freedom. No full scale tests were conducted to verify the model, but comparison of theoretical displacements with published data suggested a reasonable agreement.

Hirai (19, 20) and Tsujino and Hirai (40) introduced numerical methods to solve eq. (2.1). Their work, concerned with bolted wood joints with steel side-members, separated the curvilinear load-embedment curve (Fig. 2.2) into several equivalent linear sections. Harai (19) then solved eq. (2.2) numerically using a stepwise linear analysis. The general solution of eq. (2.2) was divided into segments to account for different layer properties and then solved simultaneously. The numerical analysis seemed to somewhat overestimate the joint stiffness because the bolt displacement in the steel side plate was neglected. Hirai (20) investigated this effect experimentally and incorporated the results into the original model to characterize joint behavior more closely.

Aune and Patton-Mallory (5) have recently reported on the theoretical procedure for predicting load-bearing capacities of two- and three-member nailed joints. They applied European-based yield theory which assumes that the nail is embedded into the wood foundation until the yield stress of the nail is reached. Nails enter the plastic region at one or more points depending on the joint type. Nail embedment can be simulated either by plastic behavior

beyond the nail-yield moment, or by a fourth-root curve to describe the wood embedment curve. Use of the fourth-root curve, obtained through virtual work, also produced joint deformation in the model. In a companion research report, Aune and Patton-Mallory (6) verified their theoretical model. Although the yield-theory model included neither the effects of friction between members nor axial forces in the nail, accurate prediction of yield load was observed.

2.2. Empirical modeling

In 1966, Mack (26) showed that the load-slip curve of a nailed joint up to 0.1-in. slip can be described by the empirical exponential equation:

$$P = (Aw + B)(1 - e^{-Cw})^{D} \qquad (2.6)$$

where: P = applied load;
w = slip; and
A,B,C,D = nonlinear constants obtained by testing.

This equation, while similar in nature to eq. (2.4) described by Foschi (12), seemed to be too complicated. Mack (26) attempted to derive an empirical equation of simpler form to fit data up to 0.1-in. slip but was unsuccessful. He did, however, find a simpler and reasonably accurate equation for joint slip less than 0.02 in.:

$$R = Ad^{B} \qquad (2.7)$$

where: d = slip;
A,B = nonlinear regression constants; and
R = reduced load, defined as $\frac{P_w}{P_d}$;

where: P_w = load at slip w; and
P_d = load at slip d, $0 \leq d \leq 0.02$ in.

Beineke and Suddarth (8) used an empirical model that replaced actual die-punched truss-plate connections with an equivalent single solid piece of wood with identical stiffness properties. This model, which was used to estimate stiffness only, used axial stiffness indexes for plate length classes as determined by linear regression. Although experimental results were used to determine the axial stiffness indexes, no verification of the joint stiffness prediction was presented.

Suddarth et al. (38) tension tested 322 truss-plate joints to failure and used multiple regression to correlate joint strength and stiffness with specific gravity and moisture content. Regression results showed that specific gravity is definitely related to joint stiffness and strength. Moisture content was also found to be a significant variable in the regression analysis. The authors also reported coefficients of variation between 10 and 15 percent, indicating that variations in joint properties are less important in probabilistic engineering than corresponding lumber characteristics.

In a similar study, Palka (33) tested 360 truss-plate-joint specimens in tension to determine and model the

effect of relative density on load-slip behavior. Using different grades, species, and plate orientations, he used multiple regression techniques to determine different regression models for each of the 12 treatment conditions. The empirical function used in the analysis was of the form:

$$P_i = (A_i + B_i + C_i w^2) [1 - e^{(-D_i w)}] \qquad (2.8)$$

where: P = applied load;
w = joint slip; and
A_i, B_i, C_i, D_i = empirically fitted parameters for the ith treatment cell.

Noguchi (31) tested truss-plate butt joints in pure bending and found that the maximum bending moment was insensitive to variation in wood strength. However, the maximum bending moment could be approximated by a linear function of the distance from the compressive face of wood members to the extreme tensile edge of a plate. Noguchi also reported that the neutral axis, although appearing at first in the center of the truss-plate, shifted toward the compressive face of the joint as the load was increased. This shift was accentuated upon closure of a small initial gap between butt joints.

III. THEORETICAL PROCEDURE

There are many factors affecting the behavior of truss-plate joints (36). The most significant factor is the interaction between the truss-plate tooth and the wood member. Of all the models used to describe this interaction, beam-on-elastic-foundation theory has been the most successful and appears the most promising. Therefore, the model used in this study will be based upon beam-on-elastic-foundation theory. However, three modifications will be introduced in this study: the wood foundation will be considered to behave nonlinearly (14), the moment of inertia of the tooth will change along its length, and nonlinear terms in the governing differential equation relating tooth withdrawal resistance to axial tooth loading will be included in the solution.

3.1. Modeling Principles

Figure 3.1 illustrates the flow of tasks performed in this investigation. The beam-on-elastic-foundation theory applied in this investigation is based on the model described by Hetenyi (18). Because of an inelastic foundation and friction, nonlinear terms are introduced into the governing differential equations. The inelastic foundation modulus is determined by nonlinear regression of data obtained in tests of duplicated plate tooth bearing

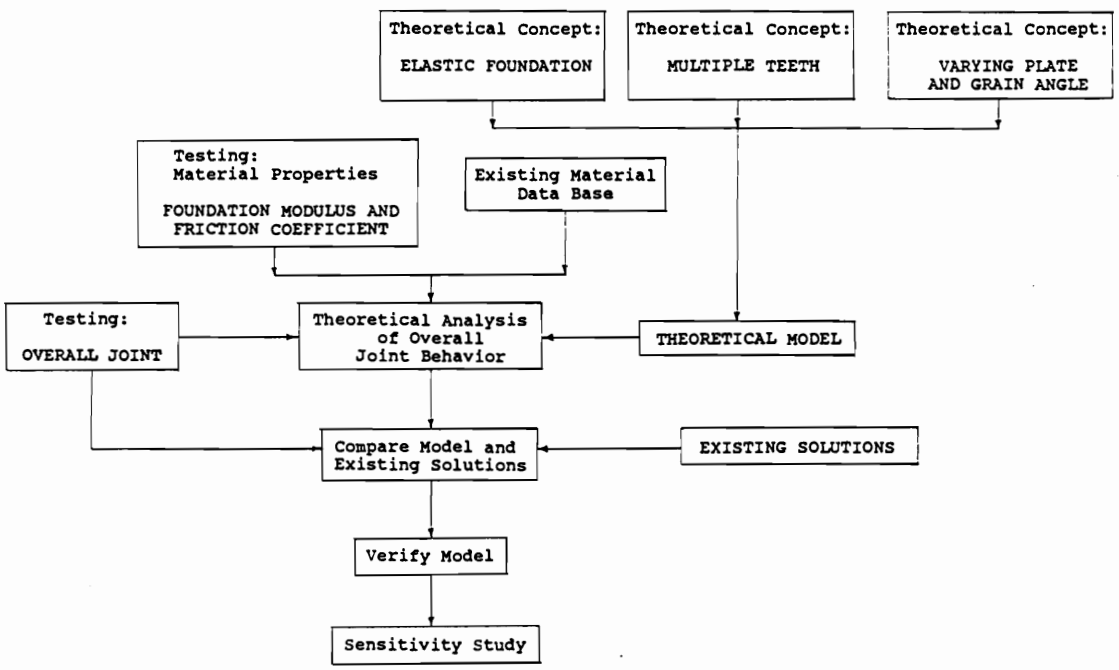

Figure 3.1. Flow chart of modeling procedures.

on wood. The nonlinearity is included by a linear step-by-step procedure, while the differential equation defining conditions in each step were solved by a Runge-Kutta technique. Interaction between teeth was determined in a separate, nonlinear finite element analysis.

3.2. Beam-On-Elastic-Foundation Concept

3.2.1. Nonlinear Differential Equation Governing Tooth-Wood Interaction

Figure 3.2 illustrates the simplest case for an elastic beam of finite length on an elastic foundation, which neglects the effect of axial force and friction between the beam and foundation. Kuenzi (24) showed that this configuration is governed by eq. (2.1). The general solution of eq. (2.1) is of the form

$$y = e^{\lambda x}(C_1 \cos \lambda x + C_2 \sin \lambda x) + e^{-\lambda x}(C_3 \cos \lambda x + C_4 \sin \lambda x) \qquad (3.1)$$

where λ is defined by eq. (2.2) and constants C_1 through C_4 are determined by loading and boundary conditions. Derivatives of eq. (3.3) can be used to determine slope, moment, and shear at any point, x, along the length of the beam.

The loading regime for truss-plate teeth is more complicated than that illustrated in Fig. 3.2. Three loading conditions are present in all teeth: lateral

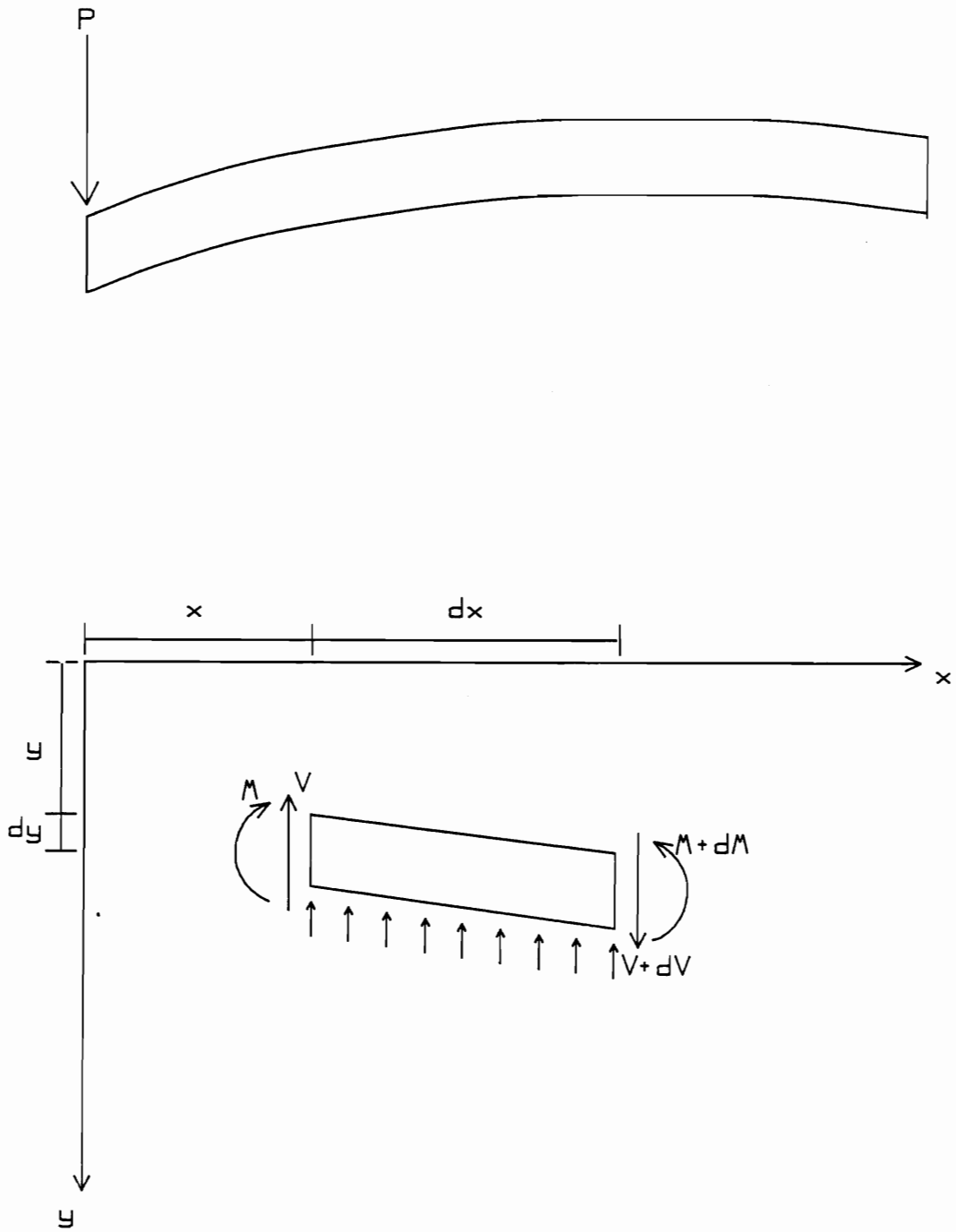

Figure 3.2. (a) Cross-section and (b) free-body diagram of elastic beam of finite length, L, on an elastic foundation.

shear, moment, and axial (Fig. 3.3). The lateral shear load, generally the only load considered in analyzing nailed joints, has been studied in detail by other researchers (24, 12, 5). The moment is caused by the resistance of the tooth to rotate about the point of its attachment to the plate. The axial load is a withdrawal force that appears after load is applied and the tooth deforms, which alters the governing differential equation from eq. (2.1) to the form (18):

$$EI\frac{d^4y}{dx^4} - N\frac{d^2y}{dx^2} + ky = 0 \qquad (3.2)$$

where all the symbols are defined in Fig. 3.3.

The general solution of eq. (3.2) takes the form of

$$y = (C_1e^{\alpha x} + C_2e^{-\alpha x})\cos \beta x + (C_3e^{\alpha x} + C_4e^{-\alpha x})\sin \beta x \qquad (3.3)$$

where

$$\alpha = \quad ^2 + \frac{N}{4EI}$$

$$\beta = \quad ^2 - \frac{N}{4EI}$$

The particular solution is dependent upon loading and boundary conditions. Solutions exist for cases with axial and shear load and for axial load and moment. Overall closed-form solutions could then be obtained by

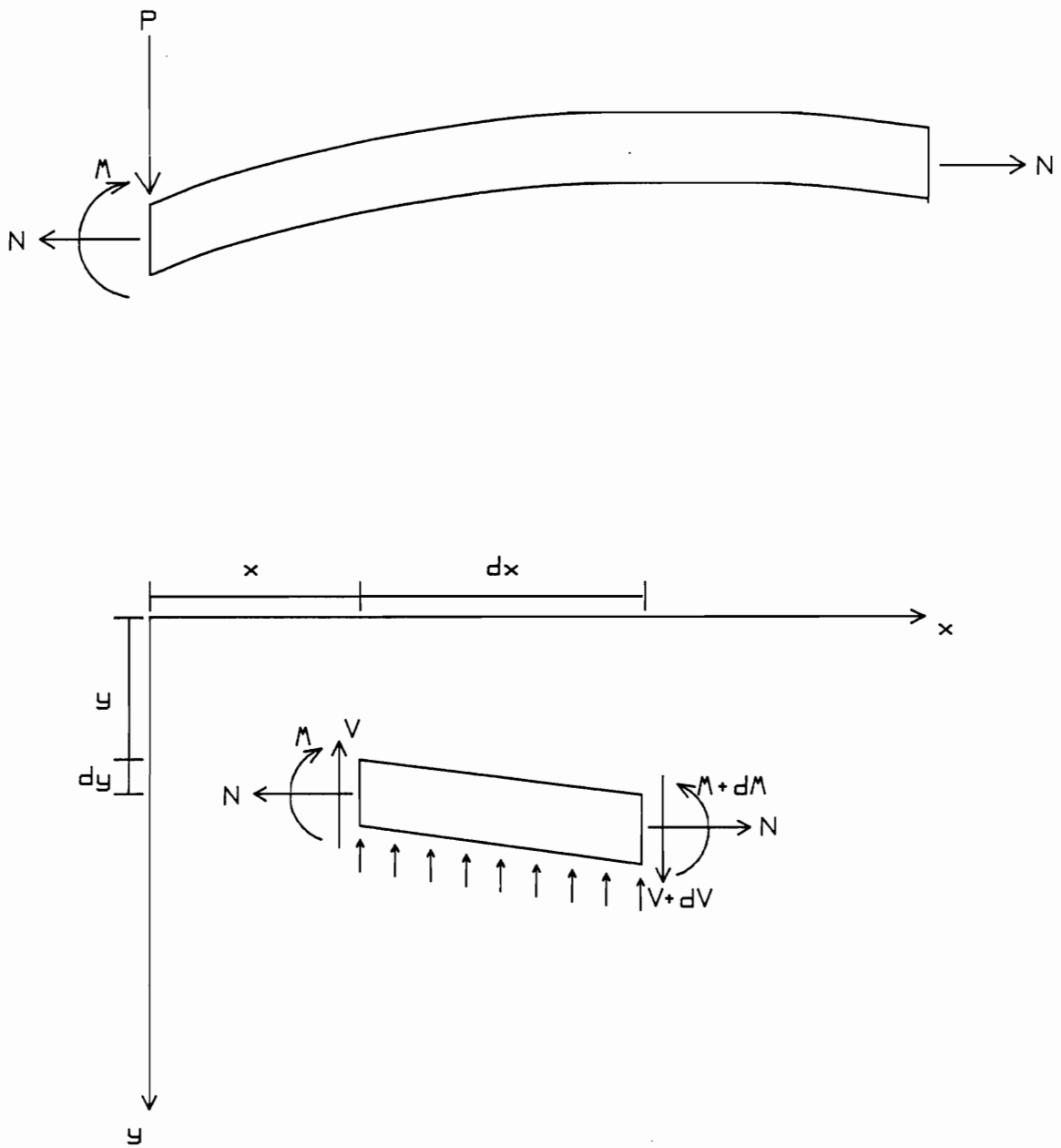

Figure 3.3. (a) Cross-section and (b) free-body diagram of beam on an elastic foundation with lateral shear, moment, and axial loading considered.

superposition (18). Although the superimposed solution more closely approximates the behavior of a tooth than does the first model with only lateral shear load, adding axial load as shown in Fig. 3.3 does not result in an accurate model. This is because the axial load only exists at the tooth head but not at the tooth end. The axial load is transferred along the tooth length by friction between the tooth and wood (Fig. 3.4).

The governing differential equations for the system shown in Fig. 3.4 are derived next. Beginning with summing forces in the x-and y-direction, the following is obtained:

$$dV = k\ y\ dx \tag{3.4}$$

$$dN = \mu\ k\ y\ dx \tag{3.5}$$

where μ is the friction coefficient between the tooth and wood. Differentiation of eq. (3.5) gives:

$$\boxed{\frac{d^2N}{dx^2} = \mu\ k \frac{dy}{dx}} \tag{3.6}$$

Summing moments about the center of the right side of the free-body diagram in Fig. 3.4 gives:

$$-dM - N\ dy + Vdx + \frac{\mu kyb}{2}\ dx + \frac{ky}{2}(dx)^2 = 0 \tag{3.7}$$

Division of eq. (3.7) by dx and using the known differential equation, $EI(d^2y/dx^2) = -M$ gives

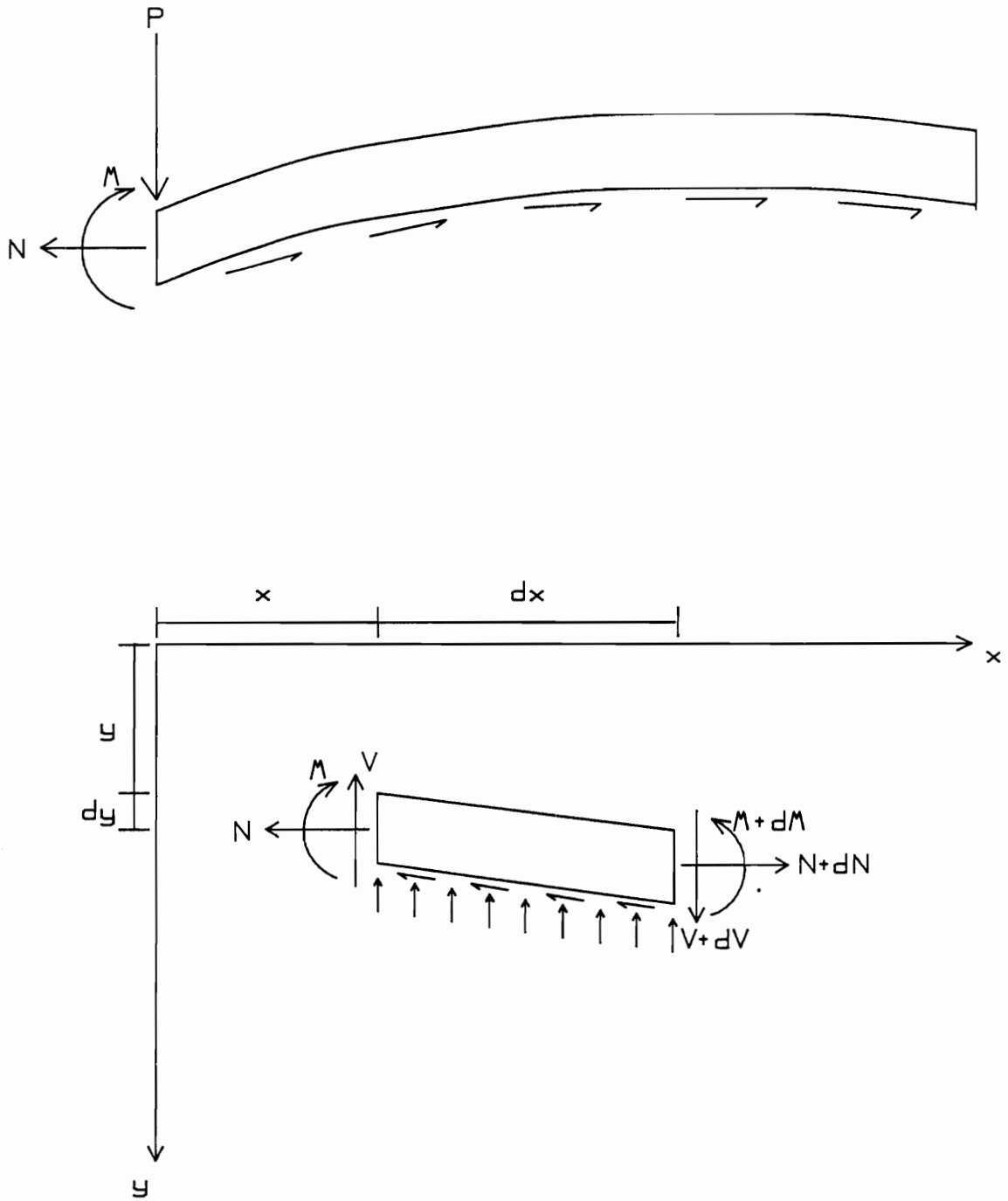

Figure 3.4. (a) Cross-section and (b) free-body diagram of a beam on an elastic foundation with lateral shear, moment, and axial load in conjunction with friction.

$$EI \frac{d^3y}{dx^3} - N \frac{dy}{dx} + V + \frac{\mu kb}{2} y + \frac{ky}{2} dx = 0 \qquad (3.8)$$

Differentiation of eq. (3.8) results in

$$EI \frac{d^4y}{dx^4} - \frac{dN}{dx} \frac{dy}{dx} - N \frac{d^2y}{dx^2} + \frac{dV}{dx} + \frac{\mu kb}{2} \frac{dy}{dx} = 0 \qquad (3.9)$$

Substitution of eqs. (3.4), (3.5), and (3.6) into eq. (3.9) gives

$$EI \frac{d^4y}{dx^4} - \mu ky \frac{dy}{dx} - N \frac{d^2y}{dx^2} + ky + \frac{b}{2} \frac{d^2N}{dx^2} = 0 \qquad (3.10)$$

Resubstitution of eq. (3.6) into eq. (3.10) and rearranging gives the final governing differential equation:

$$\boxed{\frac{d^4y}{dx^4} - \frac{N}{EI} \frac{d^2y}{dx^2} + \frac{ky}{EI} + \frac{(b/2 - y)}{EI} \frac{d^2N}{dx^2} = 0} \qquad (3.11)$$

Eqs. (3.6) and (3.11) are the two differential equations which govern the behavior of the system. The variables k and N are functions of y which makes eq. (3.11) nonlinear, and thus a closed-form solution is not possible. As an alternative, a Runge-Kutta numerical analysis was employed.

3.2.2. Runge-Kutta Technique

The Runge-Kutta technique is useful for solving initial-value, first-order linear or nonlinear differential equations of the form (21):

$$\frac{dy}{dx} = f(y,x) \tag{3.12}$$

$$y(x_0) = y_0 \tag{3.13}$$

The general technique is illustrated in Figure 3.5. It is assumed that the solution to eq. (3.12) is known in the interval $0 \leq x \leq x_i$. The objective is to advance the solution by interval h to $x_{i+1} = x_i + h$. The desired solution y_{i+1} is then obtained in terms of y_i, $f(y_i,x_i)$, and $f(y,x)$ which are evaluated for various estimates of y between x_i and x_{i+1}.

3.2.2.1. Basic Concept

Formulas of the Runge-Kutta type have been successfully used in solving many types of ordinary differential equations (21). The type used in this study is usually referred to as <u>the</u> fourth-order Runge-Kutta coefficients:

$$q_4^{(i+1)} = q_4^{(i)} + h\left[\frac{1}{6}f(q_4^{(i)},x^{(i)}) + f(\frac{1}{3}q_1^{(i+)},x^{(i+)}) + \frac{1}{3}f(q_2^{(i+)},x^{(i+)}) + \frac{1}{6}f(q_3^{(i+1)},x^{(i+1)})\right] \tag{3.14a}$$

where:

$$q_1^{(i+)} = q_4^{(i)} + \frac{h}{2} f(q_4^{(i)},x^{(i)}); \tag{3.14b}$$

$$q_2^{(i+)} = q_4^{(i)} + \frac{h}{2} f(q_1^{(i+)},x^{(i+)}); \text{ and} \tag{3.14c}$$

$$q_3^{(i+1)} = q_4^{(i)} + h\, f(q_2^{(i+)},x^{(i+)}). \tag{3.14d}$$

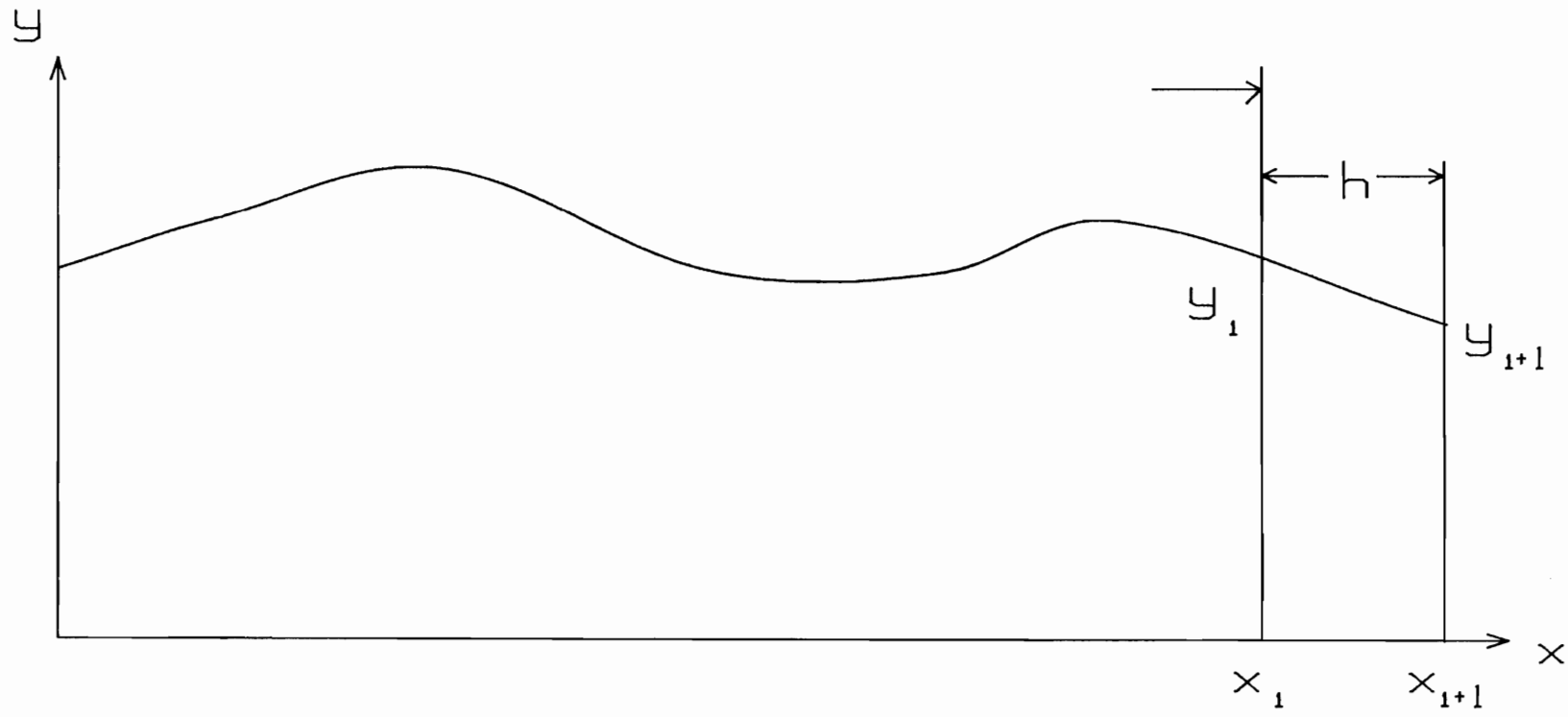

Figure 3.5. Graphic representation of Runge-Kutta technique for initial-value, first-order differential equation.

Coefficient calculations proceed from the previous estimate, (i), along the interval h until the current estimate is calculated at (i+1). The intermediate coefficients $q_1^{(i+\ )}$, $q_2^{(i+\ )}$, and $q_3^{(i+1)}$ must be computed in the order given since they are interdependent.

There are two shortcomings with the use of the Runge-Kutta technique in this study. First, the technique requires that the differential equations be of first order while this study has governing differential equations of second (eqs. (3.6)) and fourth order and (eq. (3.12)). This shortcoming can be corrected by breaking the two equations into six equivalent first order differential equations. Second, the technique is applicable to initial-value problems whereas the problem used in this study is a boundary-value problem. However, the boundary-value problem can be transformed into an initial-value problem through the use of derivatives.

To illustrate changing the boundary- to the initial-value problem, consider the following:

$$y'' + Ay = B \qquad (3.15)$$

$$y(0) = 0, \text{ and } y(1) = 0.$$

where: $y'' = \frac{d^2y}{dx^2}$

This can be transformed to the initial value problem:

$$y'' + Ay = B \qquad (3.16)$$

$$y(0) = 0 \text{ and } y'(0) = \alpha$$

where α is unknown, and must be chosen such that $y(1) = 0$ and thus the boundary values of eq. (3.15) remain intact (21). If a value is arbitrarily chosen for α and eq. (3.16) is solved by a Runge-Kutta technique, the solution might appear graphically as shown in Figure 3.6. Since $y(1)$ is not zero, the original boundary value of eq. (3.15) has not been reproduced. (As $y(1)$ is a function of the chosen value of α, it will be denoted as $y_1(\alpha)$.) To bring $y_1(\alpha)$ closer to the boundary value of 0, the strategy is to reduce α. Seeking the correct value of α such that the boundary condition at x=1 is satisfied can be stated as searching for α such that:

$$y_1(\alpha) = y(1) = 0 \qquad (3.17)$$

As this is a root solving problem, only two estimates of the root of eq. (3.17) are needed. These two estimates, say α^0 and α^1, are used to solve the initial value problem (3.16), yielding $y_1(\alpha^0)$ and $y_1(\alpha^1)$. A new estimate of α could then be obtained using a Newton-Raphson technique:

$$\alpha^2 = \alpha^0 - \frac{y_1(\alpha^0)}{[y_1(\alpha^0) - y_1(\alpha^1)]/(\alpha^0 - \alpha^1)} \qquad (3.18)$$

This process is then continued until convergence.

3.2.2.2. Application of Runge-Kutta Technique to Higher Order Differential Equations

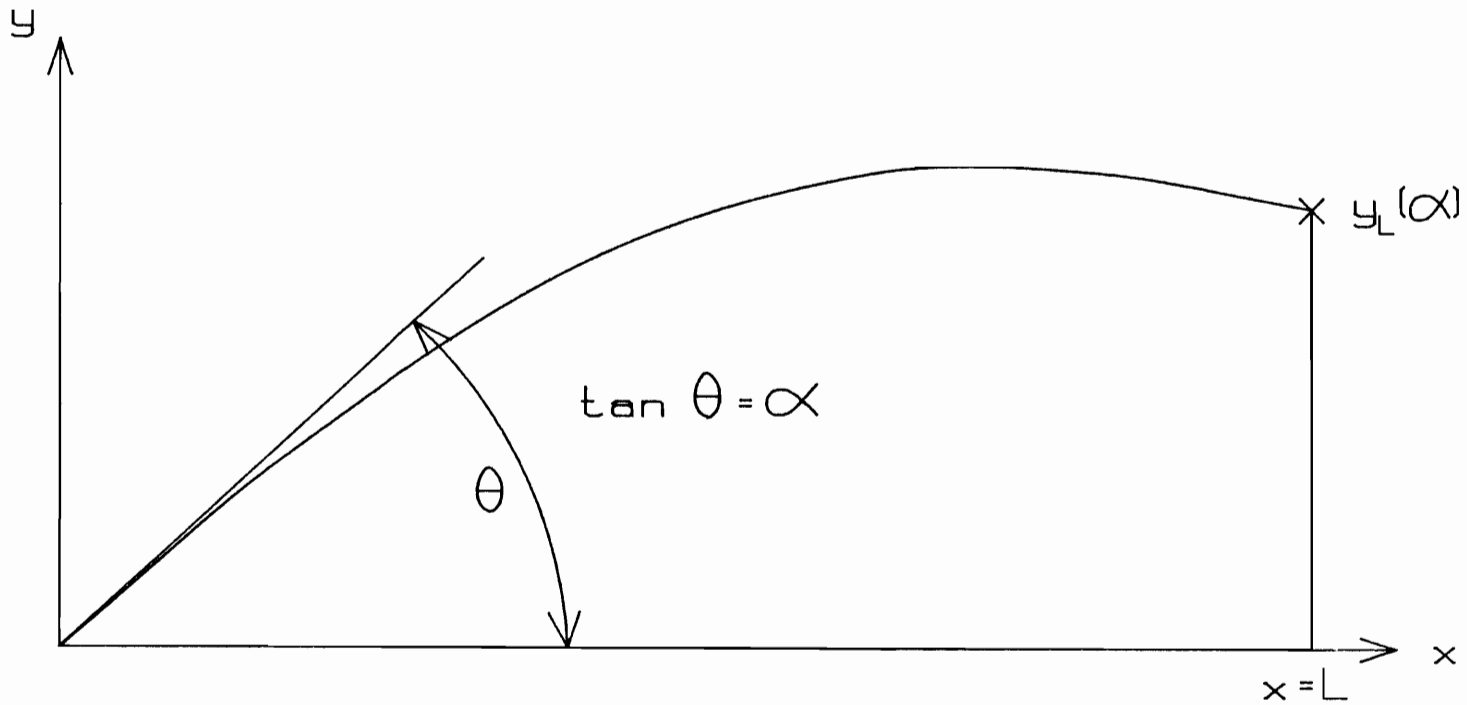

Figure 3.6. Graphical representation for solution of second order differential equation with boundary conditions using Runge-Kutta technique.

The technique described in the previous section was expanded to solve the differential equations which govern truss-plate joints. The first step consisted of making the following substitution in eqs. (3.6) and (3.11):

$$z = x / L \tag{3.19}$$

which transformed x into the dimensionless variable z. Thus, Eqs. (3.6) and (3.11) became

$$y^{iv} = \frac{NL^2}{EI} y'' - \frac{kL^4}{EI} y - (\frac{b}{2} - y)\frac{L^2}{EI} N'' \tag{3.20}$$

$$N'' = \mu\, k\, L\, y' \tag{3.21}$$

$$y'(0) = 0 \qquad y''(1) = 0$$

$$y'''(0) = \frac{-P}{EI} \qquad y'''(1) = 0$$

$$N(0) = N \qquad N(1) = 0$$

This can be set up as a series of first order equations by letting

$$\begin{aligned} s_1 &= y \\ s_2 &= y' \\ s_3 &= y'' \\ s_4 &= y''' \\ s_5 &= N \\ s_6 &= N' \end{aligned} \tag{3.22}$$

The resulting first-order differential equations representing eqs. (3.20) and (3.21) are

$$
\begin{aligned}
s_1' &= s_2 \\
s_2' &= s_3 \\
s_3' &= s_4 \\
s_4' &= \frac{L^2}{EI}\left[s_5 s_3 - kL^2 s_1 - \left(\frac{b}{2} - s_1\right)s_6\right] \\
s_5' &= s_6 \\
s_6' &= \mu\, k\, L\, s_2
\end{aligned}
\qquad (3.23)
$$

$$
\begin{aligned}
s_2(0) &= 0 & s(0)_1 &= \alpha_1 \\
s_4(0) &= -P/EI & s(0)_3 &= \alpha_2 \\
s_5(0) &= N & s(0)_6 &= \alpha_3
\end{aligned}
$$

The reduction of eqs. (3.20) and (3.21) to a set of first-order differential equations with initial conditions allowed the use of a Runge-Kutta technique. The estimates of the roots α_1, α_2, and α_3 must be chosen such that the boundary conditions are satisfied. If the newly calculated roots do not equal the boundary conditions:

$$
\begin{aligned}
\alpha_1 &= s_3(1) = 0 \\
\alpha_2 &= s_4(1) = 0 \\
\alpha_3 &= s_5(1) = 0
\end{aligned}
\qquad (3.24)
$$

then a Newton-Raphson method analagous to eq. (3.18) is applied to modify the estimates of the roots. This process is continued to convergence.

However, the three root estimates of s_3, s_4, and s_5 are now a function of not only distance along the length of

the tooth but also the choices of the three root estimates:

$$\begin{aligned} s_3 &= s_3\,(z,\ \alpha_1,\ \alpha_2,\ \alpha_3) \\ s_4 &= s_4\,(z,\ \alpha_1,\ \alpha_2,\ \alpha_3) \\ s_5 &= s_5\,(z,\ \alpha_1,\ \alpha_2,\ \alpha_3) \end{aligned} \tag{3.25}$$

To solve for eq. (3.23), partial derivatives must be taken with respect to α_1, α_2, and α_3. If we let:

$$\begin{aligned} u_j &= \frac{\delta s_j}{\delta \alpha_1} \\ v_j &= \frac{\delta s_j}{\delta \alpha_2} \\ w_j &= \frac{\delta s_j}{\delta \alpha_3} \end{aligned} \tag{3.26}$$

in which j = 1, 2, 3, 4, 5, or 6.

By following the procedure used for eq. (3.22), we can obtain an additional 18 first order differential equations in terms of u, v, and w:

$$\begin{aligned} t_1' &= t_2 \\ t_2' &= t_3 \\ t_3' &= t_4 \end{aligned} \tag{3.27}$$

$$t_4' = \frac{L^2}{EI}\left[t_5 s_3 + t_3 s_5 - kL^4 t_1 - (\frac{b}{2} - t_1)s_6 - (\frac{b}{2} - s_1)t_6\right]$$

$$t_5' = t_6$$

$$t_6' = \mu\, k\, L\, t_2$$

where t = u, v, or w.

In solving eq. (3.23), the initial conditions for a tooth embedded in a wood foundation (Fig. 3.4) are:

$$\frac{\delta s_j}{\delta \alpha_1}(0) = u_j(0) = a_j$$

$$\frac{\delta s_j}{\delta \alpha_2}(0) = v_j(0) = b_j \qquad (3.28)$$

$$\frac{\delta s_j}{\delta \alpha_3}(0) = w_j(0) = c_j$$

where j = 1, 2, 3, 4, 5, or 6; and $a_j = 0$ for all j's except $a_1 = 1$; $b_j = 0$ for all j's except $b_3 = 1$; and $c_j = 0$ for all j's except $c_6 = 1$.

Eqs. (3.23) through (3.28) are summarized in Tables 3.1 and 3.2. The system of 24 first-order differential equations (Table 3.1) with initial conditions (Table 3.2) can be solved using Runge-Kutta technique directly by using the interval i to estimate the values for interval i+1. The following three steps need to be completed to reach the

final solution: determination of Runge-Kutta coefficients, summation of these coefficients, and iteration until the process converges.

There are four Runge-Kutta coefficients for each equation shown in Table 3.1, making a total of 96 coefficients. These coefficients are determined by the same procedure outlined in section 3.2.2.1. and are analagous to eq. (3.14). They are denoted as $q_{m,n}$:

where:
$$q_{1,n}^{(i+)} = q_{4,n}^{(i)} + \frac{h}{2} f(q_{4,n}^{(i)}, z_{t,n}^{(i)}); \qquad (3.29b)$$

$$q_{2,n}^{(i+)} = q_{4,n}^{(i)} + \frac{h}{2} f(q_{1,n}^{(i+)}, z_{t,n}^{(i+)}); \text{ and} \qquad (3.29c)$$

$$q_{3,n}^{(i+1)} = q_{4,n}^{(i)} + h f(q_{2,n}^{(i+)}, z_{t,n}^{(i+)}). \qquad (3.29d)$$

$$q_{4,n}^{(i+1)} = q_{4,n}^{(i)} + h \left[\frac{1}{6} f(q_{4,n}^{(i)}, z_{t,n}^{(i)}) + f(\frac{1}{3} q_{1,n}^{(i+)}, z_{t,n}^{(i+)}) + \frac{1}{3} f(q_{2,n}^{(i+)}, z_{t,n}^{(i+)}) + \frac{1}{6} f(q_{3,n}^{(i+1)}, z_{t,n}^{(i+1)})\right] \qquad (3.29a)$$

where: m = Runge-Kutta coefficients 1, 2, 3, and 4;
n = 1,2,3,4,5,6 when t = s;
n = 7,8,9,10,11,12 t = u (z evaluated for α_1);
n = 13,14,15,16,17,18 t = v (z evaluated for $\alpha 2$);
n = 19,20,21,22,23,24 t = w (z evaluated for α_3);
h = interval length; and
$z_{n,t}^{(l)}$ = value of z differentiated with respect to α_j (j=1,2,3), at l^{th} interval location (i = interval origin, i+ = interval midpoint, and i+1 = interval terminus).

Now that the Runge-Kutta coefficients have been calculated for a particular interval, the values for all 24 first

Table 3.1 First-order differential equations equivalent to higher-order equations (3.20) and (3.21).

$$
\frac{d}{dz}
\begin{bmatrix}
s_1 \\ s_2 \\ s_3 \\ s_4 \\ s_5 \\ s_6 \\
u_1 \\ u_2 \\ u_3 \\ u_4 \\ u_5 \\ u_6 \\
v_1 \\ v_2 \\ v_3 \\ v_4 \\ v_5 \\ v_6 \\
w_1 \\ w_2 \\ w_3 \\ w_4 \\ w_5 \\ w_6
\end{bmatrix}
=
\begin{bmatrix}
s_2 \\
s_3 \\
s_4 \\
L^2/EI\left[s_5 s_3 - kL^2\, s_1 - (b/2 - s_1)s_6\right] \\
s_6 \\
\mu\, k\, L\, s_2 \\
u_2 \\
u_3 \\
u_4 \\
L^2/EI\left[(u_5 s_3 + s_5 u_3) - kL^2\, u_1 - (b/2 - u_1)s_6 - (b/2 - s_1)u_6\right] \\
u_6 \\
\mu\, k\, L\, u_2 \\
v_2 \\
v_3 \\
v_4 \\
L^2/EI\left[(v_5 s_3 + s_5 v_3) - kL^2\, v_1 - (b/2 - v_1)s_6 - (b/2 - s_1)v_6\right] \\
v_6 \\
\mu\, k\, L\, v_2 \\
w_2 \\
w_3 \\
w_4 \\
L^2/EI\left[(w_5 s_3 + s_5 w_3) - kL^2\, w_1 - (b/2 - w_1)s_6 - (b/2 - s_1)w_6\right] \\
w_6 \\
\mu\, k\, L\, w_2
\end{bmatrix}
$$

Table 3.2. Initial conditions for the first-order differential equations representing the behavior of a tooth embedded in wood.

$s_1(0)$	α_1	α_1
$s_2(0)$	0	0
$s_3(0)$	α_2	α_2
$s_4(0)$	-P/EI	-P/EI
$s_5(0)$	N	N
$s_6(0)$	α_3	α_3
$s_{1_{\alpha_1}}(0)$	$u_1(0)$	0
$s_{2_{\alpha_1}}(0)$	$u_2(0)$	0
$s_{3_{\alpha_1}}(0)$	$u_3(0)$	1
$s_{4_{\alpha_1}}(0)$	$u_4(0)$	0
$s_{5_{\alpha_1}}(0)$	$u_5(0)$	0
$s_{6_{\alpha_1}}(0)$	$u_6(0)$	0
$s_{1_{\alpha_2}}(0)$ =	$v_1(0)$ =	0
$s_{2_{\alpha_2}}(0)$	$v_2(0)$	0
$s_{3_{\alpha_2}}(0)$	$v_3(0)$	0
$s_{4_{\alpha_2}}(0)$	$v_4(0)$	0
$s_{5_{\alpha_2}}(0)$	$v_5(0)$	0
$s_{6_{\alpha_2}}(0)$	$v_6(0)$	1
$s_{1_{\alpha_3}}(0)$	$w_1(0)$	1
$s_{2_{\alpha_3}}(0)$	$w_2(0)$	0
$s_{3_{\alpha_3}}(0)$	$w_3(0)$	0
$s_{4_{\alpha_3}}(0)$	$w_4(0)$	0
$s_{5_{\alpha_3}}(0)$	$w_5(0)$	0
$s_{6_{\alpha_3}}(0)$	$w_6(0)$	0

order differential equations can be calculated as follows:

$$t_j^{i+1} = t_j^i + \frac{h}{6}\left[q_{m,j}^{(i+1)} + 2q_{m,j+6}^{(i+1)} + 2q_{m,j+12}^{(i+1)} + q_{m,j+18}^{(i+1)}\right] \qquad (3.30)$$

where: $j = 1,2,3,4,5,6$; and
$m = 1$ when $t = s$;
$m = 2$ $t = u$;
$m = 3$ $t = v$; and
$m = 4$ $t = w$.

3.2.2.3. Procedure for Evaluating Displacements and Forces for Complete Tooth

A set of 24 equations defined by eq. (3.30) is developed for each interval along the tooth length. The size of h affects the accuracy of the final results (23). Too small or too large an interval may result in erroneous solutions due to round-off error or lack of precision. To determine an appropriate h for this study, a preliminary study was conducted in which h was varied between 5% to 15% of tooth length; the results showed little variation between the solutions.

Equations defined by eq. (3.30) are evaluated for each iteration cycle. The results are then checked whether convergence has been attained. This is done by comparing the known boundary conditions with variables calculated in the last cycle for variables $s_3(1, \alpha_1, \alpha_2, \alpha_3)$, $s_4(1, \alpha_1, \alpha_2, \alpha_3)$, and $s_5(1, \alpha_1, \alpha_2, \alpha_3)$. These variables were chosen because they were the original known boundary conditions.

The difference between the current solutions and the variables is calculated as follows:

$$\begin{bmatrix} \Delta\alpha_1 \\ \Delta\alpha_2 \\ \Delta\alpha_3 \end{bmatrix} = \begin{bmatrix} u_3 & v_3 & w_3 \\ u_4 & v_4 & w_4 \\ u_5 & v_5 & w_5 \end{bmatrix}^{-1} \begin{bmatrix} s_3 \\ s_4 \\ s_5 \end{bmatrix} \qquad (3.31)$$

where: $\Delta\alpha_i$ = difference between boundary condition and Runge-Kutta variables at end of iteration cycle due to root estimate $i = 1,2,3$; and

$u_3 - s_5$ = Runge-Kutta variables evaluated at $(1, \alpha_1, \alpha_2, \alpha_3)$.

If the differences between the Runge-Kutta variables at the end of the iteration cycle and their accompanying boundary conditions are less than a prescribed tolerance, the system has converged. If the differences are greater than the tolerance, then new root estimates are calculated. These new root estimates then replace the original root estimates in eq. (3.23) for a new iteration cycle. The entire Runge-Kutta process is then repeated until convergence.

New root estimates are calculated from the differences between the Runge-Kutta variables obtained at the end of the last iteration cycle and the boundary conditions:

$$\begin{bmatrix} \alpha_1^1 \\ \alpha_2^1 \\ \alpha_3^1 \end{bmatrix} = \begin{bmatrix} \alpha_1 \\ \alpha_2 \\ \alpha_3 \end{bmatrix} - \begin{bmatrix} \Delta\alpha_1 \\ \Delta\alpha_2 \\ \Delta\alpha_3 \end{bmatrix} \qquad (3.32)$$

where: α_i^1 = new root estimate for i = 1,2,3.

In analyzing test joints, each tooth was divided into 10 intervals. The initial root estimates were chosen arbitrarily as 0.0, but were automatically updated during the iterative process. The tolerances, based on preliminary runs, were chosen such as to maximize accuracy while minimizing computer time.

3.2.2.4. Options for Varying Tooth Cross-Section and Nonlinear Foundation Modulus

The Runge-Kutta technique demonstrated in Section 3.2.2.2 is very versatile and has many advantages over other numerical analysis techniques. Runge-Kutta analysis moves along the tooth length in intervals until the entire length has been traversed. This allows for material property values to change in each interval while retaining compatibility since the solution for each interval is dependent upon the previous segment.

Although all other material properties along the tooth length were kept constant, an option in the procedure in this study provides for changes in the moment of inertia along the length of the tooth, which allows for modeling which more closely simulates actual tooth stiffness.

Another option accounting for the plastic behavior of the tooth during loading is also included in this model.

Since the loading is applied in constant increments, the loading and boundary conditions for each iteration can be altered. When the moment in the head of the tooth, calculated from the summation of $s_3(0, \alpha_1, \alpha_2, \alpha_3)$ for each iteration exceeds the yield moment of the tooth, the boundary conditions of eq. (3.20) were then modified to simulate the plastic behavior. This was accomplished by allowing the tooth to rotate while applying a constant moment, which was accomplished by changing appropriate boundary conditions.

3.2.3. Equations for Nonlinear Foundation Modulus

Two techniques, dependent on tooth orientation with respect to loading, were used in this study to determine the foundation modulus of wood. When tooth embedment caused the wood to bear on the wide face of the tooth, the resulting load-embedment trace generally had two linear regions joined by a small curvilinear section. These overall traces could best be approximated using 4 linear regions.

When wood bears on the edge face of the tooth, constant curvilinear traces were produced. These traces are best approximated by a nonlinear least squares routine. The subroutine RNSSQ in the IMSL software package was helpful in developing appropriate equations in this study.

3.3. Computer Program for Runge-Kutta Solution

The beam-on-elastic-foundation concepts discussed in the previous sections requires a great deal of computations. To facilitate with these computations, a program was written using Microsoft Fortran for the IBM-AT microcomputer. This program, called TRUSSCON, is shown in Appendix A and is summarized in Figure 3.7.

Pertinent material properties are first entered into the program as well as Runge-Kutta parameters such as step size and criteria for convergence. The program conducts some preliminary computations before going into the actual analysis.

The loading scheme used in TRUSSCON was a standard step-by-step procedure to account for nonlinearity, which involves subdividing the load acting on the tooth or teeth into small increments during which the joint is assumed to behavior linearly. For each increment, these linear responses are calculated and accumulated. The foundation modulus is based on the current load and not the incremental load.

There were two sets of initial conditions used in TRUSSCON which were dependent on the stress level in the teeth. The first set of initial conditions assumes that the tooth acts as a cantilever beam and thus the slope equals zero at the tooth-plate interface. The corresponding moment at the tooth head can be calculated

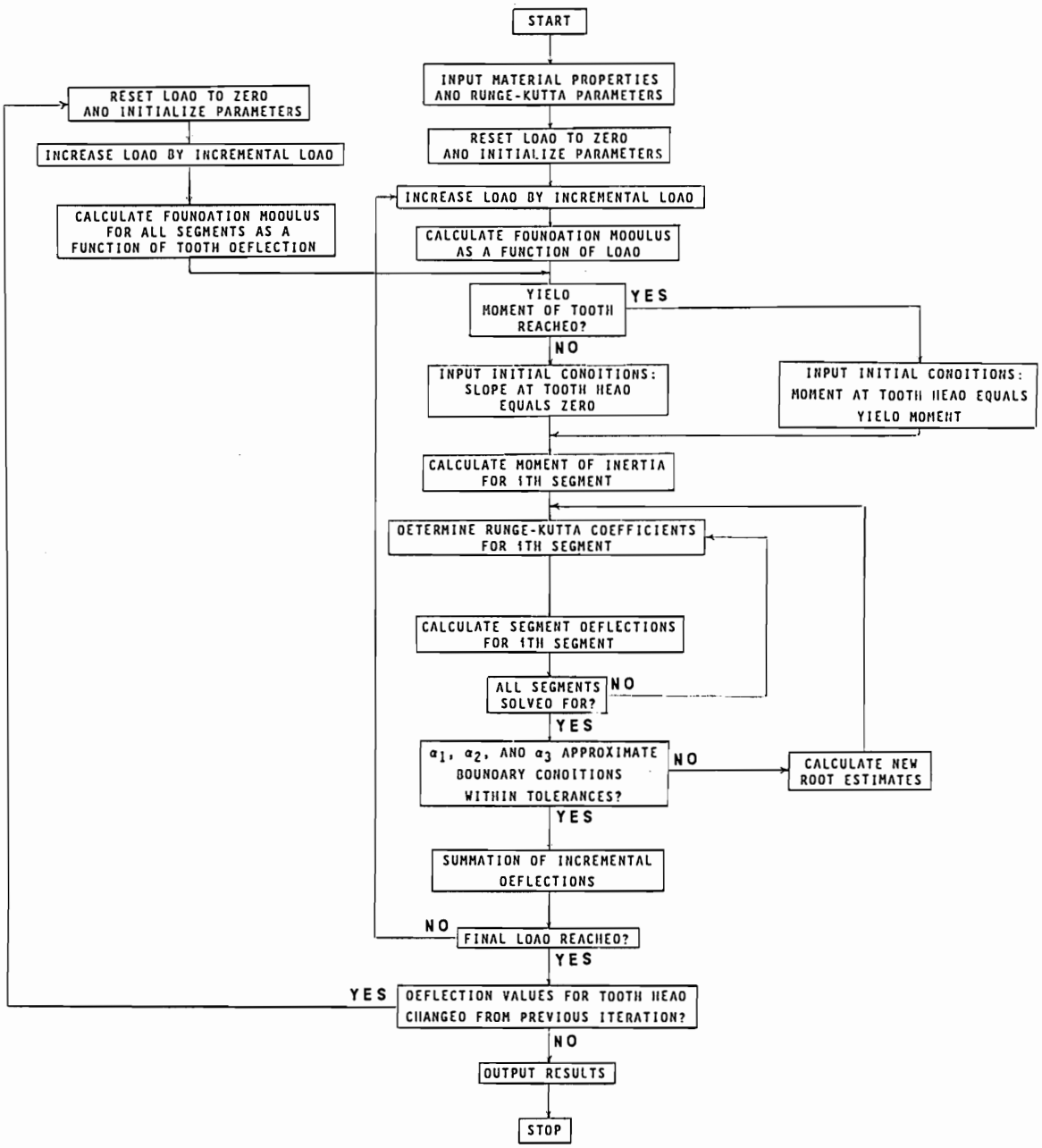

Figure 3.7. Flow chart of the program TRUSSCON used in this study to determine joint response using beam-on-elastic-foundation theory solved with Runge-Kutta techniques.

from s_3 of eq. (3.22) during the Runge-Kutta calculations. This condition remains until the stress in the tooth, determined from the calculated moment, exceeds 1.5 times the yield stress of the tooth. The plastic hinge effect caused by yielding is the basis of the second set of initial conditions, which keeps a constant restraining moment applied at the tooth-plate interface while allowing tooth rotation. The value of 1.5 times the yield stress was chosen as the plastic hinge origin because the plastic modulus of rectangular beams in bending is 1.5 (7). Thus although yielding begins in the tooth at the yield stress on the tooth surfaces, the plastic hinge develops throughout the tooth thickness while the moments become 1.5 times larger.

Termination of the program depends on the accuracy of the root estimates and the convergence of the solution. If the difference between the root estimates and the original boundary conditions exceeds certain tolerances, then the Runge-Kutta technique is repeated with newly calculated root estimates. However for the program to proceed with the next loading step there must also be deflection convergence. This convergence can be determined by comparing the displacement at the tooth head from one complete computer run to the previous run. If the difference between these two displacements is below a

prescribed tolerance and converging toward zero, then the second convergence criterion is reached.

The theoretical maximum load a joint can withstand was determined by tooth withdrawal. Tooth withdrawal occurs when the load normal to the tooth exceeds the withdrawal resistance. The normal load was taken as the product of the slope at the tooth-plate interface and the lateral load. The withdrawal resistance was the frictional resistance, as calculated from the Runge-Kutta analysis, integrated over the tooth length.

3.4. Evaluation of Interaction among Teeth

It is necessary for this study to determine if an isolated truss-plate tooth behaves identically to a tooth that is within a matrix of other teeth, so as to determine if simple addition of effects of individual teeth, as is currently used (14, 28), accounts for the overall plate behavior. Therefore, data were needed on stresses in the wood under each tooth. These stresses could not be determined using the beam-on-elastic-foundation model that is shown in the previous section, because this model only gives values for deflection, slope, moment, and shear of a single tooth. Therefore, a nonlinear finite element program was employed to determine stress contours under truss-plate teeth using various grain orientations and loading regimes.

The finite element program used in this study is a nonlinear, 2-dimensional, plane stress analysis. The program, COMCNIB1, was originally developed by White (42) for the CYBER main-frame computer using routines by Zienkiewicz (49). The microcomputer option of the final version of this program, named COMPCON (34), was used to evaluate the effect of multiple teeth in this study. The nonlinear analysis in COMPCON is based on using three discrete moduli of elasticity to describe material properties in a step-by-step analysis. The modulus of elasticity for each loading step is accomplished within the program depending on the current stresses in each finite element.

Figure 3.8 shows the three types of joints that were modeled by finite element analysis to obtain the stress contour under each tooth. The thickness of each wood finite element for joint types 1(a), 2(a), and 3(a) were based on the tooth bearing area since a preliminary analysis showed stresses act vertically. Joint types 1(a), 2(a), and 3(a) were necessary to determine the stresses acting directly under the tooth at discrete 0.05-in. segments. The amount of force acting on each 0.05 in. tooth segment could then be determined by multiplying each

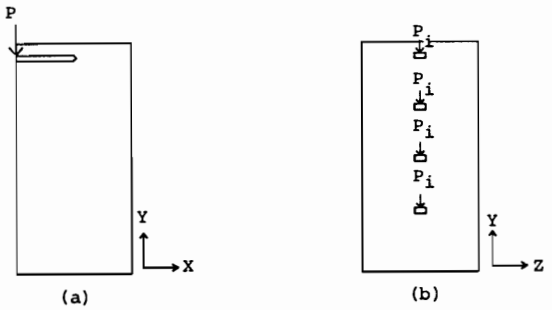

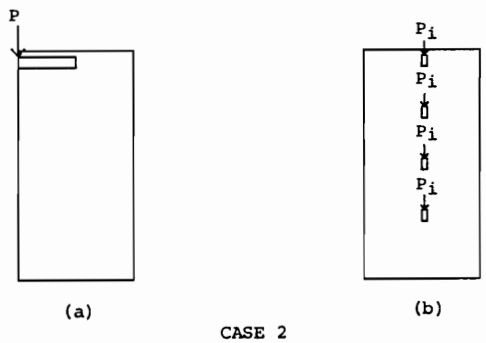

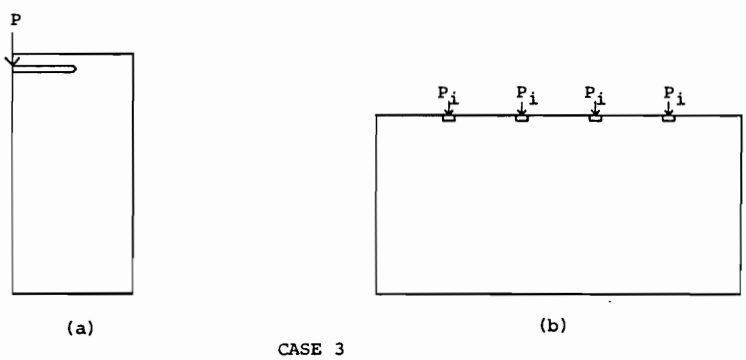

Figure 3.8. Finite element models used in this study to determine stress contours under each truss-plate tooth.

stress by its appropriate area. Joint types 1(b), 2(b), and 3(b) utilized these forces to determine the stress distribution of each 0.05 in. segment of the Y-Z plane.

IV. EXPERIMENTAL PROCEDURE

The solution for the beam-on-elastic-foundation by Runge-Kutta technique was verified by testing truss-plate joints. Seven joint types with varying number of teeth, plate angle, and grain angle were constructed and tested to obtain the data needed to assess the model accuracy. Additional tests included those to determine foundation modulus for tooth bearing, specific gravity and moisture content tests which provided the input data for the model analysis. The materials used, specimen types, and testing procedures are described in this section.

4.1. Joint Specimens

4.1.1. Material Selection

Studs: A survey of Oregon truss manufacturers, summarized in Appendix B, showed that the predominant lumber grade and species used in the construction of trusses in the upper Willamette Valley, Oregon is No. 1 and Better Douglas-fir. Therefore, two lumber samples of 30 kiln-dried, Douglas-fir No. 1 and Better grade and nominal 2- by 4-in. size were sampled from two lumber manufacturers. This lumber was kiln-dried to an average moisture content of 19 percent. The wood supply for both mills came from the Willamette Valley.

The lumber was brought to the Forest Research Laboratory where a rough estimate of specific gravity for the sampled lumber was determined by measuring overall weight and volume of each piece. Two groups of five boards, representative of the specific gravity distribution of the sampled lumber from the original group of 60, were then selected for testing.

The selected lumber was cut into 16 in. long sections with no visual defects. These sections were then placed in a Standard Room for 5 months for conditioning at a constant temperature of 70°F and relative humidity of 65 percent. These conditions provide for an equilibrium moisture content of about 12 percent.

Plates: The steel truss-plates used in this study, supplied by Gang-Nail Inc., were made of 20-gauge sheet metal, 3 in. wide and 4.5 in. long, with an average tooth density of 7.1 teeth per square in. The spacing between main columns was 0.50 in., with teeth from offset columns 0.25 in. apart (Figure 4.1). Row spacing was staggered at 0.42 in. and 0.14 in. apart. Average tooth width, thickness, and length were 0.050, 0.087, and 0.393 in., respectively.

4.1.2. Specimen construction

Figures 4.2 and 4.3 show the seven joint types tested. Joint types 1-3 were constructed to discern multiple tooth

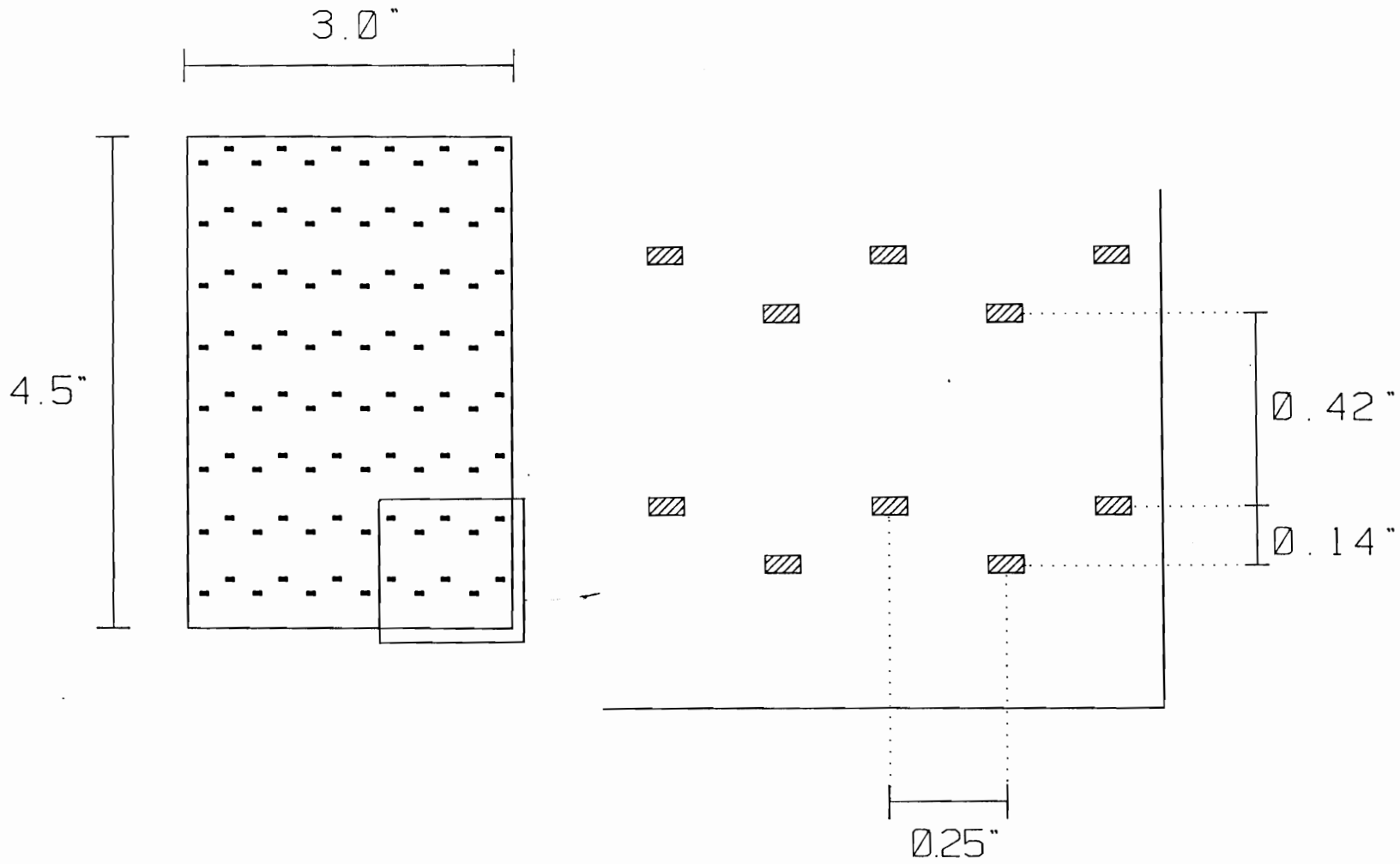

Figure 4.1. Truss plate dimensions used in this investigation.

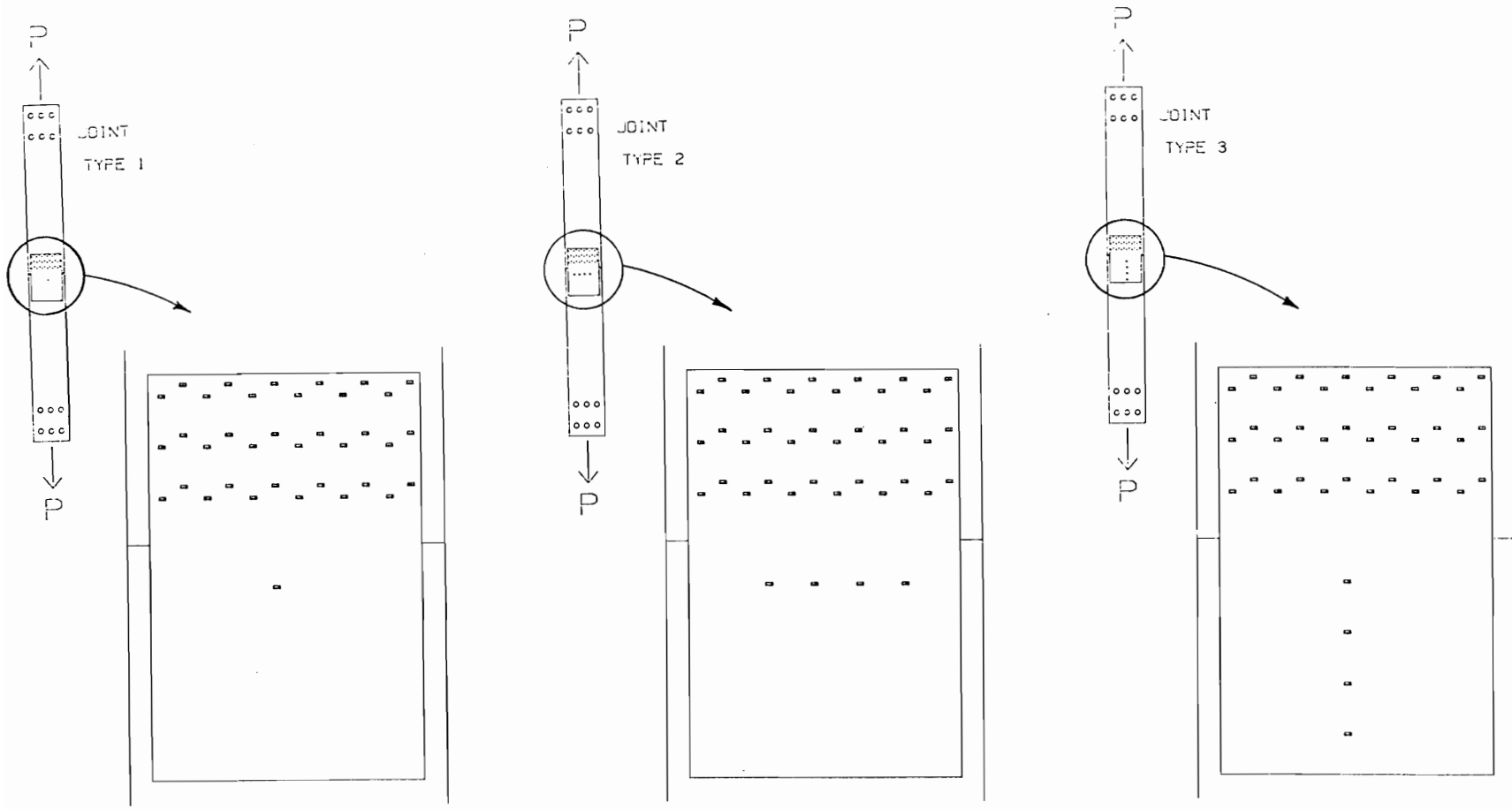

Figure 4.2. Joint types tested in this study to determine the effect of multiple teeth on truss-plate behavior. Joints shown contain (a) Type 1: single tooth, (b) Type 2: 4 teeth in a row, and (c) Type 3: 4 teeth in a column.

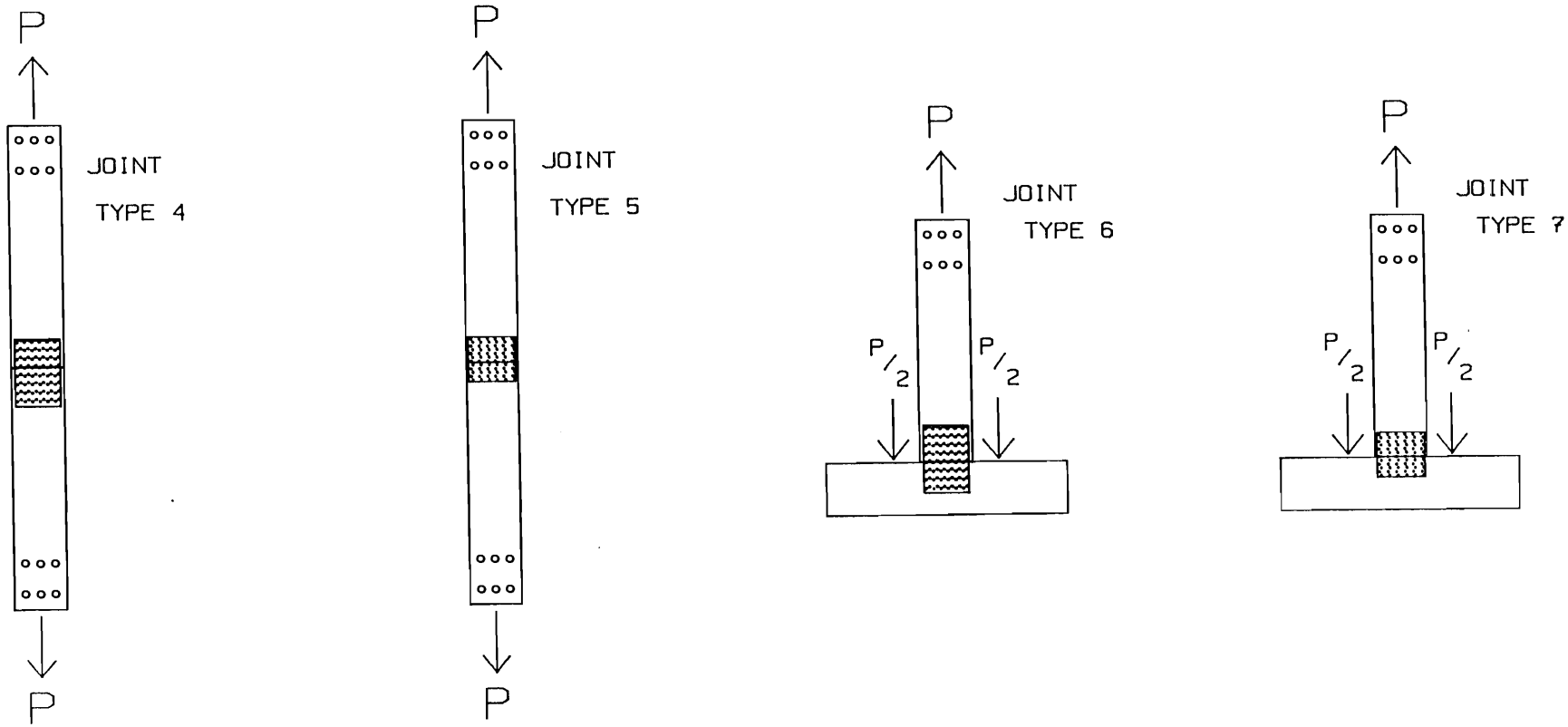

Figure 4.3. Joint types tested with complete sets of teeth to determine effect of grain and plate orientation on ultimate joint load.

complete behavior of typical truss-plate joints. The specimens for joint types 1-3 were constructed from the first group of 5 boards selected on the basis of specific gravity while joint types 4-7 were constructed from the second group.

An epoxy adhesive was applied to the teeth of the upper member of each specimen before joint assembly, thus ensuring failure in the desired lower member. The adhesive was applied to reduce slippage in the adhered portion of the joint which allowed a more precise measurement of displacements in joints tested.

In accordance with CSA S347-M1980 (9), all teeth were removed within a lumber end distance of 0.5 in. and within a lumber edge distance of 0.25 in. The teeth were removed with a milling machine which cut the teeth at the plate surface.

Joints were constructed using the apparatus shown in Figure 4.4 and in accordance with the specification prescribed by CSA S347-M1980 (9). The Canadian standard was chosen instead of ASTM D1761 (2) due to the increased flexibility regarding plate and grain geometry. Truss-plates were pressed into the lumber at a constant rate of 1.5 in./min until no gap was present between the plate and wooden members. This generally occurred at a load of about 140 lbs/tooth. The specimens were placed in a Standards room after construction for at least 72 hours

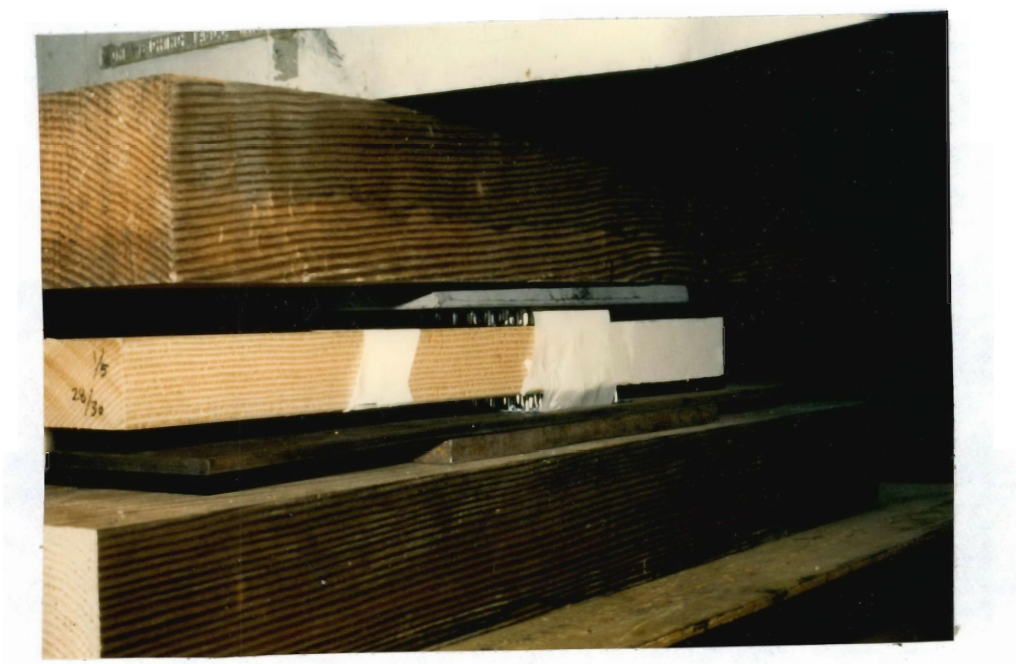

Figure 4.4. Apparatus used to assemble truss-plate joint specimens.

before testing to allow for relaxation of stresses induced by pressing and to reduce the resulting variability.

4.1.3. Testing Procedure

Figure 4.5 illustrates an assembled specimen during testing. The load was applied in tension by a 60,000-lb capacity, Tinius-Olsen, screw-driven crosshead testing machine. A constant displacement rate of 0.025 in./min was used, which produced failure in 5 to 20 minutes. A universal joint was placed between the machine and each wood member to eliminate moments imposed on joints by specimen misalignment.

Displacements were monitored by linear variable differential transducers (LVDT), and the load was monitored by a load cell. For all joints, the average of four LVDT readings located in pairs at the wood-wood juncture provided the average overall displacement between wood and plate (Fig. 4.4). The average was chosen to avoid any errors due to asymmetric specimen deflections. Load and deflection readings were acquired at a rate of 2 readings/second by an IBM-XT microcomputer with a data acquisition system.

4.2. Evaluation of Material Properties

Material properties for the joint members were necessary to model and analyze the joint behavior. This

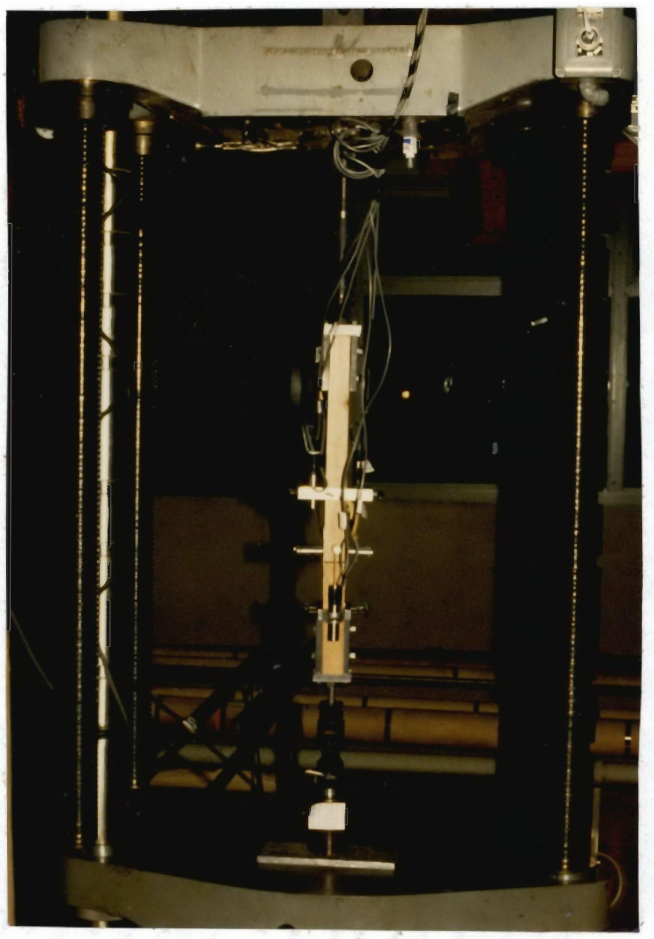

Figure 4.5. Typical joint type 1 specimen during testing.

section discusses the specimen sampling and testing procedures carried out to determine these properties.

4.2.1. Material Selection

Two 1.5- by 1.5- by 1.5-in. samples were removed from the lower member of all joint types upon failure. These samples, taken between the plate and the grip, were then labeled and stored in an impermeable package to prevent any change in moisture content.

4.2.2. Testing Procedure

The properties tested included tooth embedment, specific gravity, and moisture content.

4.2.2.1. Specific Gravity and Moisture Content

Specific gravity and moisture content were determined for each 1.5-in. specimen cube in accordance with ASTM standards D-143 (1) and D-2016 (3), respectively. Specific gravity was based on specimen weight at approximately 12 percent moisture content divided by the oven-dry volume. Moisture content was based on oven-dry weight.

4.2.2.2. Tooth embedment

There were four combinations of this test type depending on tooth and grain orientation with respect to bearing load. The tooth could either be oriented flat or

on edge while the grain orientation was either parallel or perpendicular to the applied embedment load.

The test apparatus for tooth embedment in wood is shown in Figure 4.6. A 1.5-in. metal cube, with two grooves for different tooth orientations, was clamped to one of the cube surfaces. The shape of the metal and specimen cube was dictated by the desired test type and determined as follows. An individual tooth cut from a truss-plate was driven in completely between the metal and specimen cube. The metal cube and the tooth were then removed, leaving only the specimen with a slight embedment mark made by the tooth removed. The 0.3-in. long corresponding loading head, depending on tooth orientation, was then forced into the embedded portion of the specimen at a rate of 0.035 in./min until failure. Load and deflection were monitored by a data acquisition system controlled by an IBM-XT microcomputer.

Joint types 1-3 were tested only with the wide tooth face bearing on the end grain. The load-embedment curve of joint types 1-3 were then averaged for each of the 5 boards. This provided a single foundation modulus for the entire board.

A similar procedure was used in evaluating moduli for joint types 4-7. Four orientations were tested and averaged, representing all possible tooth and grain orientations. Since in actual trusses, the bearing

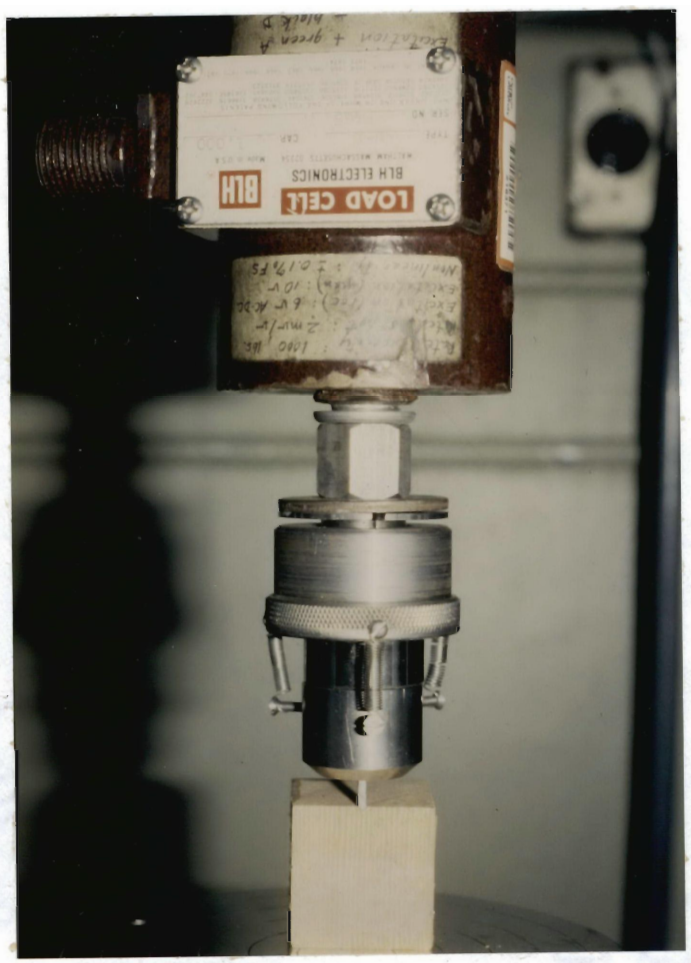

Figure 4.6. Apparatus used in this study to determine foundation modulus using tooth embedment.

stress transmitted to radial or tangential grain is a random event, no control was exercised in regard to bearing on tangential or radial grain for perpendicular to grain bearing loads. The average load-embedment curves for these joints were again averaged for each of the five boards from which they originated, resulting at the end in one average load-embedment curve for each of four tooth and grain orientations.

4.2.2.3. Tooth Withdrawal

The apparatus used for the tooth withdrawal tests is shown in Figure 4.7. A 2- by 2-in. section of truss-plate was attached to the back of an internal bond plate using hot melt adhesive. This section, consisting of 4 centrally located teeth with all other teeth removed with a milling machine, was driven a 1.5-in. specimen block until no gap was present between the wood and plate section. Another internal bond plate was then attached to the wood specimen with hot melt adhesive. The specimen with the 4-tooth section and internal bond plates was transferred to the Standards room.

Upon conditioning in the Standard room for a minimum of 24 hours, the specimen was tested at a withdrawal strain rate of 0.06 in./min. Load and deflection were monitored with a strip chart and the secant modulus and ultimate withdrawal load per tooth determined. These 4-tooth

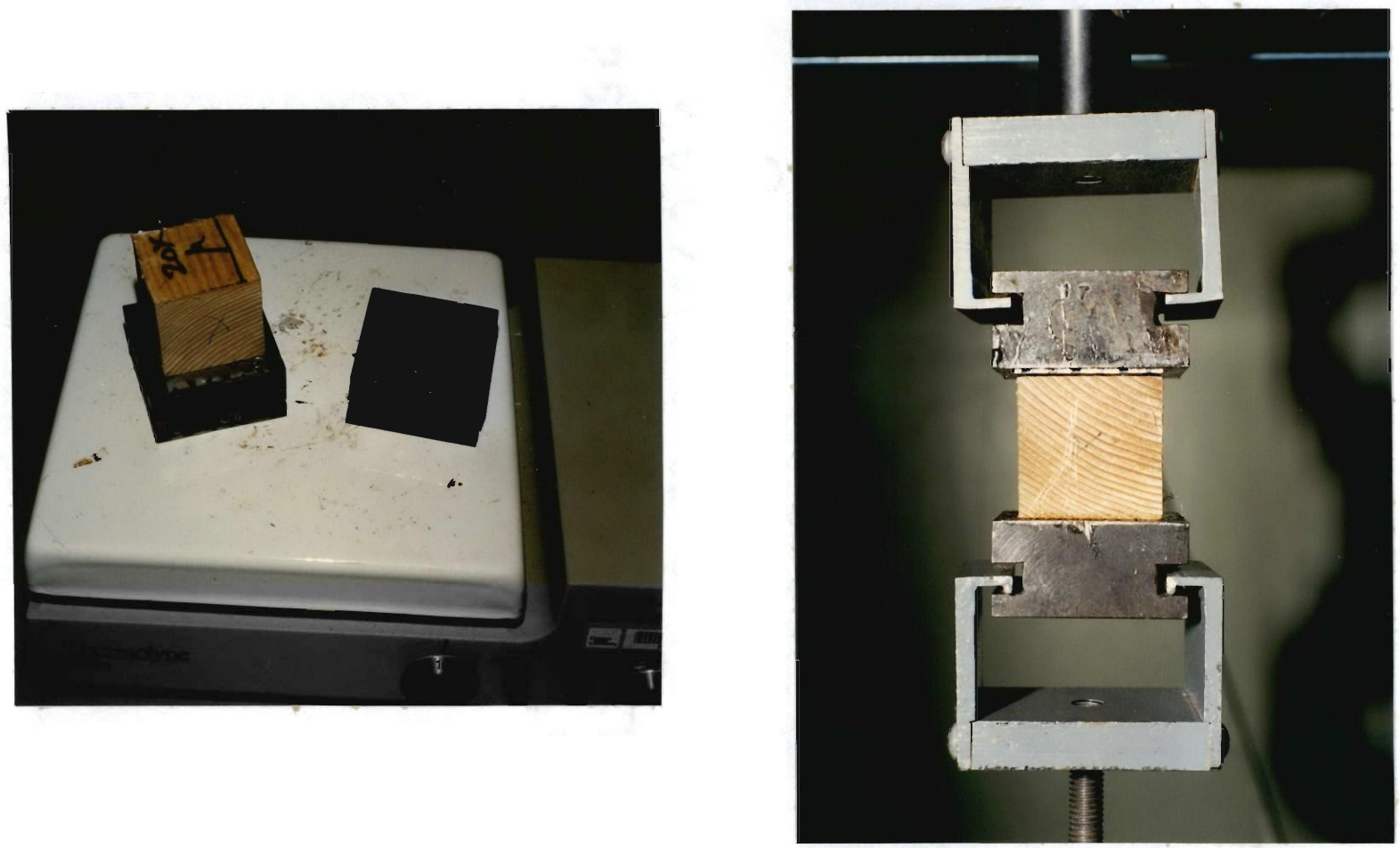

(a) (b)

Figure 4.7. Apparatus used to (a) assemble tooth withdrawal specimen, and (b) conduct withdrawal test.

were coated with an epoxy adhesive and redriven into the same wood specimen. These specimens were again conditioned in the Standards room for 24 hours and tested in withdrawal. Results of the withdrawal tests are summarized in Appendix F.

V. RESULTS AND DISCUSSION

This chapter discusses the inputs and outputs of the model developed and evaluates the accuracy of the model prediction to observations obtained in testing full scale joint specimens of type 1-7.

5.1. Specific Model for Specimens Tested

This section describes the results of the finite element analysis which provided the information needed to account for effects of rows and columns of teeth that act in groups.

5.1.1. Multiple Tooth Effect

Three finite-element joint types were modeled by finite element analysis (Fig. 3.7) to determine stress fields in the wood under the tooth pressure. The results lead to a decision about extending a single-tooth analysis to the analysis of the whole plate.

5.1.1.1. Material Data Base

Figure 5.1 shows the stiffness properties used in the 2-dimensional finite element analysis. The modulus of elasticity of wood, MOE, in the y-direction was equivalent to the average longitudinal MOE estimated from National Design Specifications (30) for No. 1 and Better Douglas-

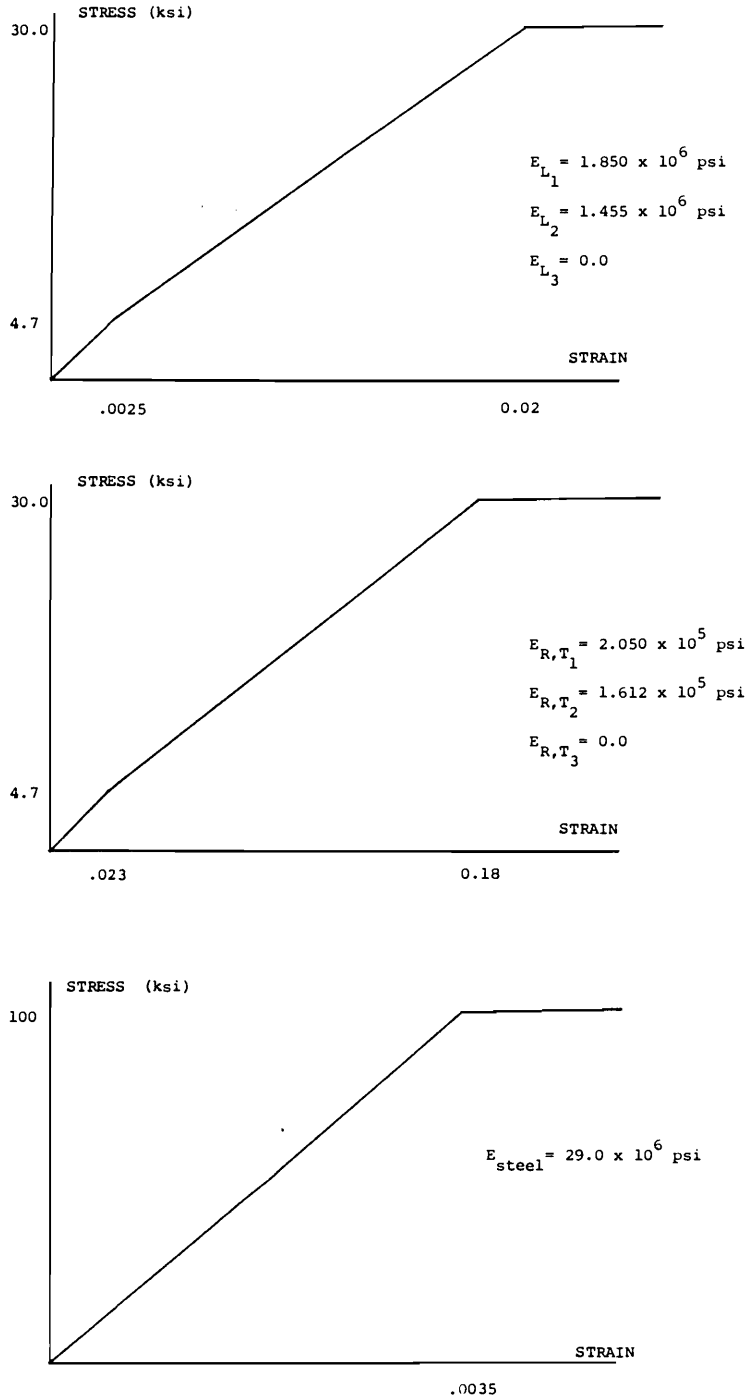

Figure 5.1. Moduli of elasticity for the finite element analysis for: (a) wood; longitudinal, (b) wood; radial and tangential, and (c) steel.

fir lumber. A single MOE value, estimated from the ratio of longitudinal MOE to radial and tangential MOE (E_T, E_R) for Douglas-fir from the Wood Handbook (41), was chosen for the x- and z-directions since a specimen had an equal probability of being oriented radially or tangentially.

The meshes used in each analysis consisted of approximately 350 rectangular elements and 25 spring elements. The spring elements (35) were necessary to account for potential gaps and to connect the tooth elements to wood elements.

5.1.1.2. Stress Distribution under a Single Tooth

Resulting stress distributions for face and edge of the tooth are shown in Figure 5.2 for a shear load of 100 lbs acting on the tooth at the wood surface. It is apparent that although the edge orientation has a smaller tooth-bearing area, the stresses under the tooth are less than those of face orientation. This is due to the increased moment of inertia and stiffness for edge orientation.

The larger stiffness for edge orientation is also evident from the patterns of stress distribution. The more flexible flat orientation has stresses which do not rapidly spread in the x-direction. However, since the edge orientation is very stiff at the tooth head, the deflections and stresses are directed further along the

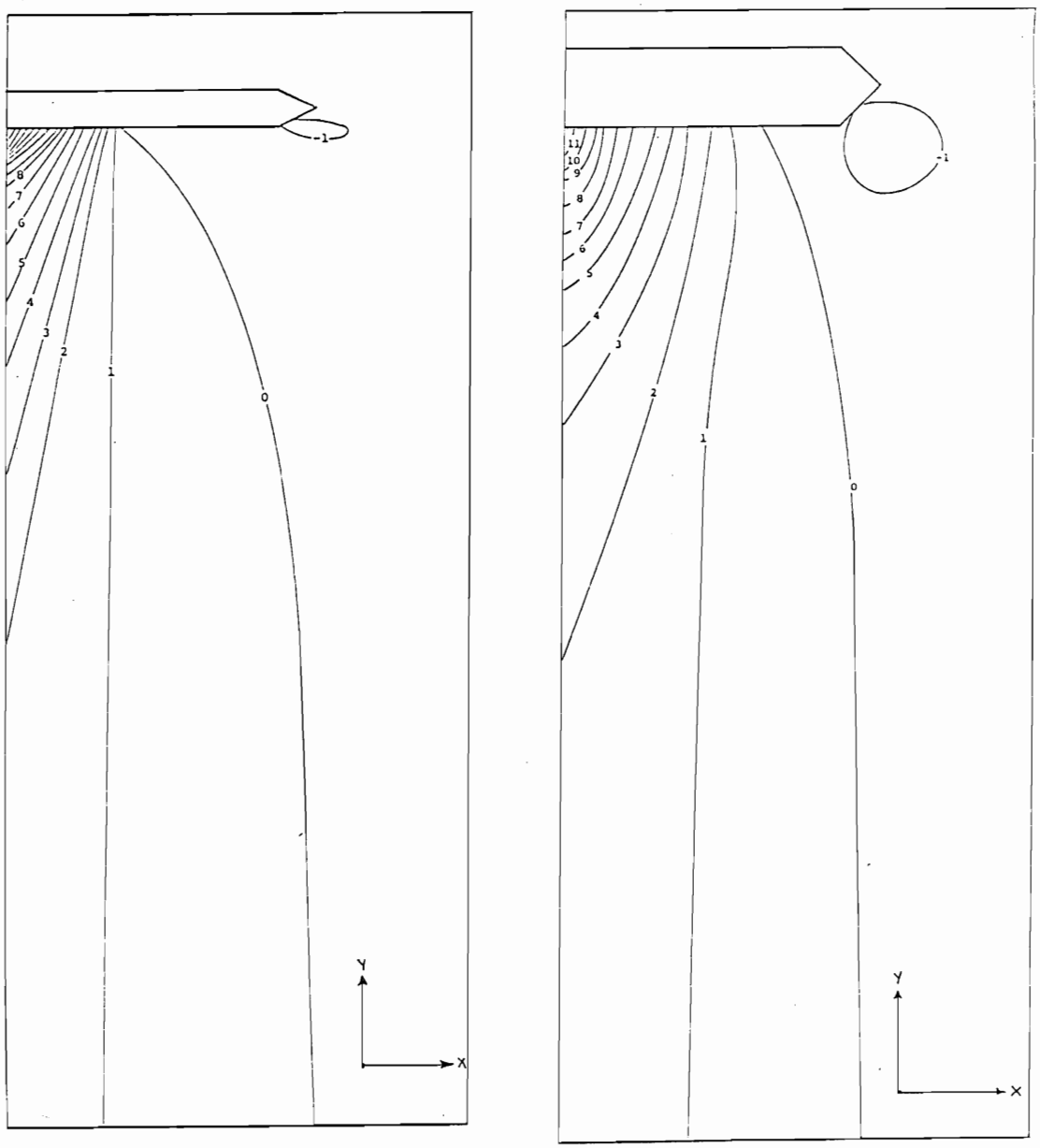

Figure 5.2. Stress distributions for (a) tooth face bearing on end grain and (b) tooth edge bearing on end grain determined by nonlinear finite element analysis (Stresses shown are in kips/in^2).

tooth resulting in a more even stress distribution.

The force distribution along each tooth illustrates this observation. Figure 5.3. shows the percent load distribution for the eight 0.05-in. sections along the tooth length. The distribution depends on the tooth orientation; the teeth bearing on edge are stiffer than on face and a greater portion of the load are carried by the ends of the tooth.

These load distributions, based on stresses directly under each corresponding 0.05-in. section, were then used to determine the applied load for second part of each multiple tooth finite-element analysis. This was done to determine how the stresses dissipate in the y-z plane and to see if and by how much these stresses among teeth overlap. This type of analysis also allows for a more detailed analysis in the areas of highest stress.

5.1.1.3. Stress Distribution among Multiple Teeth Arranged in Columns

The second part of the finite-element analysis was conducted for only the outermost 0.05-in. of tooth penetration as the stresses were the largest within that thickness. Figure 5.4 shows the stress contours in this outermost layer of the wood for teeth arranged in a column with faces bearing on end grain. The same loads were applied to each tooth. The assumption was made that each

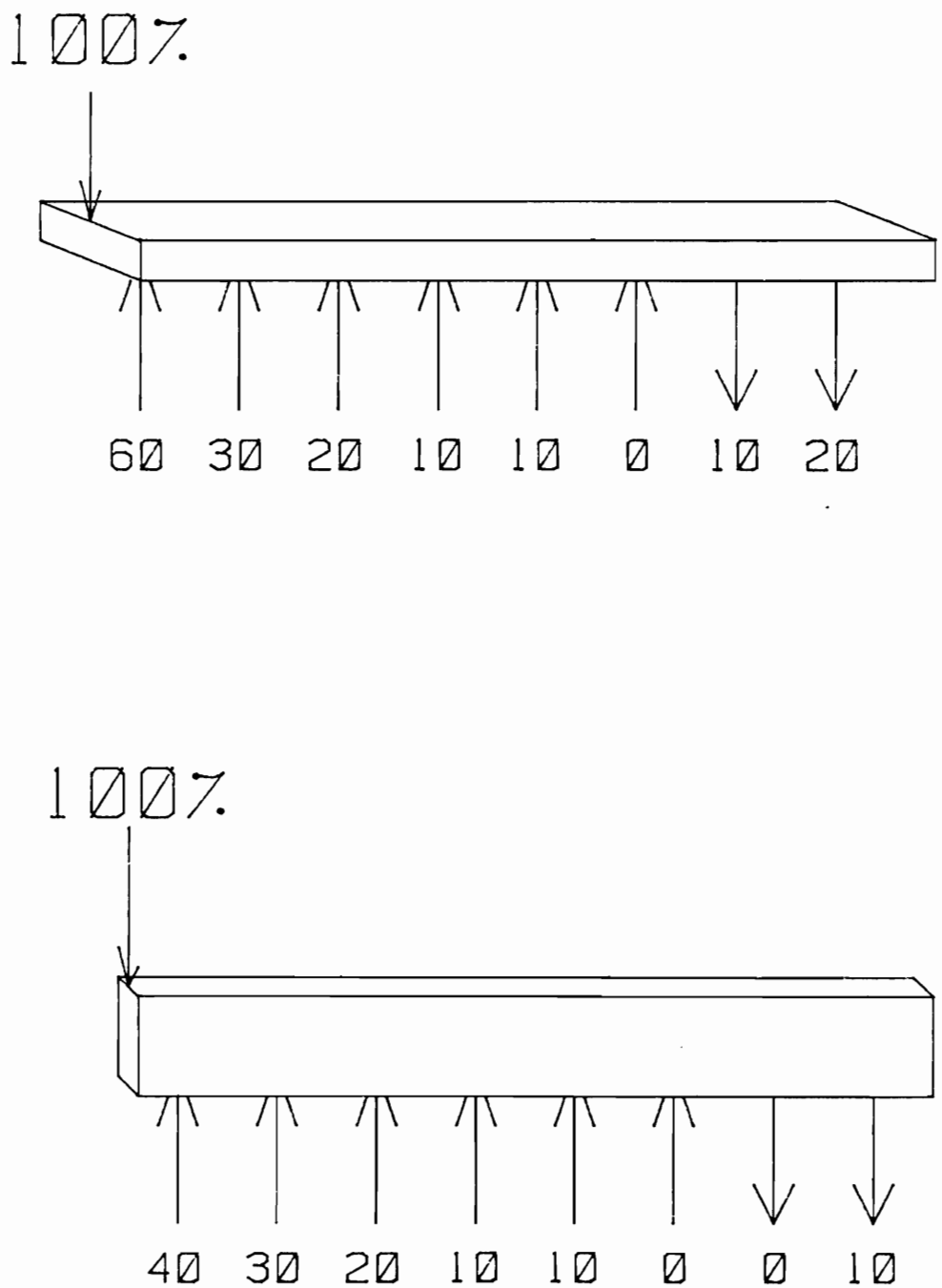

Figure 5.3. Percent of load distributed per 1/8-section of tooth length for the load applied at tooth head for: (a) face and (b) edge orientated tooth.

tooth of an actual plate carries the same load due to the relatively large stiffness of the plate in comparison with wood. Appendix C shows these stiffness differences and the justification for using the same load for each tooth.

Loads shown in Figure 5.4, which are actually the 60% of the total load carried by the outermost 0.05-in. thick layer of wood (Fig. 5.3), vary from typical prefailure loads (40 lbs ÷ 60% = 67 lbs/tooth) to typical postfailure loads (60 lbs ÷ 60% = 100 lbs/tooth).

The sequential contours of Figure 5.4 show how stresses accumulate under increasing load, and that the highest compressive stresses are concentrated around the tooth. Stresses dissipate rapidly in wood around teeth while stresses away from the teeth dissipate slower and almost at an even rate. These stresses begin to overlap as the loads approach collapse (Fig. 5.4(c)). This indicates only a minor interaction between teeth. Each tooth introduces approximately 1 ksi stress for every 10 lbs applied, which is due to the linear behavior of the high-quality wood used in the analysis.

A column arrangement of teeth which bear on edges exhibits a pattern similar to that of teeth that bear on faces (Figure 5.5). The analysis was performed for only the outermost 0.05-in. section where maximum stresses occur and 40% of the total load is transferred into the wood (Fig. 5.3). The applied loads ranged from typical

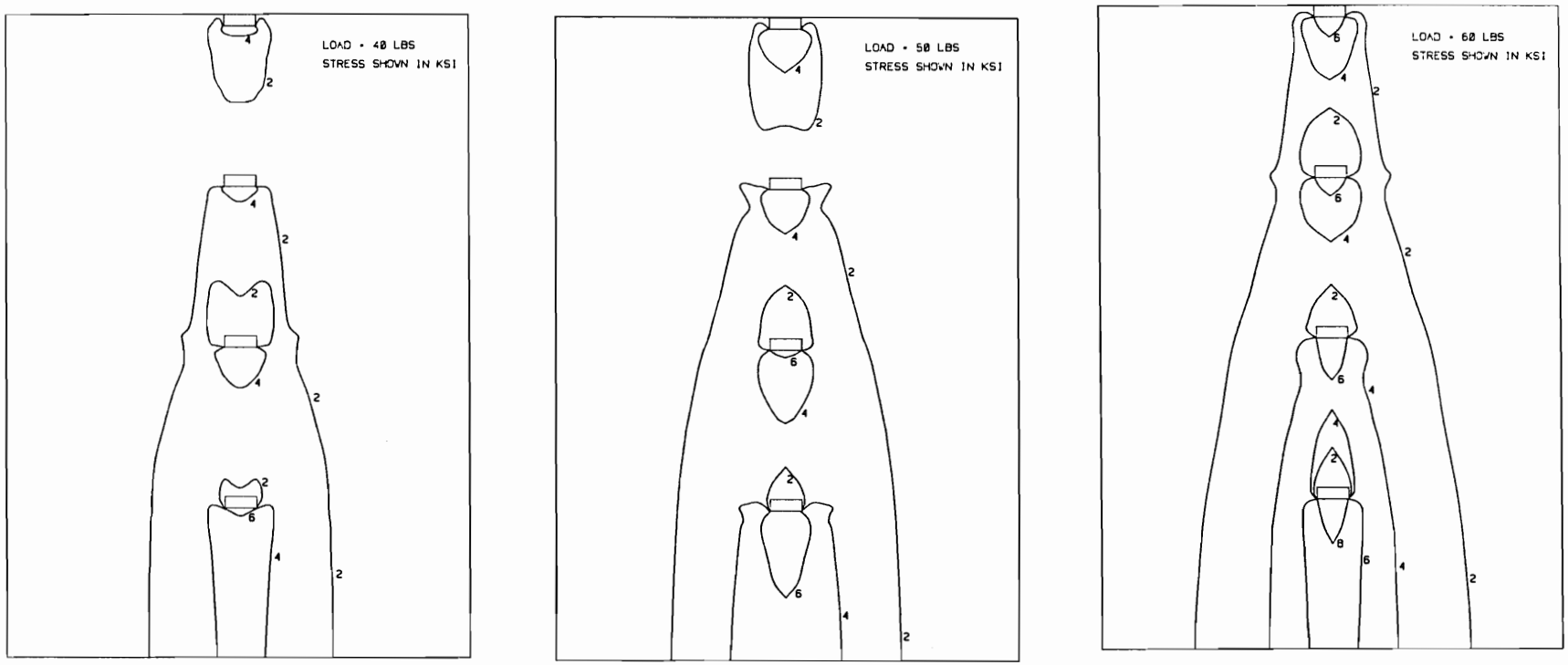

(a) (b) (c)

Figure 5.4. Stress distribution obtained in the finite-element analysis of a system with four teeth bearing on faces and arranged in a column at: (a) 67 lbs, (b) 83 lbs (typical failure load), and (c) 100 lbs per tooth.

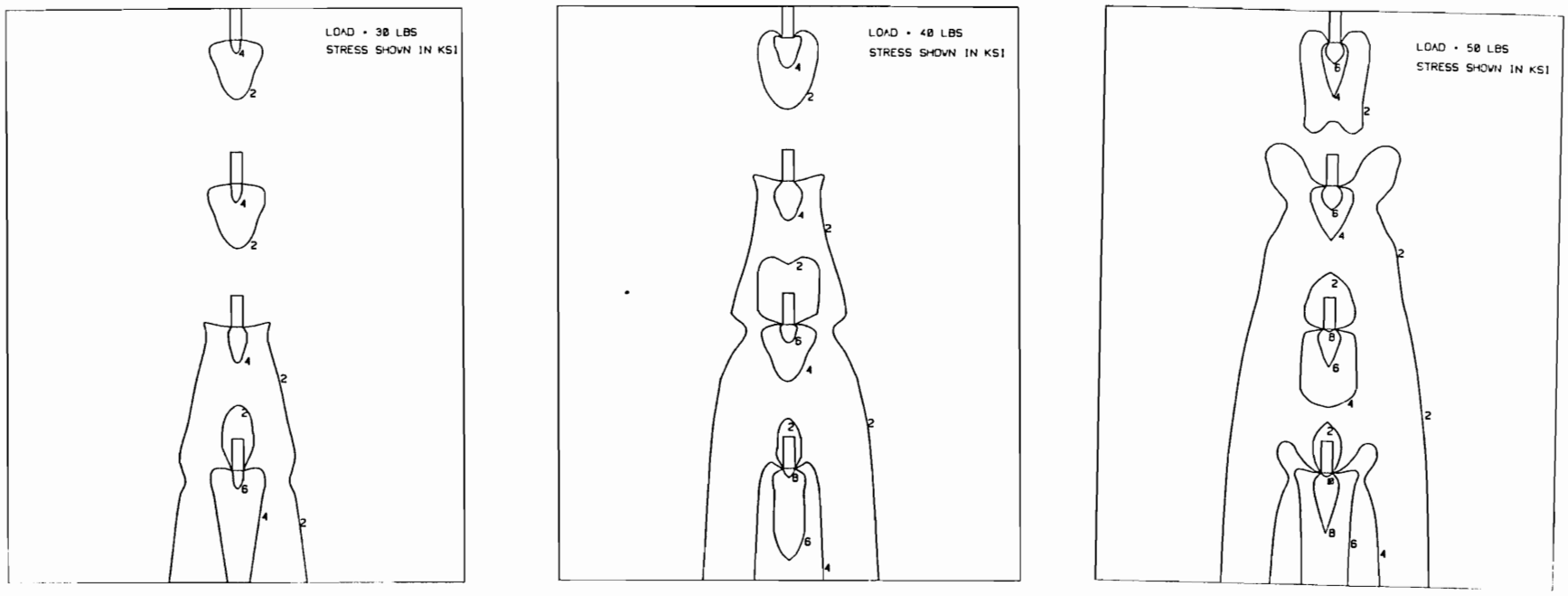

(a) (b) (c)

Figure 5.5. Stress distribution obtained in the finite-element analysis of a system with four teeth bearing on edges and arranged in a column at: (a) 75 lbs, (b) 100 lbs (typical failure load), and (c) 125 lbs per tooth.

near-failure loads of 75 lbs per tooth to an overload of 125 lbs per tooth. The smaller bearing area of the tooth results in a higher proportion of stresses located directly under the teeth. These stresses do not dissipate as quickly as those of the face orientation, which results in more stress interaction between teeth as load levels increase. The stress levels in the wood are of low magnitude, generally 2 ksi except directly under the teeth at typical failure and post-failure loads, at which the wood under the third and fourth teeth received higher stresses than the teeth above them. This is because of the small bearing area of the teeth which directs the stresses downward rather than radiating outward, compounding the stresses under the lower teeth. Therefore, although interaction between teeth is minimal at low load levels, interaction may be prevalent at collapse loads.

Interaction among the four teeth arranged in a row is much less pronounced than interaction among teeth arranged in a column. Figure 5.6 shows the results of the finite-element analysis in a row of a set of teeth bearing on edge and arranged in a row under 125 lbs per tooth, which exceeds the collapse load considerably. There is no interaction between teeth as demonstrated by the same stress patterns under each tooth. The reason is the transfer of stresses primarily in the direction of the applied load. It can be concluded that the teeth bearing

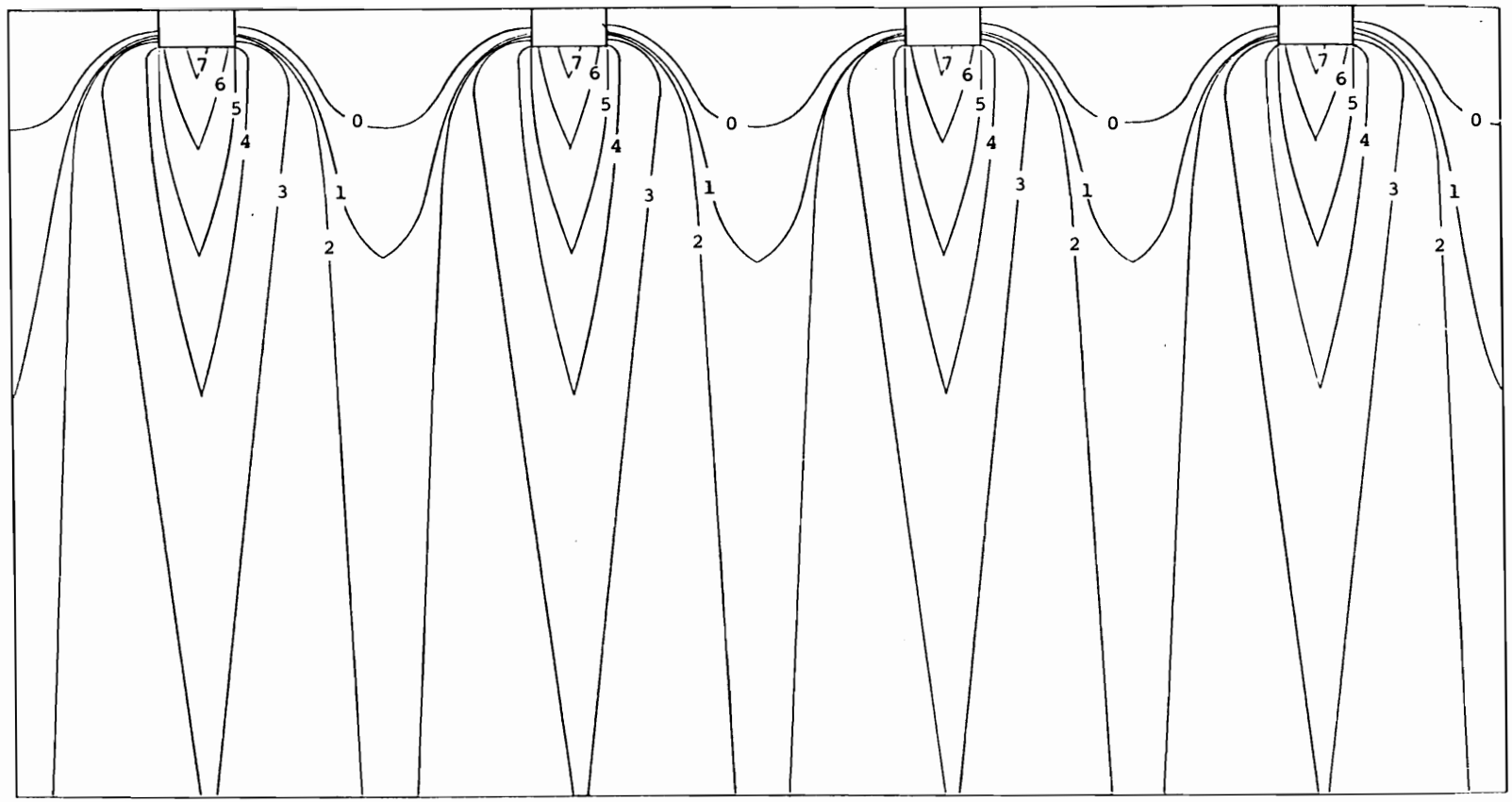

Figure 5.6. Stress pattern obtained in the finite-element analysis of four teeth in a row embedded in wood with face bearing on end grain at a load of 125 lbs/tooth.

on edge would also show no interaction as the stresses in that joint type radiate outward to an even lesser extent. For these reasons, teeth in a row are expected to carry the same load per tooth as that of a single tooth.

5.1.2. Analogy of Beam-on-Elastic-Foundation

5.1.2.1. Evaluation of Material Properties

This section discusses the existing material properties and input parameters used for the truss-plate model of this study as it relates to analyzing a plate tooth as a beam-on-elastic-foundation, and then discusses the foundation moduli used in assessing model accuracy.

Table 5.1 shows the input properties for the theoretical analysis of plate joints tested in this study. The MOE and yield stress were taken from a report by McCarthy and Wolfe (28) who used the plate gauge and type identical to the one in testing. The friction coefficient of 0.385 for nail embedment in wood was reported by Atherton (4). He determined the friction coefficient between 6d common nails on the wide and narrow face of Douglas-fir lumber. The foundation modulus, plate angle, and grain angle vary depending on test type and specimen.

Two types of teeth were found in the truss-plates used in this study; similar features except for a slight difference in length and shape. However, the differences were small enough to use the average of their

Table 5.1. Input parameters used in the theoretical analysis of experimental plate joints of this study.

MATERIAL PROPERTIES

Steel: MOE = 29.0 * 10^6 psi
Yield stress = 39,850 psi
Plastic stress = 59,775 psi

Wood: Friction coefficient = 0.385
Foundation modulus = varies
Plate and Grain angle = varies

TOOTH CHARACTERISTICS

Geometry: Overall length = 0.393 in.
No. of segments = 4

Segment #1: Length = 0.050 in.
Height = 0.0395 in.
Width = 0.113 in.

Segment #2: Length = 0.041 in.
Height = 0.044 in.
Width = 0.100 in.

Segment #3: Length = 0.241 in.
Height = 0.044 in.
Width = 0.087 in.

Segment #4: Length = 0.041 in.
Height = 0.044 in.
Width = 0.0435 in.

PROGRAM RUNNING CONSTRAINTS

Load increment = 5 lbs/tooth
No. of intervals = 10
Initial root estimates: $\alpha_1 = 0.0$
$\alpha_2 = 0.0$
$\alpha_3 = 0.0$

Tolerances:
(1) Runge-Kutta root estimates = 0.05
(2) Deflection at tooth head = 0.0005 in.

dimensions in the analysis. The average tooth had a length of 0.393 in. and was divided into 4 distinct segments due to variances in length, height, and width. The height of the rectangular segment 1, which is the segment adjacent to the plate, is basically the thickness of the plate from which the teeth were punched out. Although segments 2, 3, and 4 were punched out from the same plate thickness, their dimension was increased due to the nonrectangular shape of the tooth formed as a result of the die-punch.

5.1.2.2. Foundation Modulus of Wood

Twenty five values of foundation moduli were evaluated from test specimens. Types 1, 2, and 3 of experimental joints changed only the number and position of teeth while keeping a plate angle of 0 degrees and loading parallel to grain. Thus the five boards from which these test types originated needed only to be tested for one type of foundation modulus: tooth with its face bearing on end grain. Joint types 4, 5, 6, and 7 varied in both grain and plate orientation. Thus the 5 boards used for these test types needed all four foundation moduli: tooth face bearing on end grain, tooth edge bearing on end grain, tooth face bearing on side grain, and tooth edge bearing on side grain.

Four steps were followed to obtain the final foundation moduli. The first step involved collecting the

raw data for the load-embedment traces. Figure 5.7 shows examples of the original experimental traces for tooth flat bearing on end grain foundation moduli for two different boards. The second step was to average these traces on the basis of deflection (Figure 5.8). Deflection was the common base for averaging since the embedment tests used a constant strain rate. This constant strain rate resulted in varying embedment loads of each specimen for known deflections.

The third step involved smoothing the load-embedment traces and standardizing the traces so that the foundation moduli are based on a 1-inch tooth length. The smoothing of the traces was done by removing the initial alignment portion and extending the elastic portion of the traces to the axes origin. The initial alignment portion was removed because it was curvilinear and was due to settling of the embedment head onto the specimen and apparatus alignment, and thus not reflective of actual tooth behavior. Standardization to a 1-inch basis was done by dividing the load-embedment data by 0.30 in., which was the length of the embedment loading head used to obtain the traces. The reduced data are shown as standardized load-embedment traces in Figures 5.9 through 5.13. All original load-embedment traces are shown in Appendix D.

The fourth step involved applying the traces of Figs. 5.9 through 5.13 to evaluate numerical values which could

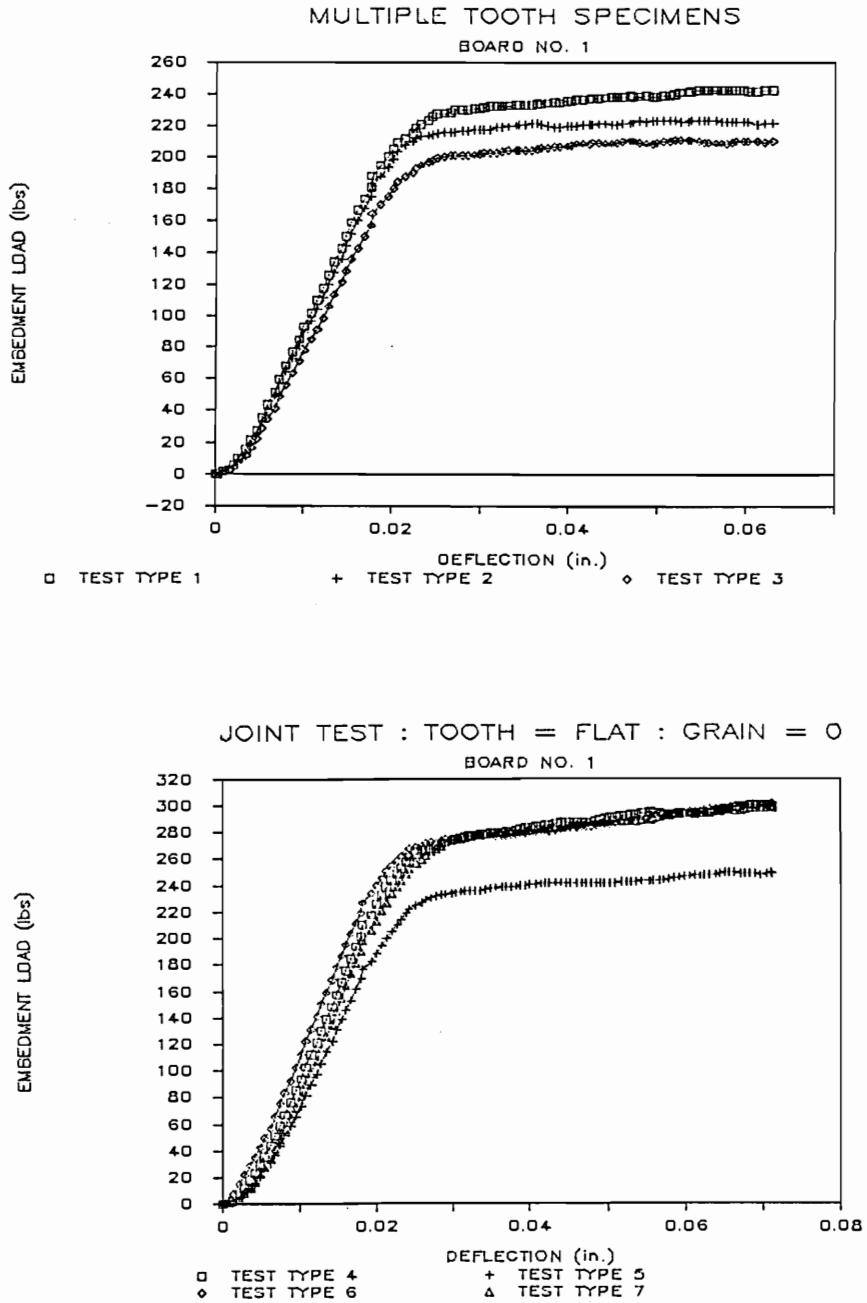

Figure 5.7. Load-embedment traces obtained in test of tooth face bearing on end grain for: (a) board no. 1, joint types 1, 2, and 3, and (b) board no. 1, joint types 4, 5, 6, and 7.

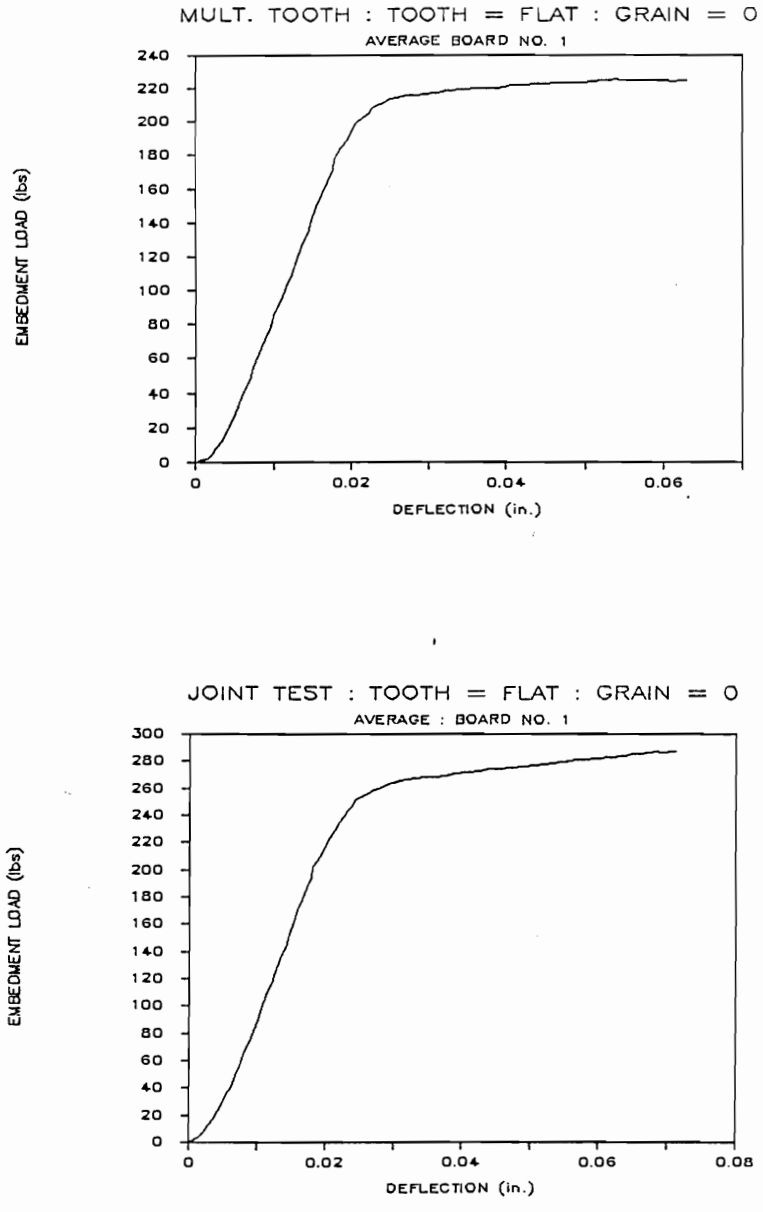

Figure 5.8. Average load-embedment traces obtained in test of tooth face bearing on end grain for: (a) board no. 1, joint types 1, 2, and 3, and (b) board no. 1, joint types 4, 5, 6, and 7.

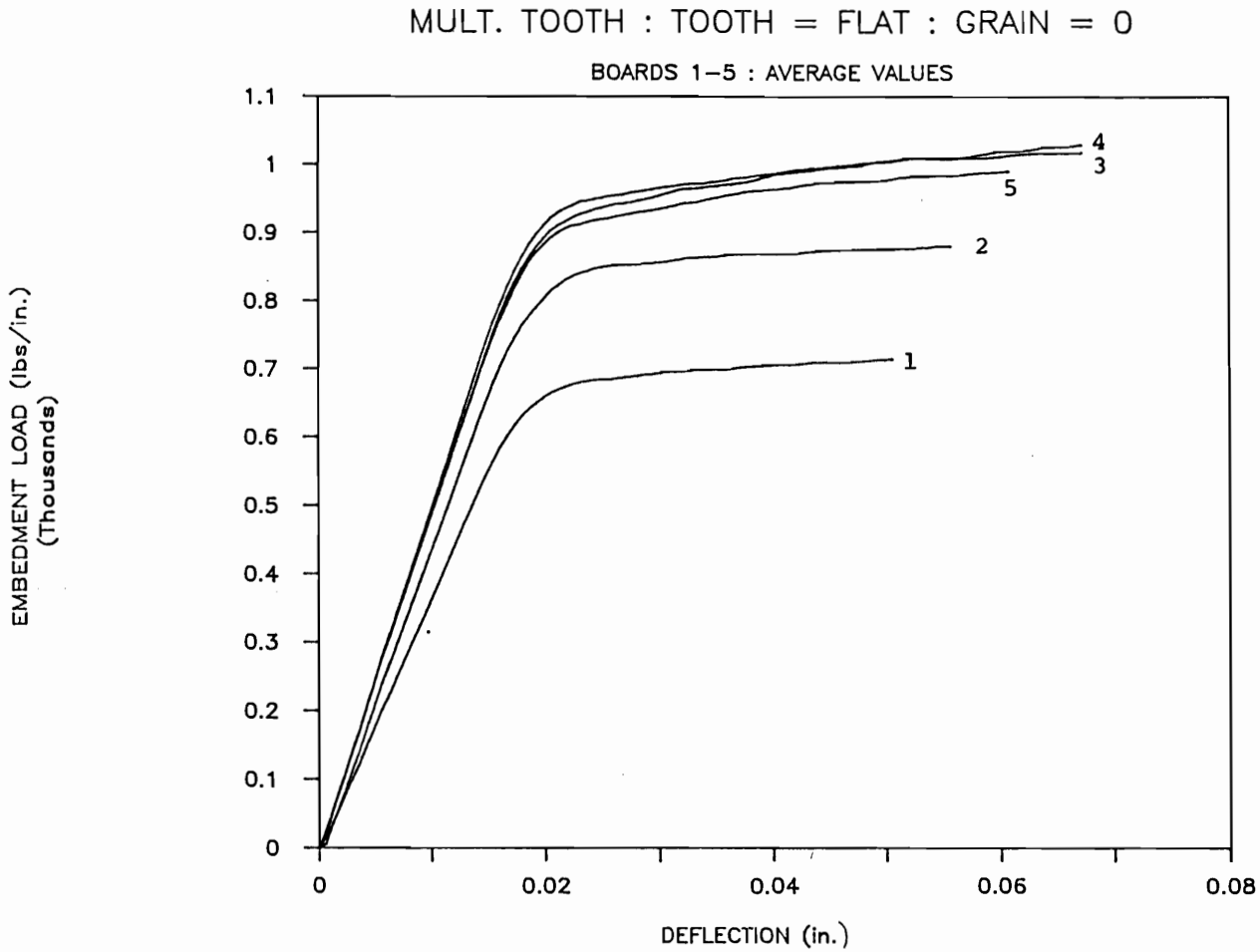

Figure 5.9. Average load-embedment traces for boards 1 through 5 adjusted for specimen alignment and standardized to 1-in. basis obtained in tests of tooth face bearing on end grain for joint types 1, 2, and 3.

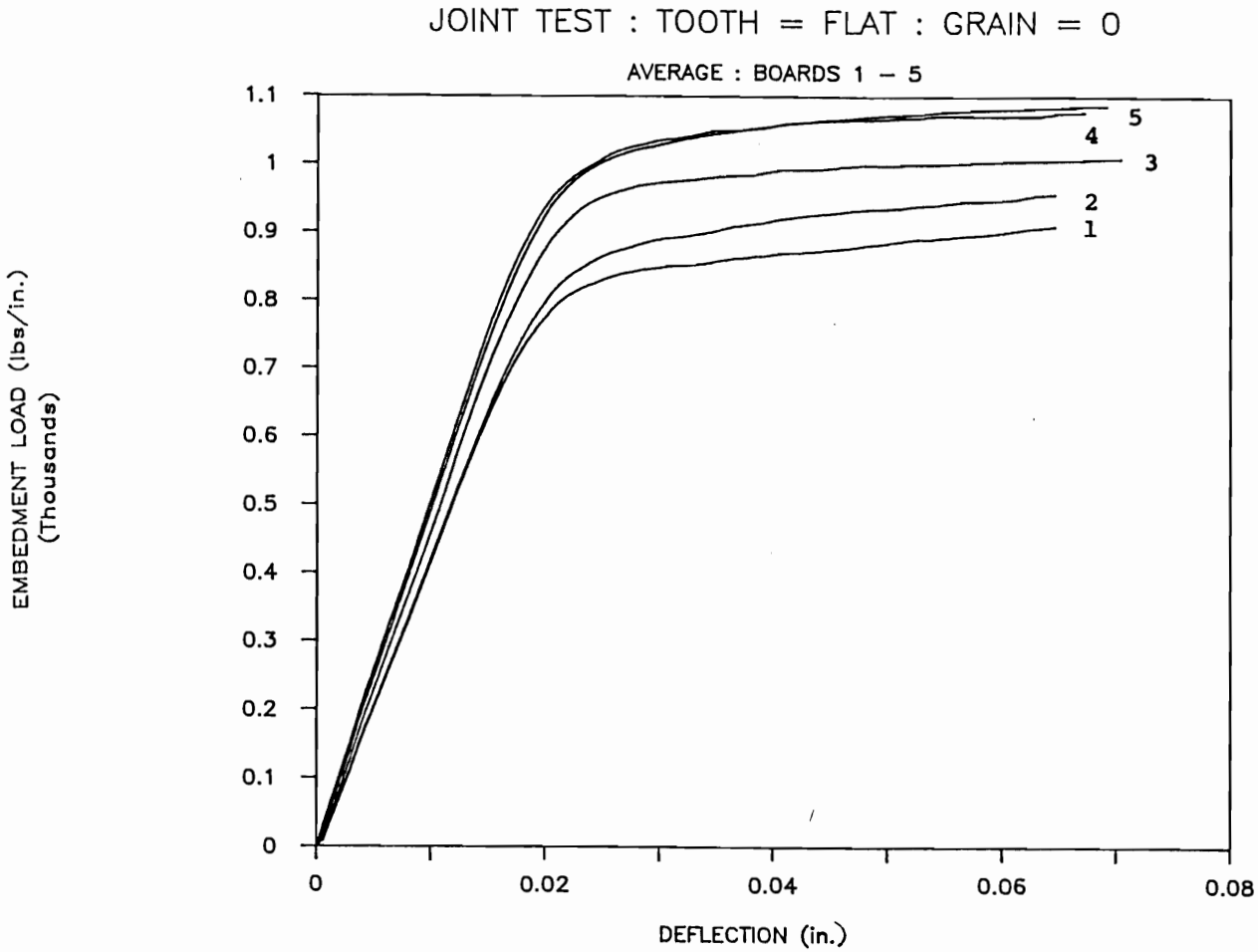

Figure 5.10. Average load-embedment traces for boards 1 through 5 adjusted for specimen alignment and standardized to 1-in. basis obtained in tests of tooth face bearing on end grain for joint types 4, 5, 6, and 7.

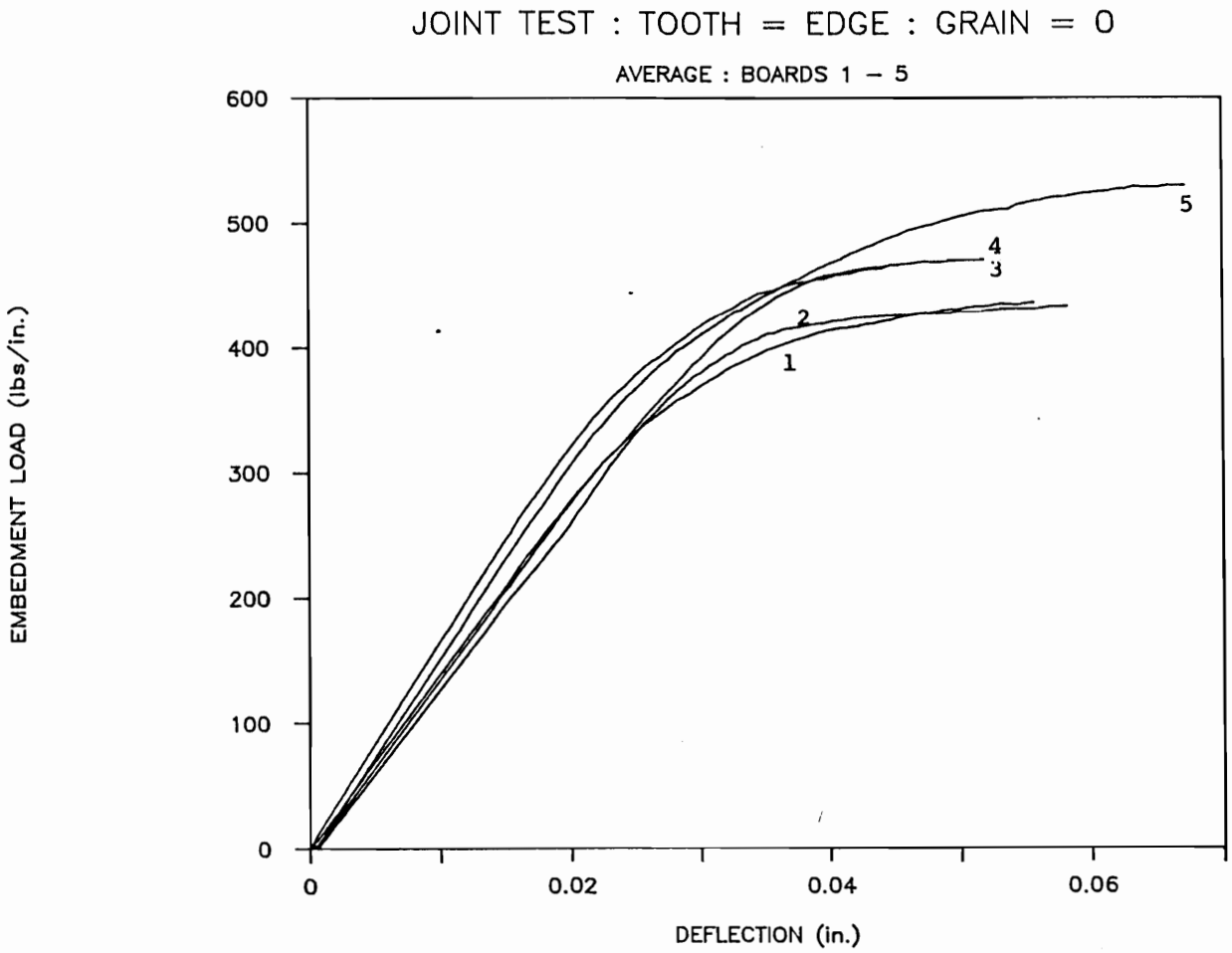

Figure 5.11. Average load-embedment traces for boards 1 through 5 adjusted for specimen alignment and standardized to 1-in. basis obtained in tests of tooth edge bearing on end grain for joint types 4, 5, 6, and 7.

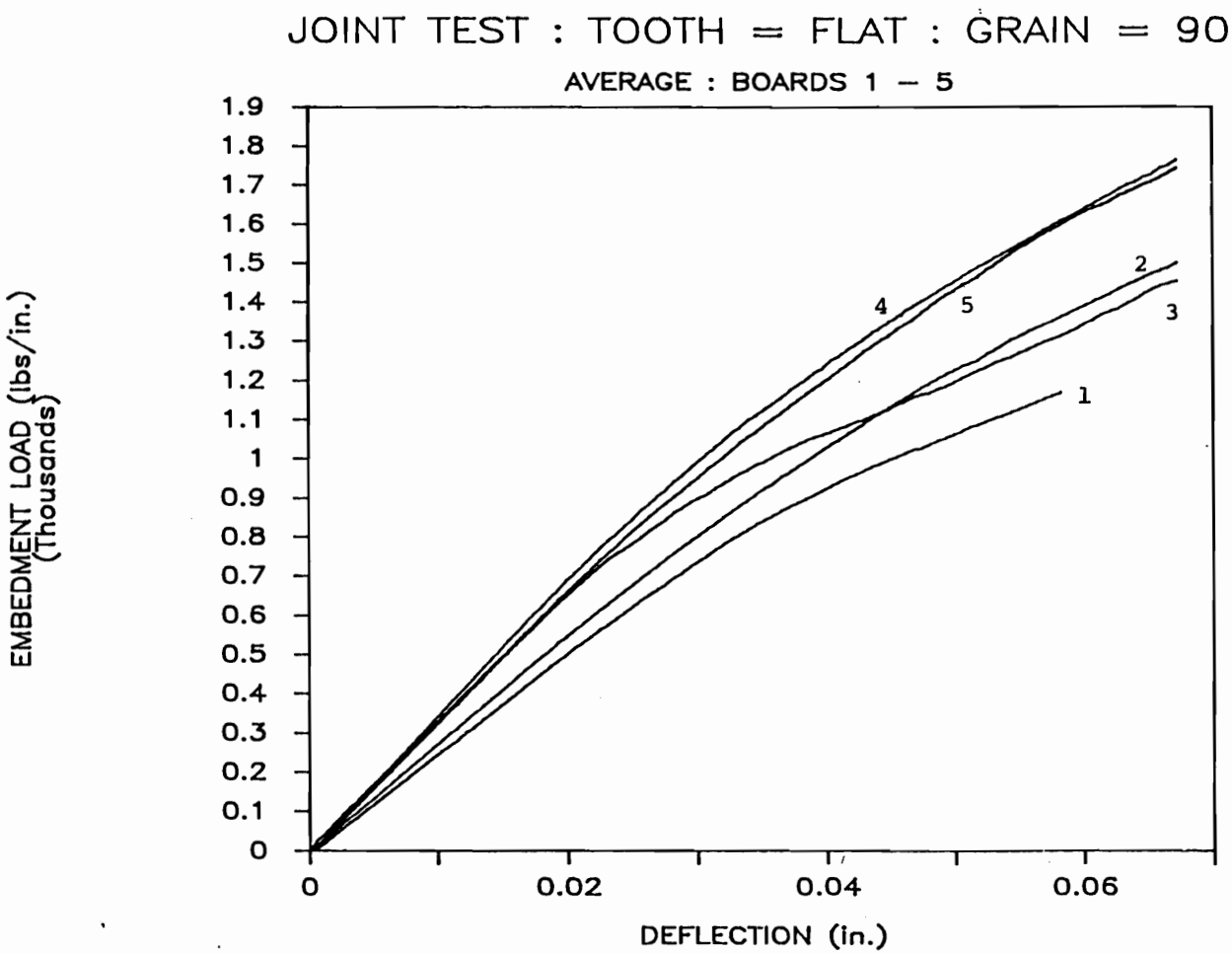

Figure 5.12. Average load-embedment traces for boards 1 through 5 adjusted for specimen alignment and standardized to 1-in. basis obtained in tests of tooth face bearing on side grain for joint types 4, 5, 6, and 7.

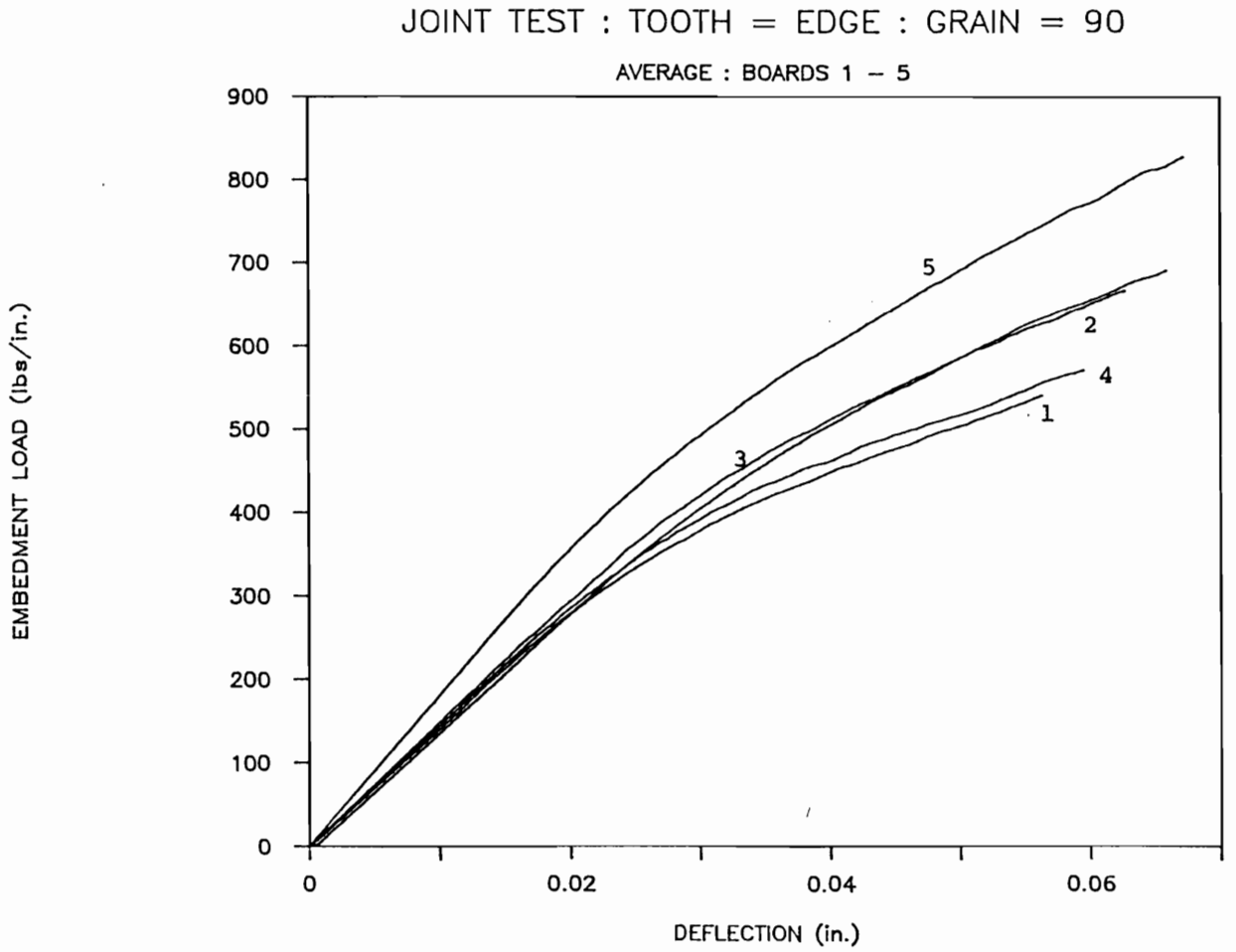

Figure 5.13. Average load-embedment traces for boards 1 through 5 adjusted for specimen alignment and standardized to 1-in. basis obtained in tests of tooth edge bearing on side grain for joint types 4, 5, 6, and 7.

be used by program TRUSSCON. Two methods were employed to accomplish this, linearization and nonlinear regression. The load-embedment traces with tooth faces bearing on end grain have 2 linear regions and only a small curvilinear region. Nonlinear curve fitting techniques were originally used to define the traces, but no exponential or polynomial equations were found which could reduce the sums of squares to an acceptable level. Therefore, traces were visually divided into linear regions with corresponding deflection limits that defined the extent of their validity. An example of this technique is illustrated in Figure 5.14.

Load-embedment traces with teeth bearing on side grain demonstrated a curvilinear behavior throughout the test. For these traces, nonlinear regression analysis was performed with exponential and polynomial functions. The following polynomial equation, based upon least sums of squares, provided the best fit:

$$y = Ax + Bx^2 \qquad (5.1)$$

where: y = load,
x = deflection, and
A, B = nonlinear regression coefficients.

Figure 5.15 shows a typical perpendicular to grain load-embedment trace along with the regression equation. The foundation modulus could be determined easily by taking the derivative of equation (5.1):

$$y' = k = A + 2Bx \qquad (5.2)$$

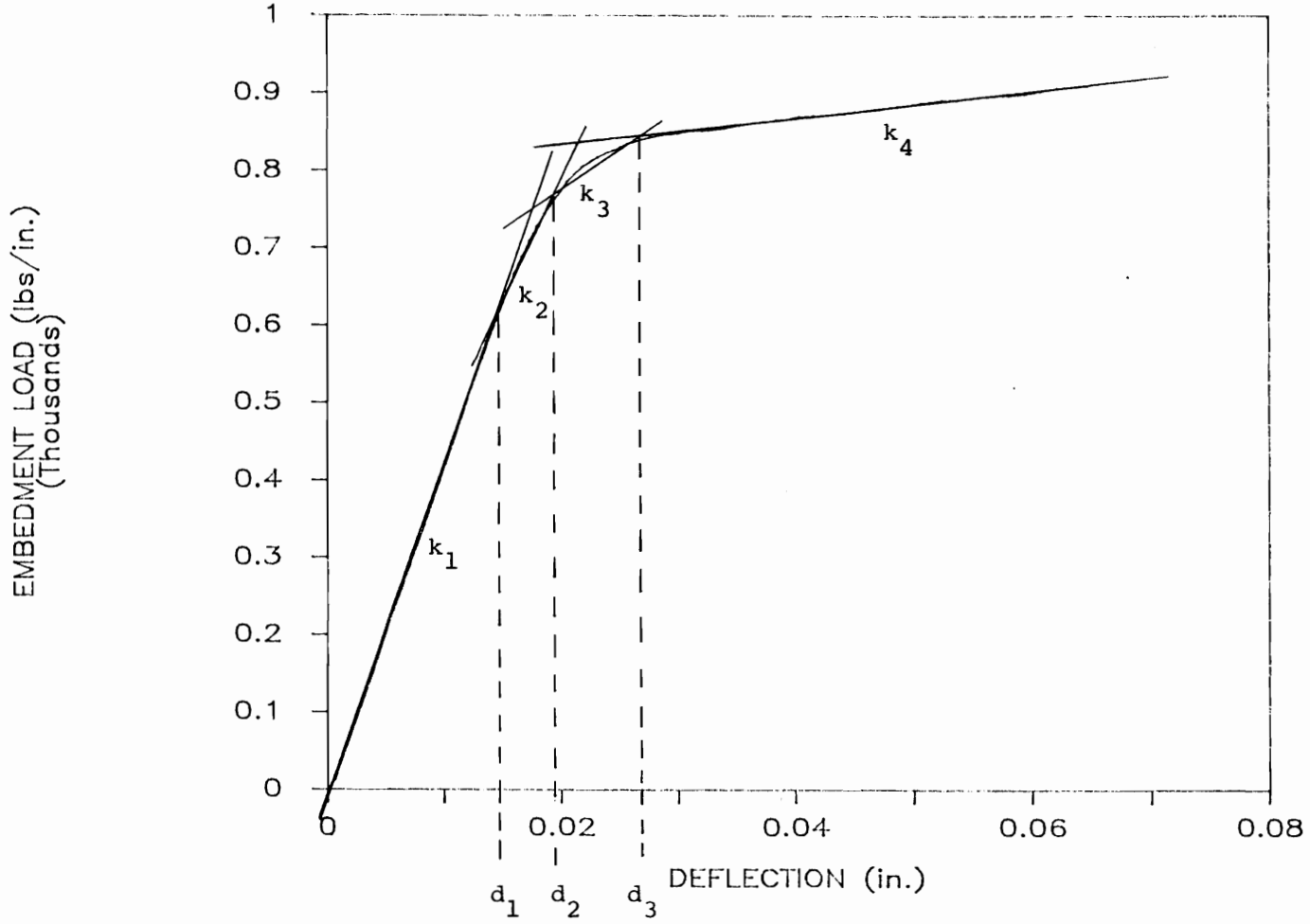

Figure 5.14. Load-embedment trace and corresponding linear moduli and deflection limits for a tooth face bearing on end grain specimen.

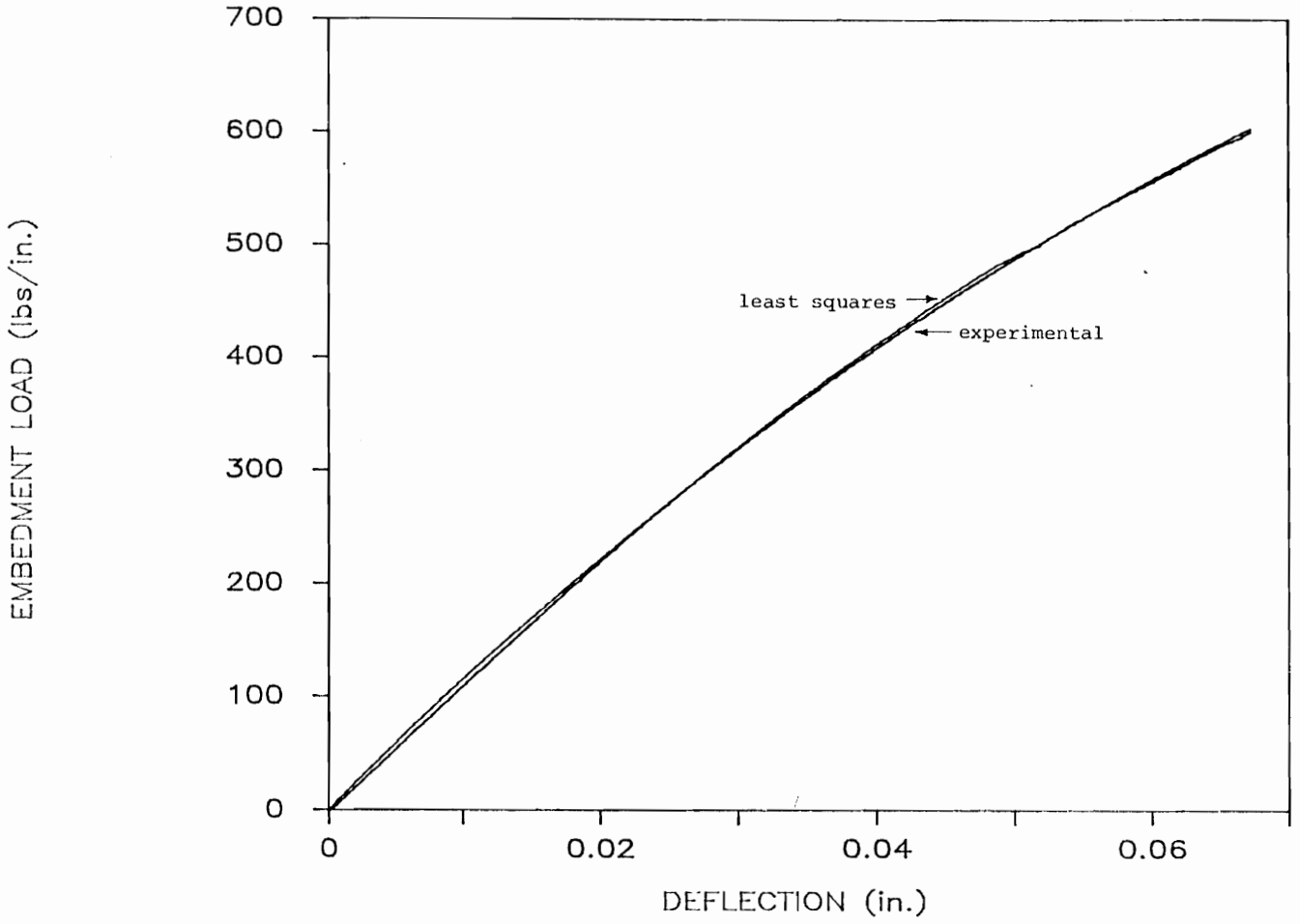

Figure 5.15. Load-embedment trace and least-squares nonlinear regression curve for a tooth bearing with face on side grain specimen.

Regression equation coefficients along with the linearized foundation moduli and deflection limits are summarized in Table 5.2.

5.2. Evaluation of the Accuracy of Theoretical Model

This section compares the theoretical prediction to experimental observations of joints with plates having one tooth, four teeth in a column, four teeth in a row, and a complete set of teeth.

5.2.1. Joints with Four Teeth in a Row or Column

Figures 5.16 through 5.18, compare theoretical and experimental traces of individual specimens. Working stresses were calculated on the basis of the average ultimate load for each joint (39). Although the model somewhat underestimates joint stiffness below the working stress, and overestimates at high loads, the general shapes and magnitudes are similar. In modeling nonlinear behavior of wood systems, the correspondence of theoretical and empirical results shown in Figs. 5.16 through 5.18 are considered acceptable.

The underestimation of the joint stiffness at low loads is probably due to difficulties with testing in evaluating the foundation modulus. Tooth length, size, and geometry vary considerably within the truss-plate. A truly accurate representation of the foundation modulus would

Table 5.2. Summary of parameters defining foundation modulus.

JOINT TYPES	FOUNDATION TYPE	BOARD NO.	A	B	k_1	k_2	k_3	k_4	d_1	d_2	d_3
1,2,3	$*k_{0A}$	1			36000.	23200.	8100.	1200.	0.015	0.018	0.0235
		2			45800.	34800.	11700.	960.	0.015	0.0185	0.024
		3			49000.	35500.	10800.	1750.	0.015	0.019	0.024
		4			46900.	29800.	6100.	1840.	0.016	0.019	0.026
		5			46900.	31400.	8500.	2160.	0.016	0.019	0.0255
4,5,6, and 7	k_{0A}	1			42600.	28800.	10100.	1750.	0.0145	0.019	0.0265
		2			42600.	34000.	11600.	2020.	0.0145	0.019	0.027
		3			47800.	36800.	11600.	1000.	0.0135	0.0205	0.027
		4			51200.	33400.	7600.	1270.	0.016	0.022	0.031
		5			50000.	31200.	7600.	1270.	0.016	0.022	0.031
	k_{90A}	1			11200.	7150.	4000.	1330.	0.021	0.029	0.038
		2			10600.	6830.	4100.	550.	0.026	0.031	0.0365
		3			11200.	8220.	3680.	820.	0.0215	0.034	0.041
		4			13200.	9200.	5030.	900.	0.018	0.0255	0.0365
		5			12500.	8660.	4160.	1060.	0.019	0.029	0.048
	k_{0E}	1	28300.	-138400.							
		2	30000.	-112400.							
		3	35900.	-224600.							
		4	38000.	-176300.							
		5	36000.	-149200.							
	k_{90E}	1	16400.	-118600.							
		2	15700.	-79500.							
		3	16600.	-94660.							
		4	16000.	-117700.							
		5	19300.	-111500.							

$*k_{ij}$: foundation modulus for i = 0, tooth bearing on face; i = 90, tooth bearing on edge; j = A, loading parallel to grain; and j = E, loading perpendicular to grain.

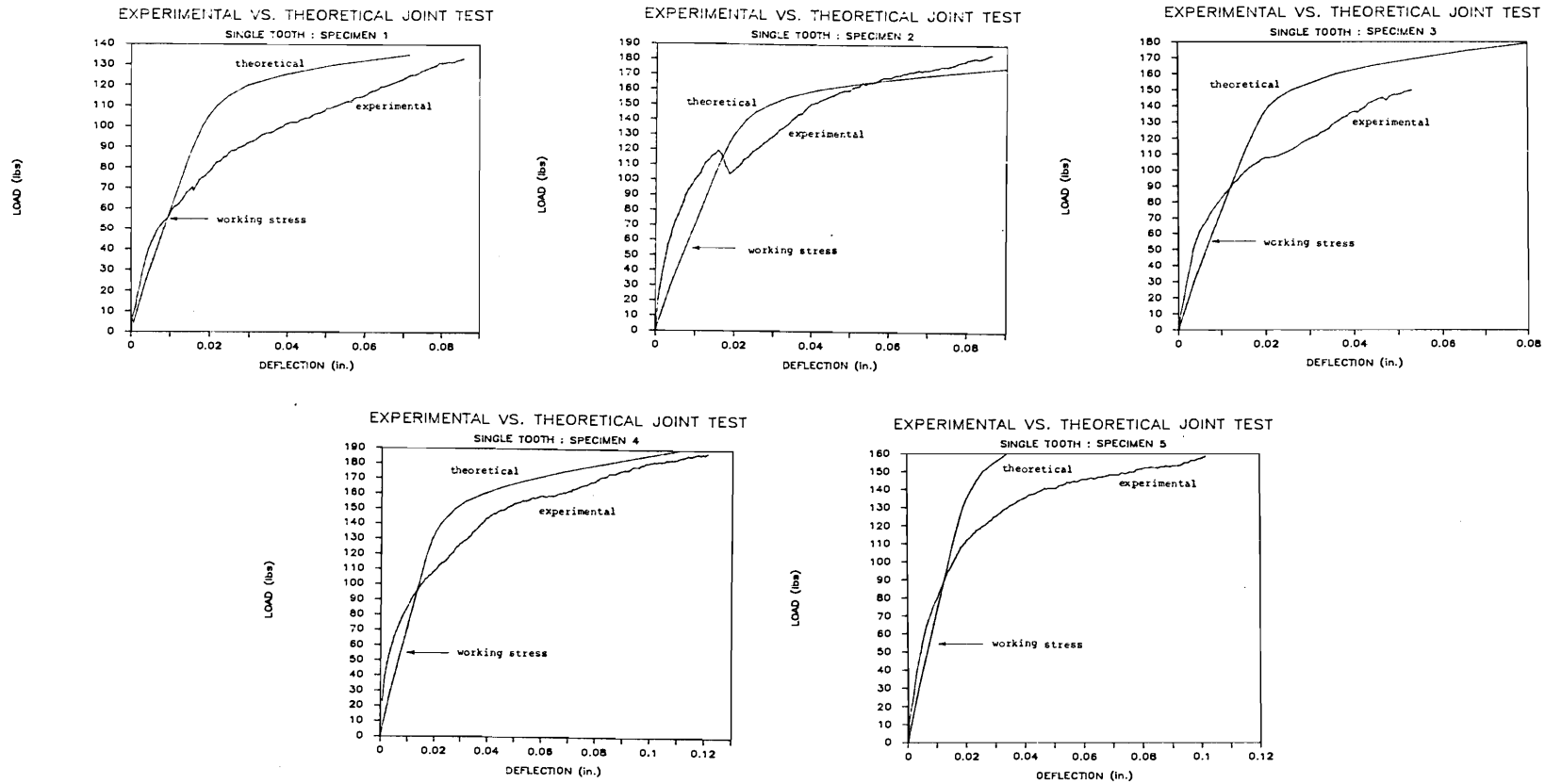

Figure 5.16. Experimental and theoretical traces for joints with one tooth (Joint type 1) with tooth face bearing on end grain.

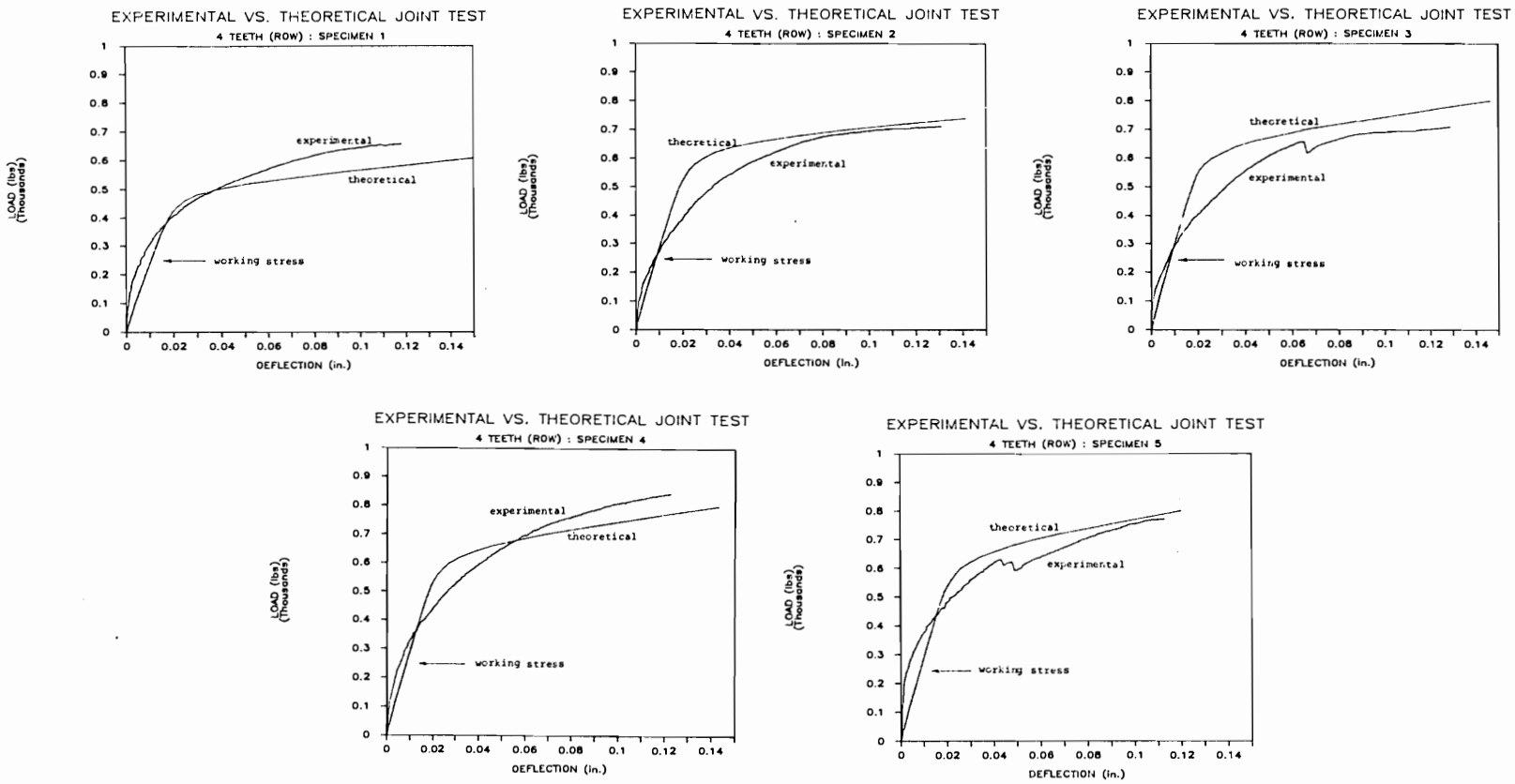

Figure 5.17. Experimental and theoretical traces for joints with 4 teeth in a row (Joint type 2) and tooth face bearing on end grain.

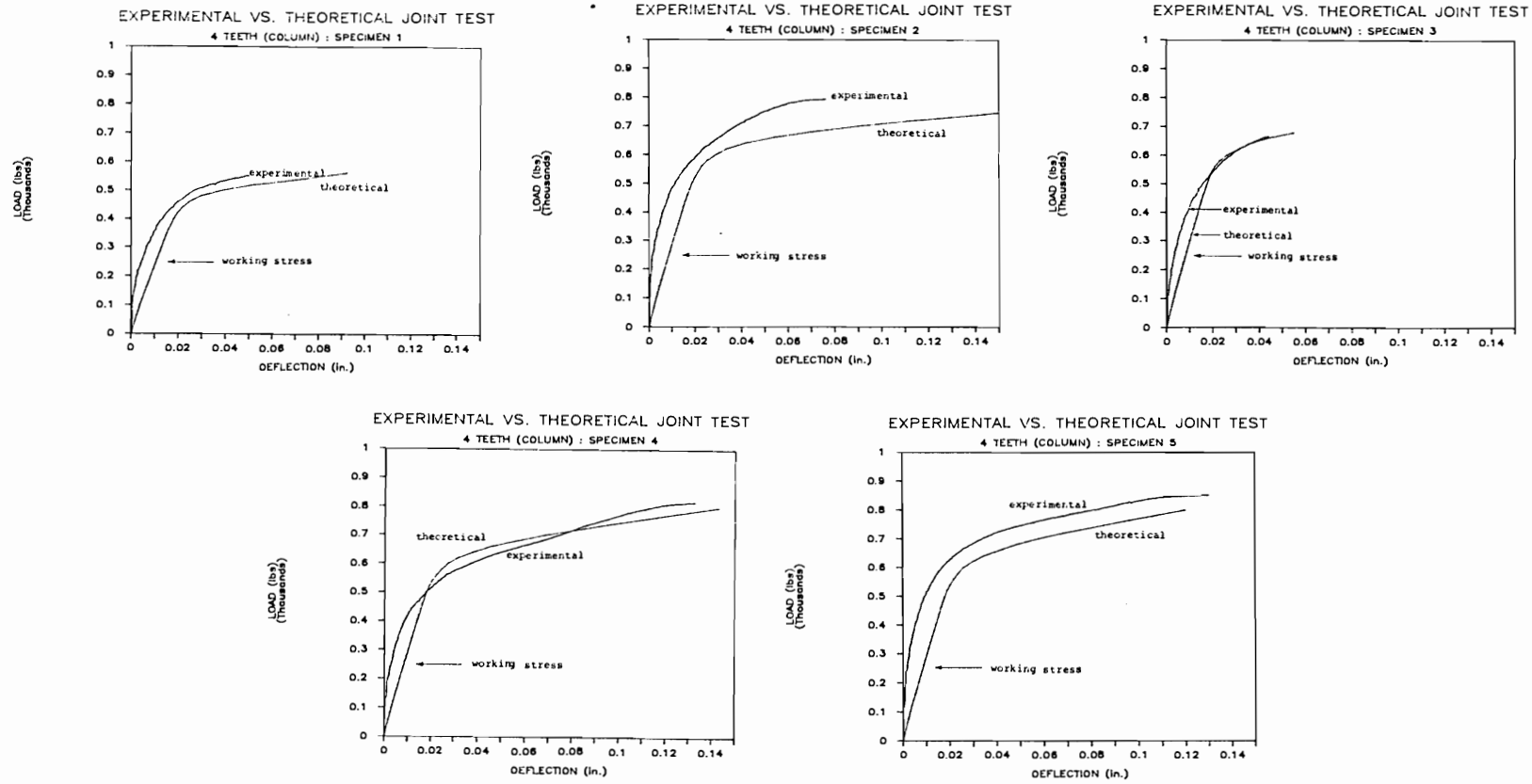

Figure 5.18. Experimental and theoretical traces for joints with 4 teeth in a column (Joint type 3) and tooth face bearing on end grain.

require removal of a statistical sample of individual teeth from a truss-plate and attaching these single teeth to a testing machine crosshead. The representative foundation modulus would then be the average of the individually tested teeth. If the predictions based on the average modulus were used in theoretical prediction, the results would be very close to the mean experimental observations. It should be noted that this reasoning applies to the entire trace length at all load levels.

No apparent difference seems to exist in the general shape of the experimental data in Figs. 5.16 through 5.18, which suggests a similar mode of failure in all 15 specimens. This failure mode can be characterized by joint failure resulting from tooth withdrawal.

Table 5.3 shows the predicted withdrawal failure loads along with the experimental ultimate loads for joint types 1, 2, and 3. The tooth furthest from the wood-wood contact in the columnar arrangement began withdrawing at approximately 80% of the ultimate load. Consequently, as the load approached failure, the same tooth withdrew first. The tooth next to it followed and then the next one resulting in a gradual withdrawal of all teeth at failure. The multiple teeth in a row which were equidistant from the wood-wood contact withdrew all at the same time when the ultimate load was reached. However, a paired t-test at the 5% significance level showed that no difference in ultimate

Table 5.3. Comparison between the theoretical and experimental ultimate loads characterized by tooth withdrawal for tooth face bearing on end grain.

SPECIMEN NO.	AVERAGE LOAD/TOOTH (lbs)			
	THEORETICAL	EXPERIMENTAL		
		TYPE 1 (single)	TYPE 2 (row)	TYPE 3 (column)
1	69.5	66.6	82.3	68.9
2	88.5	91.9	89.0	99.1
3	93.0	75.0	88.6	83.4
4	91.5	93.9	105.4	102.3
5	95.0	84.7	96.4	106.5
average	87.5	82.4	92.3	92.0

load existed between the teeth in rows and in columns despite the different failure mechanism.

The ultimate loads for column and row arrangement (Table 5.3) were averaged and tested against the loads of the single tooth showing no significant difference at the 5% signifi-cance level. However, all but one single tooth were below the failure load of specimens with teeth in rows and columns, suggesting a possibility of a smaller withdrawal load for single tooth specimens. Perhaps a larger sample size would detect this difference. The smaller ultimate load of single-tooth joints is due to their fragility. The single tooth joints were so fragile that a small but observable gap between the wood and plate developed before testing, in spite of careful handling and placement of specimens in the testing apparatus.

5.2.2. Complete Truss-Plate Joints

Figures 5.19, 5.20, 5.21, and 5.22 summarize the theoretical and experimental load-deflection traces for each specimen of the complete joint types 4, 5, 6, and 7, respectively. Tooth and grain orientation for joint type 4 was identical to types 1, 2, and 3, which permitted a further statistical comparison on the nature of load sharing in fully-toothed plates.

Traces for type 4 show a more consistent pattern than those for types 1, 2, and 3. This is because the variation

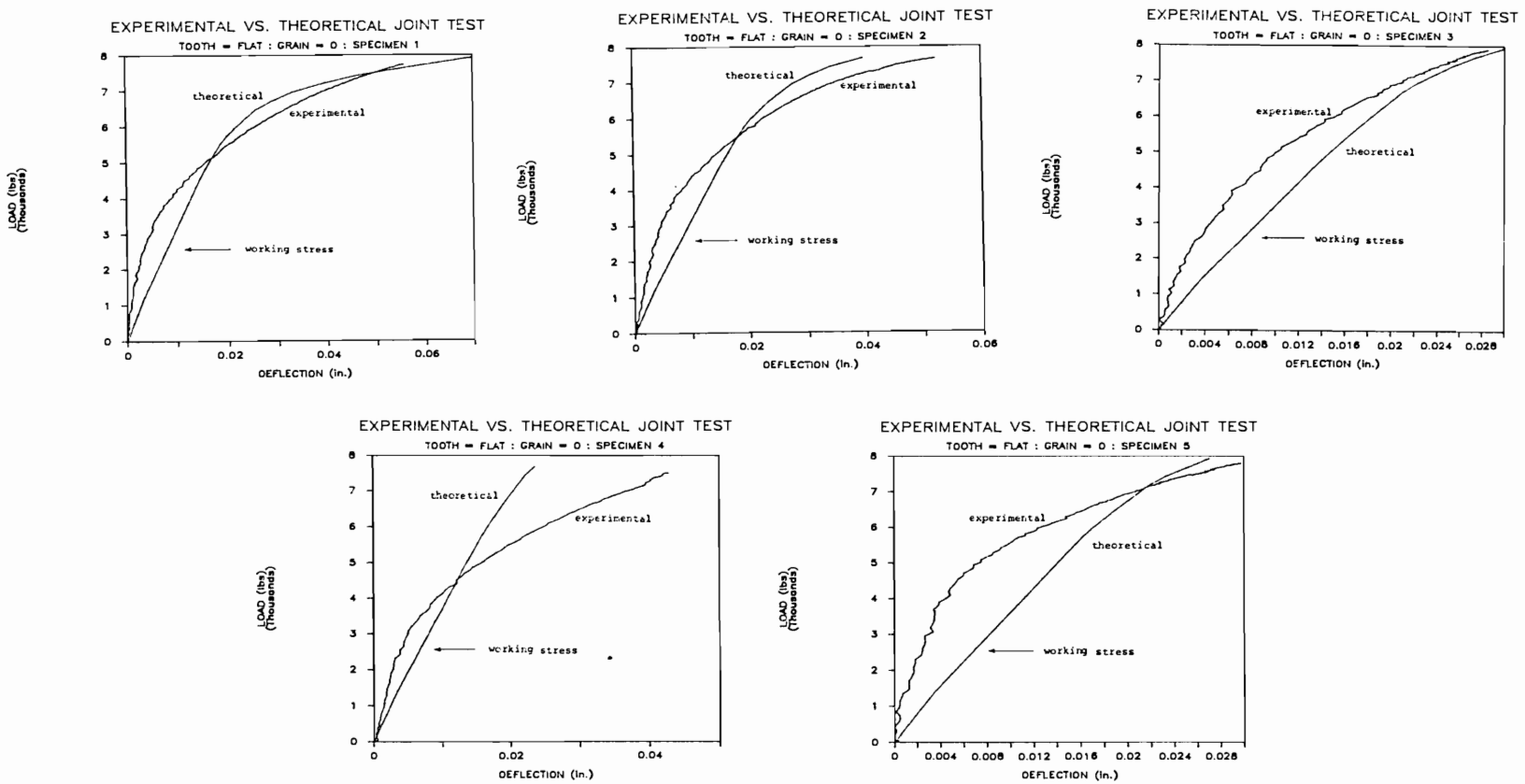

Figure 5.19. Experimental and theoretical traces for specimens 1 through 5 with tooth face bearing on end grain (joint type 4).

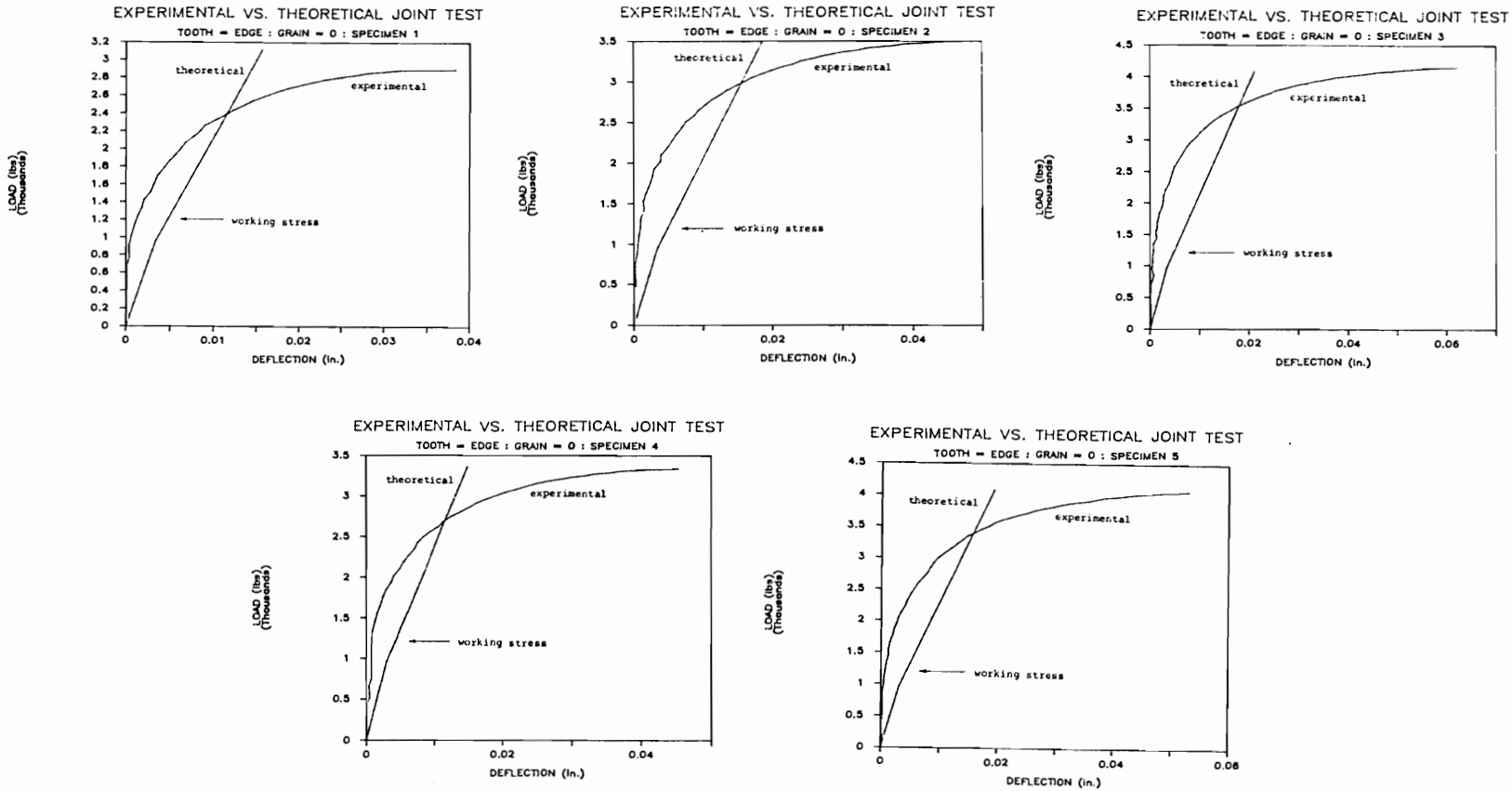

Figure 5.20. Experimental and theoretical traces for specimens 1 through 5 with tooth edge bearing on end grain (joint type 5).

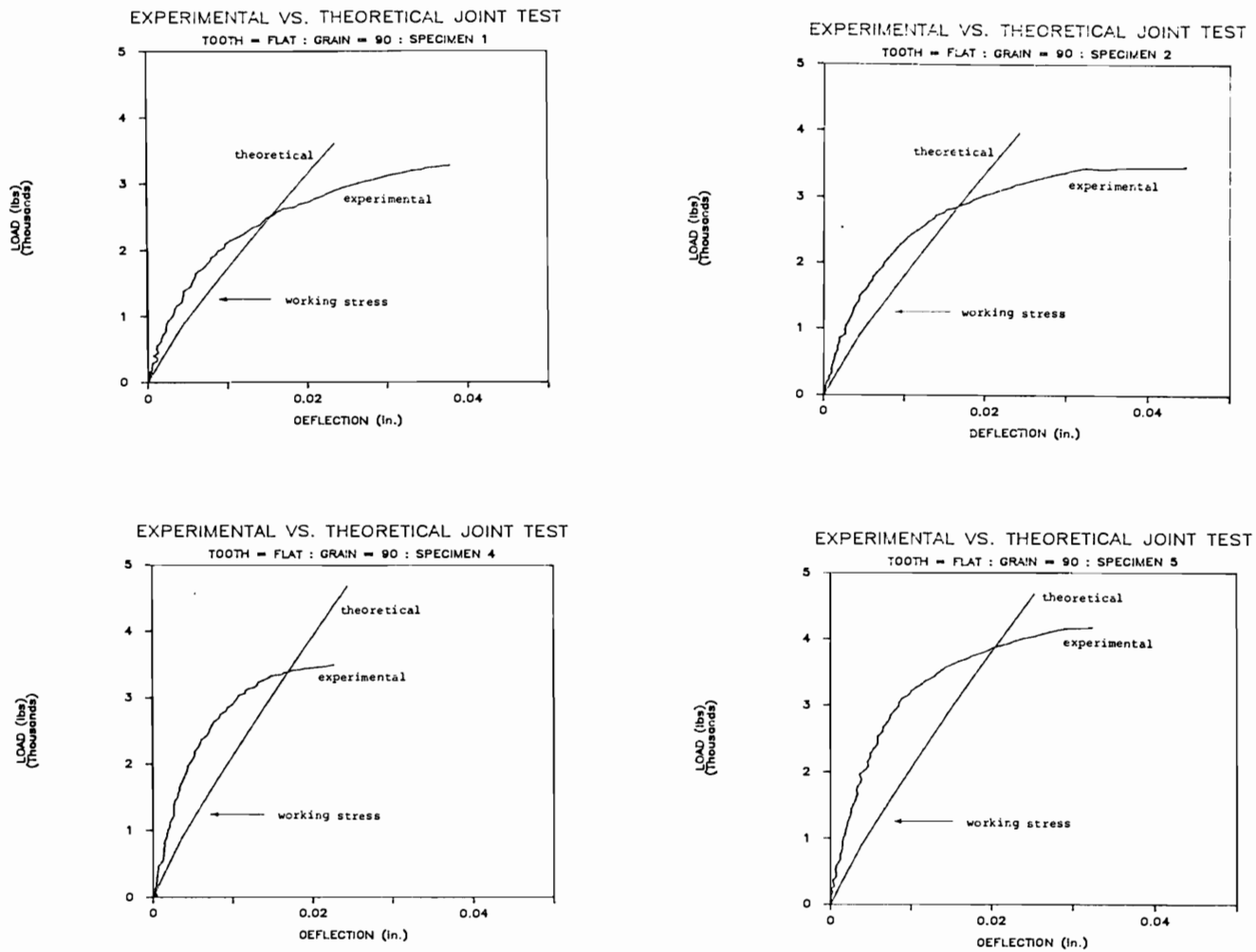

Figure 5.21. Experimental and theoretical traces for specimens 1 through 5 with tooth face bearing on side grain (joint type 6).

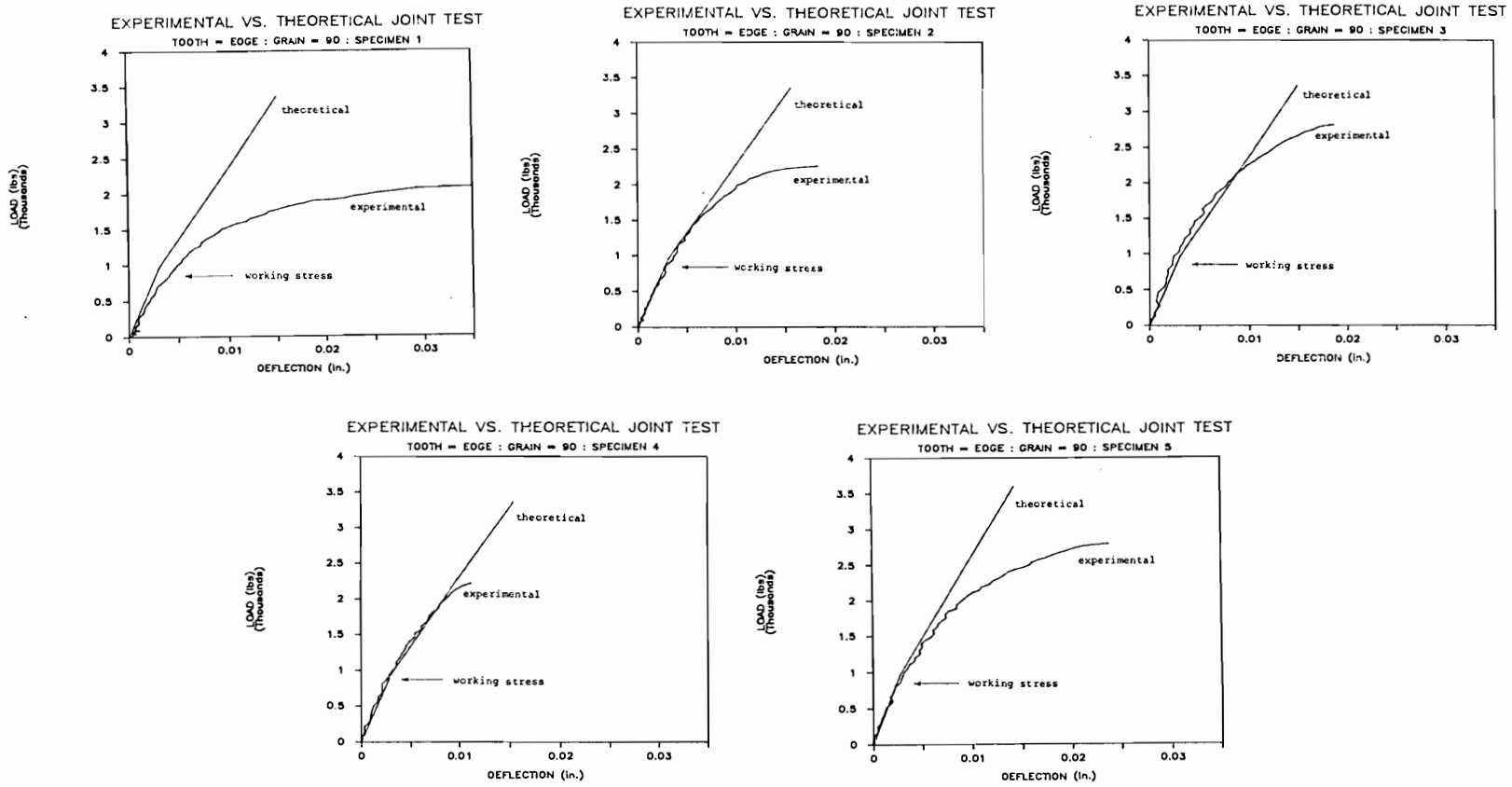

Figure 5.22. Experimental and theoretical traces for specimens 1 through 5 with tooth edge bearing on side grain (joint type 7).

in tooth size and local changes in wood foundation modulus are averaged for joints tested with fully-toothed plates. However, the general shape of the experimental and theoretical traces for test types 4 are consistent with types 1, 2, and 3 except for a sizeable decrease in the deflection at failure for type 4. The probable reason is the difference in the mode of failure. Specimens 1 and 2 exhibited wood failure by tooth withdrawal, specimens 3 and 5 failed by truss plate tensile rupture (Fig. 5.23), and testing of specimen 4 was terminated because the testing apparatus failed. Thus, the full strength of the wood in specimens 3, 4, and 5 was never reached.

Figure 5.20 shows that the theoretical model underestimates initial joint stiffness for teeth edge bearing on end grain. Although the theoretical and experimental ultimate loads are close, the shape of the curves differ. The main reason for this difference lies in the determination of the foundation modulus. The loading head used for testing specimens with tooth edge bearing was of rectangular shape with one dimension plate thickness and another tooth length. However, the die-punch process used to form the teeth substantially increases tooth thickness and thus the amount of tooth area bearing on the wood. In addition, the geometry and nonrectangular shape of the tooth in edgewise orientation also increases the bearing area especially at high load levels. As a result, the

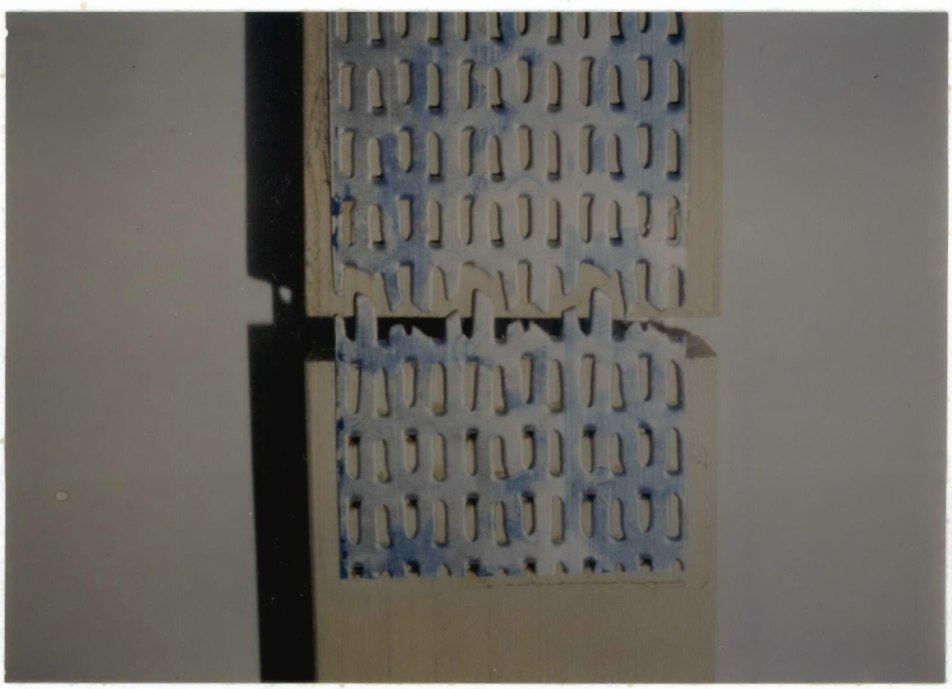

Figure 5.23. Typical failure of joint type 4 with teeth face bearing on end grain.

undersized loading head used in testing underestimated the corresponding foundation modulus at low load levels. At high load levels, sharp edges of actual teeth start cutting into wood fibers before wood crushing occurs, so that the actual joints rapidly lose their stiffness as compared to theoretical traces based on smooth edges.

The teeth bearing edgewise on end grain (type 5 specimens) had a greater resistance to rotation at their junction to the plate than the teeth bearing on face. Thus, as the loading approached ultimate loads, the moment at the tooth junction was transferred into the less stiff plate causing the plate to deform and rotate (Fig. 5.24). During this rotation, the teeth furthest from the wood-wood contact withdrew first, so that the entire load was carried by fewer teeth. This increased the moment at the remaining teeth which caused the plate to rotate more, perpetuating a chain reaction that culminated in failure.

Combined wood failure perpendicular-to-grain and plate withdrawal were the failure mechanisms for joint types 6 and 7 (Fig. 5.24). Although plate withdrawal began at about 95% of failure load, joint failure was determined by the bearing strength of the wood foundation.

The traces for joint type 6 (Fig. 2.21) show trends similar to those of type 7 (Fig. 5.22). However, the smaller difference between the theoretical and experimental traces for joint type 7 indicates that the determination of

Figure 5.24. Typical failure of joint type 5 specimen with teeth edge bearing on end grain.

Figure 5.25. Typical failure of joint types 6 and 7 illustrating wood failure.

foundation modulus to edgewise oriented teeth is less sensitive for edge bearing on side grain than on end grain. The reason is splitting of wood fibers occurs under tooth edges bearing on end grain, but splitting is absent in tooth edge bearing on side grain.

Table 5.4 compares the theoretical and experimental failure loads for joint types 4, 5, 6, and 7. The theoretical failure was based on joints reaching their withdrawal load; the tooth was assumed to withdraw where the normal component at the tooth attachment to the plate reached the frictional resistance between the wood and tooth. The failure load for specimen 4, joint type 4 was never reached due to apparatus failure. Specimen 3, joint type 6 was discarded due to equipment malfunctions.

The failure of joint type 4 was generally governed by the withdrawal strength; the model predicts the failure load of specimens 1 and 2 with sufficient accuracy, but less accurate for specimens 3 and 5 due to plate failure. Part of a problem was the selection of the coefficient of friction between the tooth and collapsed wood from tooth penetration. This coefficient is the mean value selected from a study on nailed joints; the use of the mean value did not account for variability and the collapsed wood around the tooth may differ from that around the nail.

Tooth and grain orientation for joint type 4 are same as for types 1, 2, and 3, which allows for comparison

Table 5.4. Theoretical and experimental failure loads (lbs/tooth) and mode of failure for joint types 4, 5, 6, and 7.

SPECIMEN NO.	JOINT TYPE 4			JOINT TYPE 5			JOINT TYPE 6			JOINT TYPE 7		
	Theor.	Exp.	Mode[1]	Theor.	Exp.	Mode	Theor.	Exp.	Mode	Theor.	Exp.	Mode
1	82.5	80.5	WD	59.2	60.4	WD	90.3	45.5	WF/WD	72.9	43.5	WF/WD
2	89.6	79.7	WD	56.3	73.0	WD	109.7	48.0	WF/WD	78.1	47.2	WF/WD
3	95.4	82.3	PF	56.3	86.6	WD	-	-		80.2	58.7	WF/WD
4	102.7	-		76.3	69.7	WD	127.7	48.5	WF/WD	70.8	47.1	WF/WD
5	99.4	81.2	PF	71.7	84.8	WD	129.3	58.0	WF/WD	94.2	58.3	WF/WD
average	93.9	80.9		64.0	74.9		114.3	50.0		79.2	51.0	

1: WD = plate withdrawal, PF = plate failure, and WF = wood failure perpendicular to grain.

between the test types. Joint type 1 is not included in the comparison because of the gap observed between the plate and wood member. When comparing joint type 4 to those of types 2 and 3, the following observation was made. Although the foundation modulus for joint type 4 was higher than that for joint types 2 and 3, the experimental withdrawal loads were less. This indicates a possible interaction between the teeth, which may be the result of two factors. First, the small interactive stresses that were shown by the finite element analysis to be present among the teeth arranged in columns, may be significant. Second, the possible effects of failure in wood or in steel were not included in the theoretical modeling, a point discussed in detail when evaluating the accuracy for joints 6 and 7.

Specimens of joint type 5 with teeth edges bearing on side grain all failed in withdrawal. Although a paired t-test showed no difference between the theoretical and experimental withdrawal loads at the 5% significance level, the model appears to slightly underestimate the ultimate withdrawal load. This may be due to support fixity moment at the tooth base, which caused large deformations in the plate. However, other factors may be involved, such as inaccurate estimate and large variability in the foundation modulus.

The failures of joint types 6 and 7 were characterized by wood failure in tension perpendicular-to-grain prior to tooth withdrawal or excessive wood-bearing deformation. Because failure load was based on tooth withdrawal rather than wood failure, the theoretical failure load was overestimated. Tooth withdrawal did occur, but only after wood failure.

5.3. Proposed Modifications for the Theoretical Model

5.3.1. Inclusion of Additional Failure Mechanisms

The failure criterion for the model used in this study was based on tooth withdrawal. While this is satisfactory for several teeth, it is not representative of fully-toothed plates.

A mechanism to compensate for steel failure should be included into the model to accomodate the high stresses which accumulate in the truss plate. This mechanism should address: tensile rupture of the plate, evident in some teeth face bearing on end grain specimens (joint type 4), and plate rotation, present in teeth edge bearing on end grain specimens (joint type 5).

Wood failure in tension perpendicular-to-grain was the failure mechanism for joint types 6 and 7 and should be included in the model.

5.3.2. Option for Combined Loading

A typical elbow joint showing location of loading, truss-plate, and truss-plate teeth is illustrated in Figure 5.26. Preliminary testing of these joints indicates that the theoretical model of this joint should include three distinct phases during loading. The first phase takes place when the load is first applied to the elbow joint, the wooden members rotate independently about a point on the truss plate. Under increasing load, this behavior continues until the gap separating the wooden members closes, at which time the second phase takes effect; the point of rotation starts to gradually move from the plate to the contact area between the wooden members. The third phase is characterized by joint rotation around the point in the contact area between the connected wood members.

During the first phase, the members each rotate about their own centers of rotation: determination of the centers of rotation for each member is analogous to the analysis commonly used in riveted joints (37). The center of rotation is a function of the number of teeth, the bearing area of each tooth, and the distance of these teeth from a common reference point. The contact area between members is the rotation point for the third loading phase. Interpolation can be utilized to determine the center of rotation for the second phase as it shifts between the first and third loading phases.

The total load acting on each tooth in each of the

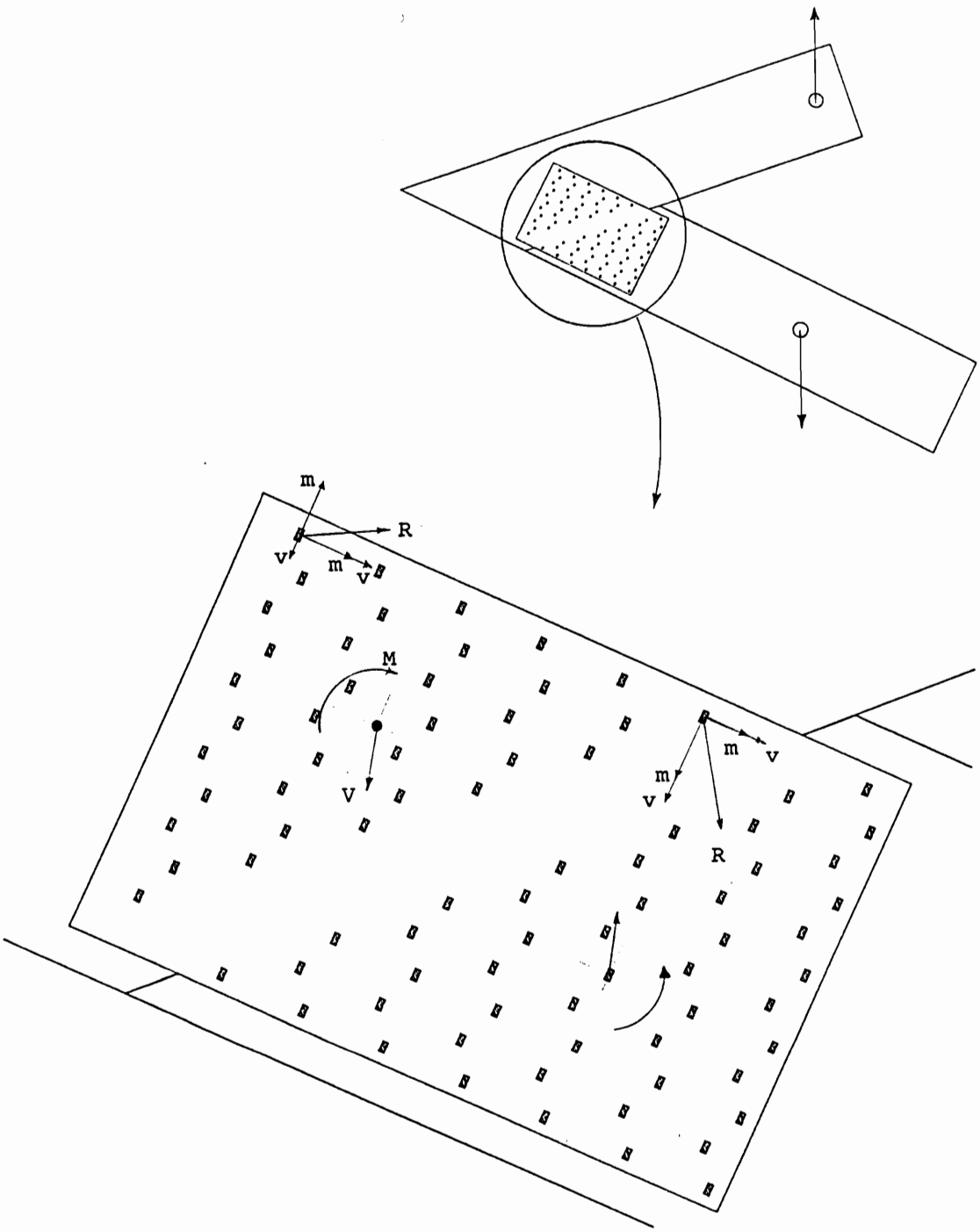

Figure 5.26. Typical elbow joint showing location of truss plate, teeth, and load application. Centers of rotation determined from shear and couple loading and resultant loads on selected teeth also shown.

three loading phases can be calculated in three steps. In the first step the shear can be divided equally among the teeth. It should be noted that the truss plate can be considered a rigid diaphragm in this analysis, allowing for an equal distribution of the shear load.

The second step involves evaluation of couple forces for each tooth that replace the moment. The force taken by each tooth depends upon its distance to the center of rotation; that is, the tooth farthest from the center of rotation takes the greatest load while the nearest tooth takes the smallest. For a nonlinear analysis, the load carried by each tooth due to the couple forces is also dependent on the current value of the foundation modulus. Nonlinear effects can be included by a linear step-by-step approach and iteration.

The third step adds the shear and couple loads vectorially to obtain the resultant load on each tooth (Fig. 5.26).

The displacements of several teeth (Fig. 5.26) with their resultant loads, could be calculated using beam-on-elastic-foundation theory described in Section 3.2. These deflections could then used to calculate the relative slip between the wooden members near the load application. A technique using Hankinson's formula, originally used by Foschi (12), can be adapted to determine the foundation modulus for teeth at various grain and plate angles. The

moment of inertia for the teeth at various angles could be transformed using Mohr's circle techniques.

5.4. Sensitivity Analysis: Effects of Material Properties

The shape of the theoretical load-displacement traces and the failure load due to withdrawal are primarily dependent on foundation modulus and friction coefficient. This section deals with the effect of these properties on the theoretical model.

5.4.1. Effect of Foundation Modulus on Theoretical Model

The foundation modulus in this study was determined from embedding simulated teeth into wood. These embedment tests demonstrated wide variability for foundation moduli among identical boards (Appendix D). In addition, the foundation moduli represent only one tooth shape and length, whereas in actuality several tooth shapes and lengths exist in each plate. These conditions make an accurate determination of foundation modulus for each tooth difficult at best. Therefore, a sensitivity study concerning the effect of foundation modulus on the theoretical model was conducted.

The sensitivity study for tooth face bearing on end grain was carried out for joint types 4, 5, 6, and 7 with wood used in constructing specimen No. 1 (Fig. 5.10). The foundation moduli were multiplied by 0.6, 0.7, 0.8, 0.9,

1.0, 1.1, 1.2, and 1.3 while the limits of linear region's load-deflection traces remained unchanged. Because Douglas-fir lumber used in this study has above average strength and stiffness, the sensitivity analysis was weighted towards the lower foundation moduli so as to encompass less dense commercial species such as western hemlock, spruce, and firs.

Results from the sensitivity analysis show that the foundation modulus alters the shape of the load-displacement traces for the same load, resulting in increased deflections for decreased foundation moduli (Fig. 5.27). These larger deflections for a given load equate to larger rotations at the tooth-plate interface, which in turn cause larger withdrawal loads.

Figures 5.28 and 5.29 show the effect of foundation modulus on complete tooth displacement and rotation. Large rotations at constant load levels result in increased withdrawal loads, explaining why the foundation modulus has a proportional effect on the theoretical failure load (Fig. 5.30).

Displacement at the theoretical failure load shows a similar proportional trend (Fig. 5.31). Smaller displacements at failure are present from these decreased foundation moduli, the result of decreased failure loads.

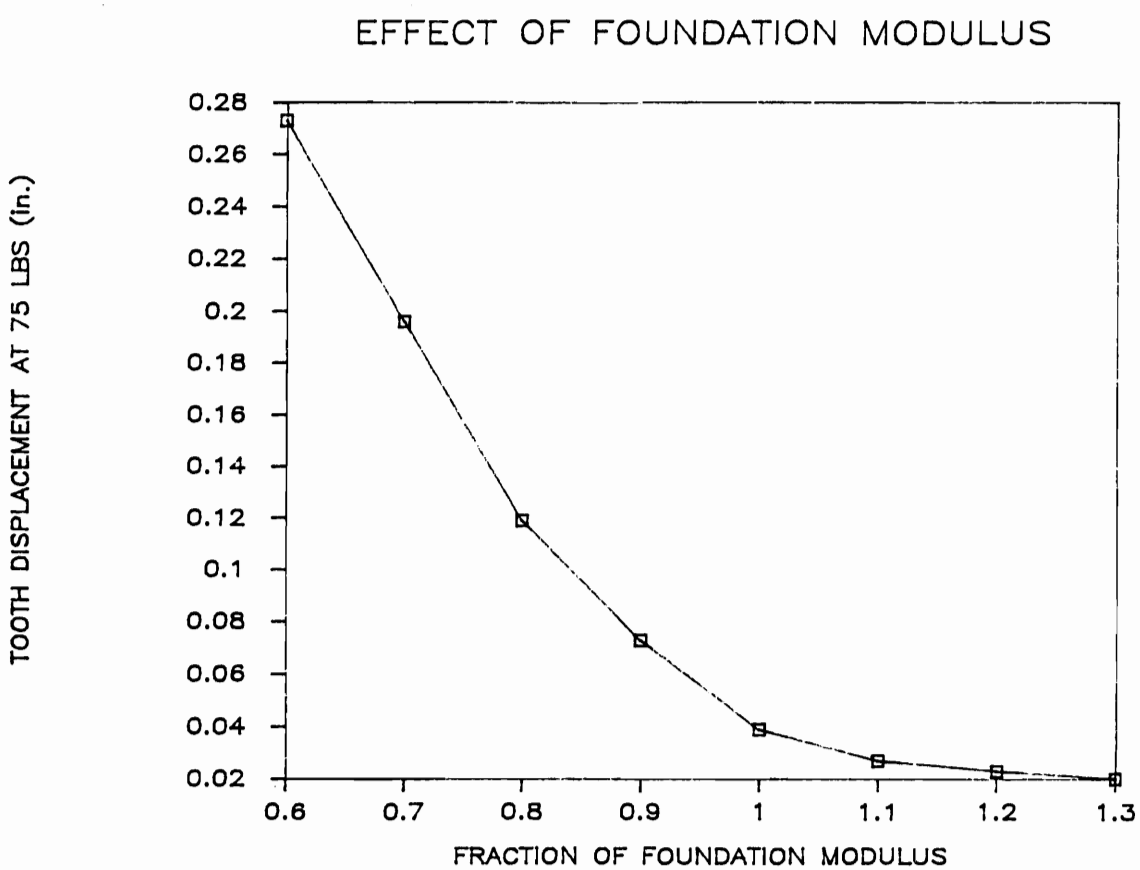

Figure 5.27. Effect of foundation modulus on the theoretical displacement at 75 lb. load per tooth for a truss-plate joint with teeth face bearing on end grain.

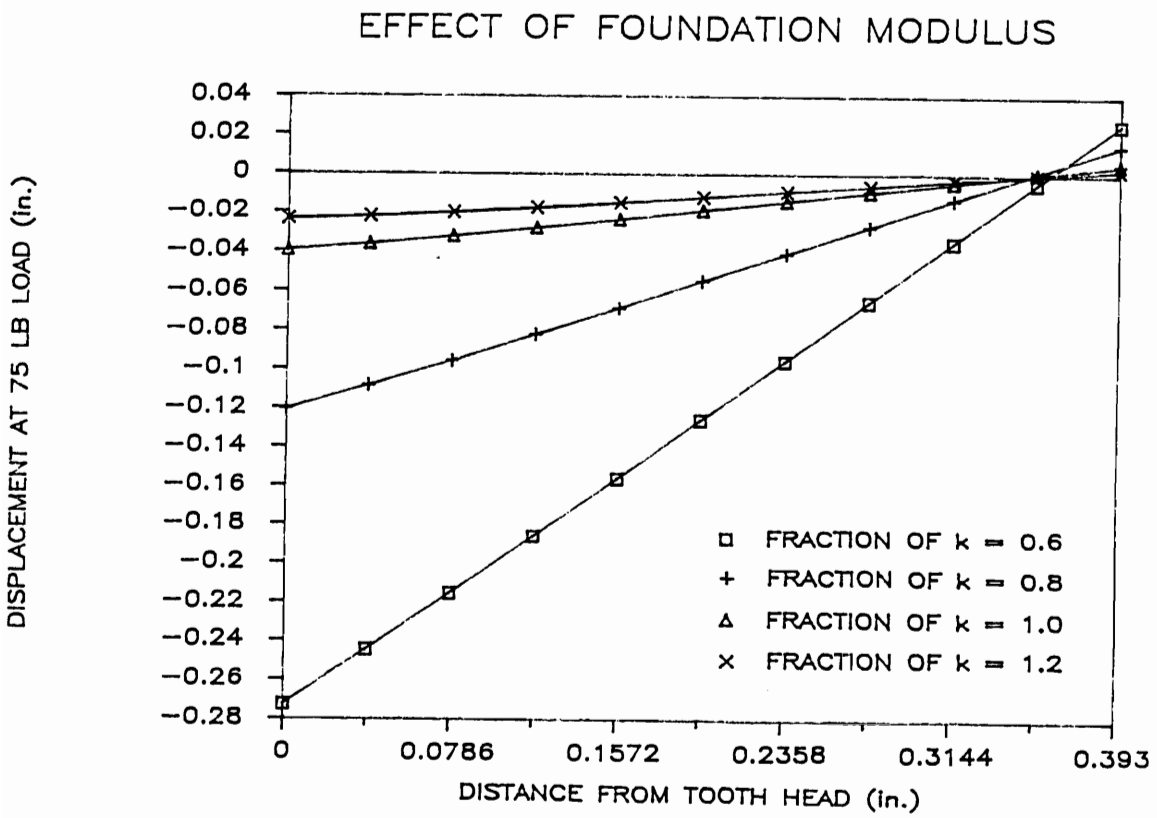

Figure 5.28. Effect of foundation modulus on the deflected tooth shape for a tooth embedded in wood with face bearing on the end grain at a constant load of 75 lb. Displacement values are given along tooth length from tooth head (tooth-plate juncture) to the tooth end (0.393 in.).

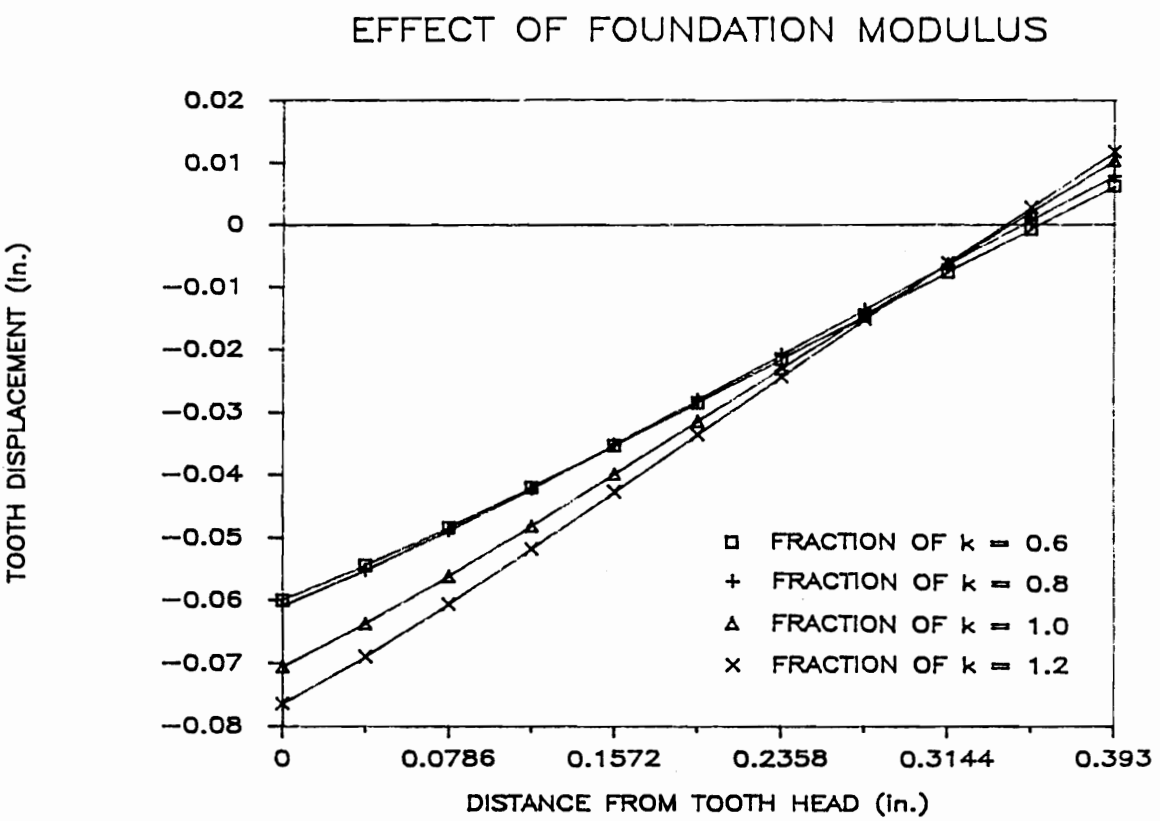

Figure 5.29. Effect of foundation modulus on the deflected tooth shape at failure load. The tooth is embedded in wood with face bearing on the end grain and displacements are given along tooth length from tooth head (tooth-plate juncture) to the tooth end (0.393 in.).

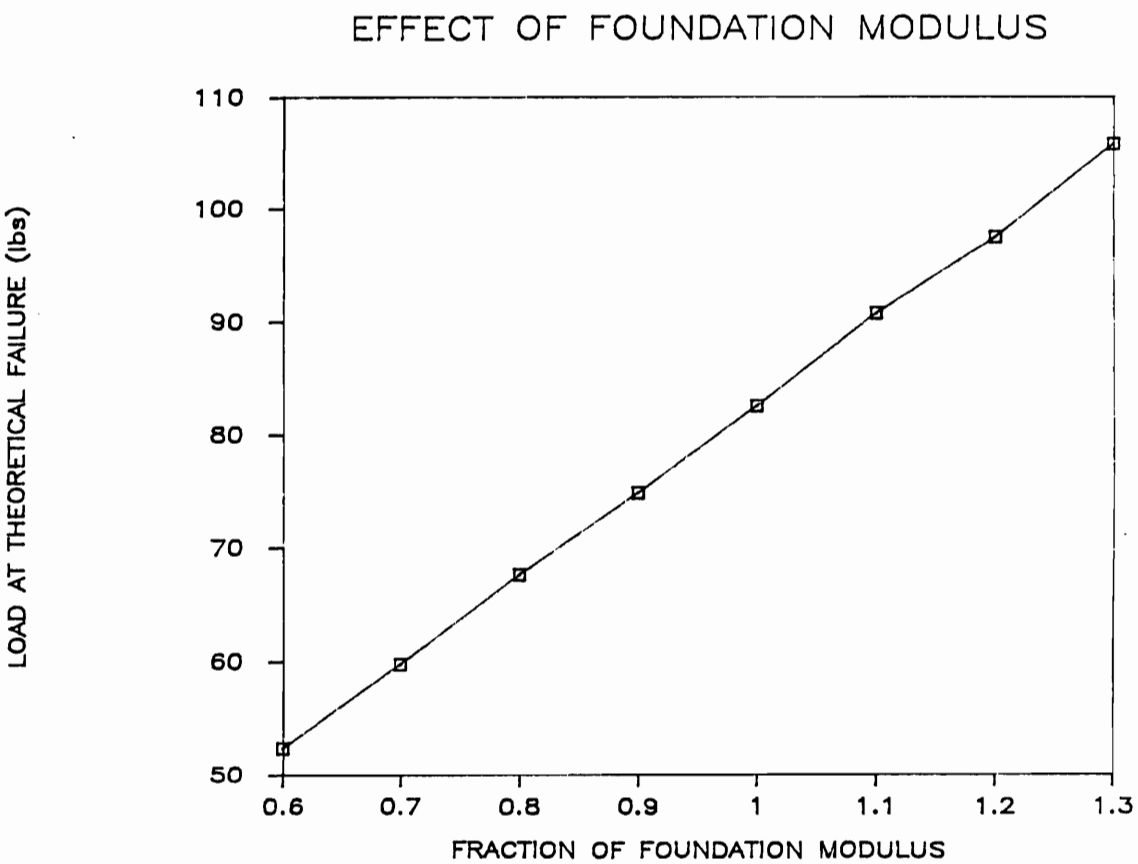

Figure 5.30. Effect of foundation modulus on the joint failure for tooth face bearing on end grain.

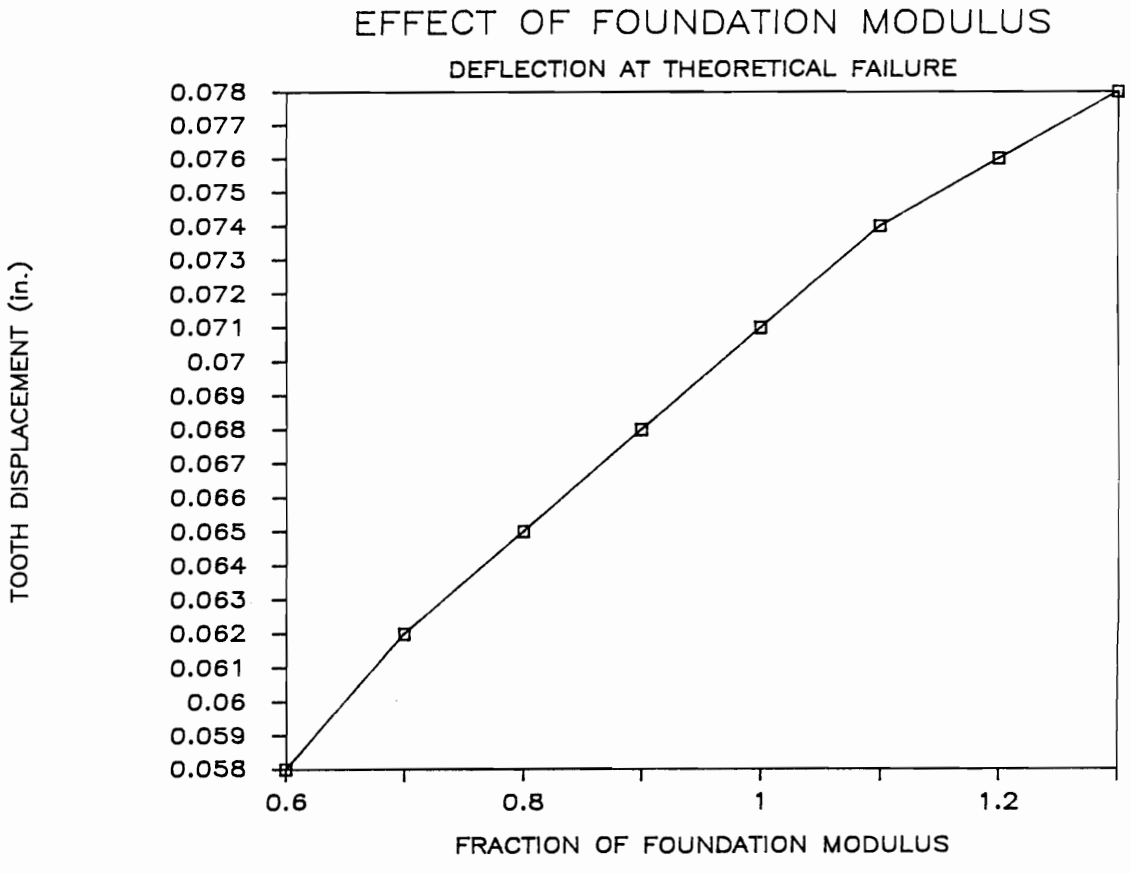

Figure 5.31. Effect of foundation modulus on joint displacement at failure for tooth face bearing on end grain.

5.4.2. Effect of Friction Coefficient

The friction coefficient used in the theoretical model was obtained from the work done by Atherton (4). He derived his friction coefficient value of 0.385 using 6d smooth common nails and Douglas-fir. He found no difference in friction coefficient between radial or tangential grain and a coefficient of variance of about nine percent, suggesting that friction coefficient does not vary much with grain orientation or between specimens.

This dissertation used the value reported by Atherton because of a similar steel-on-wood friction arrangement. However, the surface and shape between smooth, common nails and truss-plate teeth are not identical. In addition, truss plates are a proprietary item with the tooth construction varying among manufacturers. The complexity of tooth-wood friction is complicated further by the addition of epoxy to the tooth which binds with the wood during pressing (25). The results from tooth withdrawal tests (Appendix F) show that the withdrawal stiffness increases approximately 25% and the withdrawal strength increases approximately 75%. Thus a sensitivity study was conducted to determine the effect of friction coefficient on the theoretical load-displacement traces.

Figure 5.32 shows that the friction coefficient has very little effect on the shape of the tooth under a given load. That is because the friction coefficient determines

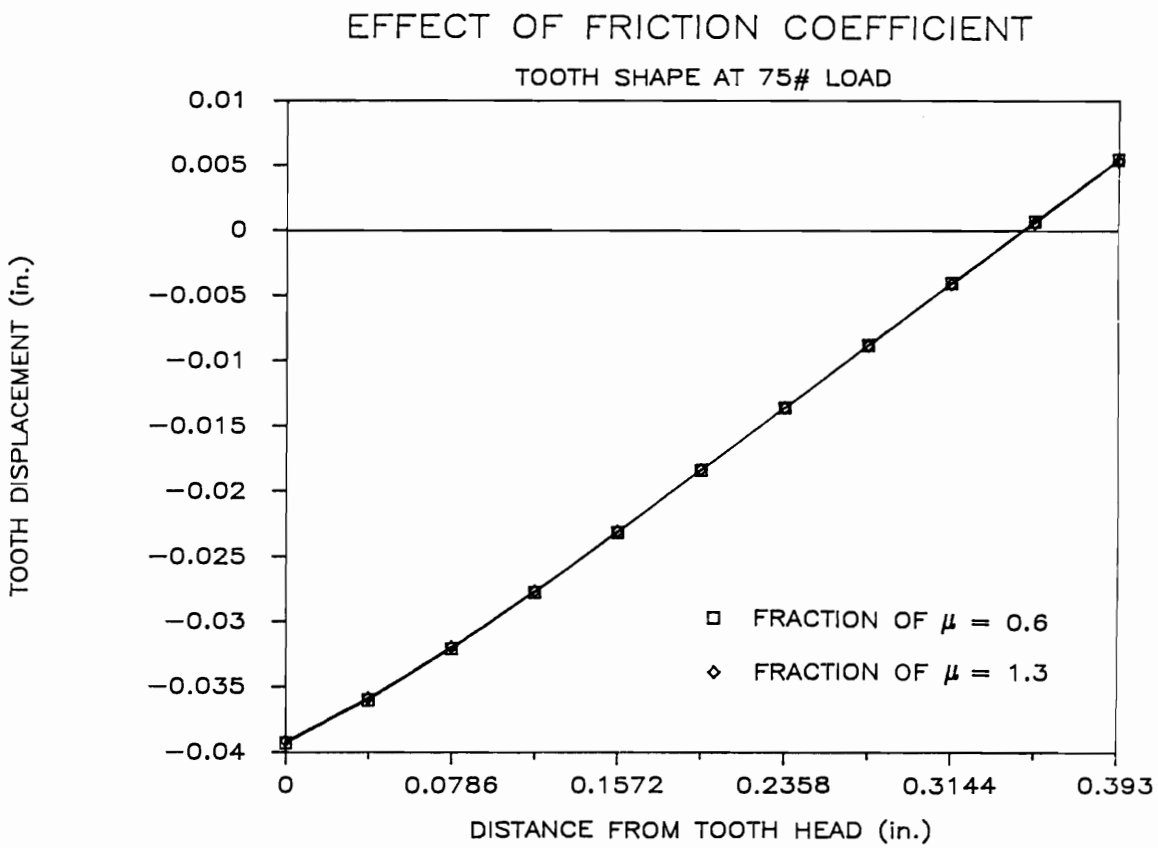

Figure 5.32. Effect of friction coefficient on the deflected tooth shape for a tooth embedded in wood with face bearing on the end grain at a constant load of 75 lb. Displacement values are given along tooth length from tooth head (tooth-plate juncture) to the tooth end (0.393 in.).

the withdrawal resistance of the tooth and has no effect on the foundation. However, when withdrawal resistance governs failure mode, the failure load is altered because of the change in withdrawal resistance (Fig. 5.33). As friction coefficient increases, the load required to overcome the frictional resistance decreases, resulting in a lower theoretical failure load.

It should be noted that the deflected tooth shape of Figure 5.32 illustrates the tooth stiffness. The vast majority of the tooth strain occur within the 25% of the tooth length closest to the plate. The deflected tooth shape in this region is concave up due to the fixity moment restricting tooth rotation. The deflected shape without the restraining moment would be concave down due to its unrestrained rotation (28).

A decrease in deflection at failure load is also present with a decrease in friction coefficient (Figs. 5.34 and 5.35). As was the case with foundation modulus, this decrease is because of the decreased load required to overcome frictional resistance.

5.4.3. Interaction Between Effects of Changes in Foundation Moduli and Friction Coefficients

The influence of foundation modulus and friction coefficient on truss-plate joint performance is difficult to identify directly from failure load and displacement at

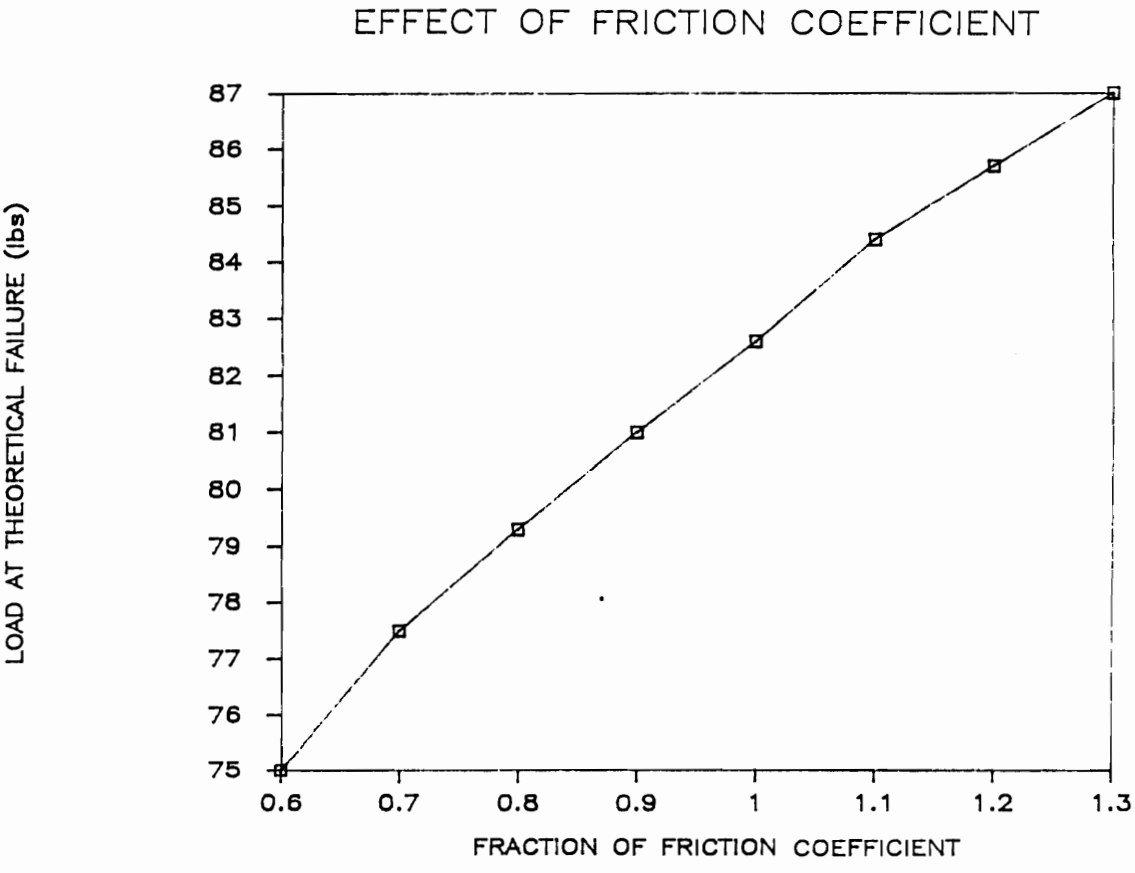

Figure 5.33. Effect of friction coefficient on joint failure load with tooth face bearing on end grain.

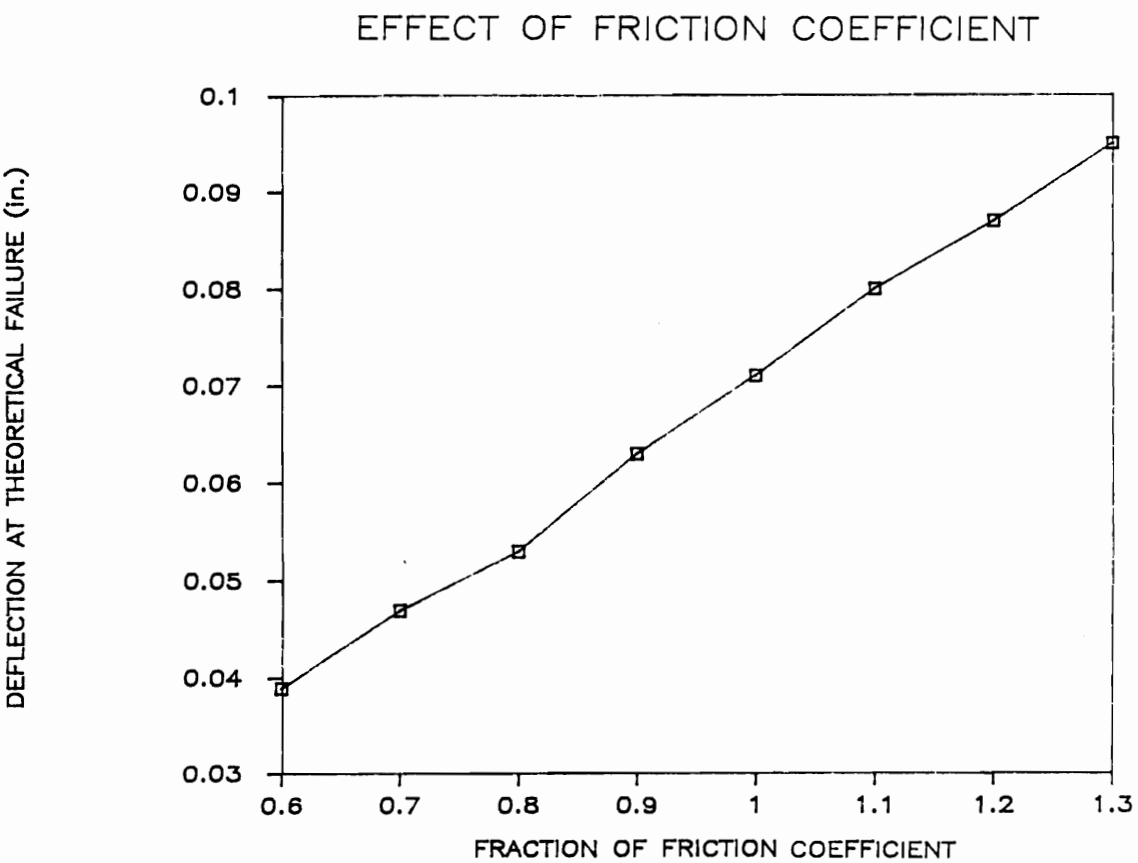

Figure 5.34. Effect of friction coefficient on joint displacement at failure with tooth face bearing on end grain.

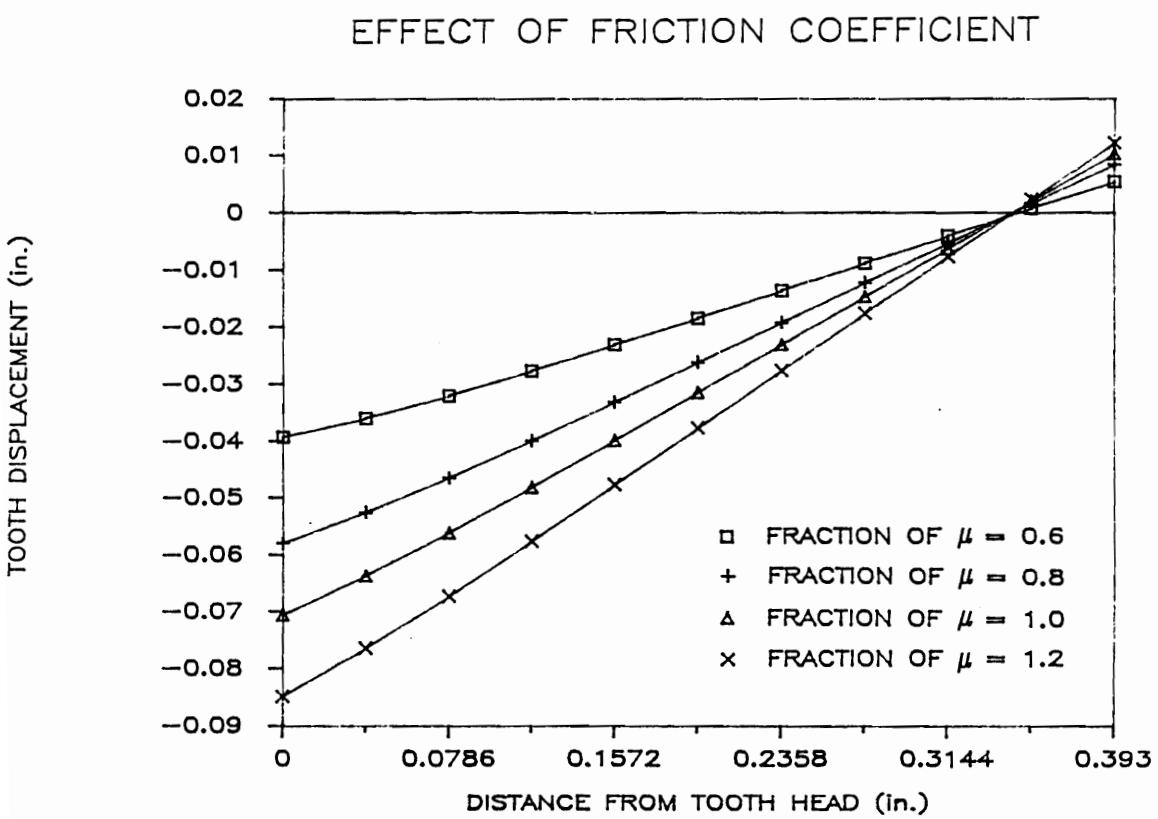

Figure 5.35. Effect of friction coefficient on the deflected tooth shape at failure load. The tooth is embedded in wood with face bearing on the end grain. Displacement values are given along tooth length from tooth head (tooth-plate juncture) to the tooth end (0.393 in.).

failure. Therefore, load and deflection factors are introduced:

$$\text{load factor} = \frac{\text{load}_{k_i,\ _i,\ \text{or}\ k_{i\ i}}}{\text{load}_{k_{1.0\ 1.0}}} \tag{5.3}$$

$$\text{displacement factor} = \frac{\text{displacement}_{k_i,\ _i,\ \text{or}\ k_{i\ i}}}{\text{displacement}_{k_{1.0\ 1.0}}} \tag{5.4}$$

in which load and displacement are at joint failure and subscripts k_i and μ_i identify the fraction of the modified parameter.

Table 5.5 illustrates changes in failure load and displacement at failure of truss-plate joints when one or both parameters are modified. Factors identified as "direct" are based on Eqs. (5.3) and (5.4) and the results of joint analysis. Factors identified as "product" are the product of the appropriate factors for single modifications. When a pair of "direct" or "product" factors is of almost the same magnitude, the modified parametets have no or negligible coupling or influence on one another.

Table 5.5 shows little difference between factors for two parameter changes and for individual parameter changes. This suggests that a negligible interaction results from coupling effects of foundation modulus and friction coefficient. This is because both parameters engage

Table 5.5. Effects of single- and multiple-parameter changes of foundation modulus, k, and friction coefficient, μ, for failure load and deflection at failure for tooth faces bearing on end grain.

Case	SINGLE PARAMETER FACTORS			
	k			
	1.3	0.6	1.3	0.6
LOAD	1.28	0.63	1.05	0.91
DEFLECTION	1.10	0.82	1.34	0.55

Case	MULTIPLE PARAMETER FACTORS			
	k1.3		k0.6	
	1.3	0.6	1.3	0.6
LOAD (Direct)[a]	1.35	1.15	0.66	0.57
(Product)[b]	1.34	1.16	0.67	0.58
DEFL (Direct)	1.46	0.62	1.10	0.44
(Product)	1.47	0.60	1.09	0.45

[a]Computed from theoretical tooth load and deflection.
[b]Product of corresponding factors for single modification.

independent mechanisms; foundation modulus controls the wood and tooth displacement, whereas friction coefficient dictates the force resisting tooth withdrawal.

Table 5.5 and Figure 5.36 demonstrate that foundation modulus affects the failure load considerably more than friction coefficient. Changing the friction coefficient in the range from 0.6 to 1.3 results in only a 10% increase in the failure load, whereas this same change in foundation modulus results in an increase of more than 100%.

Tooth displacement at theoretical failure is affected more by friction coefficient than foundation modulus (Fig. 5.37). This is due to the inability of the friction coefficient to alter the deflected shape of the tooth (Fig. 5.32). The friction coefficient thus affects the failure load which indirectly alters the deflection at failure. The foundation modulus has an even greater effect on the failure load, but in addition affects the deflected tooth shape. This deflection due to the altered tooth shape nullifies the sizable deflection changes due to the failure load.

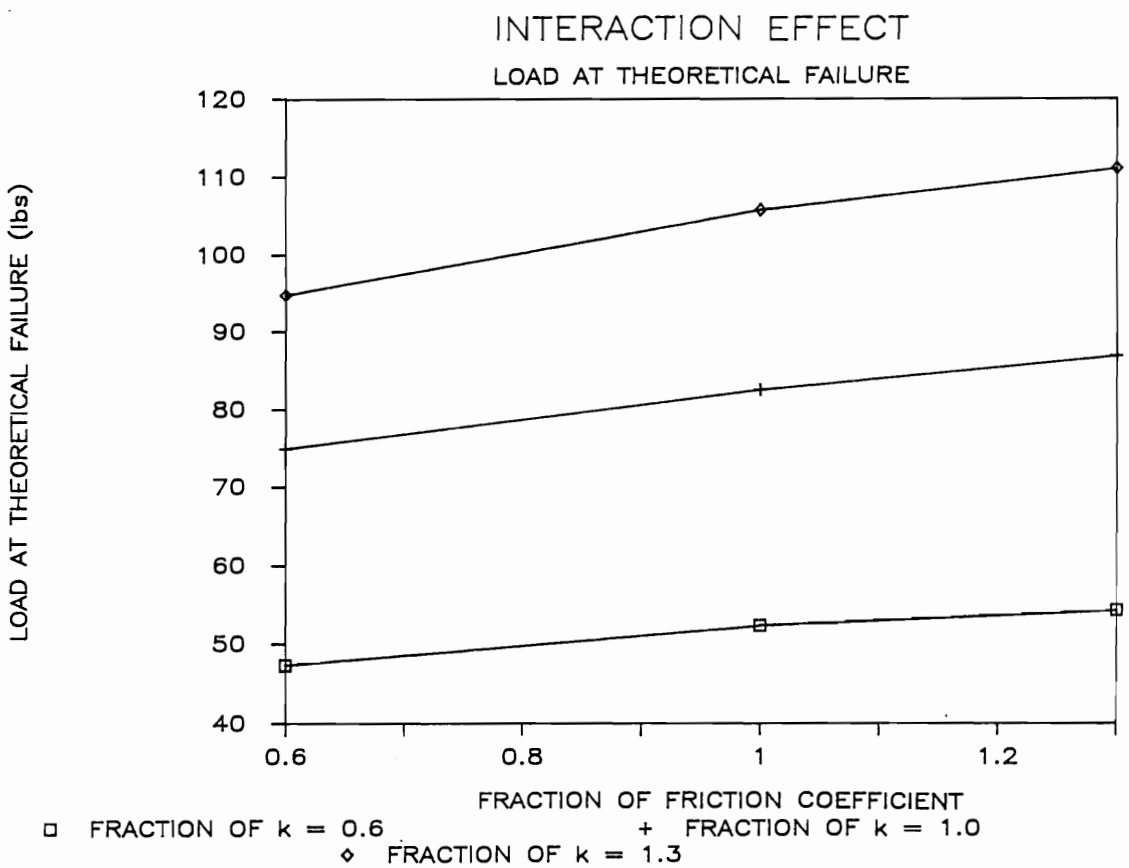

Figure 5.36. Interaction between foundation modulus and friction coefficient in terms of failure load of joints with tooth face bearing on end grain.

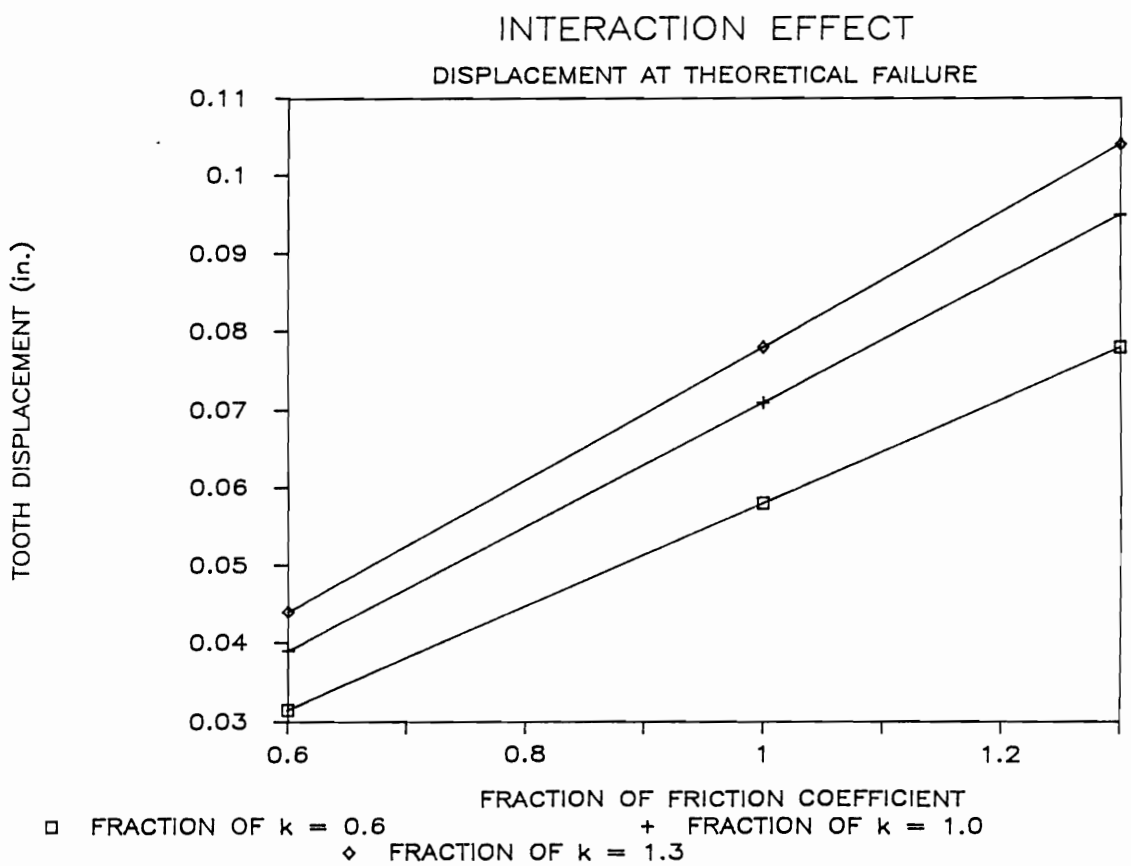

Figure 5.37. Interaction between foundation modulus and friction coefficient in terms of displacement at failure load of joints with tooth face bearing on end grain.

VI. CONCLUSIONS AND RECOMMENDATIONS

6.1. Conclusions

The conclusions drawn from this investigation pertain to the theoretical and experimental findings. The conclusions derived on the basis of the theoretical investigation are:

1. The developed theoretical model based on the beam-on-elastic-foundation analogy accurately predicts ultimate load in tooth-withdrawal mode, but overestimates ultimate load for plate and wood rupture modes. When a joint fails due to plate rupture or rotation, the model accurately predicts joint stiffness until the plate ruptures or rotates, but not the failure load. Similarly, when failure is caused in wood rupture (in tension perpendicular-to-grain), the model predicts the experimental load-deflection traces until the wood fails.
2. The Runge-Kutta numerical technique can be successfully used to solve differential equations governing the interaction between the plate tooth and wood.
3. The finite element model of plate joints with teeth faces bearing on end grain showed that higher stresses are produced in wood than those produced

by edges bearing on end grain.

4. For stresses close to collapse loads, the finite element analysis showed that when teeth in columns bear with their faces on end grain, stresses develop at a higher rate than when teeth bear on edges. This results in more stress overlapping among teeth for edge- than face-bearing teeth.
5. Finite element analysis also showed that teeth in rows display no interaction regardless of tooth orientation.
6. In the analysis based on the analogy of beam on elastic foundation, tooth withdrawal can be predicted by monitoring the developing frictional forces between the tooth and wood under stepwise loading.
7. The Runge-Kutta technique allows the analysis of teeth bearing on wood when the foundation modulus and the tooth moment of inertia vary along the tooth length.
8. A sensitivity study showed that an increase in foundation modulus: (a) decreases the amount of deflection for a given load; (b) increases the failure load; (c) increases the deflection at failure; and (d) changes the shape of the deflected tooth.

9. A sensitivity study showed that an increase in the friction coefficient: (a) has little effect on the deflection for a given load; (b) increases the failure load; (c) increases the deflection at failure; and (d) has little effect on the deflected tooth shape.
10. A sensitivity study indicated than a negligible interaction is present between foundation modulus and friction coefficient. However, foundation modulus has a much greater effect on failure load and deflection for a given load than the friction coefficient.

The following conclusions were derived on the basis of the experimental investigation:

1. Embedment tests show that teeth which bear on end grain behave linearly up to 90% of failure load, whereas teeth that bear on side grain behave entirely nonlinearly throughout the loading range.
2. When tooth faces bear on end grain, joints consisting of four teeth in a row have the same failure load as those arranged in a column, although their failure mechanism differs.
3. Testing single-tooth truss-plate joints is difficult because of the fragile nature of the joint specimens.

BIBLIOGRAPHY

1. American Society for Testing and Materials. 1986. Standard Methods of Testing Small Clear Specimens of Timber. ASTM D143-83. Annual Book of ASTM Standards, Vol. 04.09.

2. American Society for Testing and Materials. 1986. Standard Methods of Testing Mechanical Fasteners in Wood. ASTM D1761-77. Annual Book of ASTM Standards, Volume 04.09.

3. American Society for Testing and Materials. 1986. Standard Test Methods for Moisture Content of Wood. ASTM D2016-74. Annual Book of ASTM Standards, Vol. 04.09.

4. Atherton, J. C. 1982. Model for the Prediction of Nail Withdrawal Stiffness. M.Sc. Thesis, Forest Products, Oregon State University.

5. Aune, P. and Patton-Mallory, M. 1986. Lateral Load-Bearing Capacity of Nailed Joints Based on the Yield Theory: Theoretical Development. USDA Forest Service Forest Prod. Lab. Research Paper FPL-469.

6. Aune, P. and Patton-Mallory, M. 1986. Lateral Load-Bearing Capacity of Nailed Joints Based on the Yield Theory: Experimental Verification. USDA Forest Service Forest Prod. Lab. Research Paper FPL-470.

7. Beedle, L. S. 1958. Plastic Design of Steel Frames. John Wiley & Sons, Inc.

8. Beineke, L. A. and Suddarth, S. K. 1979. Modeling Joints Made with Light-Gage Metal Connector Plates. Forest Prod. J., Vol. 29(8): 39-45.

9. Canadian Standards Association. 1980. Methods of Test for Evaluation of Truss Plates Used in Lumber Joints. CSA Standard S347-M1980.

10. Cook, R. D., and Young, W. C. 1985. Advanced Mechanics of Materials. MacMillan Publishing Company

11. Egerup, A. R. 1979. European Practice and Future Development in the Design of Metal Plate Connected Wood Trusses. Proceedings, Metal Plate Wood Truss Conference. Forest Prod. Res. Soc., Madison, WI. pp. 117-122.

12. Foschi, R. O. 1974. Load-Slip Characteristics of Nails. Wood Science, Vol 7(1): 69-76.

13. Foschi, R. O. 1977. Analysis of Wood Diaphragms and Trusses. Part I: Diaphragms. Can. J. Civ. Eng. Vol. 4: 345-352.

14. Foschi, R. O. 1977. Analysis of Wood Diaphragms and Trusses. Part II: Truss-plate Connections. Can. J. Civ. Eng., Vol. 4: 345-352.

15. Foschi, R. O. 1979. Truss Plate Modeling in the Analysis of Trusses. Proc., Metal Plate Wood Truss Conference. Forest Prod. Res. Soc., Madison, WI. pp. 88-97.

16. Foschi, R. O. and Bonac, T. 1977. Load-Slip Characteristics for Connections with Common Nails. Wood Science, Vol 9(3): 118-123.

17. Foschi, R. O. and Longworth, J. 1975. Analysis and Design of Griplam Nailed Connections. J. Struc. Div., ASCE, Vol. 101, No. ST12, Proc. Paper 11766. December, 1975. pp. 2537-2555.

18. Hetenyi, M. 1946. Beams on Elastic Foundation: Theory with Applications in the Fields of Civil and Mechanical Engineering. The University of Michigan Press.

19. Hirai, T. 1983. Nonlinear Load-Slip Relationship of Bolted Wood-Joints with Steel Side-Members II. J. of Japan Wood Res. Soc., Vol. 29(12): 839-844.

20. Hirai, T. 1985. Nonlinear Load-Slip Relationship of Bolted Wood-Joints with Steel Side-Members III. J. of Japan Wood Res. Soc., Vol. 31(3): 165-170.

21. Hornbeck, R. W. 1975. Numerical Methods. Quantum Publishers.

22. Keenan, F. J., Suddarth, S. K., and Nelson, S. A. 1983. Wood Trusses and Other Manufactured Structural Components. Proceedings of the Workshop on Structural Wood Research (Milwaukee, Wisconsin). Published by the ASCE, New York, NY 10017. pp. 173-186.

23. Ketter, R. L. and Sherwood, P. P. 1969. Modern Methods of Engineering Computation. McGraw Hill Book Co.

24. Kuenzi, E. W. 1953. Theoretical Design of a Nailed or Bolted Joint Under Lateral Load. USDA Forest Service Forest Prod. Lab. Report No. 1951.

25. Lambuth, A. L. 1986. Adhesive/Nail Plate Truss Assembly. United States Patent. Patent No. 4,659,604. Patent date, 21 Apr. 1987.

26. Mack, J. J. 1977. The Load-Displacement Curve for Nailed Joints. J. of the Institute of Wood Science, Vol. 7(6): 34-36.

27. Maraghechi, K. and Itani, R. Y. 1984. Influence of Truss Plate Connectors on the Analysis of Light Frame Structures. Wood and Fiber Science, Vol. 16(3): 306-322.

28. McCarthy, M. and Wolfe, R. W. 1987. Assessment of Truss Plate Performance Model Applied to Southern Pine Truss Joints. USDA Forest Service Forest Prod. Lab. Rèsearch Paper FPL-483.

29. McLain, T. E. 1983. Mechanical Fastening of Structural Wood Members - Design and Research Status. Proceedings of the Workshop on Structural Wood Research (Milwaukee, Wisconsin). Published by the ASCE, New York, NY 10017. pp. 31-70.

30. National Forest Products Association. 1986. National Design Specifications : Wood Construction. Washington, D.C.

31. Noguchi, M. 1980. Ultimate Resisting Moment of Butt Joints with Plate Connectors Stressed in Pure Bending. Forest Prod. J., Vol 12(3): 168-175.

32. Noren, B. 1962. Nailed Joints - A Contribution of the Theoretical Analysis of Yield and Stength. Swedish Forest Prod. Res. Lab. - Meddelane. Report 123 B.

33. Palka, L. C. and Barrett, J. D. 1984. Effect of Wood Density on Truss-Plate Joint Strength. Report prepared for Science Council of British Columbia, 7671 Alderbridge Way, Richmond, B.C. Contract No. 50-69-569.

34. Polensek, A. 1976. Finite Element Analysis of Wood-Stud Walls. J. of the Struc. Div., ASCE, Vol. 102, No. ST 7, pp. 1317-1335.

35. Polensek, A. and Schimel, B. D. 1988. Analysis of Nonlinear Connection Systems in Wood Dwellings. Paper accepted for publication in Jour. of Computing in Civil Engr., ASCE.

36. Quaile, A. T. and Keenan, F. J. 1979. Truss Plate Testing in Canada: Test Procedures and Factors Affecting Strength Properties. Proc., Metal Plate Wood Truss Conference. Forest Prod. Res. Soc., Madison, WI. pp. 105-112.

37. Shigley, J. E. 1977. Mechanical Engineering Design. McGraw-Hill, Inc.

38. Suddarth, S. K., Percival, D. H., and Comus, Q. B. 1979. Variability in Tension Performance of Metal Plate Connections. Proc., Metal Plate Wood Truss Conference. Forest Prod. Res. Soc., Madison, WI. pp. 98-104.

39. Truss Plate Institute. 1978. Design Specification for Metal Plate Connected Wood Trusses. TPI-78.

40. Tsujino, T. and Hirai, T. 1983. Nonlinear Load-Slip Relationship of Bolted Wood-Joints with Steel Side-Members I. J. of Japan Wood Res. Soc., Vol. 29(12): 833-838.

41. U.S. Forest Products Lab. 1987. Wood Handbook: Wood as an Engineering Material. U.S.D.A. Agricultural Handbook No. 72. U.S. Government Printing Office. Washington, D.C.

42. White, R. H. 1975. Finite Element Analysis of End Fixity in Stud Wall Panels. M.S. Thesis. Oregon State University.

43. Wilkinson, T. L. 1971. Theoretical Lateral Resistance of Nailed Joints. J. Struc. Div. ASCE Vol. 97, No. ST5, Proc. Paper 8121, pp. 1399-1406.

44. Wilkinson, T. L. 1972. Effect of Deformed Shanks, Prebored Lead Holes, and Grain Orientation on the Elastic Bearing Constant for Laterally Loaded Nail Joints. USDA Forest Service Research Paper FPL 192.

45. Wilkinson, T. L. 1971. Analysis of Nailed Joints with Dissimilar Members. J. Struc. Div. ASCE Vol. 98, No. ST5, Proc. Paper 9189, pp. 2005-2013.

46. Wilkinson, T. L. 1974. Elastic Bearing Constants for Sheathing Materials. USDA Forest Service Research Paper FPL 224.

47. Wilkinson, T. L. 1974. Elastic Bearing Constants of Wood: Effects of Moisture Content Conditions. USDA Forest Service Research Paper FPL 235.

48. Winkler, E. 1867. Die Lehre von der Elastizitat und Festigkeit. Prag.

49. Zienkiewicz, O. C. 1971. The Finite Element Method in Engineering Science. McGraw Hill Book Co., Inc., New York, NY. pp. 254.

50. Zimmerman, H. 1888. Die Berechnung des Eisenbahnoberbaues. Berlin.

APPENDICES

APPENDIX A

TRUSS-PLATE MODEL TRUSCON

```
      IMPLICIT DOUBLE PRECISION (A-H,O-Z)
      REAL LOAD,XLNGTH,TEMPL,TEMPL1,TEMPL2,TEMPL3,TEMPL4,TEMPL5,RKL,XL
     1,CRNTP,DPSNGL,DPPAIR,K1,K2,K3,K4,LOADPR
      DIMENSION XJAC(3,3),B(3),DLTALP(3),DLTAA1(20),DLTAA2(20),
     1DLTAA3(20),ALPHA1(51,21),ALPHA2(51,21),ALPHA3(51,21),INEXT(51),
     1DLEFT(51),DRIGHT(51)
      COMMON / BLOCK / S1(21),S2(21),S3(21),S4(21),S5(21),S6(21),
     1U1(21),U2(21),U3(21),U4(21),U5(21),U6(21),V1(21),V2(21),
     1V3(21),V4(21),V5(21),V6(21),W1(21),W2(21),W3(21),W4(21),
     1W5(21),W6(21),NUMIN,H,E,FNDMOD,XMOMIN,HEIGHT,LOAD,XLNGTH,
     1FRCMOD,FRLOAD,ICOUNT,NUMEND,TLRNCE,XH(5),XW(5),XI(5),XL(5),
     1NUMSEG,XMOM(21),SHEAR(21),FND(51),DIFFAL(51),PREVK(51),DELTA1(51),
     1DELTA2(51),DELTA3(51),DELTA4(51),DELTA5(51),DELTA6(51),CRNTP,
     1TEMPS1(51,51),LCOUNT,KCOUNT
$DEBUG
      OPEN(4,FILE='LONG17.PRN',STATUS='NEW')
      OPEN(5,FILE='SYM17.PRN',STATUS='NEW')
      OPEN(7,FILE='LD17.PRN',STATUS='NEW')
C
C
**********************************************************************
C
C            PROGRAM RUNGA-KUTTA PLUS NON-LINEAR K
C
C      This program solves a set of 6 first order nonlinear differential
C   equations via the fourth-order Runga-Kutta/Newton method.  This
C   program inputs the data one variable at a time and is a step-by-step
C   linear approach to account for nonlinear foundation modulus.
C
C      Given: 6 first order o.d.e. with 3 pair of boundary conditions.
C
C      Solution:  Since Runga-Kutta(RK) needs all initial conditions,
C                 the boundary conditions must be transformed into
C                 initial conditions.  This is done using a shooting
C                 method, which results in a set of 24 o.d.e. with
C                 24 initial conditions.  This can now be solved using
C                 ordinary RK methods.
C
**********************************************************************
C
      WRITE(*,*)' WELCOME TO THE WORLD OF RUNGA-KUTTA ANALYSIS!'
      WRITE(*,*)' '
      WRITE(*,*)' ENTER 3-DIGIT SPECIMEN ID NUMBER (ex. 301)'
      READ(*,70) SPECID
 70   FORMAT(A4)
      WRITE(*,*)' ENTER THE NUMBER OF TEETH FOR PLATE UNDER STUDY'
      WRITE(*,*)'   (Note:  generally 1, 4, 24, or 48)'
      READ(*,72) NTEETH
 72   FORMAT(I2)
      NTOTLT = NTEETH*2
      WRITE(*,*)' ENTER PLATE ANGLE IN DEGREES'
      WRITE(*,*)'   (Note:  0.0 = parallel,  90.0 = perpendicular)'
      READ(*,74) PANGLE
      WRITE(*,*)' ENTER GRAIN ANGLE IN DEGREES'
```

```
      WRITE(*,*)'   (Note:  0.0 = parallel,  90.0 = perpendicular)'
      READ(*,74) GANGLE
 74   FORMAT(F4.1)
      IF (GANGLE .LT. .1) GO TO 85
C
C  ***   ENTER THE VALUES FOR THE FOUNDATION MODULUS.  ALL VALUES
C         SHOULD BE CALCULATED FOR A STANDARD ONE-INCH EMBEDMENT
C         LENGTH.   ***
C
      WRITE(*,*)' ENTER THE TWO NONLINEAR REGRESSION PARAMETERS'
      WRITE(*,*)'  (y = Ax + Bx**2)'
      WRITE(*,*)' '
      WRITE(*,*)'    A = '
      READ(*,*)VARA
      WRITE(*,*)'    B = '
      READ(*,*)VARB
      GO TO 86
 85   WRITE(*,*)' ENTER THE 3 LINEAR FOUNDATION MODULI OF EMBEDMENT CURV
     1ES'
      WRITE(*,*)' '
      WRITE(*,*)' K1 = (generally 46500.)'
      READ(*,76)K1
      WRITE(*,*)' K2 = (generally 30000.)'
      READ(*,76)K2
      WRITE(*,*)' K3 = (generally 10000.)'
      READ(*,76)K3
      WRITE(*,*)' K4 = (generally 1400.)'
      READ(*,76)K4
 76   FORMAT(F10.1)
      WRITE(*,*)' ENTER THE 2 DEFLECTION LIMITS WHICH DEFINE THE THREE L
     1INEAR K VALUES'
      WRITE(*,*)' '
      WRITE(*,*)' DLIM1 = (generally 0.016)'
      READ(*,77)DLIM1
      WRITE(*,*)' DLIM2 = (generally 0.019)'
      READ(*,77)DLIM2
      WRITE(*,*)' DLIM3 = (generally 0.024)'
      READ(*,77)DLIM3
 77   FORMAT(F10.6)
C
C   ***   ENTER SOME INITIAL DATA  (DEFAULT VALUES)  ***
C
 86   E = 29000000.
      YLDSTR = 39850.
      FNLSTR = YLDSTR * 1.5
      XMOMIN = 0.00000080466
      HEIGHT = 0.046875
      WIDTH = 0.09375
      NUMSEG = 4
      ZERO = 0.0
      IF (PANGLE .EQ. 0.0) THEN
      XH(1) = .0395
      XH(2) = .044
      XH(3) = .044
```

```
      XH(4) = .044
      XH(5) = .044
      XW(1) = .113
      XW(2) = .100
      XW(3) = .087
      XW(4) = .0435
      XW(5) = .0435
      ELSE
      XW(1) = .0395
      XW(2) = .044
      XW(3) = .044
      XW(4) = .044
      XW(5) = .044
      XH(1) = .113
      XH(2) = .100
      XH(3) = .087
      XH(4) = .0435
      XH(5) = .0435
      ENDIF
      XL(1) = .050
      XL(2) = .041
      XL(3) = .241
      XL(4) = .061
      XL(5) = .000
      XI(1) = .000
      XI(2) = .000
      XI(3) = .000
      XI(4) = .000
      XI(5) = .000
      LOAD = 100.0
      XLNGTH = .393
      FRCMOD = 0.385
      FRLOAD = 1.
      DPPAIR = 5.0
      NUMIN = 10
      ITERAT = 0
      TLRNCE = 0.05
      CRNTP = 0.0
C
C     WRITE(*,*)' ENTER TOOTH MOD OF ELASTICITY (USUALLY 29000000.)'
C     READ(*,10)E
C10   FORMAT(F14.4)
C     WRITE(*,*)' ENTER TOOTH LENGTH (USUALLY 0.5)'
C     READ(*,11)XLNGTH
C11   FORMAT(F6.3)
C     WRITE(*,*)' ENTER THE NUMBER OF DISCRETE TOOTH SEGMENTS (USUALLY 4
C    1, BUT MAX = 5)'
C     READ(*,12)NUMSEG
C12   FORMAT(I1)
C     WRITE(*,*)' ENTER TOOTH SEGMENT LENGTHS, USUALLY.125, .125, .125 A
C    1ND .125 (5F6.2)'
C     READ(*,13)XL(1),XL(2),XL(3),XL(4),XL(5)
C13   FORMAT(5F6.2)
C     WRITE(*,*)' ENTER TOOTH HEIGHTS, USUALLY .05, .045, .045, AND .04
```

```
C     1 (5F6.2)'
C      READ(*,14)XH(1),XH(2),XH(3),XH(4),XH(5)
C14    FORMAT(5F6.2)
C      WRITE(*,*)' ENTER TOOTH SEGMENT WIDTHS, USUALLY .12, .10, .08, AND
C     1 .06 (5F6.2)'
C      READ(*,15)XW(1),XW(2),XW(3),XW(4),XW(5)
C15    FORMAT(5F6.2)
       WRITE(*,*)' ENTER APPLIED LOAD PER TOOTH PAIR (USUALLY 150.)'
       READ(*,16) LOAD
 16    FORMAT(F10.4)
C      WRITE(*,*)' ENTER WITHDRAWAL LOAD (USUALLY 150.)'
C      READ(*,18) FRLOAD
C18    FORMAT(F10.4)
C      WRITE(*,*)' ENTER FOUNDATION MODULUS (USUALLY 50000.)'
C      READ(*,20) FNDMOD
C20    FORMAT(F10.2)
C      WRITE(*,*)' ENTER FRICTION MODULUS (USUALLY 0.4, ALWAYS < 1.0)'
C      READ(*,22) FRCMOD
C22    FORMAT(F6.4)
C      WRITE(*,*)' ENTER YIELD STRESS IN PSI ( USUALLY 39850.)'
C      READ(*,24) YLDSTR
C24    FORMAT(F6.0)
C
       TEMPL = 0.
       DO 150 J=1,NUMSEG
       TEMPL = TEMPL + XL(J)
 150   XI(J) = XW(J)/12.*XH(J)**3
       XMOMIN = XI(1)
C
C    ***   SET TOLERANCE LIMIT AND INTERVAL LENGTH   ***
C
C      WRITE(*,*)' ENTER TOLERANCE FOR GUESSES (USUALLY 0.05)'
C      READ(*,28)TLRNCE
C28    FORMAT(F10.7)
       WRITE(*,*)' ENTER NO. OF INTERVALS (UP TO 20 INTERVALS)'
       READ(*,40) NUMIN
 40    FORMAT(I3)
       DO 48  J=1,NUMIN
       FND(J) = FNDMOD
 48    CONTINUE
       WRITE(*,29)XW(1),XH(1)
 29    FORMAT(' XW(1) = ',F20.15,/,' XH(1) =' ,F20.15)
 41    H = XLNGTH/NUMIN
       NUMEND = NUMIN + 1
C
C    ***   GUESS THREE INITIAL CONDITIONS WHICH WILL REPLACE BOUNDARY
C          CONDITIONS.  THESE IC's WILL CHANGE USING RK AND NEWTON
C          METHODS.  THE ITERATION PROCESS WILL STOP WHEN THE UPDATED
C          IC's VARY LESS THAN THE PRESTATED TOLERANCE OR IF THE NUMBER
C          OF ITERATIONS EXCEEDS 100.
C
C      WRITE(*,*)' ENTER 3 INITIAL GUESSES, SEPARATED BY BLANKS (3F6.2)'
C      WRITE(*,*)' NOTE: USUAL GUESSES ARE 0.001,-.044, AND -40.0'
C      READ(*,50)ORIGA1,ORIGA2,ORIGA3
```

```
C50   FORMAT(3F6.2)
C
C   ***   BEGIN STEP-BY-STEP ANALYSIS (NON-LINEAR k)   ***
C
      PLSTCM = YLDSTR * XW(1) * XH(1)**2.0 / 6.0
      HINGEM = PLSTCM * 1.5
      WRITE(*,*)' ENTER LOAD INCREMENT SIZE PER PAIR (USUALLY 5 LBS)'
      READ(*,55) DPPAIR
 55   FORMAT(F5.2)
      DPSNGL = DPPAIR/2
      NUMPIN = INT(LOAD/DPPAIR)
      FRFCTR = 0.5
C     WRITE(*,*)' ENTER FRICTION FACTOR, WHICH DETERMINES WITHDRAWAL LOA
C    1D (USUALLY 0.5)'
C     READ(*,*)FRFCTR
      DO 315 I=1,NUMPIN
      ALPHA1(I,1) = ORIGA1
      ALPHA2(I,1) = ORIGA2
      ALPHA3(I,1) = ORIGA3
 315  INEXT(I) = 1
C     WRITE(4,90)SPECID,NTEETH,PANGLE,GANGLE,VARA,VARB,VARC
C     WRITE(7,90)SPECID,NTEETH,PANGLE,GANGLE,VARA,VARB,VARC
C90   FORMAT(//,' SPECIMEN ID NO. ',A4,//,' NO. OF TEETH = ',I2,//,
C    1' PLATE ANGLE (degrees) = ',F5.1,//,' GRAIN ANGLE (degrees) = ',
C    1F5.1,//,' A = ',F12.2,//,' B = ',F12.2,//,' C = ',F12.5,///)
      IF(GANGLE .GT. .1) GO TO 94
      WRITE(4,91)SPECID,NTEETH,PANGLE,GANGLE,K1,DLIM1,K2,DLIM2,K3,DLIM3,
     1K4
      WRITE(7,91)SPECID,NTEETH,PANGLE,GANGLE,K1,DLIM1,K2,DLIM2,K3,DLIM3,
     1K4
 91   FORMAT(//,' SPECIMEN ID NO. ',A4,//,' NO. OF TEETH (pairs) = ',I2,
     1//,' PLATE ANGLE (degrees) = ',F5.1,//,' GRAIN ANGLE (degrees) = '
     1,F5.1,//,' K1 = ',F12.2,10X,' DEFL. LIMIT1 = ',F8.5,//,' K2 = '
     1,F12.2,10X,' DEFL. LIMIT2 = ',F8.5,//,' K3 = ',F12.2,10X,
     1' DEFL. LIMIT3 = ',F8.5,//,' K4 = ',F12.2,///)
      GO TO 115
 94   WRITE(4,92)SPECID,NTEETH,PANGLE,GANGLE,VARA,VARB
      WRITE(7,92)SPECID,NTEETH,PANGLE,GANGLE,VARA,VARB
 92   FORMAT(//,' SPECIMEN ID NO. ',A4,//,' NO. OF TEETH (pairs) = ',I2,
     1//,' PLATE ANGLE (degrees) = ',F5.1,//,' GRAIN ANGLE (degrees) = '
     1,F5.1,//,'  A = ',F12.2,//,'  B = ',F12.2,///)
C
C   ***   THE MAIN SECTION OF THE PROGRAM.  THIS IS THE BEGINNING OF
C         TRIPLE NESTED DO LOOP SECTION:
C           (1) INNERMOST LOOP (500); DETERMINES VALUES OF EACH TOOTH
C                    SEGMENT FOR A GIVEN LOAD,
C           (2) CENTRAL LOOP (310); INCREASES CURRENT LOAD BY A SMALL
C                    LOAD (DELTA LOAD) UNTIL THE FULL LOAD HAS BEEN
C                    APPLIED; AND
C           (3) OUTERMOST LOOP (300); REPEATS (1) AND (2) TILL ERRORS
C                    ASSOCIATED WITH ITERATIVE PROCESS ARE LESS THAN
C                    A SPECIFIED TOLERANCE.   ***
C
C   ***   REDO ENTIRE RK PROCEDURE, BUT ALTER k VALUES FOR NEWLY
```

```
C          CALCULATED DEFLECTIONS (i.e.  k is function of defl.)   ***
C
 115  DO 300 K=1,20
      KCOUNT = K
      WRITE(*,403)KCOUNT
 403  FORMAT('                              KCOUNT = ',I4)
      PREVDE = DELTA1(1)
      FLOAD1 = 0.0
      FLOAD2 = 0.0
      DSLOPE = 0.0
      CRNTP = 0.0
      DO 302 M=1,NUMEND
      DELTA1(M) = 0.0
      DELTA2(M) = 0.0
      DELTA3(M) = 0.0
      DELTA4(M) = 0.0
      DELTA5(M) = 0.0
      DELTA6(M) = 0.0
      DLEFT(M) = 0.0
 302  DRIGHT(M) = 0.0
C
C   ***   INCREASE CURRENT LOAD BY DELTA LOAD   ***
C
      WRITE(7,*)'LOAD   DEFLECTION     SLOPE       MOMENT       SHEAR
     1    FR-LOAD   FR-SHEAR'
      WRITE(7,342)ZERO,ZERO,ZERO,ZERO,ZERO,ZERO,ZERO
      DO 310 L=1,NUMPIN
      LCOUNT = L
      WRITE(*,402)LCOUNT
 402  FORMAT('                              LCOUNT = ',I4)
      CRNTP = CRNTP + DPSNGL
      CRNTTP = CRNTP * NTOTLT
      LPREV = L - 1
      TRUEDP = DPSNGL * COS(DSLOPE)
      TRUEDF = 0.0
      TEMPDF = 0.0
      IF (PANGLE .GT. 89.) THEN
        TEMPDF = -DPLSTM / 0.5 * XI(1) * E / 10.
        TRUEDF = TEMPDF + (DPSNGL * SIN(DSLOPE))
      ELSE
        TEMPDF = -DPLSTM / 0.5 * XI(1) * E / 10.
        TRUEDF = TEMPDF + (DPSNGL * SIN(DSLOPE))
      ENDIF
      FRLOAD = TRUEDF
      IF (KCOUNT .NE. 1) GO TO 180
      DO 320  M=1,NUMIN
        IF (GANGLE .GT. 89.) THEN
      TEMPX = (-VARA + (VARA**2. + 4.0*VARB*DPSNGL)**.5)/2./VARB
      FND(M) = (VARA + 2.0*VARB*TEMPX) * XLNGTH
        ELSE
      FND(M) = K1 * XLNGTH
        ENDIF
 320  CONTINUE
C     WRITE(*,*)FND(1)
```

```
      GO TO 185
 180  DO 151 M=1,NUMIN
      NEXTM = M + 1
      DLEFT(M) = DLEFT(M) + TEMPS1(LCOUNT,M)
 151  DRIGHT(M) = DRIGHT(M) + TEMPS1(LCOUNT,NEXTM)
      DO 330 M=1,NUMIN
      TEMPX = DABS((DLEFT(M) + DRIGHT(M))/2.0)
      IF (GANGLE .LT. .1) GO TO 172
      FND(M) = (VARA + 2.0 * VARB * TEMPX) * XLNGTH
C     WRITE(*,*)FND(1)
      GO TO 330
 172     IF (TEMPX .LT. DLIM1) THEN
           FND(M) = K1 * XLNGTH
         ELSEIF (TEMPX .GE. DLIM1 .AND. TEMPX .LT. DLIM2) THEN
           FND(M) = K2 * XLNGTH
         ELSEIF (TEMPX .GE. DLIM2 .AND. TEMPX .LT. DLIM3) THEN
           FND(M) = K3 * XLNGTH
         ELSE
           FND(M) = K4 * XLNGTH
         ENDIF
C     WRITE(*,811)FRLOAD,FND(M)
 810  FORMAT(1X,4F10.7)
 811  FORMAT(1X,F10.1)
 330  CONTINUE
C
C   ***   END STEP-BY-STEP INPUT   ***
C
C
C   ***   ENTER INITIAL CONDITIONS FOR ALL 24 O.D.E.   ***
C
 185  ALPHA1(LCOUNT,1) = ALPHA1(LCOUNT,INEXT(LCOUNT))
      ALPHA2(LCOUNT,1) = ALPHA2(LCOUNT,INEXT(LCOUNT))
      ALPHA3(LCOUNT,1) = ALPHA3(LCOUNT,INEXT(LCOUNT))
      DO 500 I=1,20
      ICOUNT = I
      INEXT(LCOUNT) = I+1
      S1(1) = ALPHA1(LCOUNT,I)
      TEMPS1(LCOUNT,1) = S1(1)
C
C   ***   THE NEXT PAIR OF IF STATEMENTS ARE NECESSARY TO ACCOUNT
C         FOR PLASTIC HINGE
C
      IF(LCOUNT .EQ. 1) THEN
         S2(1) = 0.0
         S3(1) = ALPHA2(1,I)
         V2(1) = 0.0
         V3(1) = 1.0
         GO TO 242
      ENDIF
      IF (DELTA3(1) .LT. HINGEM) THEN
         S2(1) = 0.0
         S3(1) = ALPHA2(LCOUNT,I)
         V2(1) = 0.0
         V3(1) = 1.0
```

```
C          TEMPDM = XMOM(1)
      ELSE
         S2(1) = ALPHA2(LCOUNT,I)
         S3(1) = DPLSTM
         V2(1) = 1.0
         V3(1) = 0.0
      ENDIF
C
 242  S4(1) = TRUEDP/E/XI(1)
      S5(1) = FRLOAD
      S6(1) = ALPHA3(LCOUNT,I)
      U1(1) = 1.0
      U2(1) = 0.0
      U3(1) = 0.0
      U4(1) = 0.0
      U5(1) = 0.0
      U6(1) = 0.0
      V1(1) = 0.0
      V4(1) = 0.0
      V5(1) = 0.0
      V6(1) = 0.0
      W1(1) = 0.0
      W2(1) = 0.0
      W3(1) = 0.0
      W4(1) = 0.0
      W5(1) = 0.0
      W6(1) = 1.0
C
C   ***   CALL THE SUBROUTINE RKALGO TO DETERMINE HOW ACCURATELY THE
C         INITIAL GUESSES SIMULATED THE BOUNDARY CONDITIONS.   ***
C
      CALL RKALGO
C
C   ***   SET UP AND INVERT JACOBIAN MATRIX.  THIS IS DONE TO DETERMINE
C         HOW FAR OFF THE INITIAL GUESSES WERE.   ***
C
C
C     WRITE(*,401)I
C401  FORMAT(' VALUE AFTER CALL RKALGO.  ICOUNT = ',I4)
C
      XJAC(1,1) = U3(NUMEND)
      XJAC(1,2) = V3(NUMEND)
      XJAC(1,3) = W3(NUMEND)
      XJAC(2,1) = U4(NUMEND)
      XJAC(2,2) = V4(NUMEND)
      XJAC(2,3) = W4(NUMEND)
      XJAC(3,1) = U5(NUMEND)
      XJAC(3,2) = V5(NUMEND)
      XJAC(3,3) = W5(NUMEND)
      NSIZE = 3
      NCOL = 1
      B(1) = S3(NUMEND)
      B(2) = S4(NUMEND)
      B(3) = S5(NUMEND)
```

```
C
C
      CALL MATINV (XJAC,NSIZE,DET,INVERR)
      CALL MATMUL (XJAC,B,DLTALP,NSIZE,NSIZE,NSIZE,NCOL,MULERR)
C
C
      DLTAA1(I) = DLTALP(1)
      DLTAA2(I) = DLTALP(2)
      DLTAA3(I) = DLTALP(3)
      NEXTI = I+1
      ALPHA1(LCOUNT,NEXTI) = ALPHA1(LCOUNT,I) - DLTAA1(I)
      ALPHA2(LCOUNT,NEXTI) = ALPHA2(LCOUNT,I) - DLTAA2(I)
      ALPHA3(LCOUNT,NEXTI) = ALPHA3(LCOUNT,I) - DLTAA3(I)
      DUM1 = DABS(DLTALP(1))
      DUM2 = DABS(DLTALP(2))
      DUM3 = DABS(DLTALP(3))
C
C     WRITE(*,276)DLTALP(1),DLTALP(2),DLTALP(3)
C276  FORMAT(' DELTA-ALPHA1 = ',F14.7,/,' DELTA-ALPHA2 = ',F14.7,/,' DEL
C    1TA-ALPHA3 = ',F14.7)
C     WRITE(*,278)ALPHA1(LCOUNT,INEXT(LCOUNT)),
C    1ALPHA2(LCOUNT,INEXT(LCOUNT)),ALPHA3(LCOUNT,INEXT(LCOUNT))
C278  FORMAT(' ALPHA1 = ',F14.7,/,' ALPHA2 = ',F14.7,/,' ALPHA3 = ',F14.
C    17,/)
C
      IF (DUM1 .GT. TLRNCE) GO TO 500
      IF (DUM2 .GT. TLRNCE) GO TO 500
      IF (DUM3 .GT. TLRNCE) GO TO 500
      ICOUNT = I
      GO TO 200
C
 500  CONTINUE
C
C
C   ***   RK/NEWTON METHOD COMPLETE.  NOW UPDATE FOUNDATION MODULUS
C           AND THEN RETURN FOR ANOTHER RK/NEWTON ITERATION.   ***
C
C
C   ***   ADD SOME MORE INFO FOR STEP-BY-STEP ANALYSIS   ***
C
 200  DO 340 I=1,NUMEND
      DELTA1(I) = DELTA1(I) + S1(I)
      DELTA2(I) = DELTA2(I) + S2(I)
      DELTA3(I) = DELTA3(I) + XMOM(I)
      DELTA4(I) = DELTA4(I) + SHEAR(I)
      DELTA5(I) = DELTA5(I) + S5(I)
 340  DELTA6(I) = DELTA6(I) + S6(I)
C  **  OUTPUT LOAD-DEFL VALUES AT TOOTH HEAD.  IF OTHER LOCATIONS ARE
C      DESIRED, CHANGE (1) TO (DESIRED) IN STATEMENT BELOW.   **
      FSHEAR = 0.
      D6AVE = 0.
      DO 233 I=1,NUMIN
 233  D6AVE = D6AVE + DELTA6(I)
        IF (GANGLE .LT. 1.)THEN
```

```
          TEMPK = K2*XLNGTH
        ELSEIF (GANGLE .GT. 89. .AND. PANGLE .GT. 89.)THEN
          TEMPK = (VARA + 2.0 * VARB * XH(3) / 4.0) * XLNGTH
        ELSE
          TEMPK = (VARA + 2.0 * VARB * XH(3)) * XLNGTH
        ENDIF
      D6AVE2 = TEMPK * XH(3) / 2. * FRCMOD * XLNGTH / 4.0
      FSHEAR = (D6AVE * H) + D6AVE2
C     WRITE(*,813)TEMPK,XH(3),FRCMOD,XLNGTH,D6AVE2,D6AVE
C813  FORMAT(F7.0,5(2X,F9.5))
      DSLOPE = DELTA2(1)
      FLOAD = 0.0
      IF (PANGLE .GT. 89.) THEN
       FLOAD1 = -DPLSTM / 0.5 * XI(1) * E / 10. * LCOUNT
       FLOAD2 = -CRNTP * SIN(DSLOPE)
      ELSE
       FLOAD1 = -DPLSTM / 0.5 * XI(1) * E / 10. * LCOUNT
       FLOAD2 = -CRNTP * SIN(DSLOPE)
      ENDIF
      FLOADF = FLOAD1 + FLOAD2
C     WRITE(*,813)FLOAD1,FLOAD2,FLOADF
C813  FORMAT(3(2X,F12.5))
C     FLOADF = FRLOAD
      WRITE(7,342)CRNTTP,DELTA1(1),DELTA2(1),DELTA3(1),DELTA4(1),FLOADF,
     1FSHEAR
 342  FORMAT(F7.1,F11.7,3(F12.7),2F12.4)
C
      IF (LCOUNT .NE. 1) GO TO 310
      IF (PANGLE .LT. 1.) THEN
      DPLSTM = -1.0 * XMOM(1)/XI(1)/E/1.15
      ELSE
      DPLSTM = -1.0 * XMOM(1)/XI(1)/E/1.15
      ENDIF
 310  CONTINUE
C
C   ***   END ADDITIONAL STEP-BY-STEP ANALYSIS INFO   ***
C
      IF(ITERAT .EQ. 20) GO TO 220
      ITERAT = ITERAT + 1
      IF(ITERAT .EQ. 1) GO TO 207
      ITOTAL = 0
      DO 108 I=1,NUMIN
      DIFFAL(I) = DABS(PREVK(I)-FND(I))
      IF (DIFFAL(I) .LT. 200.)THEN
       ITOTAL=ITOTAL+1
      ELSE
       ITOTAL=ITOTAL
      ENDIF
 108  CONTINUE
      DIST = H/2.
      DO 110 I=1,NUMIN
      NEXTI = I + 1
      PREVK(I) = FND(I)
      AVEY = -(S1(I)+S1(NEXTI))/2.
```

```
      WRITE(4,234)DIST,AVEY,FND(I)
      DIST = DIST + H
  234 FORMAT(3F20.7)
  110 CONTINUE
  207 WRITE(*,307)ITERAT
  307 FORMAT(' ***  END ITERAT = ',I2,'  ***')
      DIST = 0.
      DO 236 I=1,NUMEND
      DEFLEC = -1.0*DELTA1(I)
      WRITE(4,238)DIST,DEFLEC,CRNTTP
      DIST = DIST + H
  238 FORMAT(3F13.8)
  236 CONTINUE
      DIFFER = ABS(DELTA1(1) - PREVDE)
      IF (DIFFER .LT. .0005) GO TO 220
  300 CONTINUE
C
  220 WRITE(5,*)KCOUNT
      WRITE(*,777)ICOUNT
  777 FORMAT(' VALUE RIGHT BEFORE FINAL OUTPUT.  ICOUNT = ',I4)
      WRITE(5,*)DPPAIR,LOAD,PLSTCM,HINGEM
      DIST = 0.
      DO 710 I=1,NUMEND
      DEFLEC = -1.0*DELTA1(I)
      WRITE(5,708)DIST,DEFLEC
      DIST = DIST + H
  708 FORMAT(2F15.6)
  710 CONTINUE
      WRITE(5,*)' DISTANCE   DEFLECTION     SLOPE     MOMENT    SHEAR  F
     1RICTION-FORCE  dN/dZ'
      DSTNCE = 0.
      DO 601 J=1,NUMEND
      WRITE(5,305)DSTNCE,DELTA1(J),DELTA2(J),DELTA3(J),DELTA4(J),
     1DELTA5(J),DELTA6(J)
  305 FORMAT(F8.4,F10.7,F13.6,F13.5,3F11.5)
      DSTNCE = DSTNCE + H
  601 CONTINUE
C
      CLOSE(4)
      CLOSE(5)
      CLOSE(7)
      STOP
      END

      SUBROUTINE RKALGO
      IMPLICIT DOUBLE PRECISION(A-H,O-Z)
      REAL LOAD,XLNGTH,TEMPL,TEMPL1,TEMPL2,TEMPL3,TEMPL4,TEMPL5,RKL,XL
     1,CRNTP,DPSNGL,DPPAIR
      DIMENSION XJAC(3,3),B(3),DLTALP(3),DLTAA1(21),DLTAA2(21),
     1DLTAA3(21),ALPHA1(51),ALPHA2(51),ALPHA3(51)
      COMMON / BLOCK / S1(21),S2(21),S3(21),S4(21),S5(21),S6(21),
     1U1(21),U2(21),U3(21),U4(21),U5(21),U6(21),V1(21),V2(21),
     1V3(21),V4(21),V5(21),V6(21),W1(21),W2(21),W3(21),W4(21),
     1W5(21),W6(21),NUMIN,H,E,FNDMOD,XMOMIN,HEIGHT,LOAD,XLNGTH,
```

```
     1FRCMOD,FRLOAD,ICOUNT,NUMEND,TLRNCE,XH(5),XW(5),XI(5),XL(5),
     1NUMSEG,XMOM(21),SHEAR(21),FND(51),DIFFAL(51),PREVK(51),DELTA1(51),
     1DELTA2(51),DELTA3(51),DELTA4(51),DELTA5(51),DELTA6(51),CRNTP,
     1TEMPS1(51,51),LCOUNT,KCOUNT
C
*********************************************************************
C
C      THIS SUBROUTINE CALCULATES THE COEFFICIENTS FOR THE RK NUMERICAL
C      METHOD.  THIS ALGORITHM THEN CALCULATES THE VALUES OF ALL 24
C      O.D.E. AT EACH INTERVAL STEP.
C
C      VARIABLE DESCRIPTION:
C
C         XK101 - XK124 = FIRST RK COEFFICIENT FOR S1 THROUGH W6
C         XK201 - XK224 = SECOND RK COEFFICIENT FOR S1 THROUGH W6
C         XK301 - XK324 = THIRD RK COEFFICIENT FOR S1 THROUGH W6
C         XK401 - XK424 = FOURTH RK COEFFICIENT FOR S1 THROUGH W6
C         S1(I) - S6(I) = ORIGINAL SIX DIFFERENTIAL EQUATIONS TO BE
C                         SOLVED FOR iTH ITERATION
C         U1(I) - U6(I) = SIX PARTIAL DIFFERENTIAL EQUATIONS W/ RESPECT
C                         TO ALPHA1 FOR iTH ITERATION
C         V1(I) - V6(I) = SIX PARTIAL DIFFERENTIAL EQUATIONS W/ RESPECT
C                         TO ALPHA2 FOR iTH ITERATION
C         W1(I) - W6(I) = SIX PARTIAL DIFFERENTIAL EQUATIONS W/ RESPECT
C                         TO ALPHA3 FOR iTH ITERATION
C
C
*********************************************************************
C
C
      RKL = 0.
      JCOUNT = 0
C
      DO 700 I=1,NUMIN
      JCOUNT = JCOUNT+1
C
      H = XLNGTH/NUMIN
      RKL = RKL + H
      TEMPL1 = XL(1)
      TEMPL2 = TEMPL1 + XL(2)
      TEMPL3 = TEMPL2 + XL(3)
      TEMPL4 = TEMPL3 + XL(4)
      TEMPL5 = TEMPL4 + XL(5)
        IF (RKL .LE. TEMPL1) THEN
           WIDTH = XW(1)
           HEIGHT = XH(1)
           XMOMIN = XI(1)
           GO TO 185
        ELSEIF (RKL .LE. TEMPL2) THEN
           WIDTH = XW(2)
           HEIGHT = XH(2)
           XMOMIN = XI(2)
           GO TO 185
        ELSEIF (RKL .LE. TEMPL3) THEN
```

```
            WIDTH = XW(3)
            HEIGHT = XH(3)
            XMOMIN = XI(3)
            GO TO 185
         ELSEIF (RKL .LE. TEMPL4) THEN
            WIDTH = XW(4)
            HEIGHT = XH(4)
            XMOMIN = XI(4)
            GO TO 185
         ELSE
            WIDTH = XW(5)
            HEIGHT = XH(5)
            XMOMIN = XI(5)
         ENDIF
C
 185  NEXTI = I + 1
      FNDMOD = FND(I)
      TEMP1  = S1(I)
      TEMP2  = S2(I)
      TEMP3  = S3(I)
      TEMP4  = S4(I)
      TEMP5  = S5(I)
      TEMP6  = S6(I)
      TEMP7  = U1(I)
      TEMP8  = U2(I)
      TEMP9  = U3(I)
      TEMP10 = U4(I)
      TEMP11 = U5(I)
      TEMP12 = U6(I)
      TEMP13 = V1(I)
      TEMP14 = V2(I)
      TEMP15 = V3(I)
      TEMP16 = V4(I)
      TEMP17 = V5(I)
      TEMP18 = V6(I)
      TEMP19 = W1(I)
      TEMP20 = W2(I)
      TEMP21 = W3(I)
      TEMP22 = W4(I)
      TEMP23 = W5(I)
      TEMP24 = W6(I)
C
C   ***   CALCULATE FIRST SET OF RK COEFFICIENTS   ***
C
      XK101 = TEMP2
      XK102 = TEMP3
      XK103 = TEMP4
      XK104 = 1./E/XMOMIN*TEMP5*TEMP3-FNDMOD/E/XMOMIN*TEMP1 -
     1 (HEIGHT/2.-TEMP1)/E/XMOMIN*TEMP6
      XK105 = TEMP6
      XK106 = FRCMOD*FNDMOD*TEMP2
      XK107 = TEMP8
      XK108 = TEMP9
      XK109 = TEMP10
```

```
      XK110 = 1./E/XMOMIN*(TEMP11*TEMP3 + TEMP5*TEMP9) - FNDMOD
     1/E/XMOMIN*TEMP7 - (HEIGHT/2.-TEMP7)*TEMP6/E/XMOMIN -
     1 (HEIGHT/2.-TEMP1)*TEMP12/E/XMOMIN
      XK111 = TEMP12
      XK112 = FRCMOD*FNDMOD*TEMP8
      XK113 = TEMP14
      XK114 = TEMP15
      XK115 = TEMP16
      XK116 = 1./E/XMOMIN*(TEMP17*TEMP3 + TEMP5*TEMP15) - FNDMOD
     1/E/XMOMIN*TEMP13 - (HEIGHT/2.-TEMP13)*TEMP6/E/XMOMIN -
     1 (HEIGHT/2.-TEMP1)*TEMP18/E/XMOMIN
      XK117 = TEMP18
      XK118 = FRCMOD*FNDMOD*TEMP14
      XK119 = TEMP20
      XK120 = TEMP21
      XK121 = TEMP22
      XK122 = 1./E/XMOMIN*(TEMP23*TEMP3 + TEMP5*TEMP21) - FNDMOD
     1/E/XMOMIN*TEMP19 - (HEIGHT/2.-TEMP19)*TEMP6/E/XMOMIN -
     1 (HEIGHT/2.-TEMP1)*TEMP24/E/XMOMIN
      XK123 = TEMP24
      XK124 = FRCMOD*FNDMOD*TEMP20
C
C    ***   CALCULATE SECOND SET OF RK COEFFICIENTS   ***
C
      TEMP1  = S1(I) + H/2.0*XK101
      TEMP2  = S2(I) + H/2.0*XK102
      TEMP3  = S3(I) + H/2.0*XK103
      TEMP4  = S4(I) + H/2.0*XK104
      TEMP5  = S5(I) + H/2.0*XK105
      TEMP6  = S6(I) + H/2.0*XK106
      TEMP7  = U1(I) + H/2.0*XK107
      TEMP8  = U2(I) + H/2.0*XK108
      TEMP9  = U3(I) + H/2.0*XK109
      TEMP10 = U4(I) + H/2.0*XK110
      TEMP11 = U5(I) + H/2.0*XK111
      TEMP12 = U6(I) + H/2.0*XK112
      TEMP13 = V1(I) + H/2.0*XK113
      TEMP14 = V2(I) + H/2.0*XK114
      TEMP15 = V3(I) + H/2.0*XK115
      TEMP16 = V4(I) + H/2.0*XK116
      TEMP17 = V5(I) + H/2.0*XK117
      TEMP18 = V6(I) + H/2.0*XK118
      TEMP19 = W1(I) + H/2.0*XK119
      TEMP20 = W2(I) + H/2.0*XK120
      TEMP21 = W3(I) + H/2.0*XK121
      TEMP22 = W4(I) + H/2.0*XK122
      TEMP23 = W5(I) + H/2.0*XK123
      TEMP24 = W6(I) + H/2.0*XK124
      XK201 = TEMP2
      XK202 = TEMP3
      XK203 = TEMP4
      XK204 = 1./E/XMOMIN*TEMP5*TEMP3 -FNDMOD/E/XMOMIN*TEMP1 -
     1 (HEIGHT/2.-TEMP1)/E/XMOMIN*TEMP6
      XK205 = TEMP6
```

```
      XK206 = FRCMOD*FNDMOD*TEMP2
      XK207 = TEMP8
      XK208 = TEMP9
      XK209 = TEMP10
      XK210 = 1./E/XMOMIN*(TEMP11*TEMP3 + TEMP5*TEMP9) - FNDMOD
     1/E/XMOMIN*TEMP7 - (HEIGHT/2.-TEMP7)*TEMP6/E/XMOMIN -
     1 (HEIGHT/2.-TEMP1)*TEMP12/E/XMOMIN
      XK211 = TEMP12
      XK212 = FRCMOD*FNDMOD*TEMP8
      XK213 = TEMP14
      XK214 = TEMP15
      XK215 = TEMP16
      XK216 = 1./E/XMOMIN*(TEMP17*TEMP3 + TEMP5*TEMP15) - FNDMOD
     1/E/XMOMIN*TEMP13 - (HEIGHT/2.-TEMP13)*TEMP6/E/XMOMIN -
     1 (HEIGHT/2.-TEMP1)*TEMP18/E/XMOMIN
      XK217 = TEMP18
      XK218 = FRCMOD*FNDMOD*TEMP14
      XK219 = TEMP20
      XK220 = TEMP21
      XK221 = TEMP22
      XK222 = 1./E/XMOMIN*(TEMP23*TEMP3 + TEMP5*TEMP21) - FNDMOD
     1/E/XMOMIN*TEMP19 - (HEIGHT/2.-TEMP19)*TEMP6/E/XMOMIN -
     1 (HEIGHT/2.-TEMP1)*TEMP24/E/XMOMIN
      XK223 = TEMP24
      XK224 = FRCMOD*FNDMOD*TEMP20
C
C    ***   CALCULATE THE THIRD SET OF RK COEFFICIENTS   ***
C
      TEMP1  = S1(I) + H/2.0*XK201
      TEMP2  = S2(I) + H/2.0*XK202
      TEMP3  = S3(I) + H/2.0*XK203
      TEMP4  = S4(I) + H/2.0*XK204
      TEMP5  = S5(I) + H/2.0*XK205
      TEMP6  = S6(I) + H/2.0*XK206
      TEMP7  = U1(I) + H/2.0*XK207
      TEMP8  = U2(I) + H/2.0*XK208
      TEMP9  = U3(I) + H/2.0*XK209
      TEMP10 = U4(I) + H/2.0*XK210
      TEMP11 = U5(I) + H/2.0*XK211
      TEMP12 = U6(I) + H/2.0*XK212
      TEMP13 = V1(I) + H/2.0*XK213
      TEMP14 = V2(I) + H/2.0*XK214
      TEMP15 = V3(I) + H/2.0*XK215
      TEMP16 = V4(I) + H/2.0*XK216
      TEMP17 = V5(I) + H/2.0*XK217
      TEMP18 = V6(I) + H/2.0*XK218
      TEMP19 = W1(I) + H/2.0*XK219
      TEMP20 = W2(I) + H/2.0*XK220
      TEMP21 = W3(I) + H/2.0*XK221
      TEMP22 = W4(I) + H/2.0*XK222
      TEMP23 = W5(I) + H/2.0*XK223
      TEMP24 = W6(I) + H/2.0*XK224
      XK301 = TEMP2
      XK302 = TEMP3
```

```
      XK303 = TEMP4
      XK304 = 1./E/XMOMIN*TEMP5*TEMP3 -FNDMOD/E/XMOMIN*TEMP1 -
     1 (HEIGHT/2.-TEMP1)/E/XMOMIN*TEMP6
      XK305 = TEMP6
      XK306 = FRCMOD*FNDMOD*TEMP2
      XK307 = TEMP8
      XK308 = TEMP9
      XK309 = TEMP10
      XK310 = 1./E/XMOMIN*(TEMP11*TEMP3 + TEMP5*TEMP9) - FNDMOD
     1/E/XMOMIN*TEMP7 - (HEIGHT/2.-TEMP7)*TEMP6/E/XMOMIN -
     1 (HEIGHT/2.-TEMP1)*TEMP12/E/XMOMIN
      XK311 = TEMP12
      XK312 = FRCMOD*FNDMOD*TEMP8
      XK313 = TEMP14
      XK314 = TEMP15
      XK315 = TEMP16
      XK316 = 1./E/XMOMIN*(TEMP17*TEMP3 + TEMP5*TEMP15) - FNDMOD
     1/E/XMOMIN*TEMP13 - (HEIGHT/2.-TEMP13)*TEMP6/E/XMOMIN -
     1 (HEIGHT/2.-TEMP1)*TEMP18/E/XMOMIN
      XK317 = TEMP18
      XK318 = FRCMOD*FNDMOD*TEMP14
      XK319 = TEMP20
      XK320 = TEMP21
      XK321 = TEMP22
      XK322 = 1./E/XMOMIN*(TEMP23*TEMP3 + TEMP5*TEMP21) - FNDMOD
     1/E/XMOMIN*TEMP19 - (HEIGHT/2.-TEMP19)*TEMP6/E/XMOMIN -
     1 (HEIGHT/2.-TEMP1)*TEMP24/E/XMOMIN
      XK323 = TEMP24
      XK324 = FRCMOD*FNDMOD*TEMP20
C
C   ***   CALCULATE THE FOURTH SET OF RK COEFFICIENTS   ***
C
      TEMP1  = S1(I) + H*XK301
      TEMP2  = S2(I) + H*XK302
      TEMP3  = S3(I) + H*XK303
      TEMP4  = S4(I) + H*XK304
      TEMP5  = S5(I) + H*XK305
      TEMP6  = S6(I) + H*XK306
      TEMP7  = U1(I) + H*XK307
      TEMP8  = U2(I) + H*XK308
      TEMP9  = U3(I) + H*XK309
      TEMP10 = U4(I) + H*XK310
      TEMP11 = U5(I) + H*XK311
      TEMP12 = U6(I) + H*XK312
      TEMP13 = V1(I) + H*XK313
      TEMP14 = V2(I) + H*XK314
      TEMP15 = V3(I) + H*XK315
      TEMP16 = V4(I) + H*XK316
      TEMP17 = V5(I) + H*XK317
      TEMP18 = V6(I) + H*XK318
      TEMP19 = W1(I) + H*XK319
      TEMP20 = W2(I) + H*XK320
      TEMP21 = W3(I) + H*XK321
      TEMP22 = W4(I) + H*XK322
```

```
      TEMP23 = W5(I) + H*XK323
      TEMP24 = W6(I) + H*XK324
      XK401 = TEMP2
      XK402 = TEMP3
      XK403 = TEMP4
      XK404 = 1./E/XMOMIN*TEMP5*TEMP3 -FNDMOD/E/XMOMIN*TEMP1 -
     1 (HEIGHT/2.-TEMP1)/E/XMOMIN*TEMP6
      XK405 = TEMP6
      XK406 = FRCMOD*FNDMOD*TEMP2
      XK407 = TEMP8
      XK408 = TEMP9
      XK409 = TEMP10
      XK410 = 1./E/XMOMIN*(TEMP11*TEMP3 + TEMP5*TEMP9) - FNDMOD
     1/E/XMOMIN*TEMP7 - (HEIGHT/2.-TEMP7)*TEMP6/E/XMOMIN -
     1 (HEIGHT/2.-TEMP1)*TEMP12/E/XMOMIN
      XK411 = TEMP12
      XK412 = FRCMOD*FNDMOD*TEMP8
      XK413 = TEMP14
      XK414 = TEMP15
      XK415 = TEMP16
      XK416 = 1./E/XMOMIN*(TEMP17*TEMP3 + TEMP5*TEMP15) - FNDMOD
     1/E/XMOMIN*TEMP13 - (HEIGHT/2.-TEMP13)*TEMP6/E/XMOMIN -
     1 (HEIGHT/2.-TEMP1)*TEMP18/E/XMOMIN
      XK417 = TEMP18
      XK418 = FRCMOD*FNDMOD*TEMP14
      XK419 = TEMP20
      XK420 = TEMP21
      XK421 = TEMP22
      XK422 = 1./E/XMOMIN*(TEMP23*TEMP3 + TEMP5*TEMP21) - FNDMOD
     1/E/XMOMIN*TEMP19 - (HEIGHT/2.-TEMP19)*TEMP6/E/XMOMIN -
     1 (HEIGHT/2.-TEMP1)*TEMP24/E/XMOMIN
      XK423 = TEMP24
      XK424 = FRCMOD*FNDMOD*TEMP20
C
C   ***   CALCULATE THE NEXT ITERATIVE VALUE FOR THE 24 RK VALUES   ***
C
      S1(NEXTI) = S1(I) + H/6.*(XK101 + 2*XK201 + 2*XK301 + XK401)
      S2(NEXTI) = S2(I) + H/6.*(XK102 + 2*XK202 + 2*XK302 + XK402)
      S3(NEXTI) = S3(I) + H/6.*(XK103 + 2*XK203 + 2*XK303 + XK403)
      S4(NEXTI) = S4(I) + H/6.*(XK104 + 2*XK204 + 2*XK304 + XK404)
      S5(NEXTI) = S5(I) + H/6.*(XK105 + 2*XK205 + 2*XK305 + XK405)
      S6(NEXTI) = S6(I) + H/6.*(XK106 + 2*XK206 + 2*XK306 + XK406)
      U1(NEXTI) = U1(I) + H/6.*(XK107 + 2*XK207 + 2*XK307 + XK407)
      U2(NEXTI) = U2(I) + H/6.*(XK108 + 2*XK208 + 2*XK308 + XK408)
      U3(NEXTI) = U3(I) + H/6.*(XK109 + 2*XK209 + 2*XK309 + XK409)
      U4(NEXTI) = U4(I) + H/6.*(XK110 + 2*XK210 + 2*XK310 + XK410)
      U5(NEXTI) = U5(I) + H/6.*(XK111 + 2*XK211 + 2*XK311 + XK411)
      U6(NEXTI) = U6(I) + H/6.*(XK112 + 2*XK212 + 2*XK312 + XK412)
      V1(NEXTI) = V1(I) + H/6.*(XK113 + 2*XK213 + 2*XK313 + XK413)
      V2(NEXTI) = V2(I) + H/6.*(XK114 + 2*XK214 + 2*XK314 + XK414)
      V3(NEXTI) = V3(I) + H/6.*(XK115 + 2*XK215 + 2*XK315 + XK415)
      V4(NEXTI) = V4(I) + H/6.*(XK116 + 2*XK216 + 2*XK316 + XK416)
      V5(NEXTI) = V5(I) + H/6.*(XK117 + 2*XK217 + 2*XK317 + XK417)
      V6(NEXTI) = V6(I) + H/6.*(XK118 + 2*XK218 + 2*XK318 + XK418)
```

```
      W1(NEXTI) = W1(I) + H/6.*(XK119 + 2*XK219 + 2*XK319 + XK419)
      W2(NEXTI) = W2(I) + H/6.*(XK120 + 2*XK220 + 2*XK320 + XK420)
      W3(NEXTI) = W3(I) + H/6.*(XK121 + 2*XK221 + 2*XK321 + XK421)
      W4(NEXTI) = W4(I) + H/6.*(XK122 + 2*XK222 + 2*XK322 + XK422)
      W5(NEXTI) = W5(I) + H/6.*(XK123 + 2*XK223 + 2*XK323 + XK423)
      W6(NEXTI) = W6(I) + H/6.*(XK124 + 2*XK224 + 2*XK324 + XK424)
C
      TEMPS1(LCOUNT,NEXTI) = S1(NEXTI)
      XMOM(NEXTI) = -S3(NEXTI) * E * XMOMIN
      SHEAR(NEXTI) = -S4(NEXTI) * E * XMOMIN
C
 700  CONTINUE
C
      DSTNCE = 0.
      DO 601 J=1,NUMEND
      XMOM(1) = -S3(1) * E * XI(1)
      SHEAR(1) = -S4(1) * E * XI(1)
      DSTNCE = DSTNCE + H
 601  CONTINUE
C
      RETURN
      END


C
*MATINV
$NODEBUG
$NOFLOATCALLS
$TITLE:'Matrix Inversion Routine'
      SUBROUTINE MATINV( ARRAY, NORDER, DET, INVERR )
CP  The precision of this routine may be changed by changing the REAL
CP  declaration to REAL*8, and/or using the IMPLICIT declaration below.
      IMPLICIT DOUBLE PRECISION ( A-H, O-Z )
      PARAMETER  ( MAXORD = 100, EPS = 0.0001 )
      DIMENSION         ARRAY(NORDER,NORDER)
      INTEGER  IK(MAXORD), JK(MAXORD), PROW, PCOL
      EQUIVALENCE  ( PROW, PCOL ), ( NROW, NCOL )
      LOGICAL  INVERR
*****************************************************************************
*                                                                           *
*  Routine to invert square matrix "ARRAY" (of order "NORDER") by a         *
*  modified Gauss-Jordan elimination.  The inverse matrix is                *
*  accumulated in the space vacated by the input matrix during              *
*  computation rather than using the traditional two matrices.              *
*  The determinant "DET" is also calculated.  The method is described       *
*  in Philip R. Bevington's "Data Reduction and Error Analysis for the      *
*  Physical Sciences"; McGraw-Hill; 1969.  In fact, this routine is an      *
*  updated version of one that appears in Appendex B (op-cit).              *
*                                                                           *
*  By convention, PROW and PCOL (which are one and the same) point to       *
*  the "pivot row" and "pivot column".  Similiarly, NCOL and NROW point     *
*  to the "max row" and "max col" (order) of the matrix.                    *
*                                                                           *
*                                  D. E. Cawlfield,  MCC 124                *
```

```
*                                   30 Nov 1982                                *
*                                                                              *
********************************************************************************
      IF ( NORDER .GT. MAXORD )     THEN
          WRITE(*,*) ' **** ABORT FROM MATINV, CURRENT MAXORD= ', MAXORD
          STOP ' *ERROR*  ORDER GT MAXORD (MATINV)'
      ENDIF

      INVERR = .FALSE.
      DET    =      1.
      NCOL   = NORDER
C
C  ********DEBUG*******
C     WRITE(*,*)((ARRAY(I,J),J=1,NORDER),I=1,NORDER)
C     OPEN(4,FILE = 'MATINV.OUT',STATUS = 'NEW')
C     WRITE(4,6)((ARRAY(I,J),J=1,NORDER),I=1,NORDER)
C6    FORMAT(' TRANSFERRED ARRAY',/,6(1X,F10.7))
C     CLOSE(4)
C  ******END DEBUG*****
C
      DO  100, PCOL = 1, NCOL

C  Find largest element A(IROW,ICOL) in rest of matrix . . .
          AMAX = 0.
          DO  10, ICOL = PCOL, NCOL
          DO  10, IROW = PROW, NROW
            DUMMY1 = ARRAY(IROW,ICOL)
            DUMMY2 = AMAX
               IF ( DABS(DUMMY1) .GT. DABS(DUMMY2) )   THEN
                    AMAX     = ARRAY(IROW,ICOL)
                    IK(PROW) = IROW
                    JK(PCOL) = ICOL
               ENDIF
   10     CONTINUE
C
C*******************************************************************************
C  ***** A B N O R M A L   E X I T *****
C*******************************************************************************

          IF ( AMAX .EQ. 0. )     THEN
               WRITE(*,*) ' *** Error from MATINV, pivot point is zero'
               INVERR = .TRUE.
               RETURN
          ENDIF

C*******************************************************************************
C          WRITE(*,'(A,1X,I2)') ' Pivoting: ', PCOL
C  Interchange rows & columns to put AMAX in ARRAY(PROW,PCOL) . . .

          IROW = IK(PROW)
          IF ( IROW .GT. PROW )     THEN
               DO  20, ICOL = 1, NCOL
                    SAVE             = ARRAY(PROW,ICOL)
                    ARRAY(PROW,ICOL) = ARRAY(IROW,ICOL)
```

```
                    ARRAY(IROW,ICOL) = - SAVE
   20           CONTINUE
                ENDIF

                ICOL = JK(PROW)
                IF ( ICOL .GT. PCOL )     THEN
                     DO  30, IROW = 1, NROW
                          SAVE             = ARRAY(IROW,PCOL)
                          ARRAY(IROW,PCOL) = ARRAY(IROW,ICOL)
                          ARRAY(IROW,ICOL) = - SAVE
   30                CONTINUE
                ENDIF
C  Accumulate elements of Inverse matrix . . .

                DO  40, IROW = 1, NROW
                     IF ( IROW .NE. PROW )     THEN
                          ARRAY(IROW,PCOL) = -ARRAY(IROW,PCOL) / AMAX
                     ENDIF
   40           CONTINUE

                DO  50, ICOL = 1, NCOL
                DO  50, IROW = 1, NROW
                     IF ( IROW .NE. PROW .AND. ICOL .NE. PCOL )     THEN
                          ARRAY(IROW,ICOL) = ARRAY(IROW,ICOL)
     &                         + ARRAY(IROW,PCOL) * ARRAY(PROW,ICOL)
                     ENDIF
   50           CONTINUE
C
C
                DO  60, ICOL = 1, NCOL
                     IF ( ICOL .NE. PCOL )     THEN
                          ARRAY(PROW,ICOL) = ARRAY(PROW,ICOL) / AMAX
                     ENDIF
   60           CONTINUE

                ARRAY( PROW, PCOL ) = 1. / AMAX

                DET = DET * AMAX

  100 CONTINUE
C
C  Restore ordering of matrix . . .

           DO 200, L = 1, NORDER
                PCOL = NORDER - L + 1
                ICOL = IK(PCOL)
                IF ( ICOL .GT. PCOL )     THEN
                     DO  110, IROW = 1, NROW
                          SAVE             =  ARRAY(IROW,PCOL)
                          ARRAY(IROW,PCOL) = -ARRAY(IROW,ICOL)
                          ARRAY(IROW,ICOL) =  SAVE
  110                CONTINUE
                ENDIF
```

```
            IROW = JK(PROW)
            IF ( IROW .GT. PROW )     THEN
                 DO  120, ICOL = 1, NCOL
                      SAVE              =  ARRAY(PROW,ICOL)
                      ARRAY(PROW,ICOL) = -ARRAY(IROW,ICOL)
                      ARRAY(IROW,ICOL) =  SAVE
  120            CONTINUE
            ENDIF

  200 CONTINUE
C
C
      RETURN

      END
$NOLIST
$LIST
      SUBROUTINE MATMUL( A, B, C, MROW, MCOL, NROW, NCOL, MULERR )
      PARAMETER( MAXORD = 100 )
      IMPLICIT DOUBLE PRECISION (A-H,O-Z)
      DIMENSION A(MROW,MCOL), B(NROW,NCOL), C(MROW,NCOL)
      LOGICAL MULERR
**********************************************************************
* Your basic matrix-multiplication routine.  Multiplies A[mrow by mcol]*
* by B[nrow by ncol] to yield C[mrow,ncol].                           *
**********************************************************************
C
C      MULERR = .FALSE.
      IF ( MCOL .NE. NROW ) THEN
           WRITE(*,*) ' MATMUL error...MCOL <> NROW ', MCOL, NROW
           MULERR = .TRUE.
           RETURN
      ENDIF

C In Fortran, access the array in row order for efficiency ...

      DO 10, JCOL = 1, NCOL
      DO 10, IROW = 1, MROW
           ZETA = 0.
           DO 20, KKKK = 1, MCOL
                ZETA = ZETA + A(IROW,KKKK) * B(KKKK,JCOL)
   20      CONTINUE
           C(IROW,JCOL) = ZETA
   10 CONTINUE
      END
$NOLIST
$LIST
```

APPENDIX B

TRUSS MANUFACTURER SURVEY

MANUFACTURER	APPROXIMATE DAILY OUTPUT	CONNECTOR	LUMBER INFORMATION
AT-Wood Manufacturing Eugene, OR (503)688-8671	50 Roof trusses	Truss-plates	Doug-fir (#1/better and MSR 2100f)
Century Truss Co. Dayton, OR (503)868-7871	40 Roof trusses	Truss-plates	80% Doug-fir (#1/better) 20% Hem/fir (MSR 2100f)(dry)
Lakeview Bld. Mat. Lakeview, OR (503)947-4071	150 Roof trusses	Truss-plates	Doug-fir (mostly #1/better)(green or dry)
Moshofsky Enter. Eugene, OR (503)461-0880	70 Roof trusses	Truss-plates	Doug-fir (mostly #1/better)(green or dry)
Norton Lumber Co. Phoenix, OR (503)535-1533	50 Roof trusses	Truss-plates	Doug-fir (#1/better)(90% green : 10% dry)
Relco Roof & Floor Harrisburg, OR (503)995-6311	110 Roof trusses	Truss-plates	Doug-fir (#1/better)(90% green : 10% dry)
Rigid Truss Co. Amity, OR (503)835-8373	400 trusses	Truss-plates and plywood gussets	Hem/fir (dry) Doug-fir (#1/better)(green) web: 2x3 (#1/better),2x4 Doug-fir (stud)(green)
Roof & Floor Components, Inc. Salem, OR (503)378-0727	35 trusses	Plywood gussets	Doug-fir (MSR)(12% M.C.) Hem/fir (MSR)(12% M.C.)
Trus-Joist Corp. Hillsboro, OR (503)648-6641	200 trusses	Steel pin connectors	60% mix of Hem/fir,Doug-fir (MSR 2400f)(dry) 40% Laminated Veneer Lumber
Truss Components Cornelius, OR (503)357-2118	100 trusses	Truss-plates	80% Doug-fir (MSR 1750f)(green) 20% Hem/fir (MSR 1650f)(dry)
Tualatin Valley Builders Supply Lake Oswego, OR	200 Roof trusses	Truss-plates	Doug-fir (MSR)(90% green : 10% dry)
Prec. Roof Trusses Clackamas, OR (503)656-2983	150 Roof trusses	Truss-plates	Doug-fir (mostly #1/better, some MSR)(green)

APPENDIX C

PLATE-WOOD STIFFNESS COMPARISON

Load Distribution among Multiple Teeth in a Column:

It is necessary to determine the percentage of the total load that each tooth in a column supports. A free-body diagram representation of 4 teeth in a column is shown in Figure C1.

There are 3 spring types shown in Fig. C1. The rotational spring, k_{rot}, represents the resistance to rotation for each tooth as related to the truss-plate. The elongation of the plate can be represented by treating the plate as a series of columns. This elongation can be characterized by the stiffness, k_{plate}. The ability of the wood foundation to resist deflections caused by the i^{th} tooth can be summarized by the stiffness, k_i. This constant is directly related to the foundation modulus of the wood.

The mechanical system of Fig. C1 can be described by:

$$\{Q\} = [K]\{d\} \qquad (C1)$$

where: $\{Q\}$ = system of applied loads;
$[K]$ = stiffness matrix; and
$\{d\}$ = resulting displacements.

To create the stiffness matrix for eq. (C1), the following relationship can be used (Laursen, 1983):

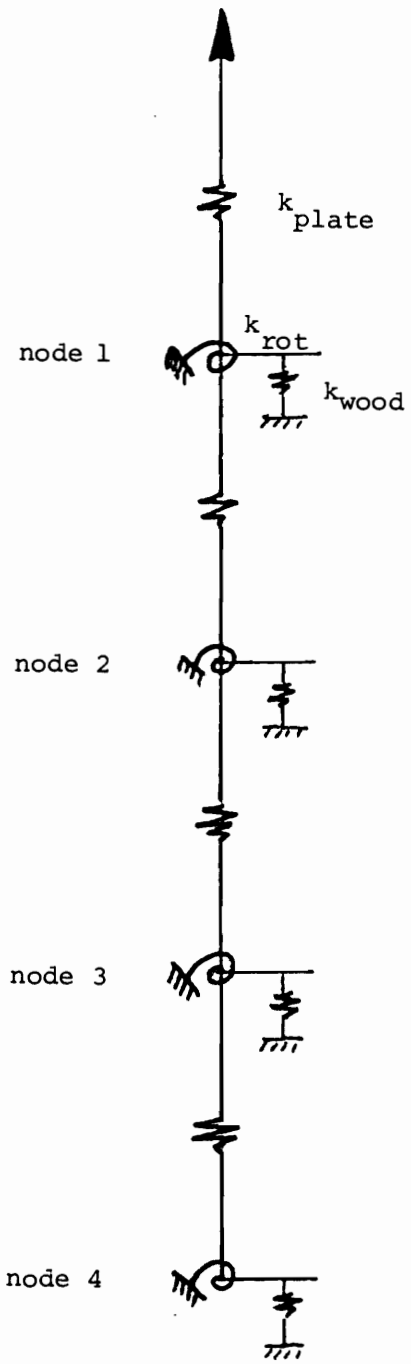

Figure C1. Stiffness representation of 4 truss-plate teeth embedded in wood with an applied load.

$$\begin{bmatrix} P_1 \\ V_1 \\ M_1 \\ P_2 \\ V_2 \\ M_2 \end{bmatrix} = E \begin{bmatrix} \frac{k_{eff}}{E} & & & & & \\ 0 & \frac{12I}{L^3} & & & \text{Symmetric} & \\ 0 & \frac{6I}{L^2} & \frac{4I}{L} & & & \\ -\frac{k_{eff}}{E} & 0 & 0 & \frac{k_{eff}}{E} & & \\ 0 & -\frac{12I}{L^3} & -\frac{6I}{L^2} & 0 & \frac{12I}{L^3} & \\ 0 & \frac{6I}{L^2} & \frac{2I}{L} & 0 & -\frac{6I}{L^2} & \frac{4I}{L} \end{bmatrix} \begin{bmatrix} 1 \\ 1 \\ 1 \\ 2 \\ 2 \\ 2 \end{bmatrix} \qquad \text{(C2)}$$

The overall system stiffness matrix can be assembled by overlapping the local stiffness matrices of eq. (C2). The overall system matrix can be reduced to include only the significant parameters. Since no moment is present at the applied load (node 1) and the truss-plate is assumed to remain vertical, M_1 and V_i can be eliminated.

The overall stiffness matrix is governed by the effective stiffness of the truss-plate and wood. The effective stiffness coefficient is the result of k_i and k_{plate} for each node acting in series. For two springs acting in series, we get the following equation:

$$k_{eff} = \frac{1}{\frac{1}{k_i} + \frac{1}{k_{plate}}} \qquad \text{(C3)}$$

Comparing the effective stiffness with the wood stiffness will give us the relative stiffness difference.

All four tooth and grain geometries are shown in the examples below. The deflections for the wood are taken from the complete joint tests. The dimensions of the truss-plate are used to determine plate stiffness.

1) Tooth = flat : grain = parallel

$$k_{plate} = \frac{(29300000)(.2)(.04)}{(.5)} = 4.69 * 10^5 \text{ lbs/in.}$$

$$k_{wood} = \frac{75 \text{ lbs}}{0.08 \text{ in}} = 938 \text{ lbs/in.}$$

$$k_{eff} = 936 \text{ lbs/in.}$$

difference = 2/938 = 0.2%

2) Tooth = flat : grain = perpendicular

$$k_{plate} = 4.69 * 10^5 \text{ lbs/in.}$$

$$k_{wood} = \frac{42 \text{ lbs}}{0.03 \text{ in.}} = 1400 \text{ lbs/in.}$$

$$k_{eff} = 1396 \text{ lbs/in.}$$

difference = 4/1400 = 0.3%

3) Tooth = edge : grain = parallel

$$k_{plate} = \frac{(29300000)(.2)(.04)}{(.2)} = 1.17 * 10^6 \text{ lbs/in.}$$

$$k_{wood} = \frac{83 \text{ lbs}}{0.04 \text{ in.}} = 2083 \text{ lbs/in.}$$

$$k_{eff} = 2079 \text{ lbs/in.}$$

difference = 4/2083 = 0.2%

4) Tooth = edge : grain = perpendicular

$$k_{plate} = 1.17 * 10^6 \text{ lbs/in.}$$

$$k_{wood} = \frac{52 \text{ lbs}}{0.02 \text{ in.}} = 2600 \text{ lbs}$$

$$k_{eff} = 2594 \text{ lbs/in.}$$

$$\text{difference} = 6/2600 = 0.2\%$$

The difference between the effective stiffness and the wood stiffness is 0.2% in all teeth and grain orientations. Thus, for the joint types used in this study, it was justified to assume a rigid plate in comparison to the wood stiffness.

APPENDIX D

LOAD-EMBEDMENT TRACES

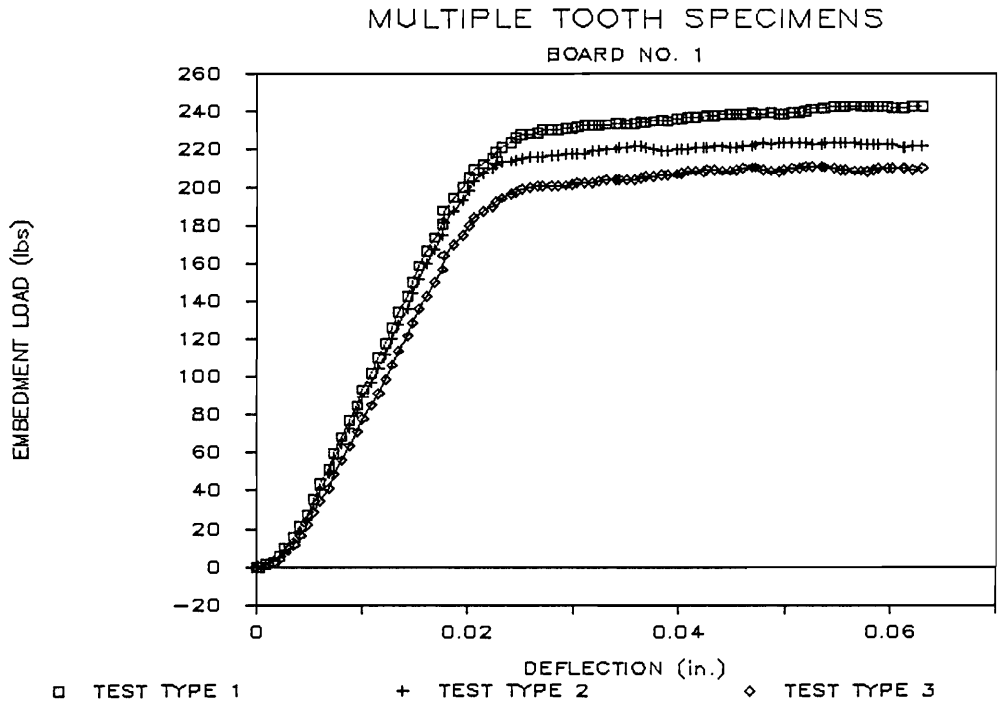
MULTIPLE TOOTH SPECIMENS
BOARD NO. 1
EMBEDMENT LOAD (lbs)
260
240
220
200
180
160
140
120
100
80
60
40
20
0
-20
0
0.02
0.04
0.06
DEFLECTION (in.)
TEST TYPE 1
TEST TYPE 2
TEST TYPE 3

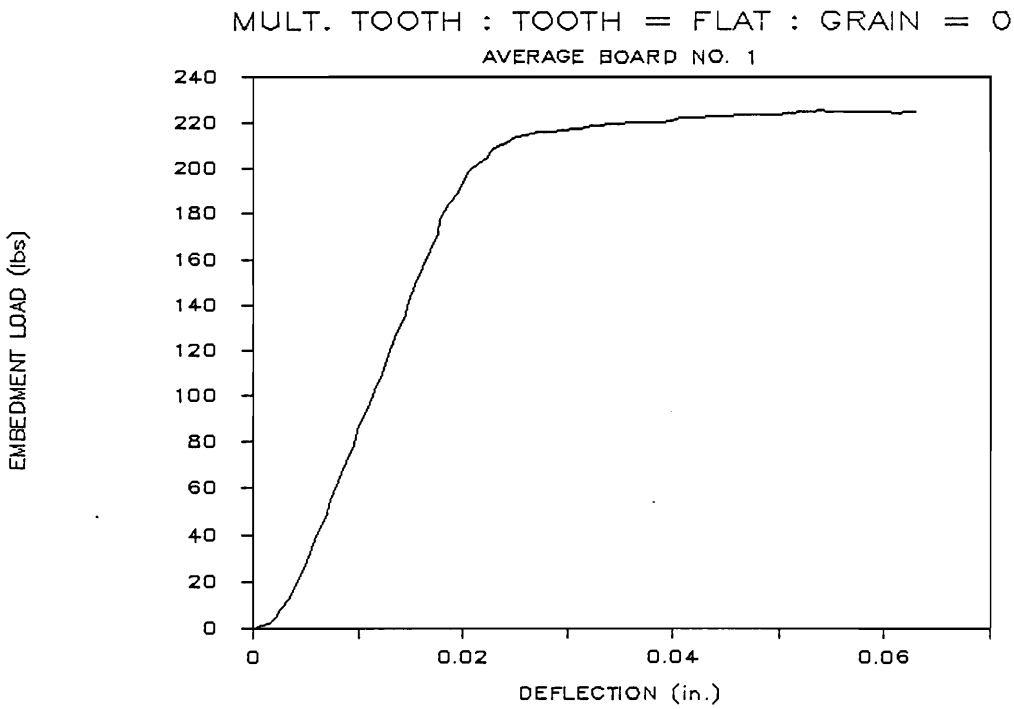
MULT. TOOTH : TOOTH = FLAT : GRAIN = 0
AVERAGE BOARD NO. 1
EMBEDMENT LOAD (lbs)
240
220
200
180
160
140
120
100
80
60
40
20
0
0
0.02
0.04
0.06
DEFLECTION (in.)

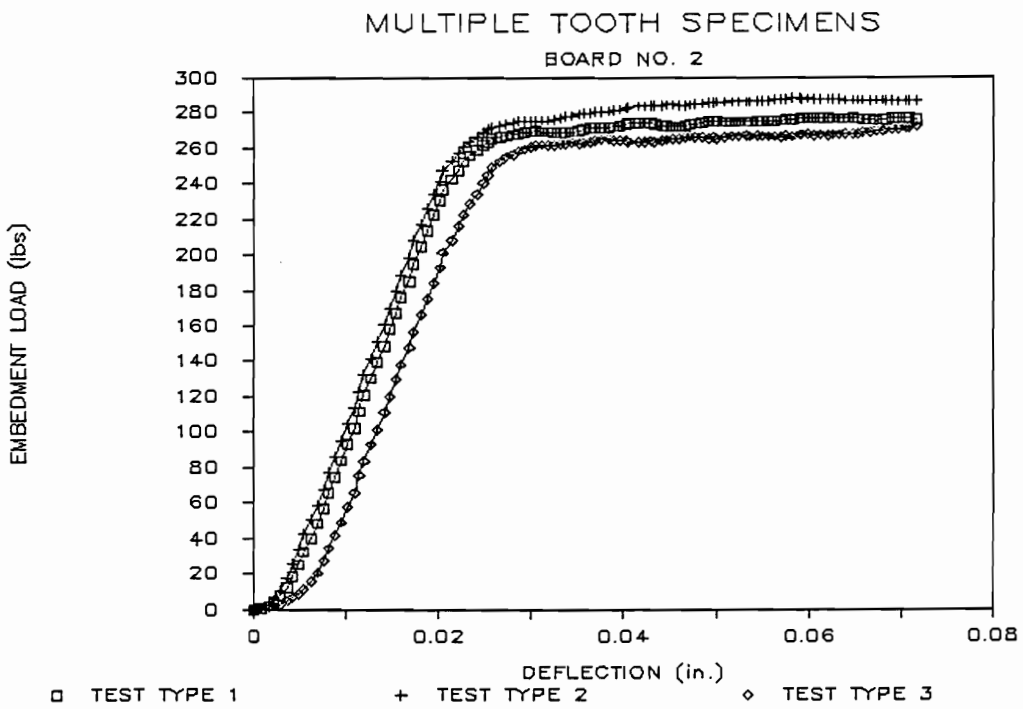
MULTIPLE TOOTH SPECIMENS
BOARD NO. 2
EMBEDMENT LOAD (lbs)
300
280
260
240
220
200
180
160
140
120
100
80
60
40
20
0
0
0.02
0.04
0.06
0.08
DEFLECTION (in.)
TEST TYPE 1
TEST TYPE 2
TEST TYPE 3

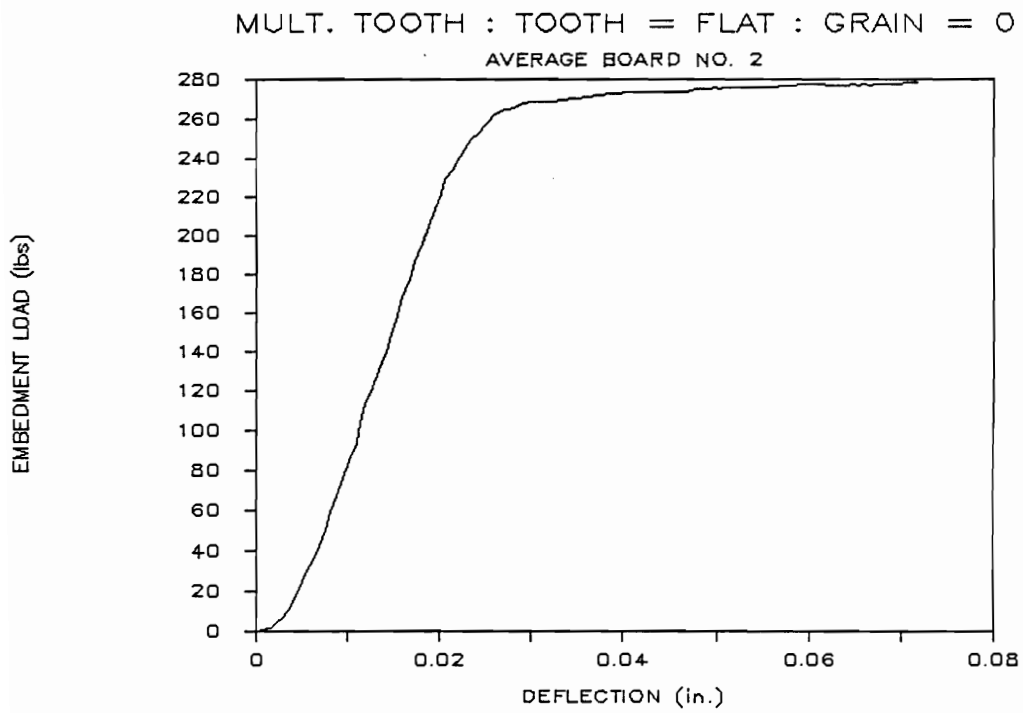
MULT. TOOTH : TOOTH = FLAT : GRAIN = 0
AVERAGE BOARD NO. 2
EMBEDMENT LOAD (lbs)
280
260
240
220
200
180
160
140
120
100
80
60
40
20
0
0
0.02
0.04
0.06
0.08
DEFLECTION (in.)

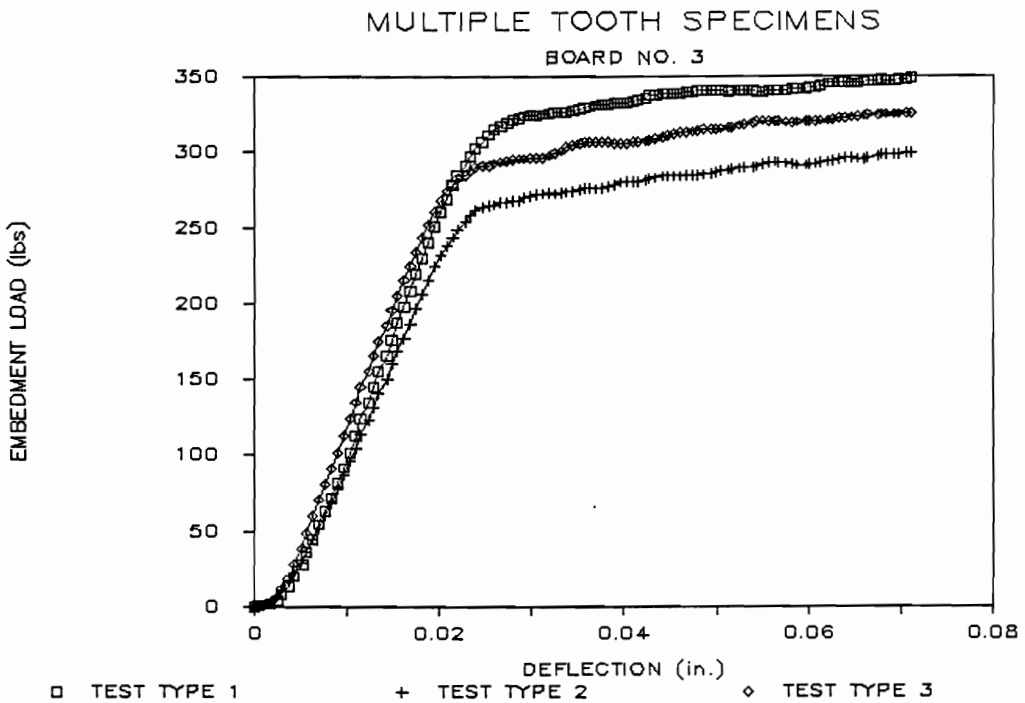
MULTIPLE TOOTH SPECIMENS
BOARD NO. 3
EMBEDMENT LOAD (lbs)
350
300
250
200
150
100
50
0
0
0.02
0.04
0.06
0.08
DEFLECTION (in.)
TEST TYPE 1
TEST TYPE 2
TEST TYPE 3

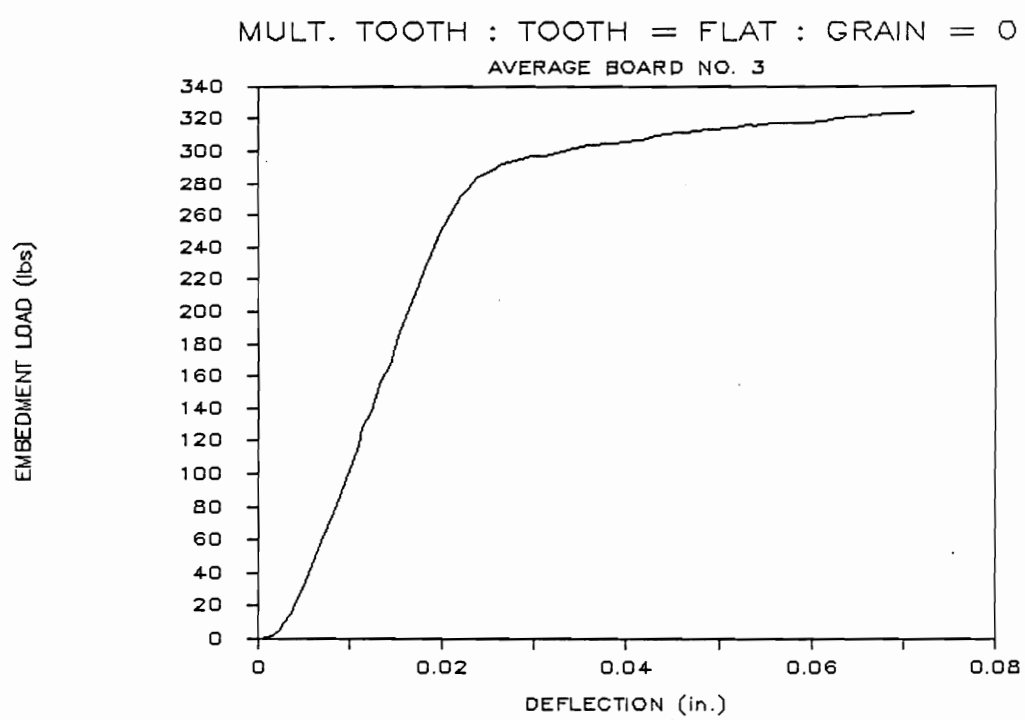
MULT. TOOTH : TOOTH = FLAT : GRAIN = 0
AVERAGE BOARD NO. 3
EMBEDMENT LOAD (lbs)
340
320
300
280
260
240
220
200
180
160
140
120
100
80
60
40
20
0
0
0.02
0.04
0.06
0.08
DEFLECTION (in.)

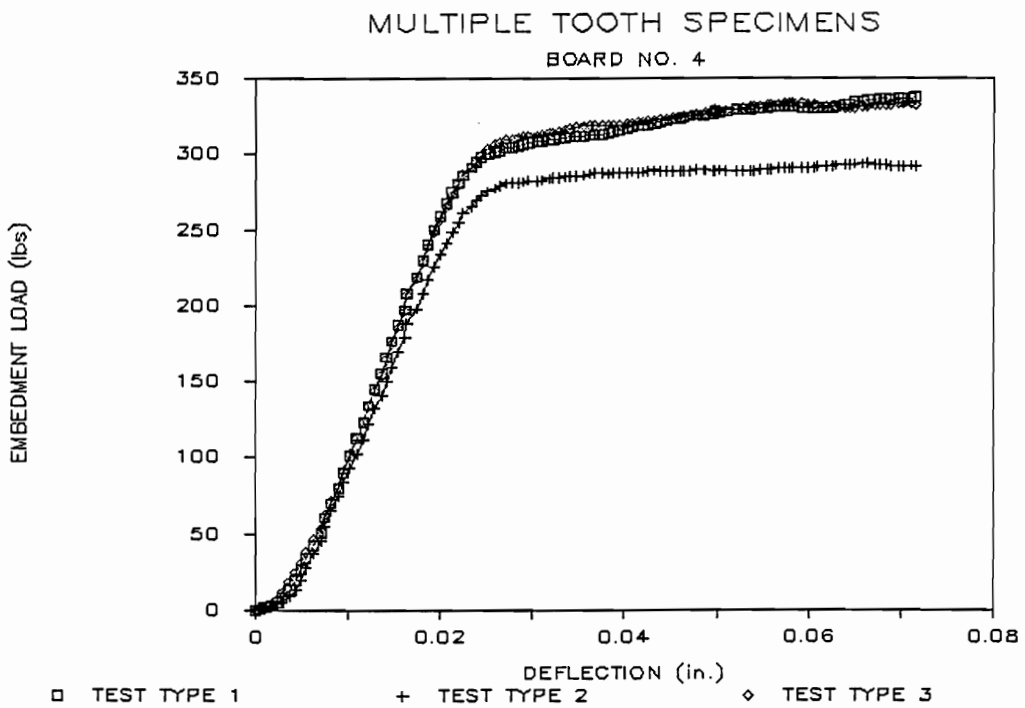
MULTIPLE TOOTH SPECIMENS
BOARD NO. 4
EMBEDMENT LOAD (lbs)
350
300
250
200
150
100
50
0
0
0.02
0.04
0.06
0.08
DEFLECTION (in.)
TEST TYPE 1
TEST TYPE 2
TEST TYPE 3

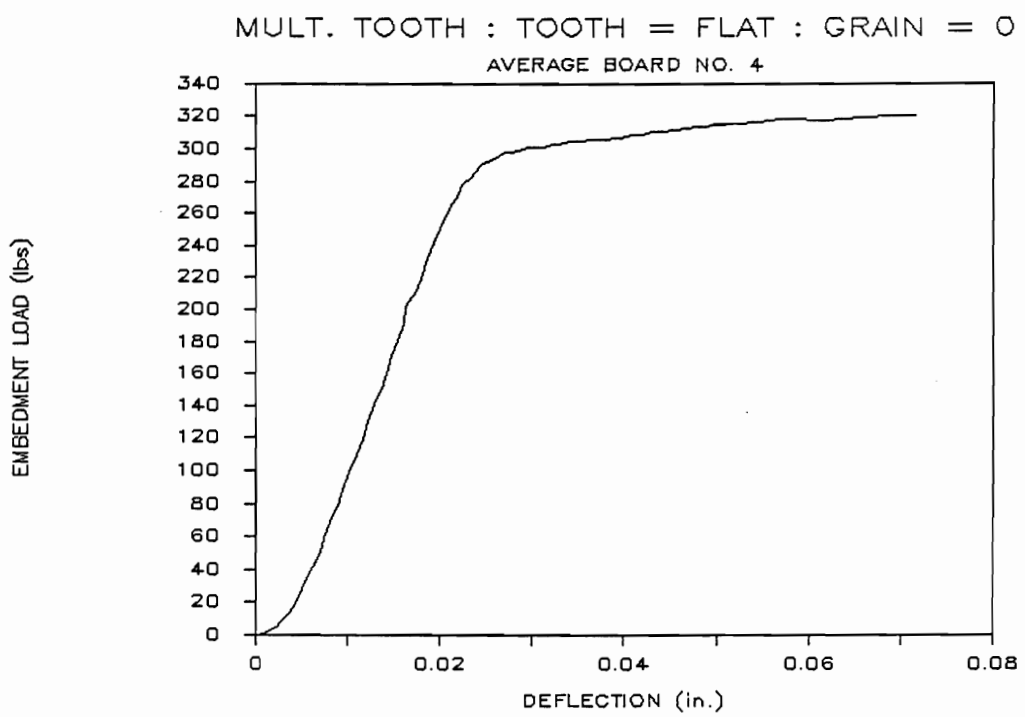
MULT. TOOTH : TOOTH = FLAT : GRAIN = 0
AVERAGE BOARD NO. 4
EMBEDMENT LOAD (lbs)
340
320
300
280
260
240
220
200
180
160
140
120
100
80
60
40
20
0
0
0.02
0.04
0.06
0.08
DEFLECTION (in.)

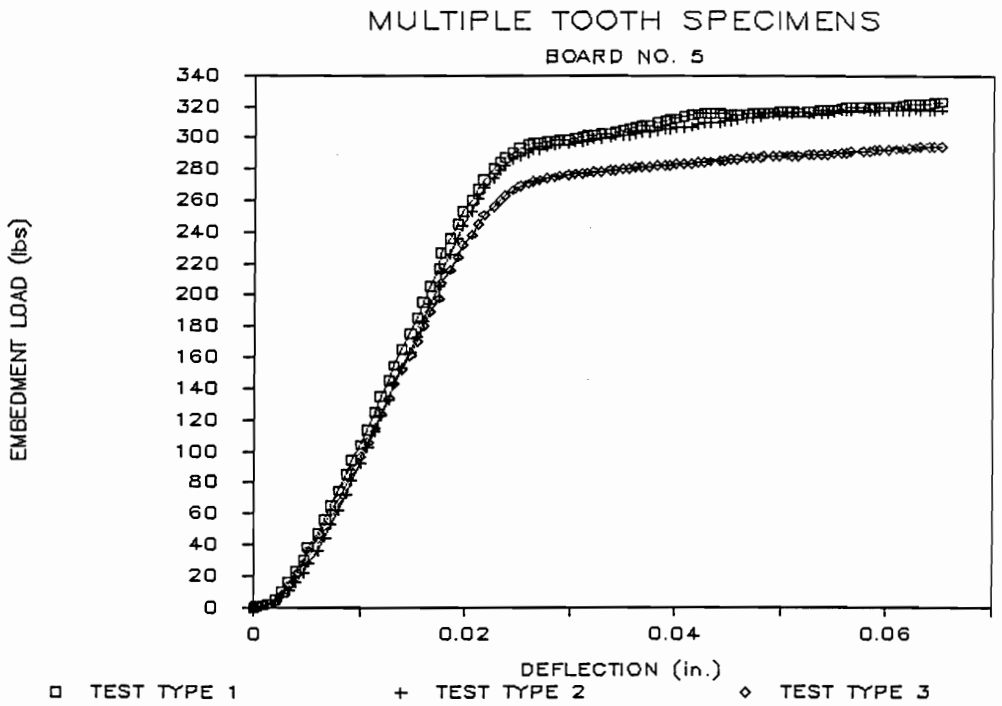
MULTIPLE TOOTH SPECIMENS
BOARD NO. 5
EMBEDMENT LOAD (lbs)
340
320
300
280
260
240
220
200
180
160
140
120
100
80
60
40
20
0
0
0.02
0.04
0.06
DEFLECTION (in.)
TEST TYPE 1
TEST TYPE 2
TEST TYPE 3

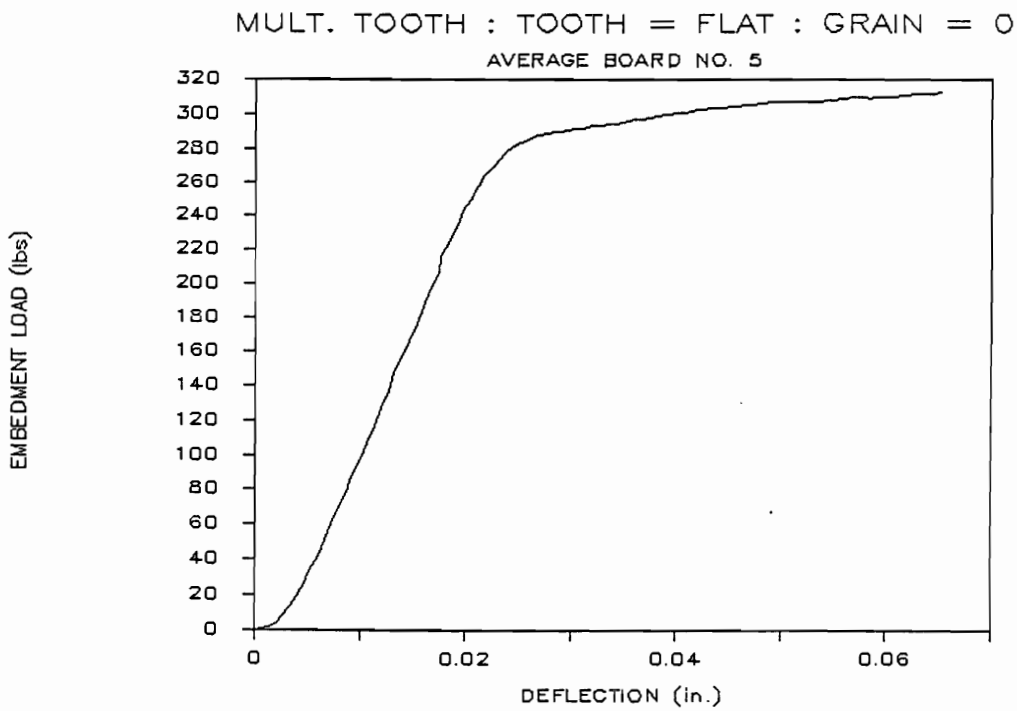
MULT. TOOTH : TOOTH = FLAT : GRAIN = 0
AVERAGE BOARD NO. 5
EMBEDMENT LOAD (lbs)
320
300
280
260
240
220
200
180
160
140
120
100
80
60
40
20
0
0
0.02
0.04
0.06
DEFLECTION (in.)

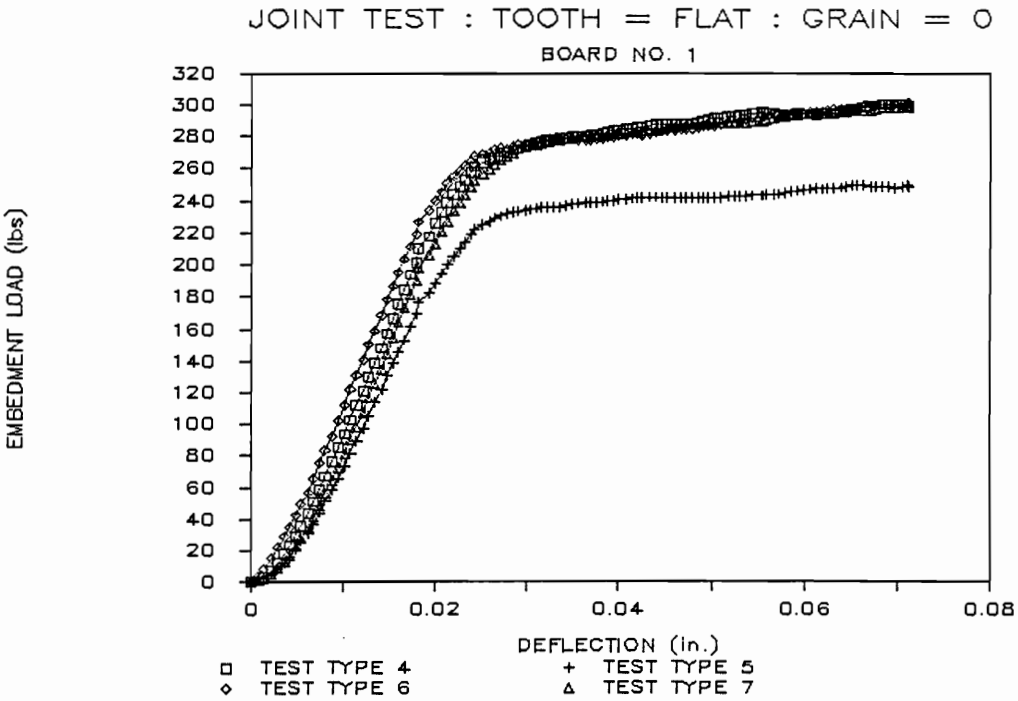
JOINT TEST : TOOTH = FLAT : GRAIN = 0
BOARD NO. 1
EMBEDMENT LOAD (lbs)
320
300
280
260
240
220
200
180
160
140
120
100
80
60
40
20
0
0
0.02
0.04
0.06
0.08
DEFLECTION (in.)
TEST TYPE 4
TEST TYPE 5
TEST TYPE 6
TEST TYPE 7

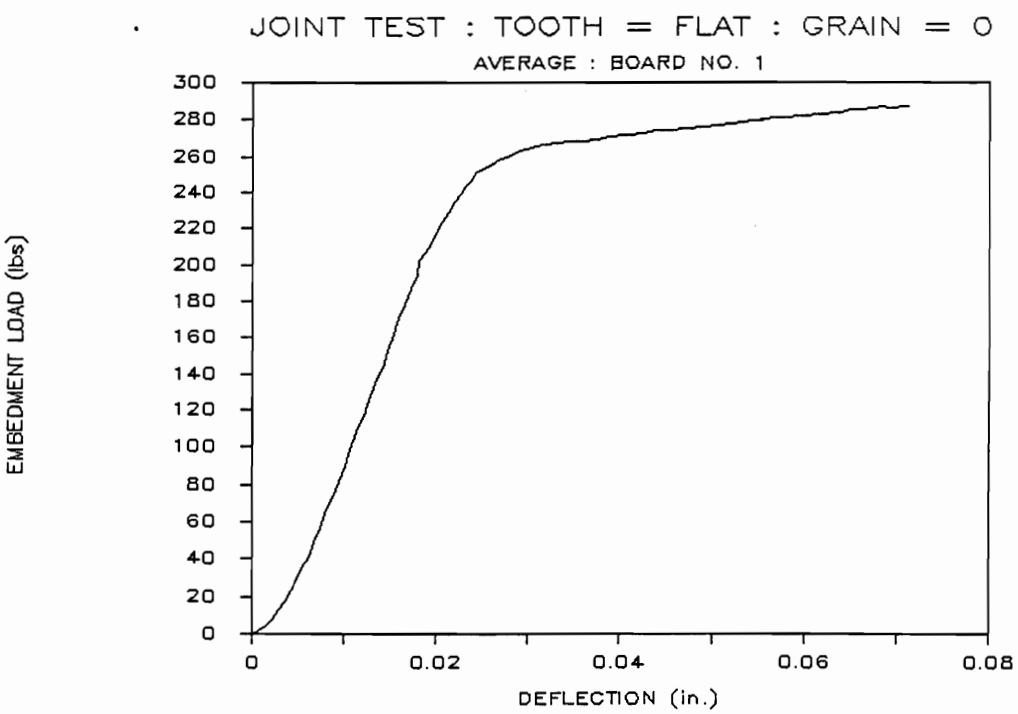
JOINT TEST : TOOTH = FLAT : GRAIN = 0
AVERAGE : BOARD NO. 1
EMBEDMENT LOAD (lbs)
300
280
260
240
220
200
180
160
140
120
100
80
60
40
20
0
0
0.02
0.04
0.06
0.08
DEFLECTION (in.)

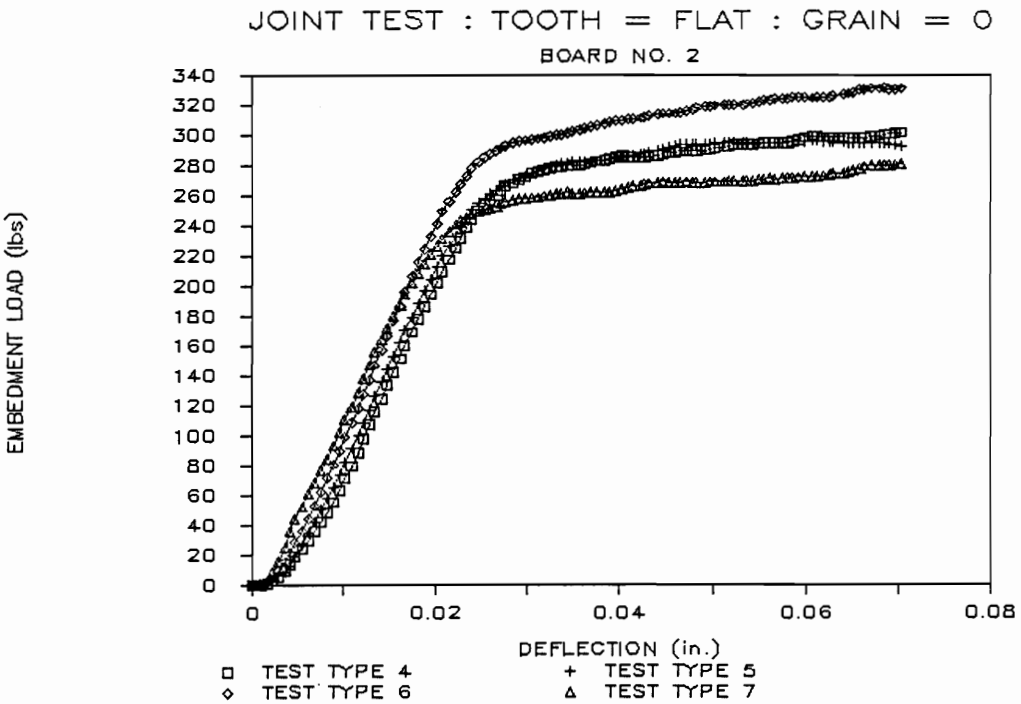
JOINT TEST : TOOTH = FLAT : GRAIN = 0
BOARD NO. 2
EMBEDMENT LOAD (lbs)
340
320
300
280
260
240
220
200
180
160
140
120
100
80
60
40
20
0
0
0.02
0.04
0.06
0.08
DEFLECTION (in.)
TEST TYPE 4
TEST TYPE 5
TEST TYPE 6
TEST TYPE 7

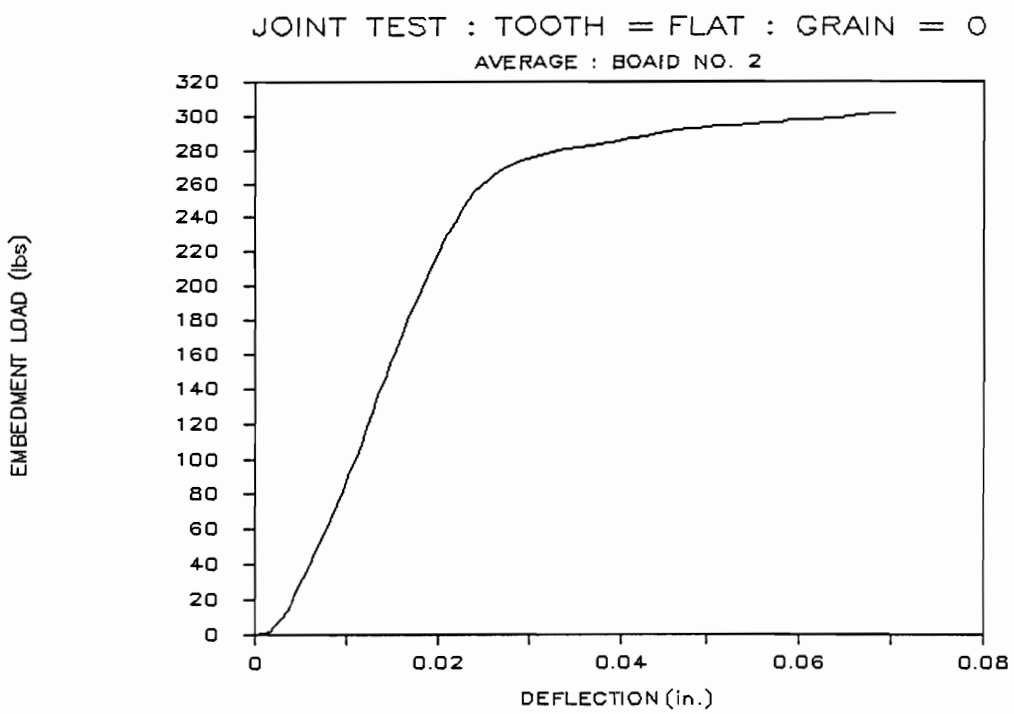
JOINT TEST : TOOTH = FLAT : GRAIN = 0
AVERAGE : BOAID NO. 2
EMBEDMENT LOAD (lbs)
320
300
280
260
240
220
200
180
160
140
120
100
80
60
40
20
0
0
0.02
0.04
0.06
0.08
DEFLECTION (in.)

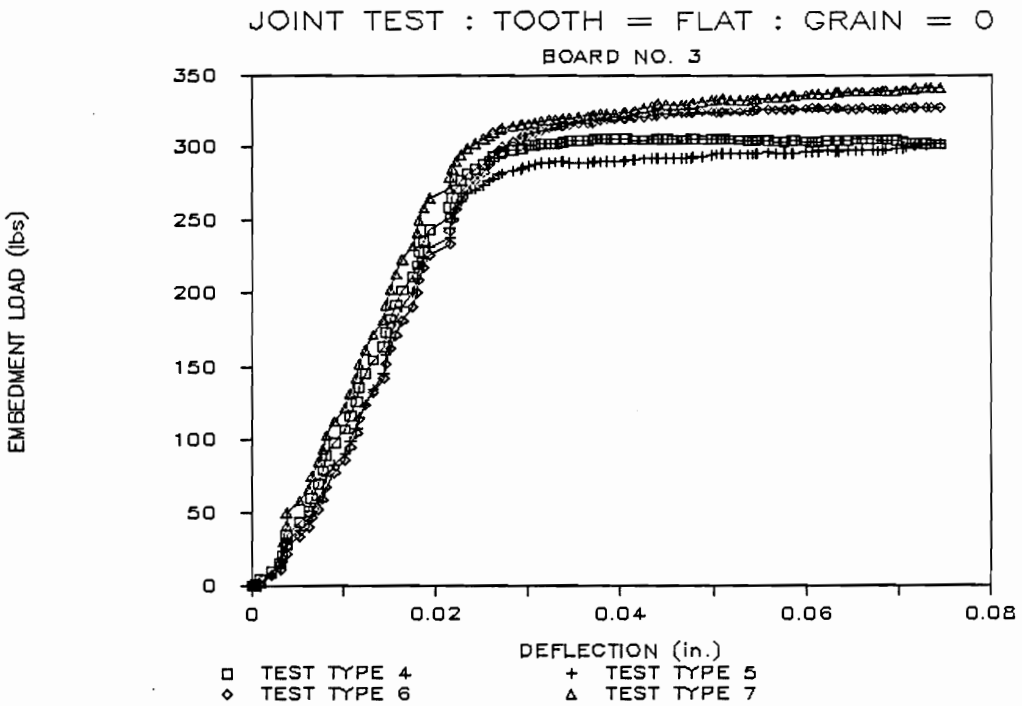
JOINT TEST : TOOTH = FLAT : GRAIN = 0
BOARD NO. 3
EMBEDMENT LOAD (lbs)
350
300
250
200
150
100
50
0
0
0.02
0.04
0.06
0.08
DEFLECTION (in.)
TEST TYPE 4
TEST TYPE 5
TEST TYPE 6
TEST TYPE 7

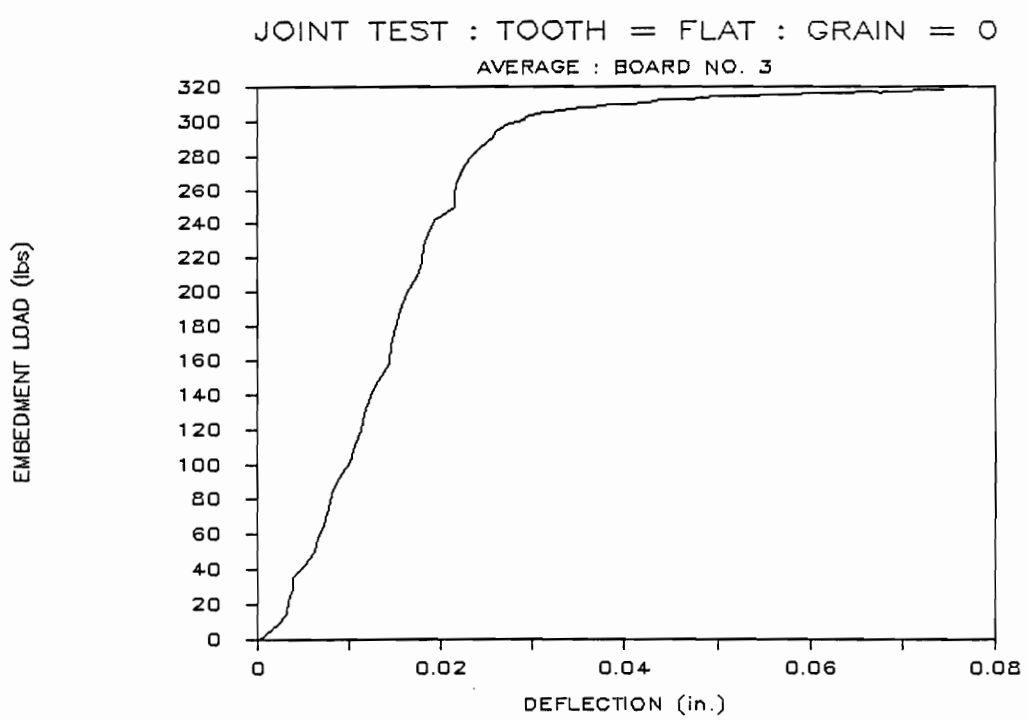
JOINT TEST : TOOTH = FLAT : GRAIN = 0
AVERAGE : BOARD NO. 3
EMBEDMENT LOAD (lbs)
320
300
280
260
240
220
200
180
160
140
120
100
80
60
40
20
0
0
0.02
0.04
0.06
0.08
DEFLECTION (in.)

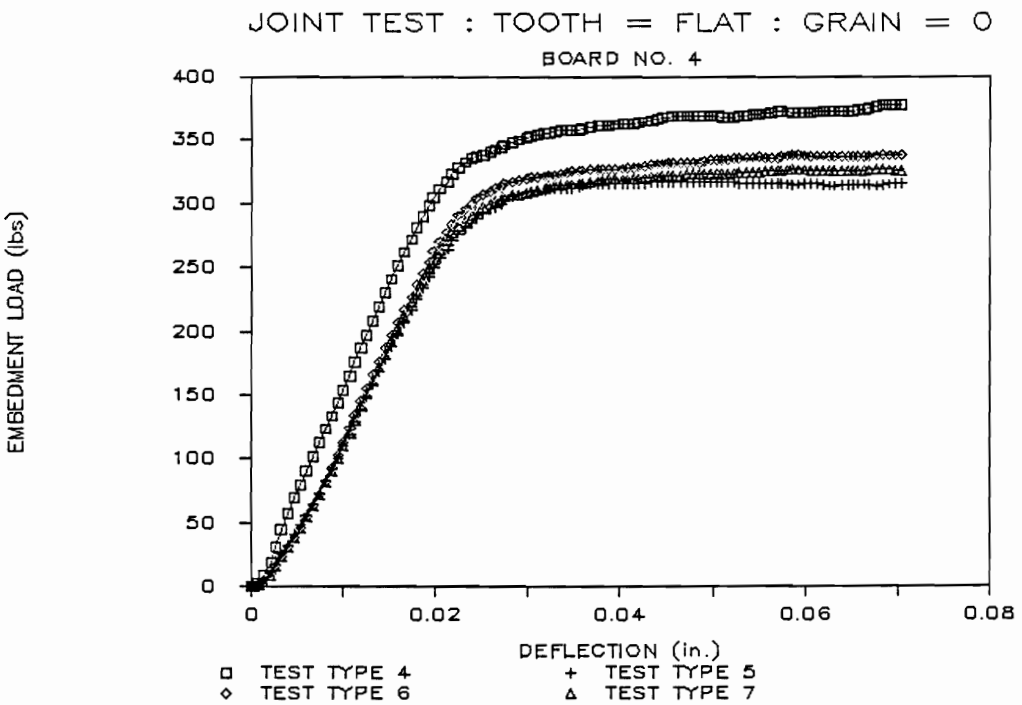
JOINT TEST : TOOTH = FLAT : GRAIN = 0
BOARD NO. 4
EMBEDMENT LOAD (lbs)
400
350
300
250
200
150
100
50
0
0
0.02
0.04
0.06
0.08
DEFLECTION (in.)
TEST TYPE 4
TEST TYPE 5
TEST TYPE 6
TEST TYPE 7

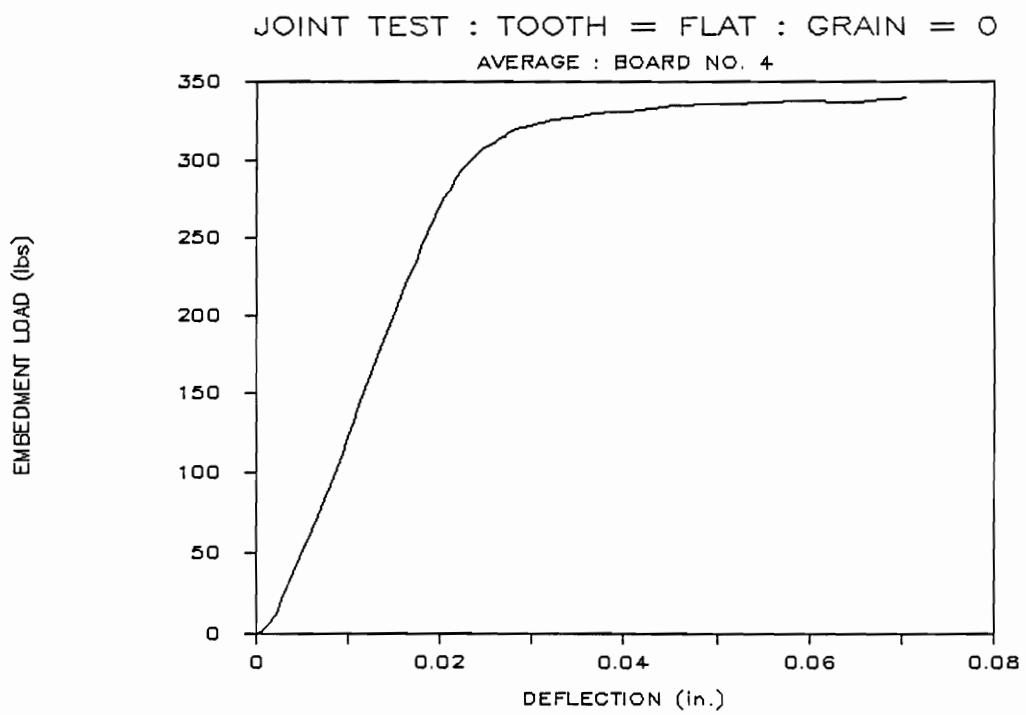
JOINT TEST : TOOTH = FLAT : GRAIN = 0
AVERAGE : BOARD NO. 4
EMBEDMENT LOAD (lbs)
350
300
250
200
150
100
50
0
0
0.02
0.04
0.06
0.08
DEFLECTION (in.)

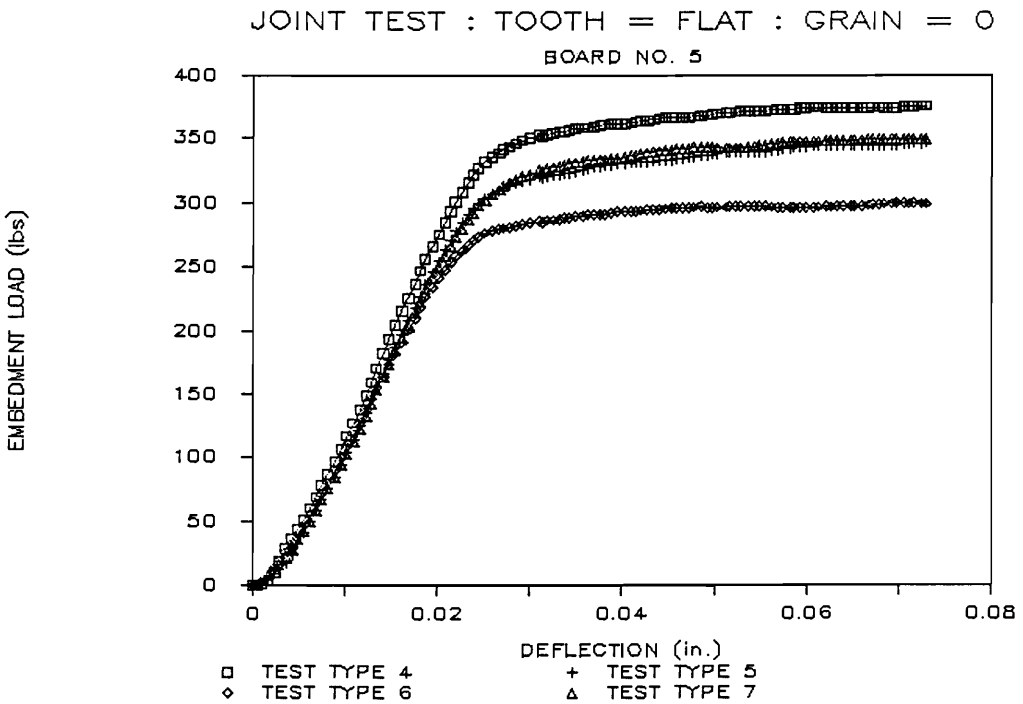
JOINT TEST : TOOTH = FLAT : GRAIN = 0
BOARD NO. 5
EMBEDMENT LOAD (lbs)
400
350
300
250
200
150
100
50
0
0
0.02
0.04
0.06
0.08
DEFLECTION (in.)
TEST TYPE 4
TEST TYPE 5
TEST TYPE 6
TEST TYPE 7

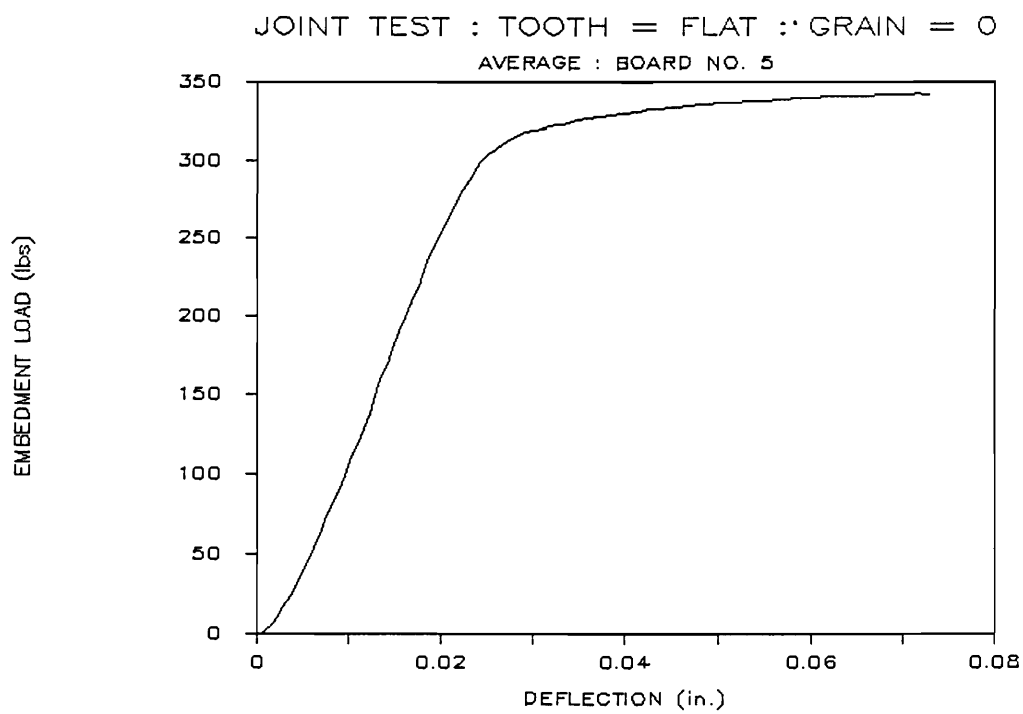
JOINT TEST : TOOTH = FLAT : GRAIN = 0
AVERAGE : BOARD NO. 5
EMBEDMENT LOAD (lbs)
350
300
250
200
150
100
50
0
0
0.02
0.04
0.06
0.08
DEFLECTION (in.)

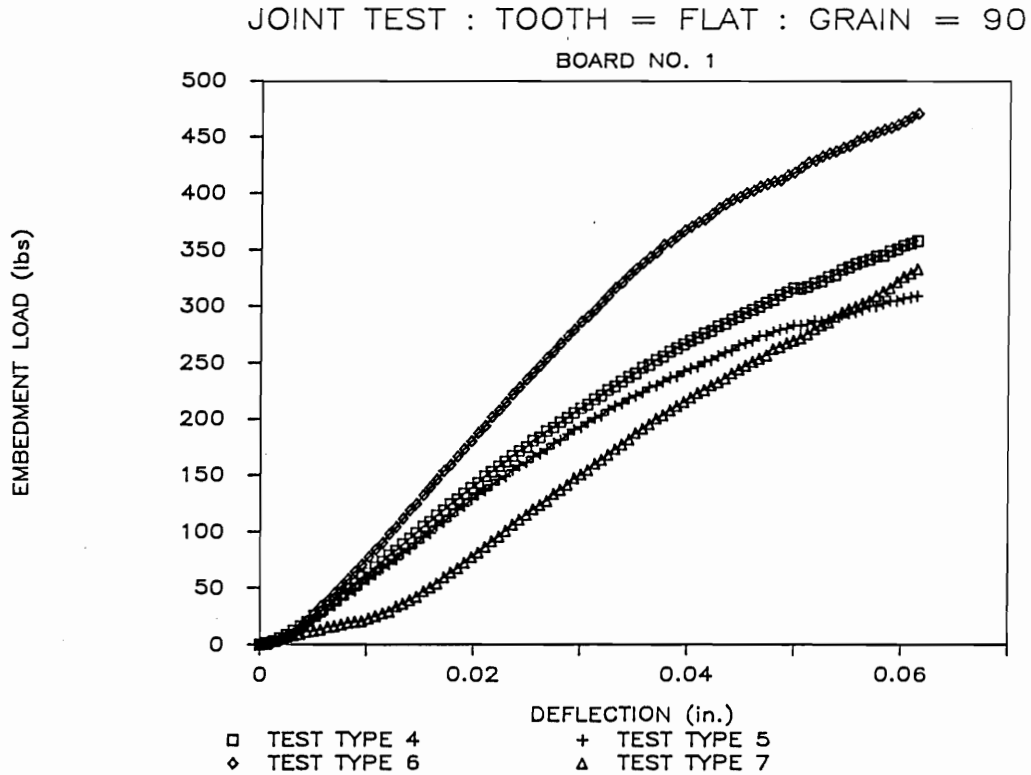
JOINT TEST : TOOTH = FLAT : GRAIN = 90
BOARD NO. 1
EMBEDMENT LOAD (lbs)
500
450
400
350
300
250
200
150
100
50
0
0
0.02
0.04
0.06
DEFLECTION (in.)
TEST TYPE 4
TEST TYPE 5
TEST TYPE 6
TEST TYPE 7

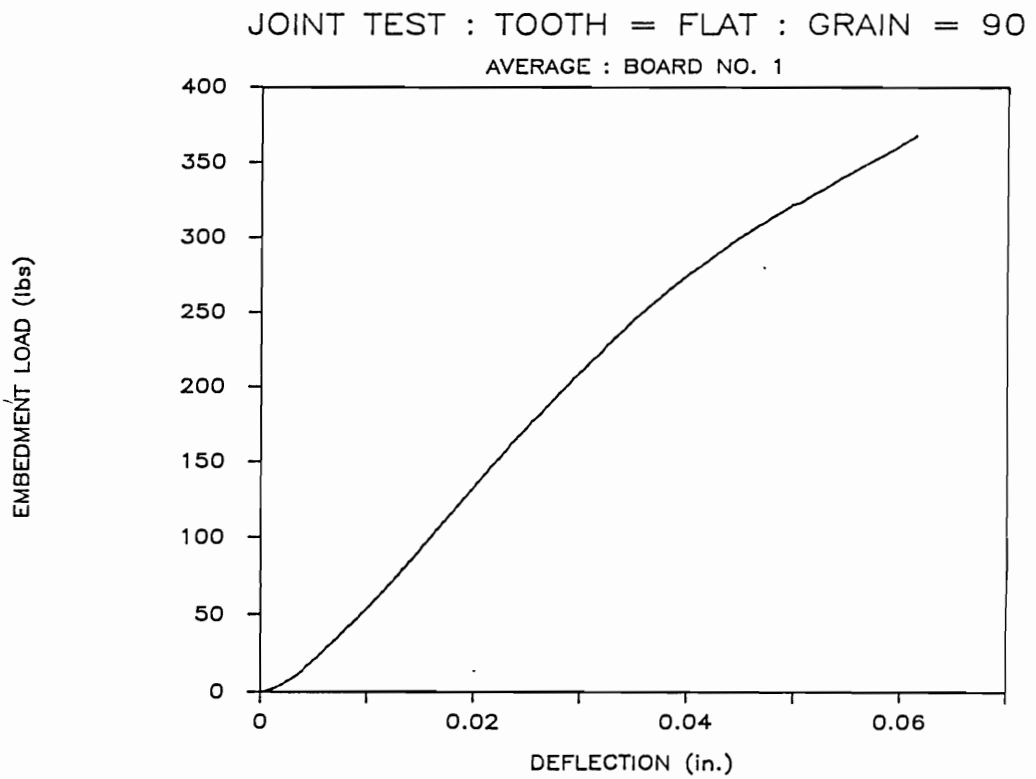
JOINT TEST : TOOTH = FLAT : GRAIN = 90
AVERAGE : BOARD NO. 1
EMBEDMENT LOAD (lbs)
400
350
300
250
200
150
100
50
0
0
0.02
0.04
0.06
DEFLECTION (in.)

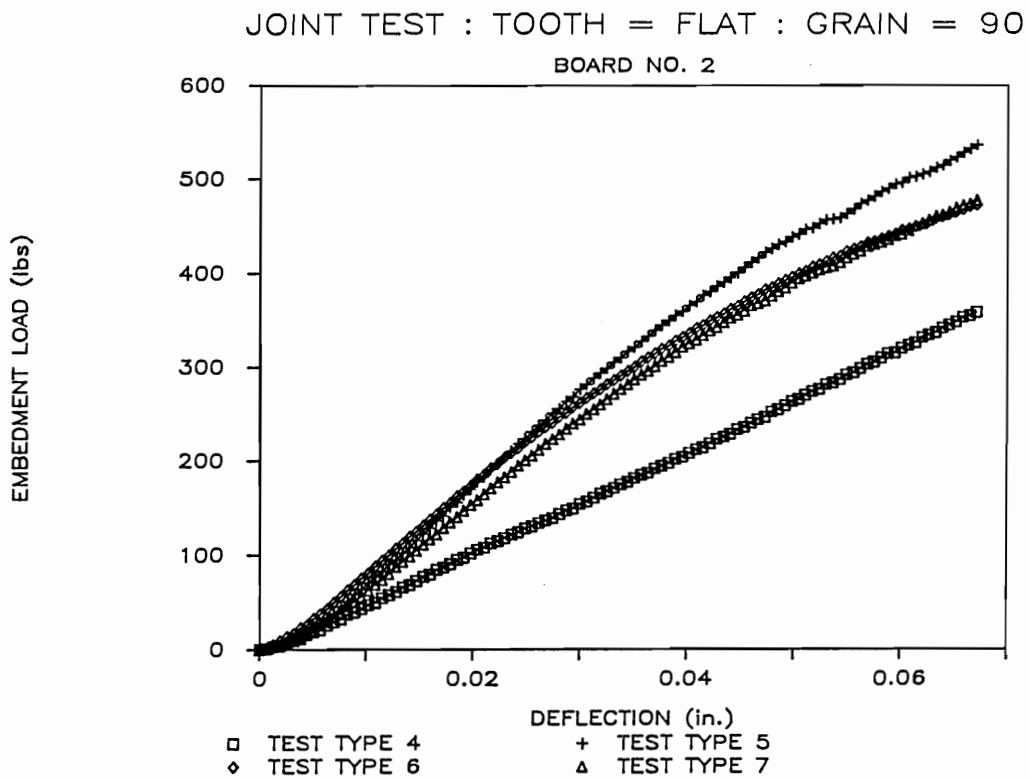
JOINT TEST : TOOTH = FLAT : GRAIN = 90
BOARD NO. 2
EMBEDMENT LOAD (lbs)
600
500
400
300
200
100
0
0
0.02
0.04
0.06
DEFLECTION (in.)
TEST TYPE 4
TEST TYPE 5
TEST TYPE 6
TEST TYPE 7

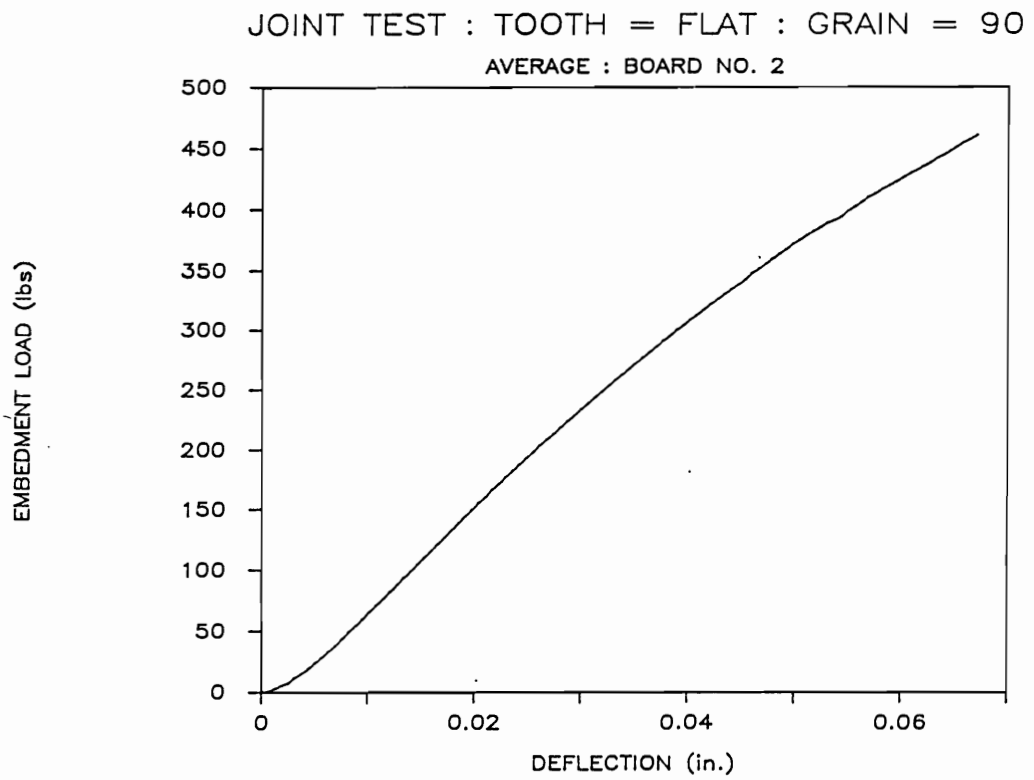
JOINT TEST : TOOTH = FLAT : GRAIN = 90
AVERAGE : BOARD NO. 2
EMBEDMENT LOAD (lbs)
500
450
400
350
300
250
200
150
100
50
0
0
0.02
0.04
0.06
DEFLECTION (in.)

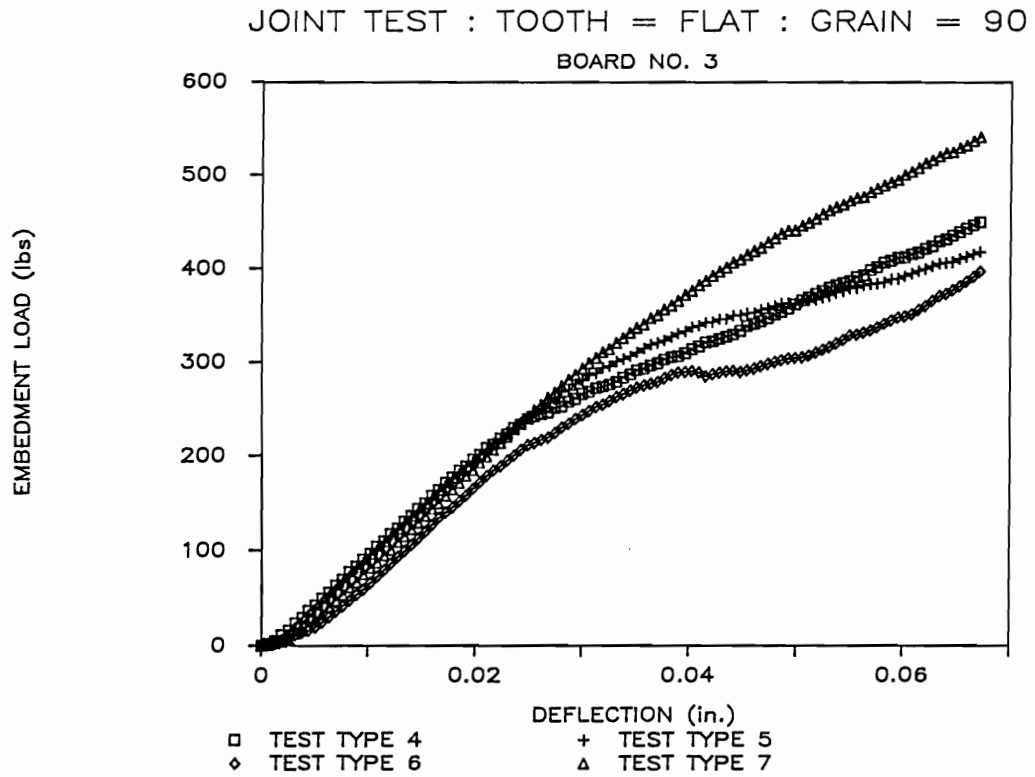
JOINT TEST : TOOTH = FLAT : GRAIN = 90
BOARD NO. 3
EMBEDMENT LOAD (lbs)
600
500
400
300
200
100
0
0
0.02
0.04
0.06
DEFLECTION (in.)
TEST TYPE 4
TEST TYPE 5
TEST TYPE 6
TEST TYPE 7

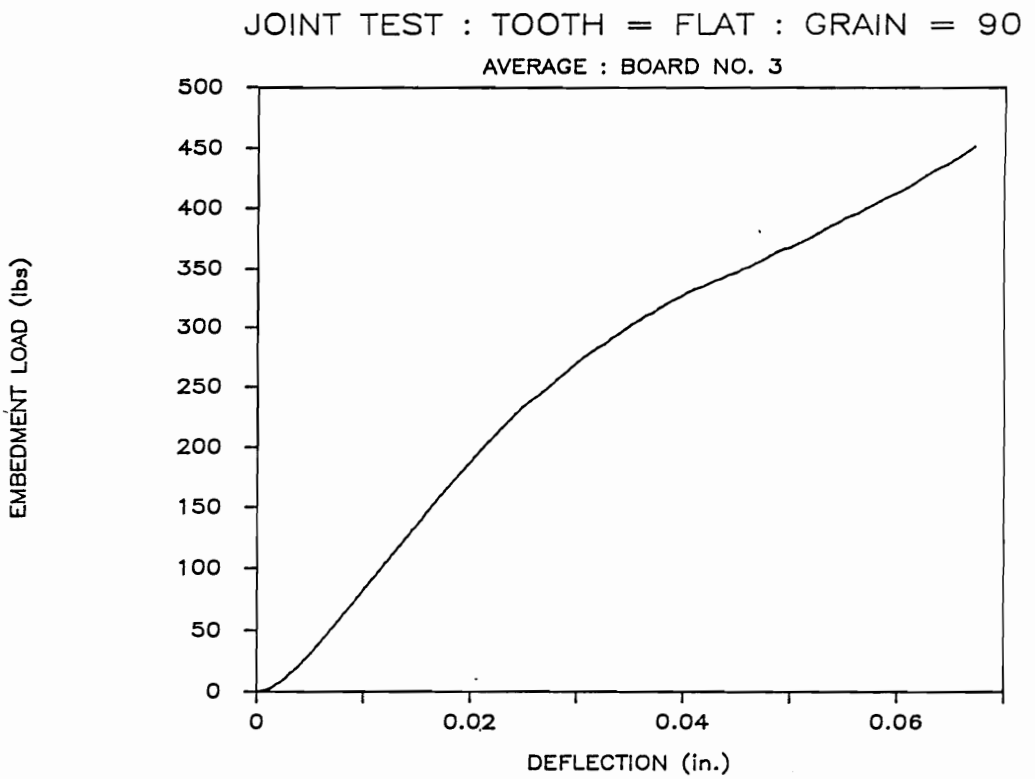
JOINT TEST : TOOTH = FLAT : GRAIN = 90
AVERAGE : BOARD NO. 3
EMBEDMENT LOAD (lbs)
500
450
400
350
300
250
200
150
100
50
0
0
0.02
0.04
0.06
DEFLECTION (in.)

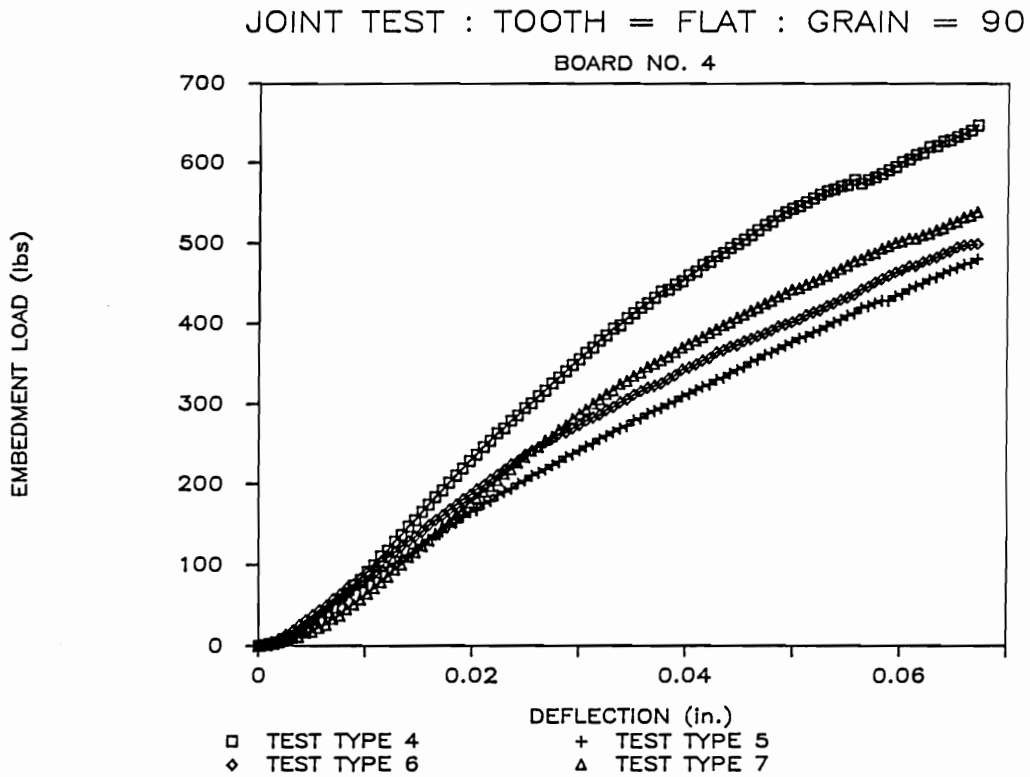
JOINT TEST : TOOTH = FLAT : GRAIN = 90
BOARD NO. 4
EMBEDMENT LOAD (lbs)
700
600
500
400
300
200
100
0
0
0.02
0.04
0.06
DEFLECTION (in.)
TEST TYPE 4
TEST TYPE 5
TEST TYPE 6
TEST TYPE 7

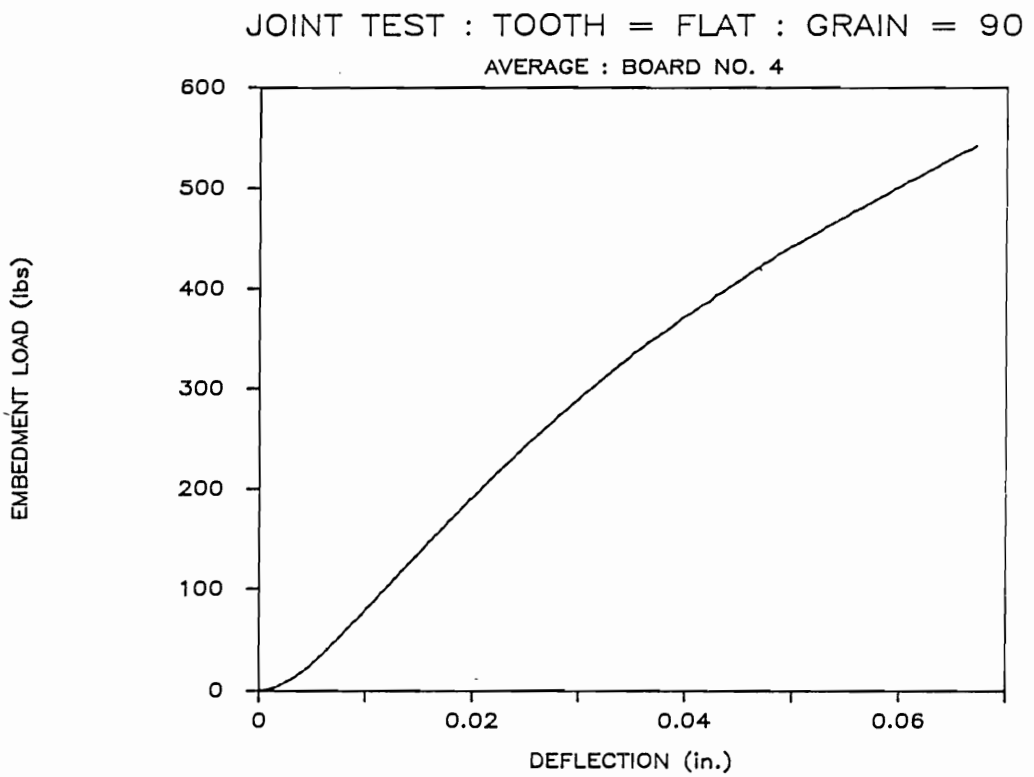
JOINT TEST : TOOTH = FLAT : GRAIN = 90
AVERAGE : BOARD NO. 4
EMBEDMENT LOAD (lbs)
600
500
400
300
200
100
0
0
0.02
0.04
0.06
DEFLECTION (in.)

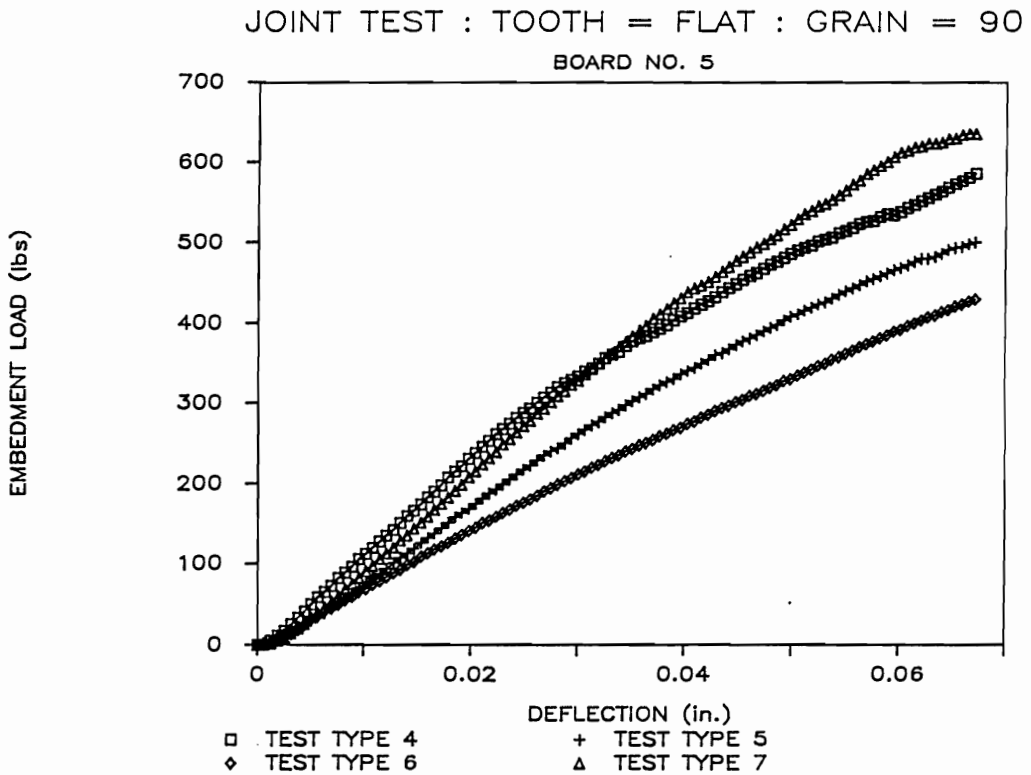
JOINT TEST : TOOTH = FLAT : GRAIN = 90
BOARD NO. 5
EMBEDMENT LOAD (lbs)
700
600
500
400
300
200
100
0
0
0.02
0.04
0.06
DEFLECTION (in.)
TEST TYPE 4
TEST TYPE 5
TEST TYPE 6
TEST TYPE 7

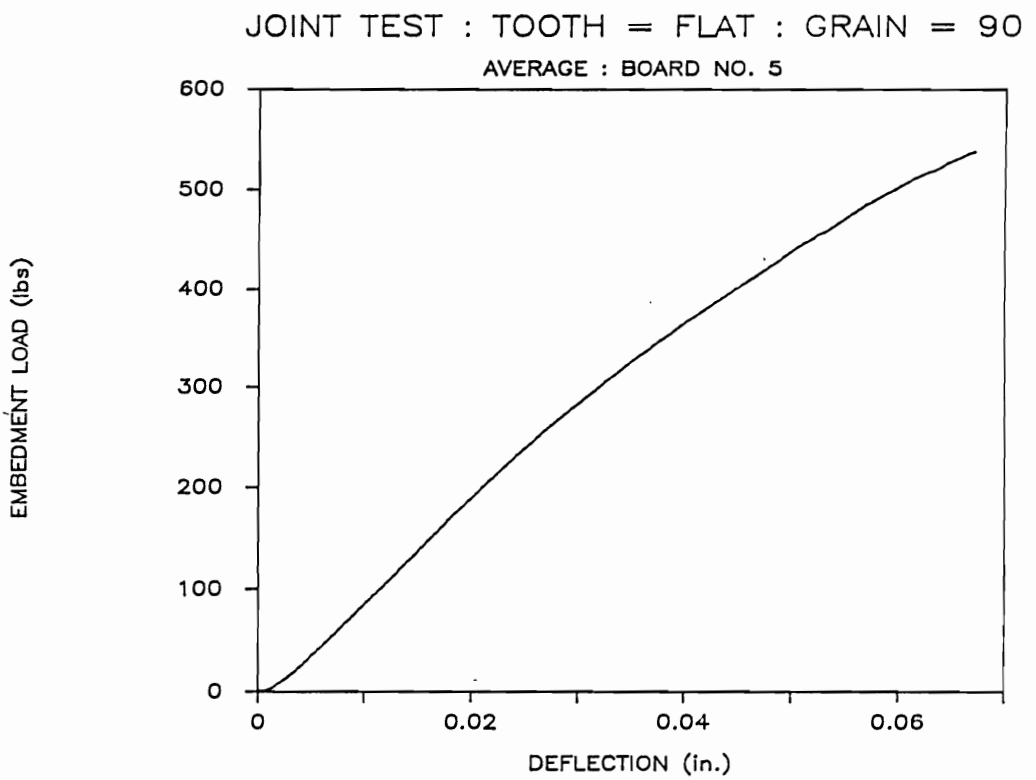
JOINT TEST : TOOTH = FLAT : GRAIN = 90
AVERAGE : BOARD NO. 5
EMBEDMENT LOAD (lbs)
600
500
400
300
200
100
0
0
0.02
0.04
0.06
DEFLECTION (in.)

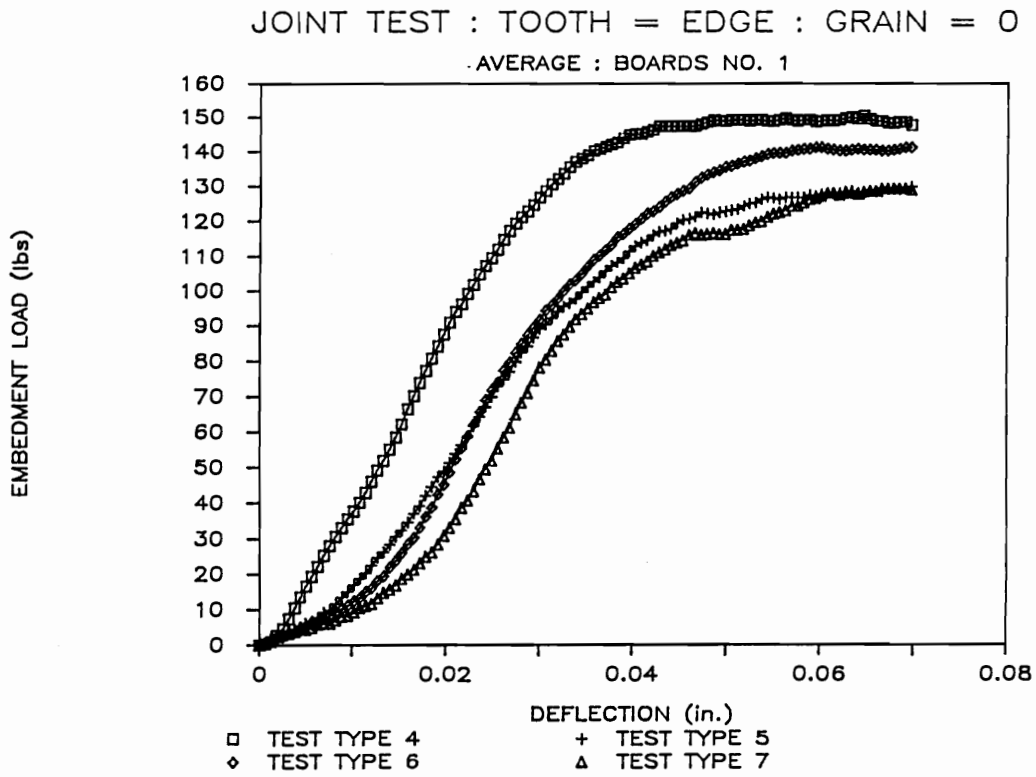
JOINT TEST : TOOTH = EDGE : GRAIN = 0
AVERAGE : BOARDS NO. 1
EMBEDMENT LOAD (lbs)
160
150
140
130
120
110
100
90
80
70
60
50
40
30
20
10
0
0
0.02
0.04
0.06
0.08
DEFLECTION (in.)
TEST TYPE 4
TEST TYPE 5
TEST TYPE 6
TEST TYPE 7

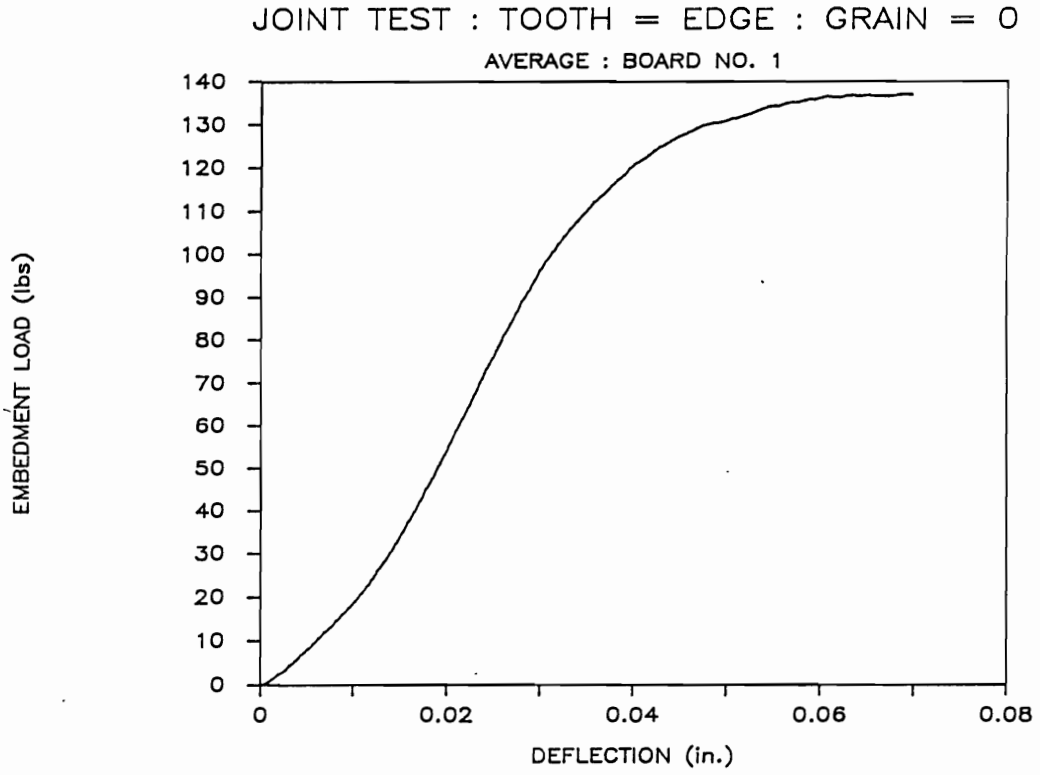
JOINT TEST : TOOTH = EDGE : GRAIN = 0
AVERAGE : BOARD NO. 1
EMBEDMENT LOAD (lbs)
140
130
120
110
100
90
80
70
60
50
40
30
20
10
0
0
0.02
0.04
0.06
0.08
DEFLECTION (in.)

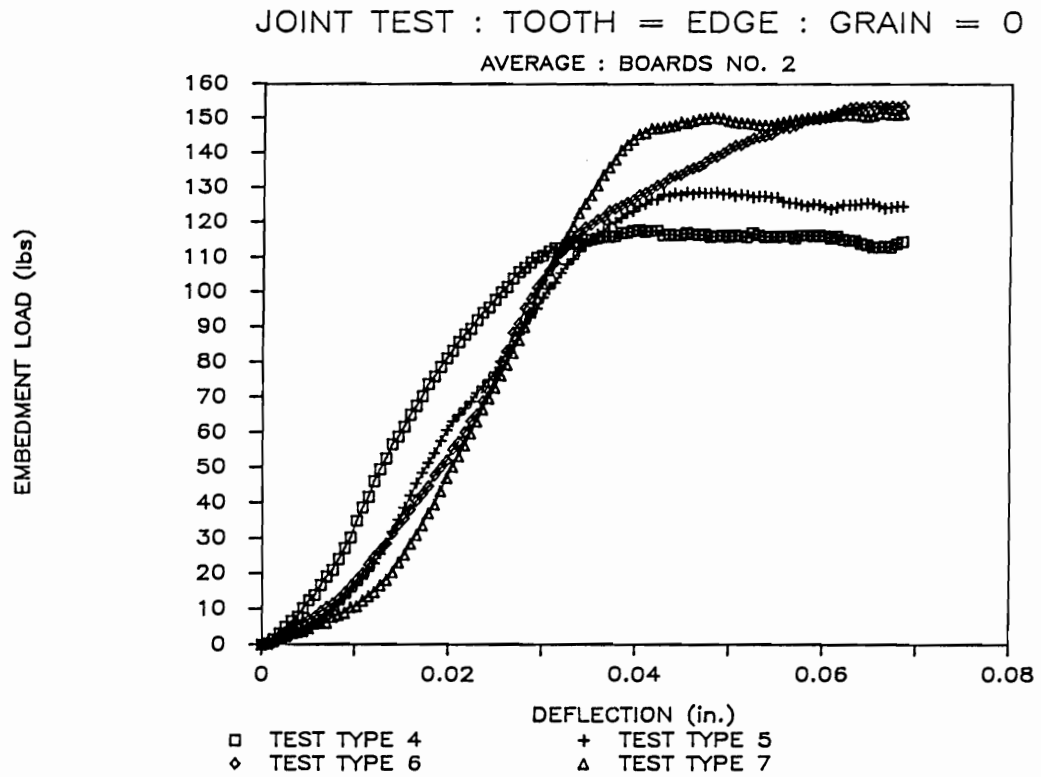
JOINT TEST : TOOTH = EDGE : GRAIN = 0
AVERAGE : BOARDS NO. 2
EMBEDMENT LOAD (lbs)
160
150
140
130
120
110
100
90
80
70
60
50
40
30
20
10
0
0
0.02
0.04
0.06
0.08
DEFLECTION (in.)
TEST TYPE 4
TEST TYPE 5
TEST TYPE 6
TEST TYPE 7

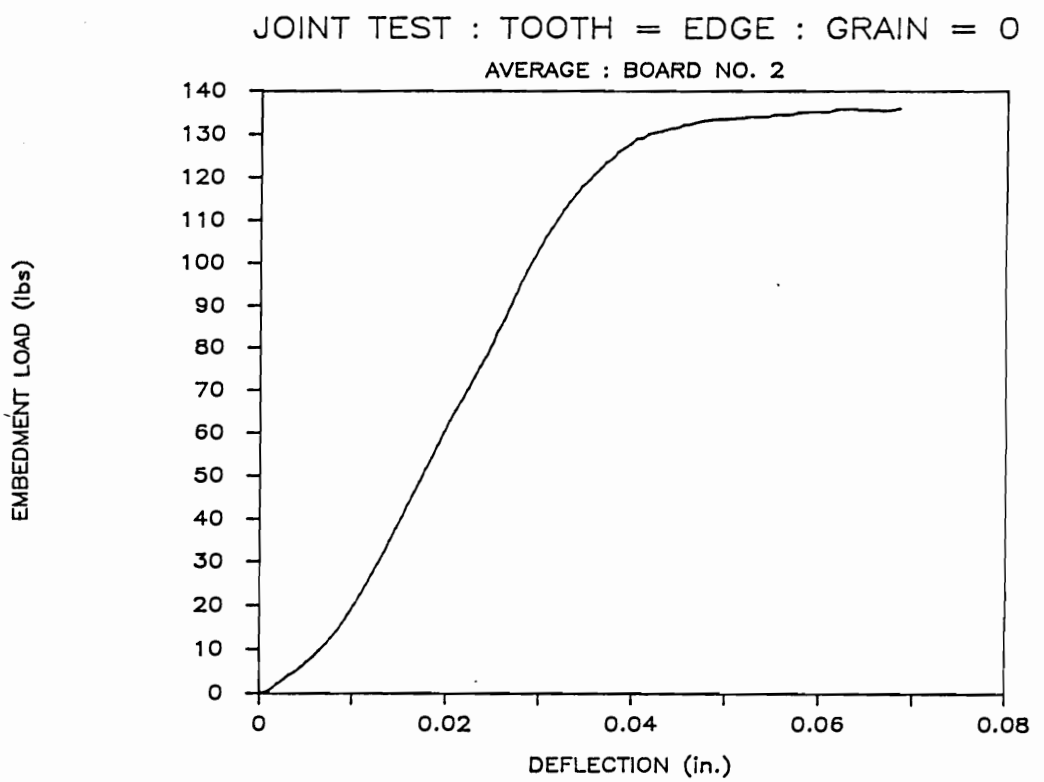
JOINT TEST : TOOTH = EDGE : GRAIN = 0
AVERAGE : BOARD NO. 2
EMBEDMENT LOAD (lbs)
140
130
120
110
100
90
80
70
60
50
40
30
20
10
0
0
0.02
0.04
0.06
0.08
DEFLECTION (in.)

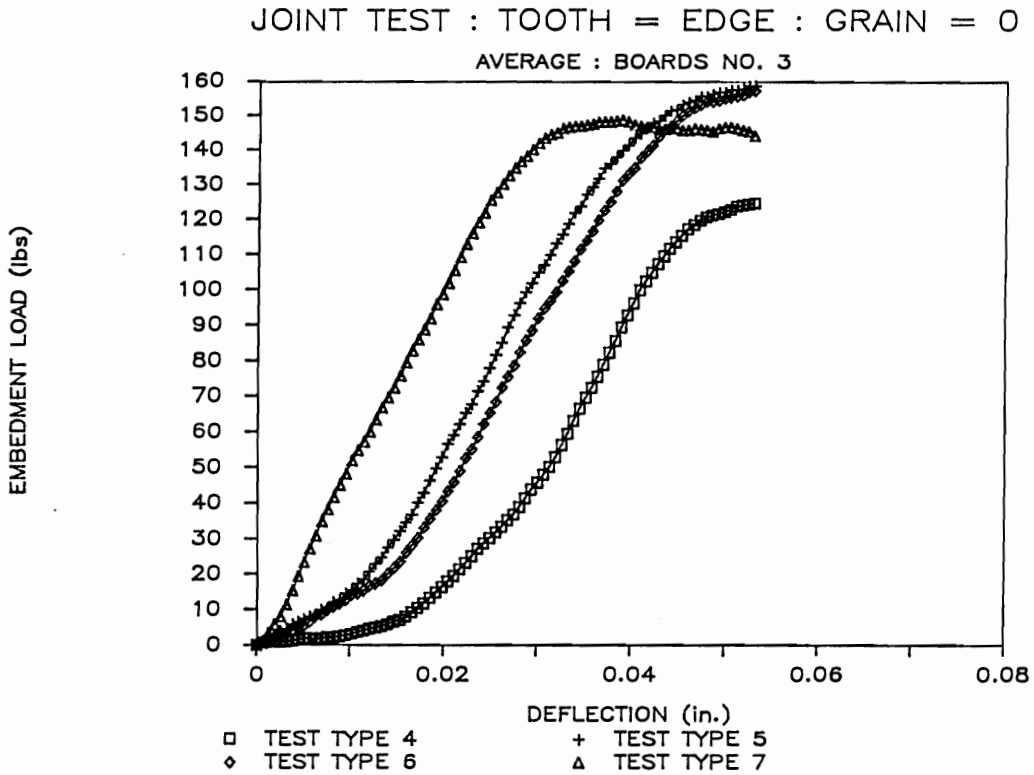
JOINT TEST : TOOTH = EDGE : GRAIN = 0
AVERAGE : BOARDS NO. 3
EMBEDMENT LOAD (lbs)
160
150
140
130
120
110
100
90
80
70
60
50
40
30
20
10
0
0
0.02
0.04
0.06
0.08
DEFLECTION (in.)
TEST TYPE 4
TEST TYPE 5
TEST TYPE 6
TEST TYPE 7

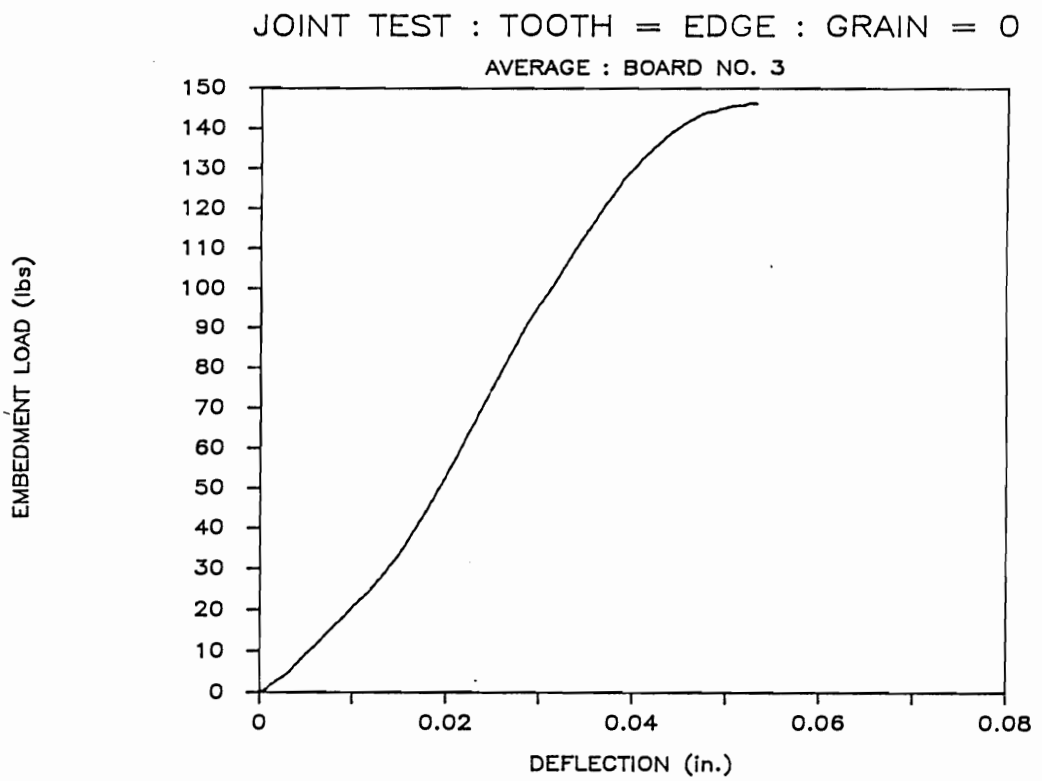
JOINT TEST : TOOTH = EDGE : GRAIN = 0
AVERAGE : BOARD NO. 3
EMBEDMENT LOAD (lbs)
150
140
130
120
110
100
90
80
70
60
50
40
30
20
10
0
0
0.02
0.04
0.06
0.08
DEFLECTION (in.)

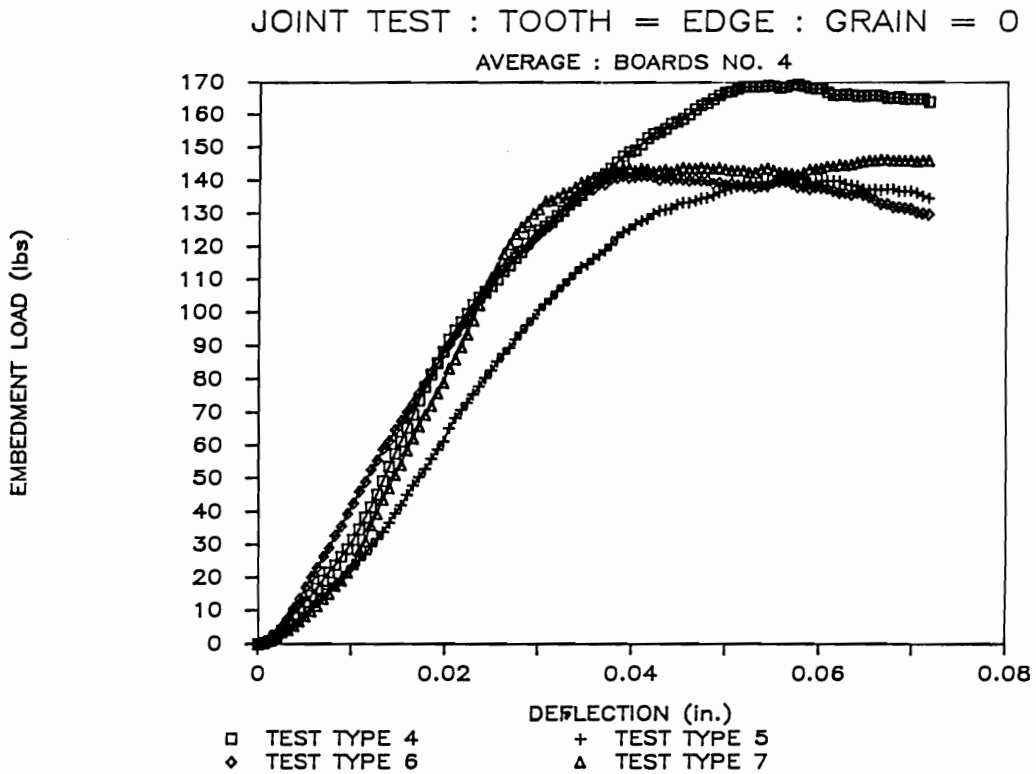
JOINT TEST : TOOTH = EDGE : GRAIN = 0
AVERAGE : BOARDS NO. 4
EMBEDMENT LOAD (lbs)
170
160
150
140
130
120
110
100
90
80
70
60
50
40
30
20
10
0
0
0.02
0.04
0.06
0.08
DEFLECTION (in.)
TEST TYPE 4
TEST TYPE 5
TEST TYPE 6
TEST TYPE 7

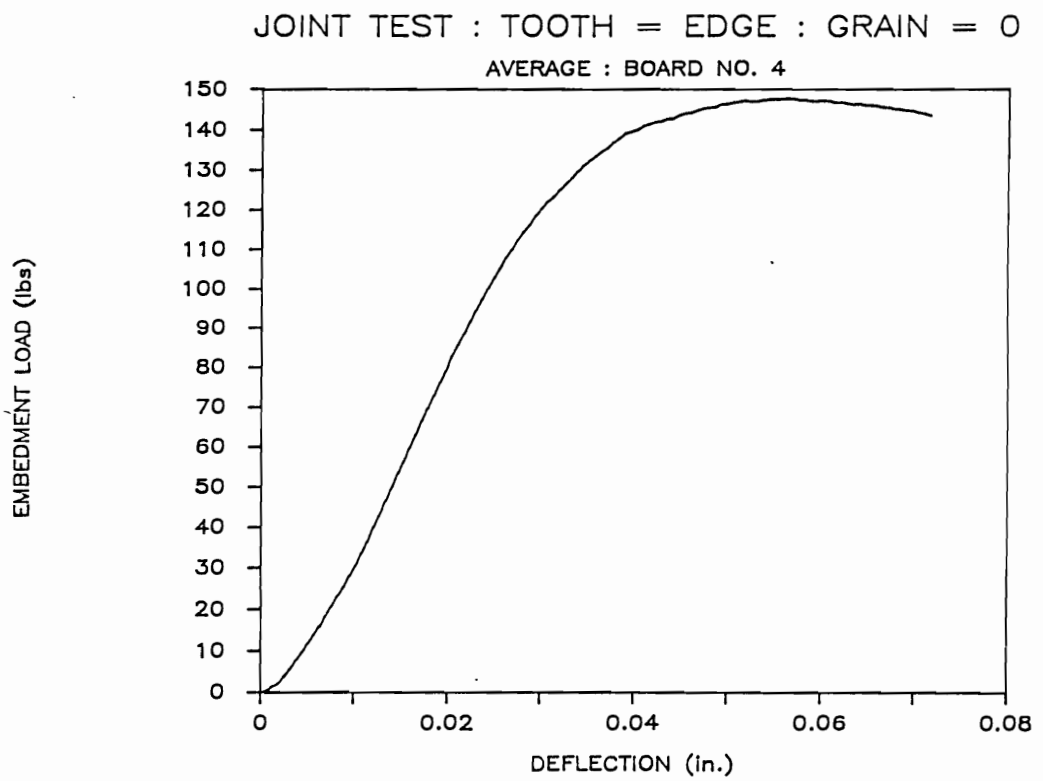
JOINT TEST : TOOTH = EDGE : GRAIN = 0
AVERAGE : BOARD NO. 4
EMBEDMENT LOAD (lbs)
150
140
130
120
110
100
90
80
70
60
50
40
30
20
10
0
0
0.02
0.04
0.06
0.08
DEFLECTION (in.)

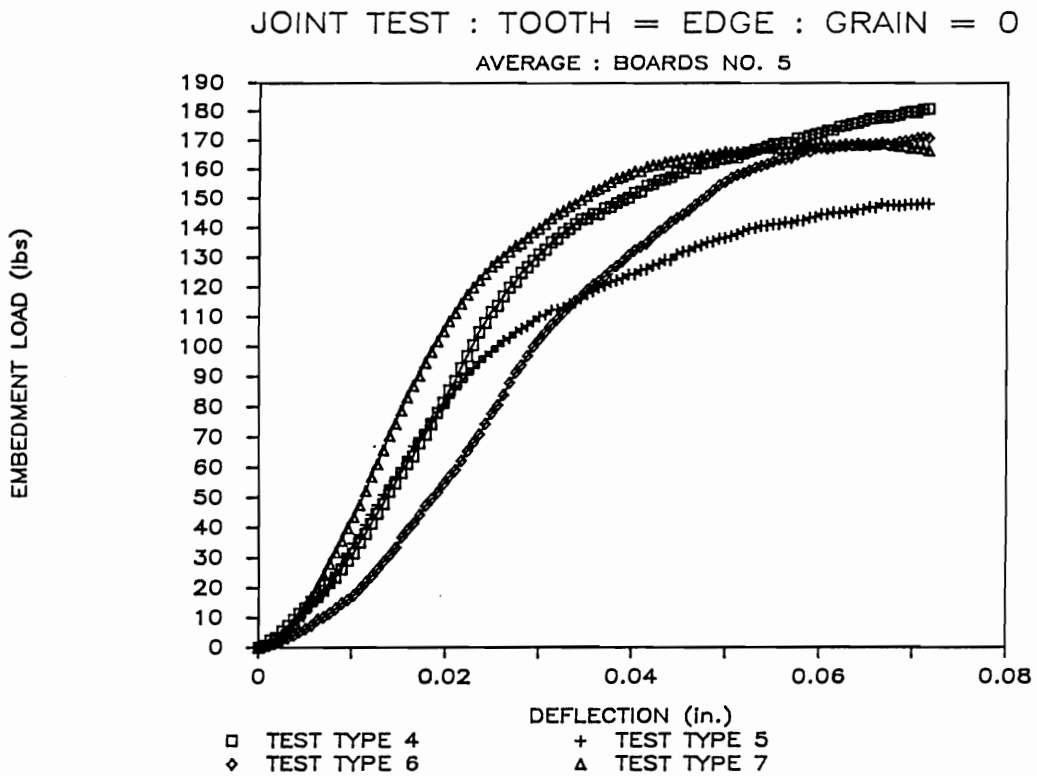
JOINT TEST : TOOTH = EDGE : GRAIN = 0
AVERAGE : BOARDS NO. 5
EMBEDMENT LOAD (lbs)
190
180
170
160
150
140
130
120
110
100
90
80
70
60
50
40
30
20
10
0
0
0.02
0.04
0.06
0.08
DEFLECTION (in.)
TEST TYPE 4
TEST TYPE 5
TEST TYPE 6
TEST TYPE 7

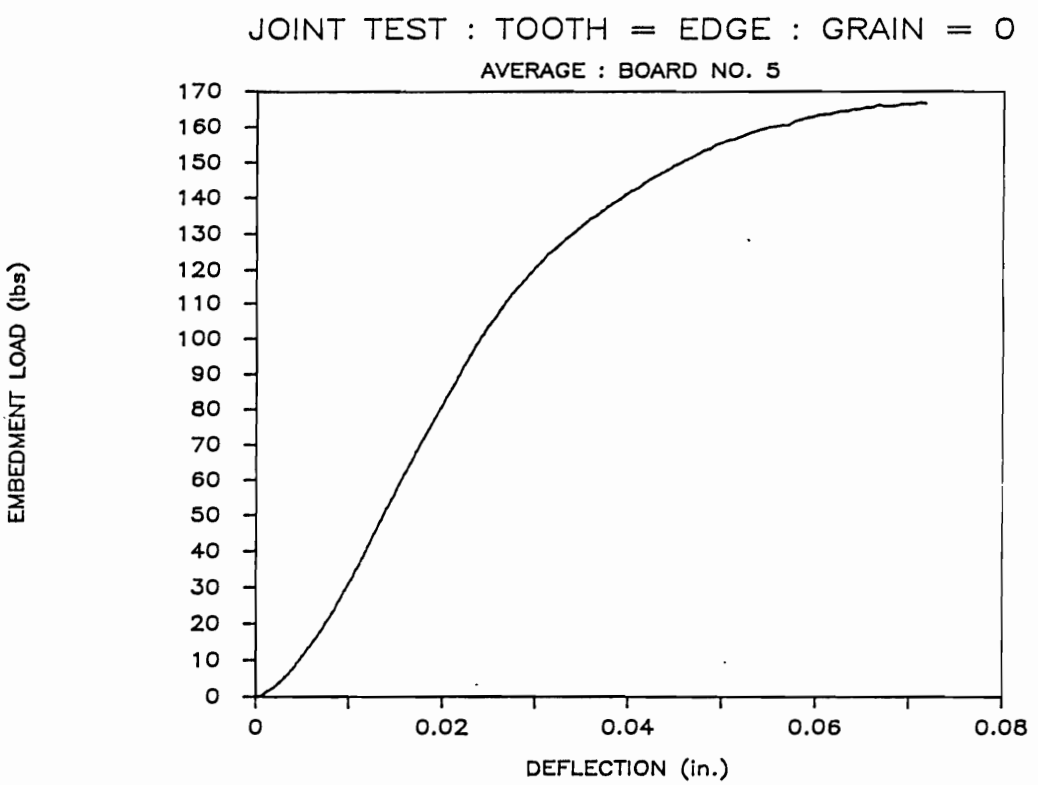
JOINT TEST : TOOTH = EDGE : GRAIN = 0
AVERAGE : BOARD NO. 5
EMBEDMENT LOAD (lbs)
170
160
150
140
130
120
110
100
90
80
70
60
50
40
30
20
10
0
0
0.02
0.04
0.06
0.08
DEFLECTION (in.)

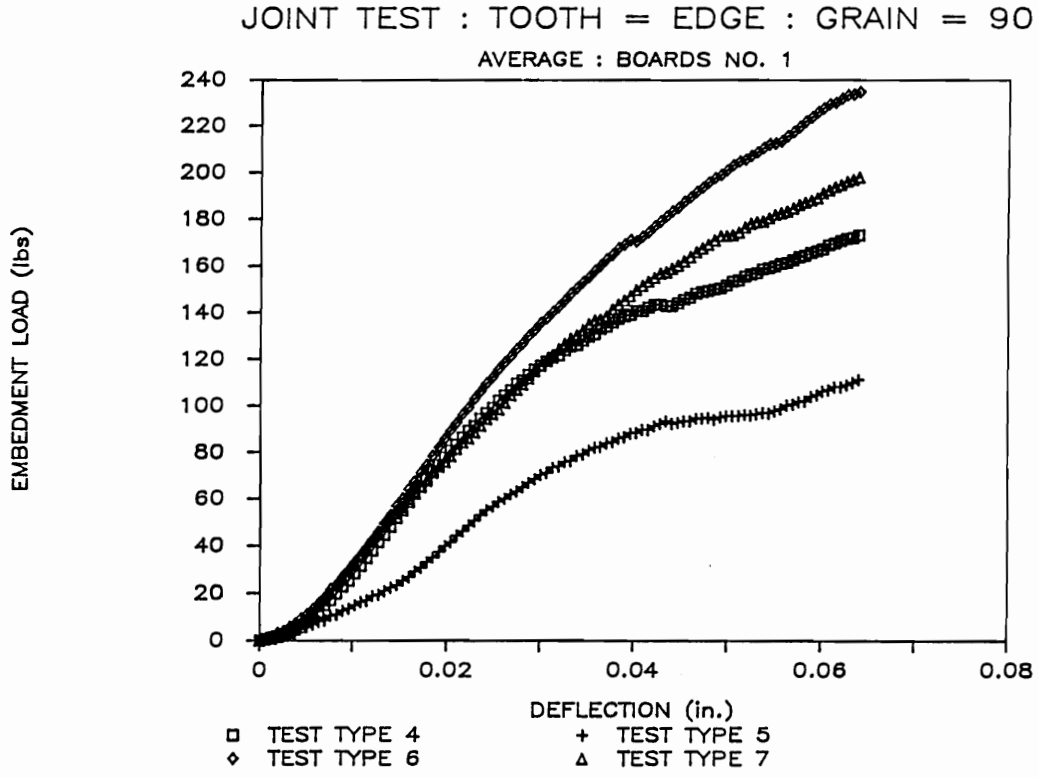
JOINT TEST : TOOTH = EDGE : GRAIN = 90
AVERAGE : BOARDS NO. 1
EMBEDMENT LOAD (lbs)
240
220
200
180
160
140
120
100
80
60
40
20
0
0
0.02
0.04
0.06
0.08
DEFLECTION (in.)
TEST TYPE 4
TEST TYPE 5
TEST TYPE 6
TEST TYPE 7

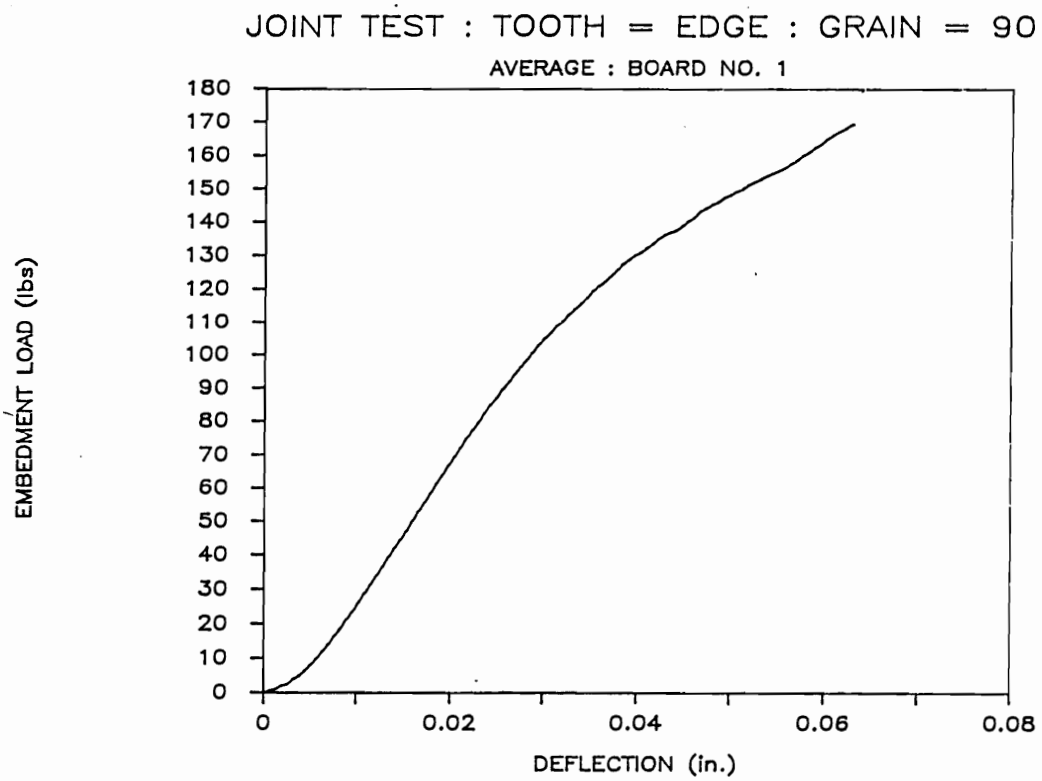
JOINT TEST : TOOTH = EDGE : GRAIN = 90
AVERAGE : BOARD NO. 1
EMBEDMENT LOAD (lbs)
180
170
160
150
140
130
120
110
100
90
80
70
60
50
40
30
20
10
0
0
0.02
0.04
0.06
0.08
DEFLECTION (in.)

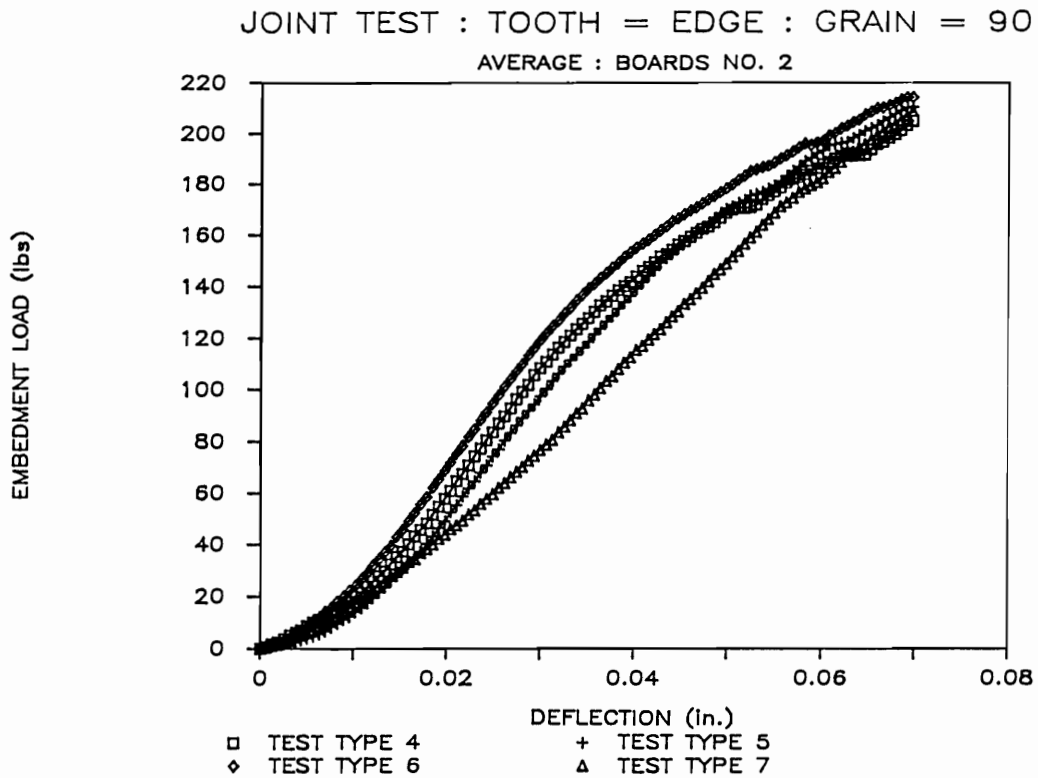
JOINT TEST : TOOTH = EDGE : GRAIN = 90
AVERAGE : BOARDS NO. 2
EMBEDMENT LOAD (lbs)
220
200
180
160
140
120
100
80
60
40
20
0
0
0.02
0.04
0.06
0.08
DEFLECTION (in.)
TEST TYPE 4
TEST TYPE 5
TEST TYPE 6
TEST TYPE 7

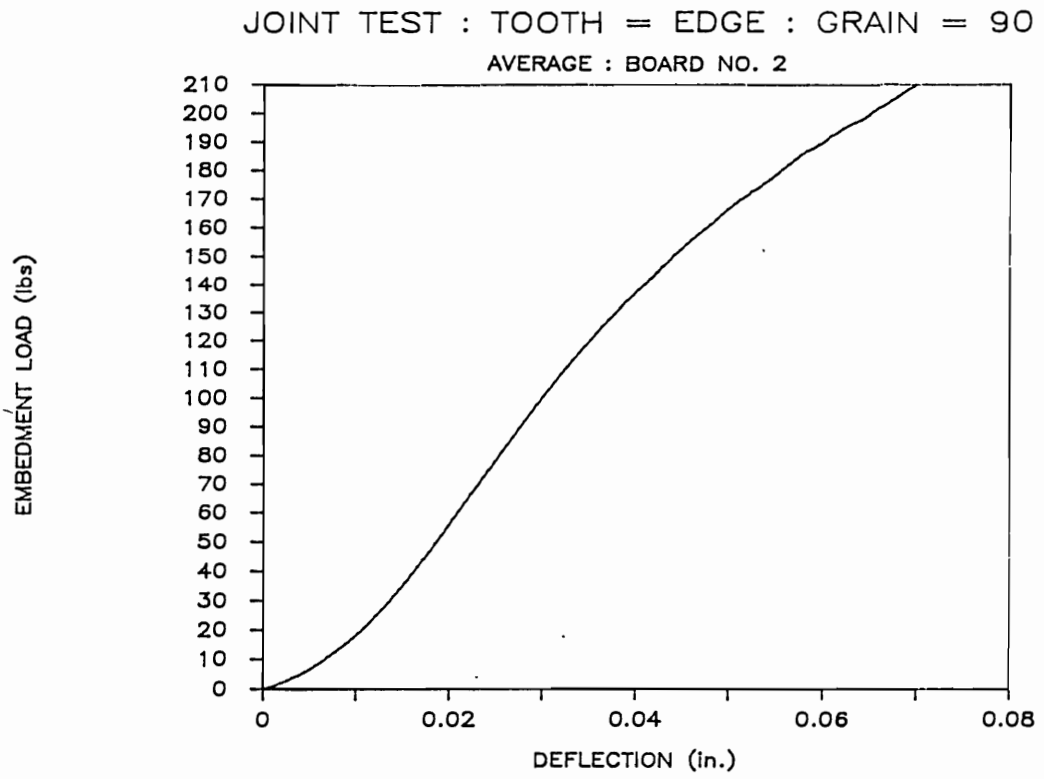
JOINT TEST : TOOTH = EDGE : GRAIN = 90
AVERAGE : BOARD NO. 2
EMBEDMENT LOAD (lbs)
210
200
190
180
170
160
150
140
130
120
110
100
90
80
70
60
50
40
30
20
10
0
0
0.02
0.04
0.06
0.08
DEFLECTION (in.)

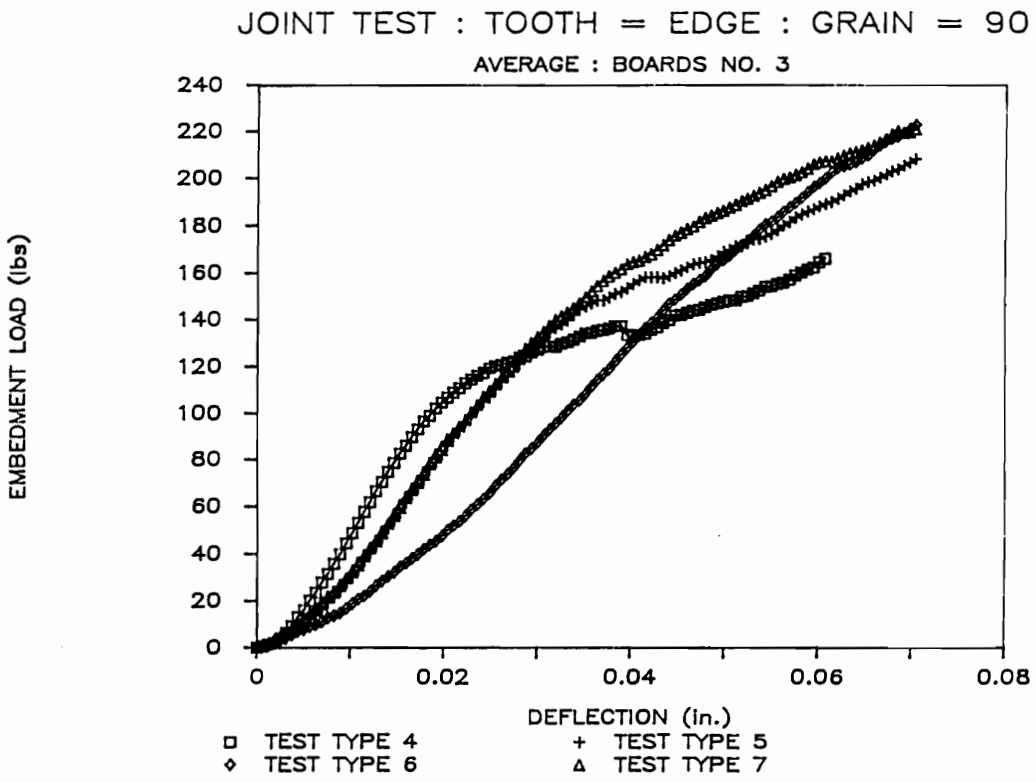
JOINT TEST : TOOTH = EDGE : GRAIN = 90
AVERAGE : BOARDS NO. 3
EMBEDMENT LOAD (lbs)
240
220
200
180
160
140
120
100
80
60
40
20
0
0
0.02
0.04
0.06
0.08
DEFLECTION (in.)
TEST TYPE 4
TEST TYPE 5
TEST TYPE 6
TEST TYPE 7

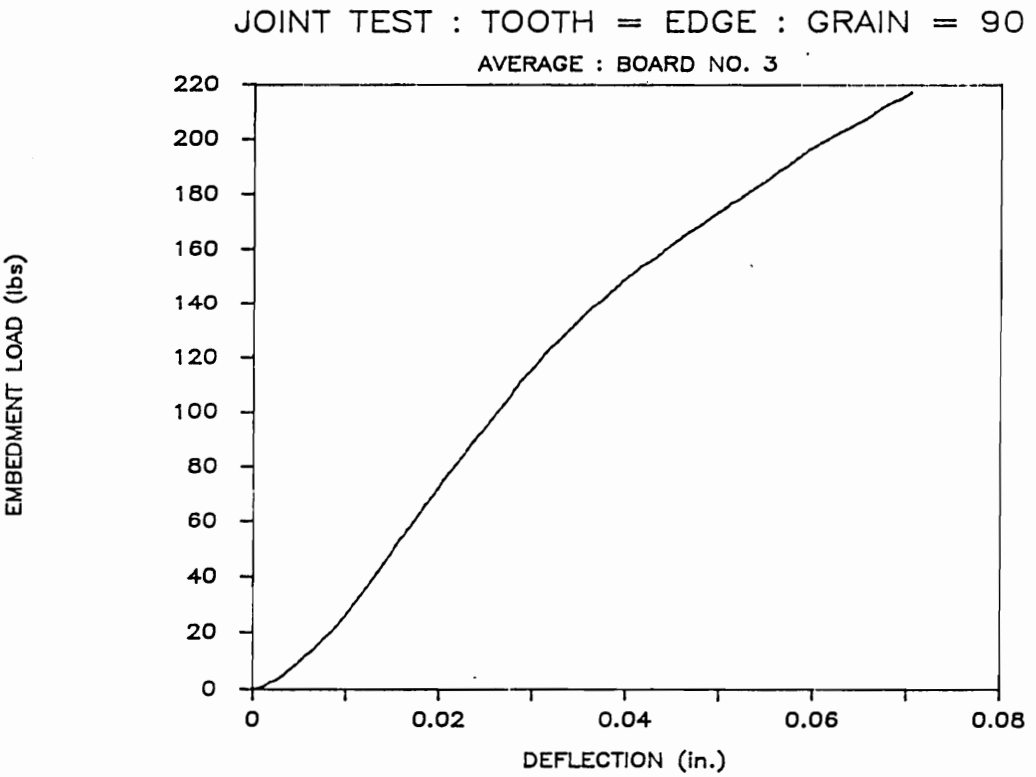
JOINT TEST : TOOTH = EDGE : GRAIN = 90
AVERAGE : BOARD NO. 3
EMBEDMENT LOAD (lbs)
220
200
180
160
140
120
100
80
60
40
20
0
0
0.02
0.04
0.06
0.08
DEFLECTION (in.)

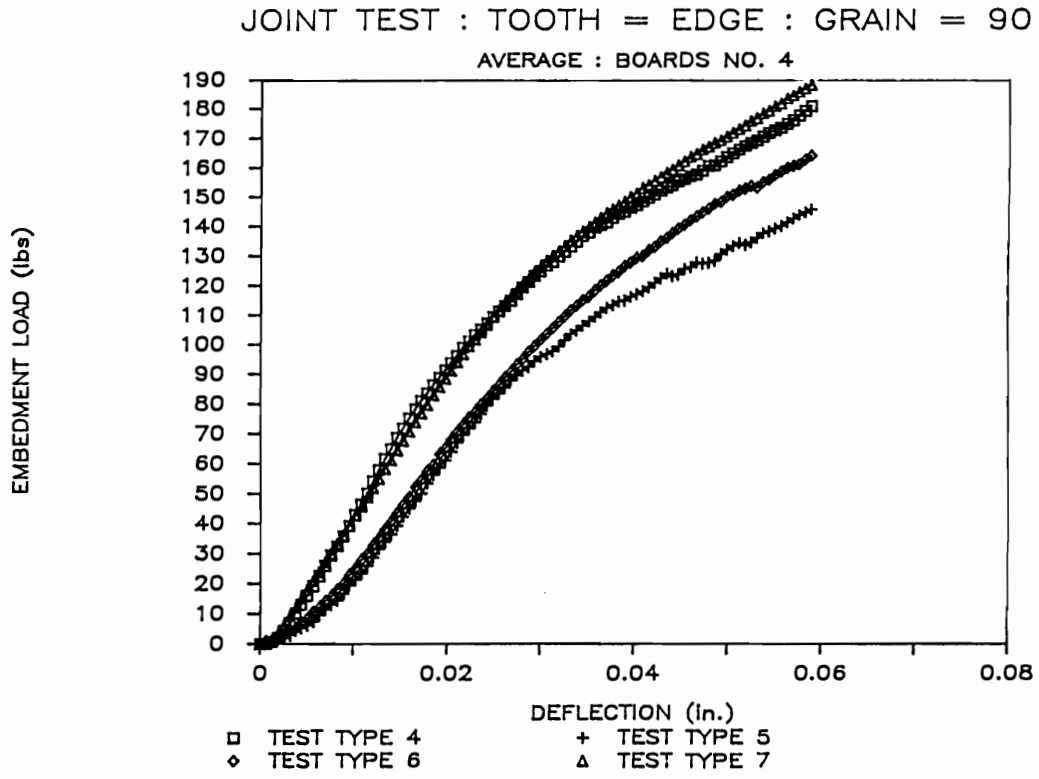
JOINT TEST : TOOTH = EDGE : GRAIN = 90
AVERAGE : BOARDS NO. 4
EMBEDMENT LOAD (lbs)
190
180
170
160
150
140
130
120
110
100
90
80
70
60
50
40
30
20
10
0
0
0.02
0.04
0.06
0.08
DEFLECTION (in.)
TEST TYPE 4
TEST TYPE 5
TEST TYPE 6
TEST TYPE 7

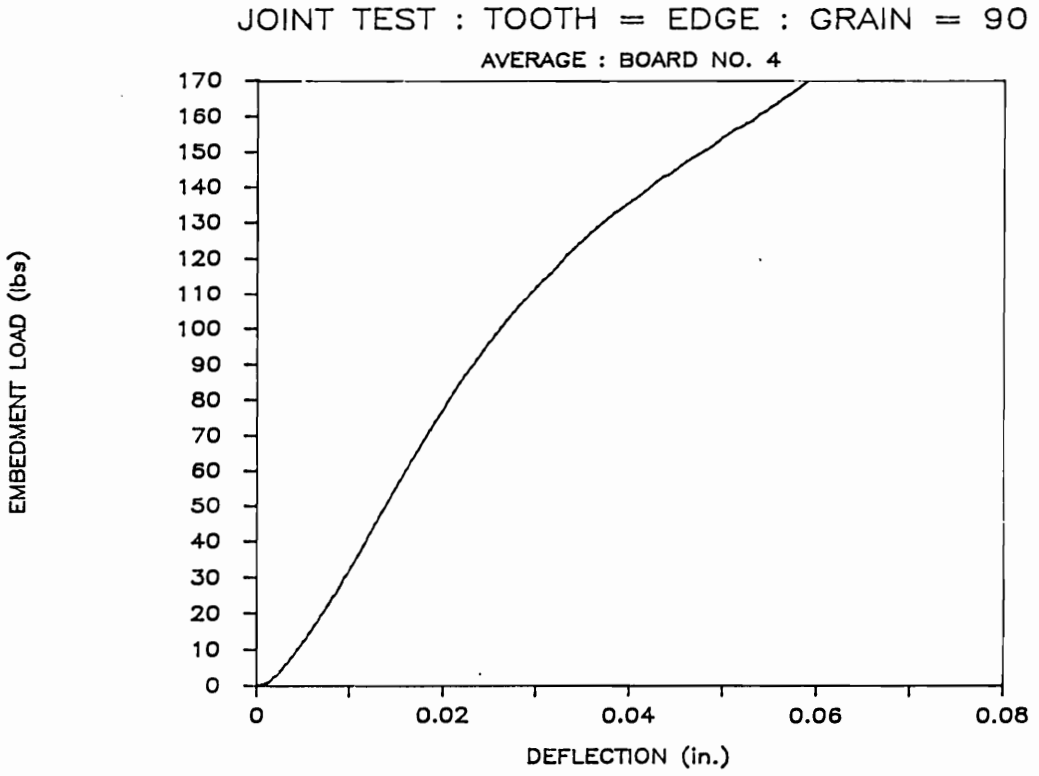
JOINT TEST : TOOTH = EDGE : GRAIN = 90
AVERAGE : BOARD NO. 4
EMBEDMENT LOAD (lbs)
170
160
150
140
130
120
110
100
90
80
70
60
50
40
30
20
10
0
0
0.02
0.04
0.06
0.08
DEFLECTION (in.)

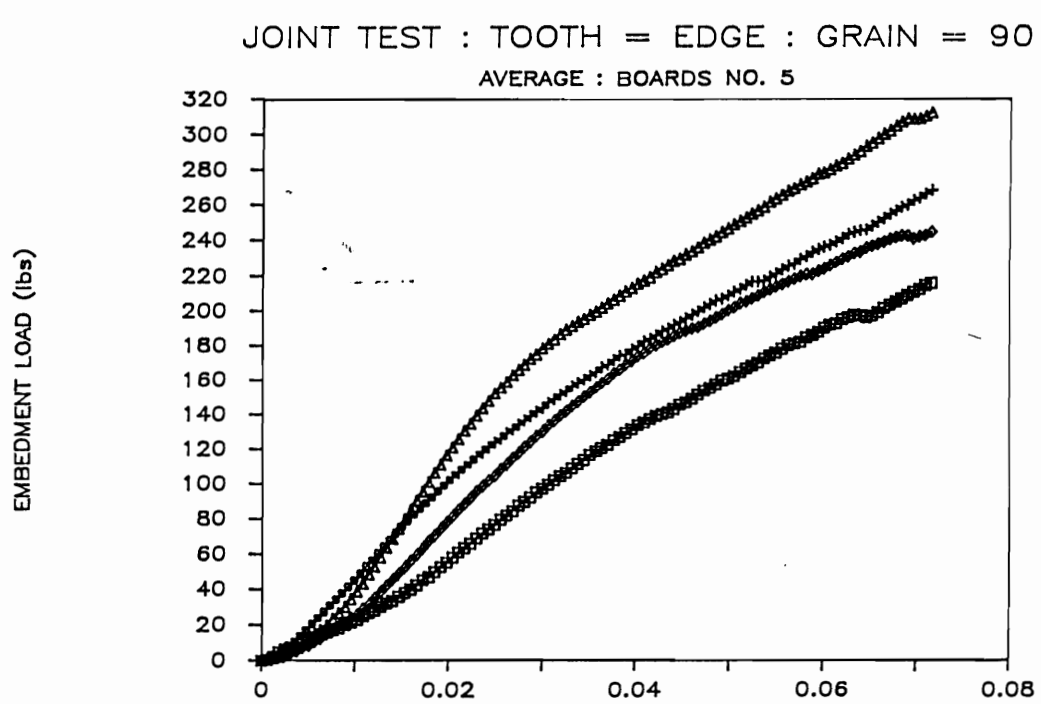
JOINT TEST : TOOTH = EDGE : GRAIN = 90
AVERAGE : BOARDS NO. 5
EMBEDMENT LOAD (lbs)
320
300
280
260
240
220
200
180
160
140
120
100
80
60
40
20
0
0
0.02
0.04
0.06
0.08
DEFLECTION (In.)
TEST TYPE 4
TEST TYPE 5
TEST TYPE 6
TEST TYPE 7

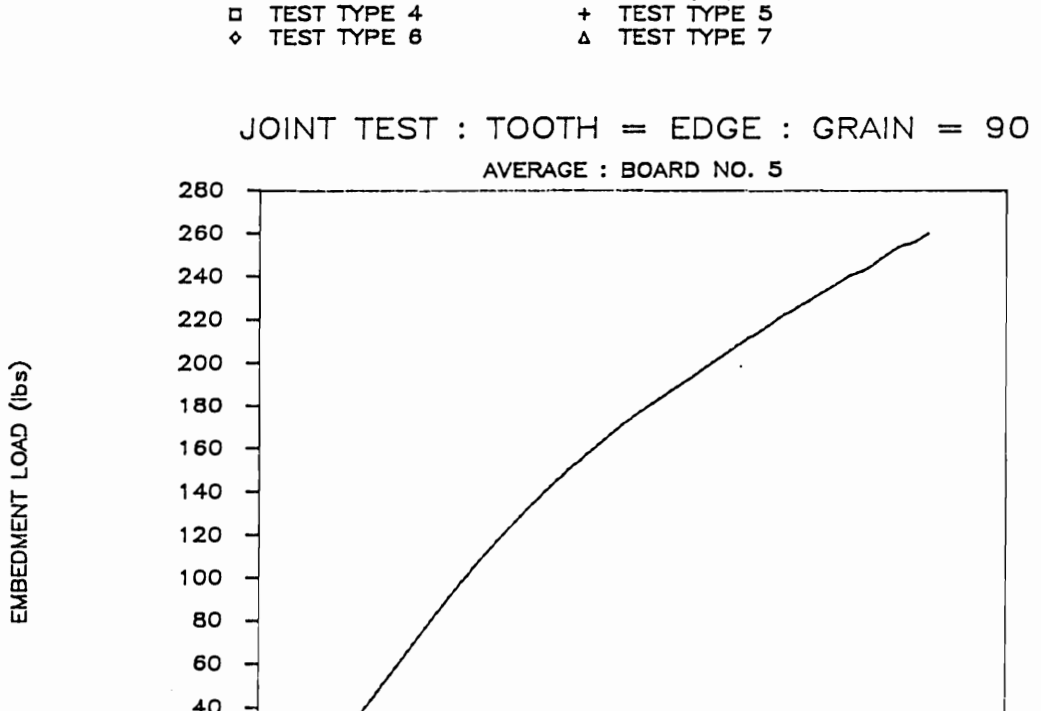
JOINT TEST : TOOTH = EDGE : GRAIN = 90
AVERAGE : BOARD NO. 5
EMBEDMENT LOAD (lbs)
280
260
240
220
200
180
160
140
120
100
80
60
40
20
0
0
0.02
0.04
0.06
0.08
DEFLECTION (in.)

APPENDIX E

SPECIFIC GRAVITY AND MOISTURE CONTENT

BOARD NO.	REPLICATE	12% MOISTURE CONTENT				OVEN-DRY	MOISTURE	SPECIFIC
		WIDTH1 (mm)	WIDTH2 (mm)	WIDTH3 (mm)	WEIGHT (gm)	WEIGHT (gm)	CONTENT (percent)	GRAVITY
MULTIPLE TOOTH JOINTS								
	1	37.83	38.05	37.95	23.68	21.31	11.1	0.39
1	2	38.07	37.94	38.07	24.41	21.89	11.5	0.40
	3	38.07	37.94	37.81	23.56	21.22	11.0	0.39
	average						11.2	0.39
	1	38.03	38.01	37.94	25.46	23.23	9.6	0.42
2	2	37.99	37.99	37.96	26.88	24.45	9.9	0.45
	3	38.01	37.90	38.00	26.00	23.66	9.9	0.43
	average						9.8	0.43
	1	38.05	37.85	38.25	27.90	25.48	9.5	0.46
3	2	38.02	37.90	38.08	27.71	25.24	9.8	0.46
	3	38.02	37.85	38.10	27.20	24.84	9.5	0.45
	average						9.6	0.46
	1	38.05	37.92	37.93	26.92	24.20	11.2	0.44
4	2	38.09	37.84	37.83	27.36	24.64	11.0	0.45
	3	38.09	37.83	37.80	26.00	23.37	11.3	0.43
	average						11.2	0.44
	1	37.96	38.03	37.77	27.62	24.78	11.5	0.45
5	2	38.20	37.89	37.88	27.82	24.97	11.4	0.46
	3	38.06	37.87	37.74	27.89	25.01	11.5	0.46
	average						11.5	0.46
COMPLETE JOINTS								
	1	38.07	37.25	37.77	24.89	22.43	11.0	0.41
	2	38.06	37.60	37.90	24.30	21.85	11.2	0.40
1	3	38.18	37.71	37.78	24.49	22.03	11.2	0.41
	4	38.05	37.69	37.96	25.20	22.66	11.2	0.42
	average						11.2	0.41
	1	38.09	37.90	38.03	24.65	22.21	11.0	0.40
	2	38.03	37.86	37.87	25.32	22.78	11.2	0.42
2	3	38.03	37.58	37.78	25.27	22.78	10.9	0.42
	4	38.06	37.79	37.89	25.64	23.13	10.9	0.42
	average						11.0	0.42
	1	38.04	37.87	37.95	27.96	25.62	9.1	0.47
	2	38.04	37.91	38.07	26.95	24.55	9.8	0.45
3	3	38.16	37.89	38.03	27.86	25.32	10.0	0.46
	4	38.14	37.86	38.06	26.38	24.01	9.9	0.44
	average						9.7	0.46
	1	38.08	37.94	37.64	30.70	27.80	10.4	0.51
	2	38.08	37.97	37.89	28.47	25.83	10.2	0.47
4	3	38.06	37.91	37.97	28.26	25.58	10.5	0.47
	4	37.99	37.92	37.90	28.55	25.87	10.4	0.47
	average						11.4	0.48
	1	37.98	37.89	37.94	28.84	26.01	10.9	0.48
	2	38.07	38.02	37.98	29.48	26.51	11.2	0.48
5	3	37.99	37.89	38.07	29.34	26.43	11.0	0.48
	4	38.04	37.65	38.33	28.50	25.67	11.0	0.47
	average						11.0	0.48

APPENDIX F

TOOTH WITHDRAWAL DATA

Table F1. Summary of withdrawal tests conducted on truss-plate section containing 4 teeth (values given in table are on a per tooth basis).

SPECIMEN	WITHOUT EPOXY		WITH EPOXY	
	SECANT MODULUS (lbs/in.)	ULTIMATE LOAD (lbs)	SECANT MODULUS (lbs/in.)	ULTIMATE LOAD (lbs)
1	250.0	16.0	245.2	25.3
2	272.7	18.3	323.9	30.8
3	369.3	37.5	520.8	51.3
4	250.0	21.0	381.3	38.0
5	262.5	16.8	293.3	33.8
6	289.1	14.3	359.4	38.5
7	197.9	16.0	231.6	33.0
8	267.0	24.3	380.7	43.5
9	342.1	28.8	453.9	39.3
average	277.8	21.4	354.5	37.1
stand. dev.	51.2	7.6	94.0	7.6